The Thesis Committee for Samarth Agrawal
Certifies that this is the approved version of the following thesis:

Investigation Of Liquid Loading Mechanism Within Hydraulic Fractures In Unconventional/Tight Gas Reservoirs And Its Impact On Productivity

APPROVED BY
SUPERVISING COMMITTEE:

Supervisor: _____
Mukul M. Sharma

_____
Kishore K. Mohanty

Investigation Of Liquid Loading Mechanism Within Hydraulic Fractures In Unconventional/Tight Gas Reservoirs And Its Impact On Productivity

by

Samarth Agrawal, B.Tech

Thesis

Presented to the Faculty of the Graduate School of

The University of Texas at Austin

in Partial Fulfillment

of the Requirements

for the Degree of

Master of Science in Engineering

The University of Texas at Austin

May 2013

Dedication

To my parents and teachers

Acknowledgements

First and foremost, I would like to take this opportunity to thank my advisor Dr. Mukul M. Sharma for his insightful guidance throughout the past two years. He was both a source of tremendous knowledge as well as inspiration for exceptional professionalism. I have learned immensely under his supervision and developed sound fundamentals regarding the discipline. I would like to thank Dr. Mohanty for sharing his expert insights about fluid flow in fractured reservoirs.

I would also like to extend my deep gratitude to all the participating members of the JIP on Hydraulic Fracturing and Sand Control at the University of Texas at Austin for their continued technical and financial support. I am deeply thankful to CMG for providing their reservoir simulation software package and support services towards the successful implementation of this project.

Among my fellow colleagues, I would like to extend my sincere gratitude to Jongsoo Hwang for his support during this project. I am also thankful to Sahil, Ripudaman, Prateek, Sriram, Evan, Do, Roman, Kyle and Natalia for making this tenure a great learning and enjoyable experience.

Last but not the least, I would like to thank my family for their tireless support and blessings.

May 2013

Abstract

Investigation Of Liquid Loading Mechanism Within Hydraulic Fractures In Unconventional/Tight Gas Reservoirs And Its Impact On Productivity

Samarth Agrawal, M.S.E.

The University of Texas at Austin, 2013

Supervisor: Mukul M. Sharma

One of the major challenges in fracturing low permeability/tight/unconventional gas formations is the loss of frac water and well productivity due to fluid entrapment in the matrix or fracture. Field results have indicated that only 15-30% of the frac fluid is recovered at the surface after flow back is initiated. Past studies have suggested that this water is trapped in the rock matrix near the fracture face and remains trapped due to the high capillary pressure in the matrix. Significant efforts have been made in the past to understand the impact of liquid blocking in hydraulically fractured conventional gas wells. Numerous remediation measures such as huff and puff gas cycling, alcohol or surfactant based chemical treatments have been proposed to reduce fracture face damage. However, when considering hydraulic fractures in unconventional reservoirs horizontal

wells, the fluid may also be trapped within the fracture itself and may impact the cleanup as well as productivity. This study shows that under typical gas flow rates in tight / shale gas formations, liquid loading within the fractures is likely to occur. Most of the previous simulation studies consider a 2D reservoir model and ignore gravity, considering the high vertical anisotropy (or extremely low vertical permeability) in these tight reservoirs matrix. However, this study presents the results of 3D simulations of liquid loading in hydraulic fractures in horizontal wells, including gravity and capillary pressure effects. Both CMG IMEX and GEM have been used to study this phenomenon in dry and wet gas cases. The impact of drawdown, fracture and reservoir properties on liquid loading and well productivity is presented. Results show that low drawdown, low matrix permeability or low initial gas rates aggravate the liquid loading problem inside the fracture and thereby impact the cleanup and gas productivity during initial production. A clear understanding of the phenomena could help in selection of optimal production facilities and well profile.

Table of Contents

List of Tables

List of Illustrations

List of Figures

Chapter 1: Introduction

1.1 Research Motivation

Unconventional oil and gas reservoirs refer to those hydrocarbon reservoirs that were historically not considered economical to produce from due to extremely small fluid permeability. However, by the end of 1990's Mitchel Energy with support from other agencies combined the "slickwater fracturing" technique, which uses water, sand, proppant and small percentage of chemical lubricants, with horizontal drilling to create multiple massive hydraulic fractures in these tight hydrocarbon bearing formations that allowed commercial recovery of hydrocarbons. Over the past 10 years the technology has evolved rapidly in this domain, especially in the area of horizontal well placement, proppant transport in fractures and geo-mechanical modeling. Advancements in hydraulic fracturing of these unconventional reservoirs has led to a massive production surge in North America.

One of the biggest concerns for the industry today is to minimize the environmental footprint of their operations while simultaneously maximizing the recovered hydrocarbons for the fixed amount of capital invested. One of the primary concerns with the use of water in these fracturing operations is its low recovery after flowback. Publically reported frac-water recovery ranges from 5-30% of the injected volume. Water utilized to initiate and propagate the fracture is assumed to get trapped in the formation matrix due to the high capillary pressures in the water wet rocks. This blocking of water on the fracture face also has an impact on the gas productivity. As the water saturation in the near fracture zone increases, the relative permeability to gas decreases significantly and impairs the gas rates. This has serious implications for the economics of the project.

This study investigates another mechanism of fluid trapping downhole and its implications on the productivity of the well. For extremely low matrix permeabilities, the gas flow rate is also expected to be small. In such a scenario, there is a high possibility of liquid (frac-water) sitting at the bottom of the fracture. This is because the low gas velocity will not be able to lift the frac-water out of the fracture against the capillary forces and gravity. To put the relative magnitude of these forces in perspective, consider the following calculations.

Assume a typical gas well in an unconventional reservoir with a gas rate of 5 MMscf/day (Q). Let the total number of fracs (N) in the well be 50, the thickness of each fracture (t) to be 0.01 ft and the lateral extent of the fracture (w) be 100ft. With a gas expansion coefficient (B_g) of 1000 scf/cf and a proppant porosity (φ) of 40%, the downhole gas velocity inside the fracture can be estimated as:

$$v = Q/(N * t * w * B_g * \varphi) = 250 \text{ ft./day} = 0.003 \text{ ft./sec}$$

To approximately compute the velocity needed to lift the liquid vertically out of the fracture, we borrow from Turner's critical velocity analysis for unloading vertical gas wells. Turner's critical velocity model assumes that liquid droplets are removed by the drag force of the gas. The critical lift velocity is that value of gas velocity at which the liquid droplet is stationary in a column of gas. A simple force balance on a single drop of liquid being removed by moving gas is represented in Illustration 1 below. Assume that the liquid droplet is removed through the pore space and is small enough to not touch the pore walls.

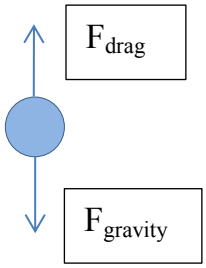

Illustration 1: Schematic of forces operating on a single liquid drop

$$F_{gravity} = \frac{g}{g_c} * (\rho_l - \rho_g) * \frac{\pi d^3}{6}$$

$$F_{drag} = \frac{1}{2g_c} * \rho_g * C_D * \frac{\pi d^2}{4} * V^2$$

Where,

ρ_l = Liquid density
ρ_g = Gas density
d = Liquid drop diameter
C_D = Drag coefficient
g = Acceleration due to gravity = 32.2 ft/sec^2
g_c = Critical acceleration of gravity = 32.2 lbm-ft/lbf-sec^2

At V = V_{crit}

$$F_{gravity} = F_{drag}$$

Assuming ρ_L = 60 lb/ft^3, ρ_G = 5 lb/ft^3 , C_D = 0.44 and d= pore throat size = 60 μm, we obtain :

$$V_{crit} = 0.459 \text{ ft/s}$$

As the calculation above indicates, the desired lift velocity for unloading the liquid and the available gas velocity in a fracture differ by almost two orders of magnitude. It is, therefore, very likely that the lower portions of fractures may be filled with liquid even after extended production. This suggests that when studying the issue of fluid recovery from hydraulically fractured horizontal wells, even if the drawdown is able to overcome the capillary pressures, the inflow gas velocity may not be high enough to lift the liquid against gravity, into the wellbore. Liquid blocked inside the fracture in this way will impact the productivity of the well and impact the cleanup of the matrix. This mechanism is illustrated below:

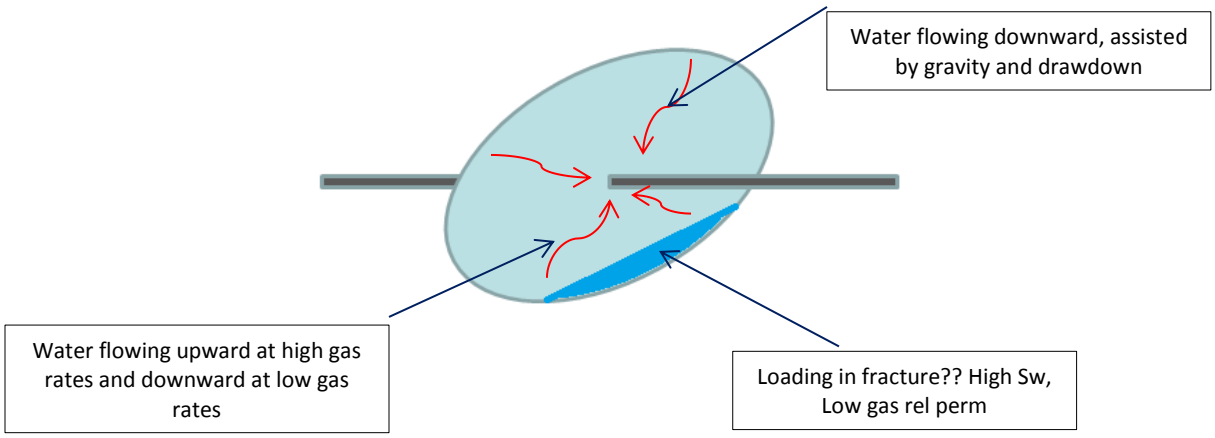

Illustration 2: Schematic of forces operating during fracture cleanup

Study of liquid loading at the bottom of a fracture is even more important considering the effect of proppant settling and fracture closure. Multiple field and experimental studies have highlighted the phenomenon of proppant settling at the bottom of a fracture after the frac-job. When the well is put back on production, the top part of the fracture is not able to withstand the closure pressure due to the absence of sufficient

proppant. In such cases, the lower portion of the fracture (with the proppant) dominates the production. If a considerable portion of the lower part of the fracture gets liquid loaded, gas production could be severely impaired. A schematic of this phenomenon is shown below.

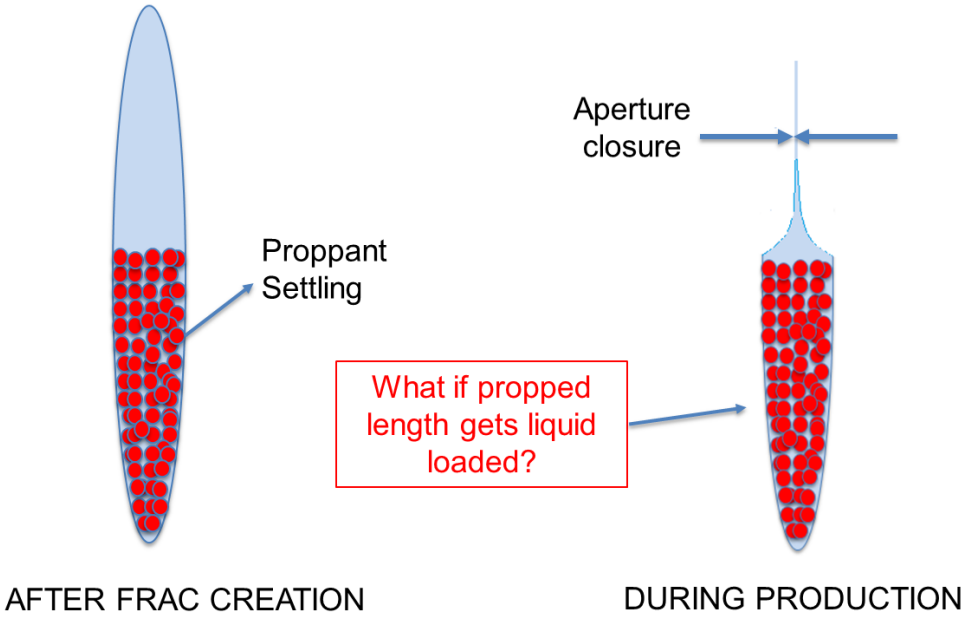

Illustration3: Impact of proppant settling and fracture closure

1.2 Research Objectives

The above discussion introduces the motivation for this study. The concept is explored using black oil and compositional, 3D numerical simulation by modeling frac-water invasion into the matrix followed by its flowback. The primary objectives of this study are as follows:

1. Model a single, bi-wing, lateral hydraulic fracture in a horizontal well in a gas reservoir and simulate frac-water flowback.
2. Study the impact of drawdown, reservoir and fracture properties on frac water loading within hydraulic fractures. A sensitivity analysis gives information about which factors play a dominant role. This information can then be used to find specific solutions.
3. Study the impact of frac water loading on productivity and gas rates.
4. Investigate the same phenomenon in a gas condensate system and study the impact of velocity dependent relative permeability and water evaporation effects (through compositional simulation). Liquid loading in fractures maybe important when dealing with condensate rich unconventional gas reservoirs. If the bottom hole flowing pressure is below the dew point of the reservoir fluid, the condensate may drop out of the gas. This condensate may also get trapped at the bottom of the fracture and impair the productivity of the well.

1.3 REVIEW OF CHAPTERS

Chapter 1 introduces the concept and the objectives of this study. The following chapters cover additional details about the different models employed, sensitivity analysis and the results of the study.

Chapter 2 offers an overview of previous research in related areas. It discusses public literature references related to the traditional liquid trapping model in fractured reservoirs. It then refers to studies that highlighted the impact of liquid blocking or trapping on well productivity. The chapter also covers references to earlier experimental

and simulation studies pertaining to condensate blocking or condensate bank formation in conventional reservoirs and its impact on well productivity. After describing the various liquid trapping/loading mechanisms in fractured reservoirs, the chapter describes remediation measures provided in literature. This is followed by a summary of recent works pertaining to simulation of unconventional reservoir performance.

Chapter 3 investigates black oil modeling and simulation of fluid injection and flowback. It begins with a brief description of the CMG IMEX^{TM} black oil simulator that was used in this study and its features, followed by a detailed description of the reservoir model. Matrix and fracture properties as well as operational controls are discussed. The chapter then illustrates the results of various sensitivity analysis scenarios for various drawdowns, matrix permeability, fracture permeability, fracture dimensions and shut-in time before flowback. In conclusion, the impact of each parameter on the fracture fluid cleanup and its impact on productivity is discussed.

Chapter 4 discusses the compositional simulation of fracturing and flow-back from a dry gas system. It begins with a brief introduction to the CMG GEM^{TM} compositional simulator used in this study and is followed by a detailed description of the model. Effects such as velocity dependent relative permeability as well as evaporation of water during flowback are included. The impact of using one or both or none of these effects on cleanup and productivity is studied.

Chapter 5 presents the flow back simulation results for a condensate rich unconventional reservoir system. Unlike previous models, this model involves three mobile phases: water, gas and oil (condensate). The chapter provides detailed information about the model parameters and the fluid properties used. Liquids with different condensate richness are studied along with the effects of velocity dependent relative permeability and water evaporation. The aim is to study the relative cleanup of

condensate and water from within the fracture and near-fracture matrix region. Its impact on gas productivity is also studied.

Chapter 6 provides the overall conclusions from this study and recommends future work in this area.

Appendices provide sample IMEX/GEM input files corresponding to the models studied.

Chapter 2: Background study

2.1 Frac Fluid Cleanup And its Impact on Gas Productivity

The issue of frac fluid loss/ invasion into the rock matrix after a stimulation operation has been widely studied in the past. The primary reason for interest in this area stems from the fact that most of the stimulations do not perform as well as expected. This is attributed to inadequate models for frac fluid cleanup and liquid trapping in the matrix. Low permeability, water wet formations have a tendency to trap the frac fluid in their pores due to high capillary pressures. This increase in aqueous phase saturation near the fracture face leads to a reduction in gas relative permeability, thereby retarding the flow of gas. Gel damage or proppant crushing within the fracture can also lead to slower frac fluid cleanup and therefore reduced gas productivity. Multiple numerical simulations as well as experimental studies have been performed over the years to study the mechanisms involved.

2.1.1 Literature Review

Tannich (1975) presented a detailed simulation study of fracture fluid cleanup and the transient productivity variation by modeling four distinct zones of interest: 1) un-damaged, virgin reservoir, 2) the invaded, damaged near fracture zone 3) the fracture itself and 4) the tubing. This study says that cleanup and productivity enhancement require not only liquid removal from the damaged matrix near the fracture but also from the fracture and tubing. The author mentions that liquid in tubing reduces productivity by increasing bottom hole flowing pressure whereas turbulence in the fracture can lead to further reduction in productivity. However, their model made no provisions for liquid build up within the fracture. In a case study mentioned in this work, the author draws

attention to the fact that gas breakthrough from the simulation was slower than the actual breakthrough and attributed this to the redistribution of frac-fluid due to gravity and capillary forces, during shut-in. In conclusion, they found that short, highly conductive fractures aid cleanup and turbulent flow in the fracture reduces productivity due to reduction in apparent permeability to gas.

Holditch (1979) presented a study of formation damage due to frac fluid injection in tight gas reservoirs. His numerical simulation based analysis investigated the effect of increased capillary pressures, decreased gas relative permeability and formation permeability due to invasion of frac fluid into water wet matrix on gas production. The study concluded that in low permeability reservoirs frac fluid invasion has an important impact on peak gas productivity. It also points out that gas production can be severely affected if drawdown is not greater than the matrix capillary pressures and if the mobility of water is not high enough to cause quick imbibition away from the matrix face. However, if the matrix permeability next to fracture is not severely damaged, the study showed cumulative gas production is not severely impacted as long as drawdown is greater than the capillary entry pressure. The study also highlighted the importance of water mobility in cleanup.

Solimon et al. (1985) present a numerical simulation based analysis of fracture fluid cleanup and its impact on gas production. Their study revealed that fracture conductivity has a key effect on the cleanup of frac fluids from tight gas reservoirs. It pointed out that the optimal conductivity required for cleanup might be higher than that necessary for gas production. However, they also noted that in very tight reservoirs the cleanup may primarily depend on the capillary pressures inside the matrix. A key conclusion was that the presence of mobile water in the fracture has a significant impact on buildup pressure response after flow back.

Montgomery et al. (1990) discuss the fracturing fluid cleanup process and its impact on the post-fracturing buildup analysis. Their study revealed that high fracture conductivity, low matrix damage and high water mobility improved frac water recovery. In cases of low formation permeability, low fracture conductivity and damage in/around fracture, conventional pressure buildup analyses were found to be unreliable. They also noted that in case of severe damage around the fracture, the pressure derivative in the buildup test will have an identifiable shape.

Bennion et al. (1994) investigate the potential mechanisms of aqueous phase trapping in the reservoir after a drilling, stimulation or work over operation. They also discuss the types of reservoirs most prone to water blocking. The study tries to quantify the productivity impairment experimentally. According to the authors, reservoirs with initial water saturation below residual water saturation, including highly oil-wet oil or gas reservoirs, are most susceptible to water blocking. They mention that the pore distribution and surface characteristics which affect the relative permeability curves are also important factors. The paper discusses reasons for initial water saturation below residual saturation and attributes it to the following possibilities: 1) Vaporization due to low pressures in geological history 2) Changes in pore structure due to compression or diagenesis in the past 3) Adsorption and hydrate formation 4) Hysteresis. The study recommends the use of non-aqueous fluids and alcohols to enhance cleanup.

May et al. (1997) looked at the issue of polymer fluid cleanup and why the recovery was often less than 50%. The compositional numerical simulation based study was used to explain why post-frac conductivity and frac length are often estimated to be lower than anticipated. The results pointed out the polymer yield stress and relative permeability are primary mechanisms controlling the fracture cleanup. The paper highlights the major mechanisms involved in cleanup: 1) effect of time and temperature

on proppants 2) gel residue and its damage to proppant pack 3) viscous fingering through proppant pack 4) effects of unbroken fluid of proppant permeability 5) Non-Darcy and multiphase flow 6) Capillary pressure effects. They suggested that better measure of cleanup would be the volume of polymer recovered rather than the load recovered, since the two are not always proportional.

Settari et al. (2002) have investigated the water blockage and fracturing associated geomechnical issues in water fracs in the Bossier play. The study utilized a coupled reservoir and geomechanics simulator which allows dynamic fracture propagation during frac-job and static fracture during flowback. The authors concluded that geomechanics played an important role on fracture productivity. Long shut-in time didn't lead to higher gas productivity.

Mahadevan et al. (2003) present a very detailed experimental study of water block removal under different rock permeability, temperature, wettability and drawdowns. Cleanup was measured through changes in gas relative permeability. The study revealed that there are two primary mechanisms for water block removal: 1) displacement of water when drawdown is greater than the capillary forces and 2) evaporative cleanup of water. The latter becomes important after a long period of gas injection to remove the water block. An important conclusion from the study was that cleanup could be accelerated by the use of solvents not only to modify the wettability but also because of its volatility. In addition to this, an increase in temperature, change of wettability from oil wet to water wet and higher drawdown, all resulted in faster cleanup. The analytical model developed in this study provides an excellent way of computing water cleanup from wells.

Kamath et al. (2003) also quantified the impact of water blocks on gas productivity through experimental observations. They concluded that water block removal or cleanup occurs in two stages: first, when water is displaced immediately after

flow back is initiated and second, during evaporative cleanup, which takes much longer time. This evaporative cleanup is reported to be expedited by using alcohol solvents. The authors note that in extremely tight reservoirs as the gas volume flowing is low, the cleanup is also very slow.

In Gdanski et al. (2005) the authors revisit Holditch (1979) and investigate the effects of formation damage on stimulated low permeability gas formations which have slow cleanup and gas production. A new numerical simulator was used to validate that permeability damage of over 90% increases the capillary pressures and thereby leads to reduction in gas production. The study points out that gas production causes water to pile up near the fracture face but it won't be produced until the capillary forces are overcome.

Jamiolahmady et al. (2007) discusses the frac fluid cleanup process in a gas condensate reservoir and its impact on gas productivity. The study models water and oil based frac fluids with different viscosities. The results indicate that using higher viscosity frac fluid provided better cleanup as depth of matrix invasion was less. They also reported that condensate drop out facilitated frac water cleanup.

Bazin et al. (2008) have done special core analysis (SCAL) on tight gas reservoir samples to study the formation damage problem and have found that matrix relative permeabilities and their hysteresis are key factors in frac fluid cleanup.

Wang et al. (2009) have also looked at this problem of modeling fracture fluid cleanup from tight gas wells. The cleanup from within the fracture is ignored in this study as the focus is on recovery from the matrix. Effects such as proppant crushing due to closure stress, polymer filter cake and gel strength were analyzed. This study points out that frac fluid cleanup is faster for lower yield stress fluids. Gel damage is also mentioned as a major cleanup inhibitor. The authors conclude that if the fracture fluid breaks down to low viscosity and behaves as a Newtonian fluid, then an F_{cd} greater than 10 will

optimize frac fluid cleanup. However, when the fluid retains a yield stress ~100 Pa then cleanup will be very slow.

Friehauf et al. (2009) has modeled the productivity of hydraulically fractured gas wells including the effects of frac fluid leak off into the matrix and has concluded that unless the permeability damage in the invaded zone is more than 90%, gas production is not significantly impacted as long as drawdown is greater than capillary pressure. He also concludes that for low permeability, depleted reservoirs energized fracturing may help mitigate the gas relative permeability reduction in the near fracture zone.

In Gdanski et al. (2010) the authors have developed a fit for purpose numerical simulator known as Fracture Cleanup and Chemistry Simulator (FCCS) to closely replicate the frac fluid flow back process. In this study, they looked at the impact of different relative permeability curves, drawdowns, drawdown rate, shut-in times and fracture conductivities on the load/ frac fluid recovery. This simulations study didn't find significant dependence of productivity on shut-in time under different relative permeability regimes. Higher water relative permeability led to higher capillary imbibition for increased shut-in time and led to reduced load recovery. However, this low recovery didn't impact gas production. For moderate quality relative permeability, effect of F_{cd} was found to be more significant than shut-in period for gas recovery. Poor quality relative permeability led to worse liquid loading near fracture face and had the most impact on gas rates.

Yu et al. (2010) look at the formation damage issue in modern unconventional reservoirs. The mathematical model includes reservoir pseudo-radial flow, reservoir-linear flow, fracture linear flow and fracture radial flow near wellbore. The study looked at fracture face skin under different frac fluid properties, reservoir conditions and large ranges of spurt and leak-off coefficients. The study concluded that fracture face skin has

minimal impact on the productivity of multi-fraced horizontal well. The authors, therefore, recommend not using expensive low-damaging fluids during fracturing operations.

Shaoul et al. (2011) investigate the importance of formation damage in unconventional reservoirs. They note that there is still a lot of speculation in the industry about the dominant mechanisms and their impact on productivity. Ideas such as 'permeability-jail' and stress sensitive matrix permeability are proposed. The study highlights the strong correlation between fracture length and fracture cleanup time. The authors also refer to the possibility of proppant pack damage and gel retention on frac fluid cleanup. However, this effect is not modeled in this study. The authors conclude that high capillary pressures alone can't explain the reduced and delayed gas productivity. The use of non-aqueous fracturing fluid is suggested for weak permeability jail scenario where it significantly helps improve early time cleanup and productivity. However, long term recovery is not affected.

Wang et al. (2012) analyzes the various damage mechanisms in unconventional reservoirs and attempts to quantify their relative impact on the gas productivity. The major effects outlined in the study include 1) fracture fluid trapping 2) proppant embedment 3) gel filter cake at frac face and 4) gel residue in proppant pack. The new analytical well productivity model developed here estimates that each of the above factors causes productivity reduction of 12.5%, 0.6%,6% and 7%. The authors conclude that formation damage due to above factors is not important in shale reservoirs.

2.2 CONDENSATE BANKING AND ITS IMPACT ON GAS PRODUCTIVITY

Gas condensate reservoirs present even more complex challenge in terms of gas productivity optimization. The reservoir fluid in these reservoirs is primarily in single phase at reservoir temperature and pressure conditions. However, if the reservoir pressure drops below the dew point during production, then condensate starts dropping out of the gas. The condensate phase is rich in higher molecular weight hydrocarbons. Since the pressure is lower near the wellbore, condensate dropout also primarily takes place there and is referred to as condensate banking. This 'bank' of liquid condensate near the wellbore is attributed to severe gas productivity impairment because it leads to gas relative permeability reduction. The region around the wellbore primarily consists of three condensate saturation zones. 1) Nearest to the wellbore is the two phase flow zone where both condensate and gas are flowing towards the wellbore. The gas relative permeability damage is maximum in this area. 2) Moving further outwards towards the reservoir boundary is the 'transition zone'. Here the condensate is still accumulating and is not yet mobile. 3) Farthest away from the wellbore is the 'native' reservoir zone where condensate drop-out hasn't begun. There is no gas relative permeability damage in this zone. The two phase flow region continues to grow with time as pressure depletion occurs further deeper into the formation.

Many of the biggest gas reservoirs around the world (for example the Arun field in Indonesia and North Field of Qatar) are condensate reservoirs and therefore, require close examination to achieve maximum gas recovery. The relative permeability alteration in the two phase flow region has been studied using analytical, numerical simulation and experimental methods.

2.2.1 Literature Review

Fussell et al. (1973) used a 1D radial model to predict well performance in three gas condensate reservoirs. The study found that condensate drop out can reduce gas productivity by an order of magnitude. Also, the condensate saturation in the near well bore region might be higher than the maximum liquid dropout in the Constant Volume Depletion (CVD) experiment. The authors noted the significance of relative permeability in determining condensate saturation in the two phase region. Shutting the well after condensate dropout and productivity loss doesn't help remove the near well bore condensate.

Clark et al. (1985) presented a 2D, radial, compositional model to predict the performance of a rich gas condensate reservoir. The model used vertically heterogeneous formation and nine component fluid characterization. High gas productivity was observed after gas breakthrough and was attributed to lower gas viscosity due to condensate drop out.

Chopra et al. (1986) developed a two phase steady state model to compute the saturation profiles near a single producing well. This study provides a theoretical, material balance based proof for the steady state two phase flow theory developed by O'Dell and Miller and modified by Fussell. It postulated that at any location within the two phase zone, the ratio of volumetric flow rates of the two phases equals the ratio of volume fractions of the two phases given by the Constant Composition Expansion (CCE) experiment at the corresponding pressure.

Fishlock et al. (1993) measured multiphase gas-condensate relative permeability experimentally. Firstly, they looked at oil and gas relative permeabilities resulting from condensation in the presence of residual water. Secondly, they examined three phase flow under combined water flood and pressure depletion. Saturation changes similar to those

in reservoir were replicated. Condensation at residual water saturation reduced gas relative permeability by about 60%. However, in the case of combined water flood with depletion, presence of condensate could increase gas relative permeability for a given gas saturation. Both water flood residual gas saturation and critical gas saturation for remobilization were reduced by about 80% of condensate saturation.

Afidick et al. (1994) studied the Arun gas condensate field in Indonesia and reported that after a long period of gas production the productivity declined sharply due to condensate drop out. The productivity declined by approximately 50% even though the gas was lean.

Barnum et al. (1995) did an extensive study of published case studies as well as Exxon field studies to analyze the factors responsible for productivity impairment after liquid dropout and its impact on hydrocarbon recovery (gas and liquid). The study noted that condensate banking most severely affects low productivity reservoirs and reservoirs with KH < 1000 mD-ft. The impact on gas productivity in the case studies ranged from approximately five fold decrease to only about a 20% decrease.

Boom et al. (1996) reported that even with low liquid content of the gas, the near well bore condensate saturation could be significantly higher, because large volume of gas passes through the region over time. According to their study the degree of impairment depends on gas and condensate mobilities.

Pope et al. (1998) presented a trapping number based relative permeability model for accurate modeling of two phase flow in the near well bore region. In their model relative permeability is a function of surface tension in addition to viscous, buoyancy and capillary forces. The capillary forces resist the movement of the condensate in the porous media. If the gas viscous force (due to its velocity), buoyancy of oil (density gradient)

and surface tension are appropriate, condensate saturation will continue to decrease. Experimental values for model parameters were obtained.

Whitson et al. (1999) developed a relative permeability model for fitting steady state oil/gas flow behavior. The authors noted that a higher capillary number can lead to higher gas relative permeability in the near well bore region and therefore, lower condensate saturations. They proposed an empirical scaling function to obtain oil/gas relative permeabilities for different rock types and regions with different end point saturations.

Narayanswamy et al. (1999) presented a detailed study on the counter-acting effects of velocity dependent relative permeability and non-Darcy flow in a single wellbore model. At high gas velocities, the capillary number increases leading to improvement in gas relative permeability. However on the other side, high velocity may also lead to non-Darcy flow which will reduce the well productivity. The two effects operate simultaneously. A case study was done using a lean gas condensate and showed that a good history match could be obtained by using the two effects in the model.

Whitson et al. (1999) have presented a study that focuses on key aspects of accurate modeling of condensate reservoirs and their performance. In this study, special steady state experimental procedures are described to obtain k_{rg} as a function of k_{rg}/k_{ro} and N_c i.e. capillary number. Measurement of saturation is not important. The authors propose that this information will help in accurate modeling of condensate reservoir performance. The experimentally measured relative permeability data was modeled using an equation containing a Corey type factor in addition to a simple one parameter correlation for the capillary number. The authors also point out that the effect of saturation hysteresis is minimal on k_{rg}. An approach is also provided to include the effects of high capillary numbers and turbulent flow.

Wang et al. (2000) detailed a method to tune EOS parameters to match the experimental behavior which is extremely important for accurate modeling of the gas condensate system in a compositional simulation.

Al-Anazi et al. (2002) performed a study to show that gas relative permeability decreased by about approximately the same amount for high or low permeability samples. However, gas relative permeability damage is more severe for higher water saturation.

Chowdhury et al. (2004) tackle the problem of using fine gridding for field scale reservoir simulations involving condensate dropout. One of the techniques commonly used is local grid refinement. However, the authors point out that using local refinement on a large scale will be computationally very extensive. In order to avoid this problem a semi-analytical solution is implemented in a compositional simulator which allows much larger grid block sizes to be used and yet provides an accurate match with the solution from models with local grid refinement. The pressures, saturations, relative permeabilities and densities calculated with the new approach match compositional simulation results with grid refinement. The method was tested for single layer, multi-layer and multi-well gas condensate reservoirs. The semi-analytical solution considers effect of high capillary number on relative permeability as well as that of Non-Darcy flow.

2.3 LIQUID TRAPPING REMEDIATION

Considering the obvious importance of liquid trapping in the matrix (frac-water or condensate) on reservoir performance, many studies have been performed in the past to find remediation strategies.

2.3.1 Literature Review

Kossack et al. (1988) studied the effect of two step injection of methane followed by nitrogen, into the well with condensate banking. The study utilized a 3D EOS compositional simulator. The nitrogen followed methane as a pressure maintaining slug.

Cullick et al. (1993) discussed the use of WAG or water alternating gas in a synthetic layered reservoir with condensate blocking. Both compositional simulations as well as experimental studies were performed and showed that the effectiveness of WAG is better than only gas injection for condensate removal. Also the total amount of gas injected was less when using WAG scheme and is therefore, a more cost effective solution.

Sanger and Hagoort (1998) investigated effectiveness of nitrogen and methane in condensate recovery. The study concluded that methane was more effective because nitrogen is prone to dispersion which affects recovery. Their work involved slim tube experiments.

Ahmed et al. (1998) studied the effectiveness of using lean gas, CO_2 and N_2 in a Huff-n-Puff process to recover condensate. Huff-n-Puff refers to gas injection followed by flow back. The authors found that Huff-n-Puff helps in reducing condensate blocking. It is most effective when gas is injected before maximum liquid drop out takes place.

El-Banbi et al. (2000) performed a full field, compositional study to investigate the effectiveness of water flood versus gas injection for liquid removal. Their study found water flood to be a better option in developing rich condensate reservoirs as gas injection becomes economically unviable.

Du et al. (2000) studied the decrease in relative permeability due to condensate dropout and then its remediation using methanol. They reported that end point relative

permeability was dependent on the use of alcohol. This was attributed to miscible displacement of oil and water by alcohol.

Jamaluddin et al. (2001) evaluated the potential of using propane and CO_2 to vaporize the condensate. The study found propane to be significantly more effective than CO_2 in high pressure, high temperature gas condensate reservoirs.

Al-Anazi et al. (2002) studied the impact of using ethanol with low and high permeability cores with condensate damage. It was observed that both for low and high permeability cores, ethanol treatment provided extended duration of high gas productivity proportional to the volume of ethanol injected.

Rai et al. (2003) studied the condensate buildup process and its treatment using core flood, by simulating the process using UT PGE's in-house compositional simulator UTCOMP. The simulation modeled condensate drop out and methanol treatment. Experimental validation was also performed. The study used five fluids ranging from lean to rich. A Corey type relative permeability model was used. It was observed that the factors affecting the gas productivity include phase end point relative permeabilities as well as the trapping model parameter values. The simulations predicted that all the condensate and water will be cleaned up by injected ethanol after few pore volumes.

Bang et al. (2005) analyzed the impact of water and methanol on the phase behavior of the reservoir hydrocarbon. The study found that adding methanol decreases liquid volume fraction and the dew point pressure of the reservoir hydrocarbon. In continuation, Bang et al. (2008) present chemical treatment solutions for hydraulically fractured wells to reduce liquid trapping and enhance gas and condensate relative permeability. A fluorinated surfactant in glycol-alcohol solvent was found to improve gas and condensate relative permeabilities significantly.

Kumar (2000) has highlighted the utility of fracturing in reducing the impact of condensate damage. Higher surface area of the fracture allows greater contact with the formation and thereby reduces the drawdown required. Lower drawdown subsequently leads to lower condensate buildup and thus aids recovery.

Gdanski (2011) presents a simulation based study of surfactant based load recovery in hydraulically fractured unconventional/tight reservoirs using a fit-for-purpose simulator fracture cleanup and chemistry simulator (FCCS). Simulations analyzed the impact of fracture and matrix permeabilities in addition to rel-perm quality and surfactant properties. The study found surfactants to be most effective when matrix rel-perms are moderately to very good. Surface tension reduction only enhanced imbibition whereas changing the wettability to neutral substantially enhanced load recovery. Fracture conductivity also played an important role in cleanup. According to the study, an ideal surfactant would be lightly adsorbing, yet render the invaded zone non-wet and provide minimal capillary pressures.

2.4 UNCONVENTIONAL FRACTURED RESERVOIR SIMULATION

In unconventional/shale oil or gas reservoirs the reservoir permeabilities are of the order of a couple of nano/micro Darcies. In order to commercially produce from these reservoirs multiple hydraulic fractures are initiated in a long horizontal well. From reservoir simulation point of view there is a huge contrast between the zones defined by the matrix and the fracture. This discontinuity leads to instabilities in numerical simulation and reliable modeling requires localized fine scale gridding near the fracture-matrix interface as well as tight numerical controls.

2.4.1 Literature Review

Hill and Thomas (1985) discuss a dual porosity dual permeability model for simulating complex fractured reservoirs. There are separate grids for fractures and matrix, multi-component fluid and a capability for inert gas injection. An efficient memory management technique is also discussed.

King et al. (1991) presented the mathematical background for the simulation of unconventional gas reservoirs and identified how it is different from conventional reservoir simulation. The major differences are due to sorption kinetics, gas-transport mechanisms, adaption to different exploitation methods and different gridding schemes.

In Osorio et al. (1997) the authors describe a 3D finite difference, fully implicitly coupled model to represent the production from tight gas reservoir. The reservoir is treated as a multiphase poro-elastic system and its deformation affects the fluid and matrix flow properties. The study showed that changes in stress state and pore pressures can impact the permeability and thereby the production significantly. The permeability reduction was found to be time (depletion) dependent and most acute near the wellbore.

Ehrl et al. (2000) investigated the simulation of hydraulically fractured horizontal wells in tight gas reservoirs. The model used local grid refinement and adjustments were made to cell sizes and permeabilities in order to achieve numerical stability. A fully implicit solution mode was adopted.

Karimi-Fard et al. (2003) highlight the challenges in the numerical simulation of water injection in discrete fractured media with capillary pressure effects. The study uses discrete fracture model in which fractures are discretized as 1D entities. It is then implemented using the Galerkin finite element method. Numerical simulations were carried out in water and mixed wet media to study the effects of matrix and fracture capillary pressures.

Cipolla et al. (2009) looked at the performance of the Barnett shale. They discuss the challenges in accurate modeling of the induced fracture networks, their complexity, their flow characteristics and pressure connectivity. In this paper, the authors compare the numerical simulation approach to the conventional production analysis approach for understanding the fracture properties. The paper looks at the distribution of conductivity within the induced fracture network, the complexity of the fracture network, the effect of desorption and matrix permeability on EUR. The study also utilizes available microseismic data in the modeling. Inferring from the microseismic data, the authors note that fractures are not planar and symmetric as normally modeled but rather a complex network of minor and major fractures. Complexity is more in shale or coal gas reservoirs as compared to tight gas. The authors also discuss the concept of using a Stimulated Reservoir Volume (SRV) as a zone of higher permeability near the primary fractures.

In Abacioglu et al. (2009) the authors look at the possibility of using a coarse grid for the simulation of hydraulic fractures rather than explicitly modeling them using fine grids as they are computationally intensive for full field simulations. The hydraulic fractures are treated as an infinitely conducting line source that happen to coincide with the edges or center of grid blocks (Nghiem 1983, Lefevre et al. 1993) The study aims to accurately model both flowing and shut-in performance for multi-fraced horizontal wells in full field models. Some of the other approaches for modeling hydraulic fractures are also discussed such as 1) modeling fractures as large effective wellbore radius or negative skin in a particular block, 2) Increasing permeabilities for coarse grids based on the properties of the fracture.(El-Ahmady et al. 2004) 3) Increasing transmissibility values for coarse grids representing fracs.

Mirzaei and Cipolla (2012) outline a workflow for the simulation of hydraulic fractures in unconventional reservoirs. It includes a new modeling technique combining

the Discrete Fracture Network (DFN) approach with the Unstructured Fracture (UF) approach (Cipolla 2011).

Darishchev et al. (2013) look at the simulation of highly heterogeneous, extremely low permeability gas reservoirs. The authors have looked at various reservoir models such as SRV, dual-porosity dual permeability and dual porosity single permeability in evaluation of unconventional reservoir performance. Pseudo-steady state flow has been assumed and grid sizes have been fine scaled logarithmically. Small grid block size helps reduce the well-block storage effect. The study found the contribution of non-SRV reservoir volume to be significant.

Moinfar (2013) presents a new dual continuum and discrete fracture model to simulate unconventional reservoir production. Large scale hydraulic fractures are modeled using discrete fracture approach called Embedded Discrete Fracture Model (EDFM), whereas small scale natural fractures are modeled using the dual continuum approach. The study shows the results of multiple 2D and 3D scenarios with varying number of fractures, orientations, presence/absence of natural fractures etc.

Wu et al. (2013) have developed a generalized mathematical model and a numerical approach for modeling of unconventional gas reservoirs including Klinkenberg effects, non-Darcy flow, gas adsorption and geomechanical effects. The model is multi-domain, multi-continuum suited to handle multi-scale heterogeneities and fractures. The authors believe the hybrid-fracture modeling approach including the discrete fracture method, MINC (Pruess et al. 1985) and single porosity modeling works the best.

Zhang et al. (2013) apply Fast Marching Method (FMM) for the solution of the Eikonal equation to complex simulation grids including unstructured grids and anisotropic permeabilities. According to the authors, this allows for rapid approximation of reservoir simulation without the need for flow simulation and also provides the time

evolution of drainage volume. The Eikonal equation describes the propagation of the pressure front. Previously Xie et al. (2012) have also looked at using FMM for unconventional reservoir analysis.

Chapter 3: Fluid Flow Back Modeling Using Black Oil Simulation

3.1 Introduction to IMEX

IMEX is CMG's implicit-explicit black oil reservoir simulator that provides capabilities such as local grid refinement, comprehensive well management, pseudo-miscible option, volatile option, polymer flooding, horizontal wells, dual porosity/permeability reservoir models and many more. It was primarily developed to study depletion, coning, water, gas, solvent and polymer injection in single and dual porosity systems.

The simulator can handle three phase black oil simulations along with capillary and gravity effects. It allows Cartesian, cylindrical and variable thickness grids. IMEX offers explicit, fully implicit and adaptive implicit solution modes. In adaptive implicit mode a few blocks are solved fully implicitly whereas the rest are solved explicitly. This is useful for studying coning near well bore or thin multilayered reservoirs. Using the adaptive implicit solver can provide time savings of up to 50%. The dual porosity option allows the discretization of matrix blocks using multi-interacting continuum (MINC) approach or a layered format called subdomain method. The MINC method provides a good representation of matrix-fracture flow. However, gravity effects are not suitably handled. The subdomain method handles that challenge.

The bottomhole pressures and block properties for blocks through which the well passes are solved fully implicitly. Multiple well controls are also provided. IMEX uses a state-of-the-art solution routine based on incomplete Gaussian elimination as a precondition step for GMRES. AIMSOL has been developed specifically for adaptive implicit Jacobian matrices. IMEX also provides two models for condensate reservoir modeling: GASWATER_WITH_CONDENSATE and VOLATILE_OIL.

There are seven different input sections and commands from one section can't be placed in any other. The seven sections are:

1. Input-Output control
2. Reservoir description
3. Component properties
4. Rock Fluid data
5. Initial conditions
6. Numerical method control
7. Well and recurrent data

3.2 SIMULATION MODEL DESCRIPTION

In this study, a 3-D, gas-water black oil reservoir model was used to simulate a single, planar, bi-wing hydraulic fracture in a horizontal wellbore. The reservoir properties used are provided in Table 1 and are based on Mullen (2010). The model is based on a 46 X 16 X 20 Cartesian grid in the X, Y, and Z direction respectively. The total volume of the reservoir simulated here is 400 ft. X 400 ft. X 100 ft. whereas that of the fracture itself is 350 ft. X 55 ft. X 0.1 ft. The horizontal wellbore of radius 0.25 ft. passes through Y= 8 and Z =10. Fine-scale gridding is employed near the fracture face along the horizontal wellbore to accurately monitor the liquid buildup in the matrix and in the fracture. The grid size increases away from the fracture face. Figure 3.1 shows, fracture within the matrix. Only half the simulated reservoir volume is depicted here.

Property/ Parameter	Value
Matrix Permeability	1 μD
Fracture Permeability	2 D
Reservoir Thickness	100 ft.
Matrix Porosity	10 %
Fracture Porosity	60 %
Fracture Height	55 ft.
Fracture Thickness	0.1 ft.
Fracture Half Length	175 ft.
Gas-Water Surface tension	40 dyne/cm
Water Density	64.3 lb/ft^3
Flowing Wellbore pressure	4500 psi
Initial Reservoir Pressure	6500 psi
Initial Water Saturation	0.2
Residual Water Saturation	0.2

Table 3.1: Base case reservoir model properties

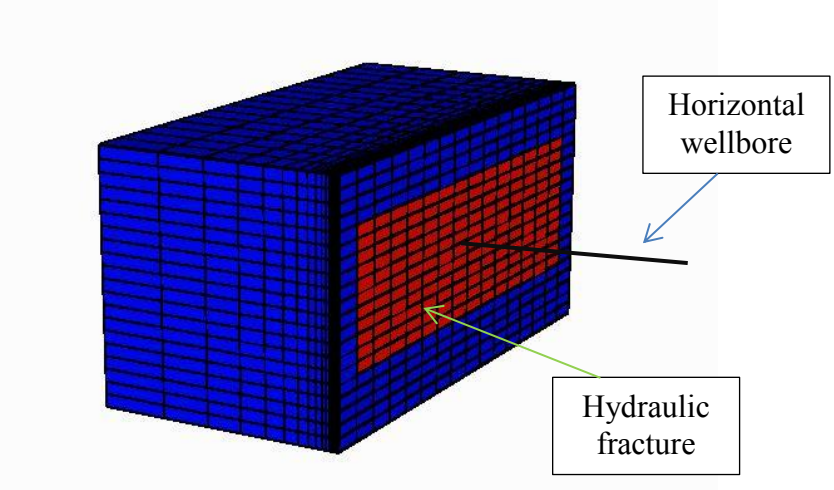

Figure 3.1: Reservoir model overview

Considering the unavailability of reliable drainage/imbibition curves for shale reservoirs, this study utilizes the J function for Berea sandstone and then scales capillary pressures according to the respective porosity and permeability of the reservoir (Appendix A4). Buoyancy effects (the Bond number) and the ratio of viscous and capillary forces (capillary number) in both the fracture and the matrix play an important role in the cleanup of the water. Pope et al. (2000) have shown that relative permeability is not just a function of interfacial tension; it also depends on trapping number. However, this velocity dependence of relative permeability is not modeled here due to the unavailability of this option in IMEX 2011. It should also be noted that the effects of evaporative cleanup (Jagannathan and Sharma, 2003 & Jagannathan et al., 2007) have not been modeled here. Matrix relative permeability characteristics have been modeled using a Corey type formulation whereas for fractures straight line rel-perms have been used considering extremely low capillary pressures. Figure 3.2 and 3.3 show the relative permeability curves for matrix and fracture respectively. To simulate the fluid loss during the fracturing operation, 1000 barrels of water were injected into the formation. This was followed by a shut-in time and then followed by flow back/ production by application of constant bottomhole pressure in the well. Various scenarios were run to investigate the impact of different reservoir or fracture properties on water blockage within the fracture and on gas recovery.

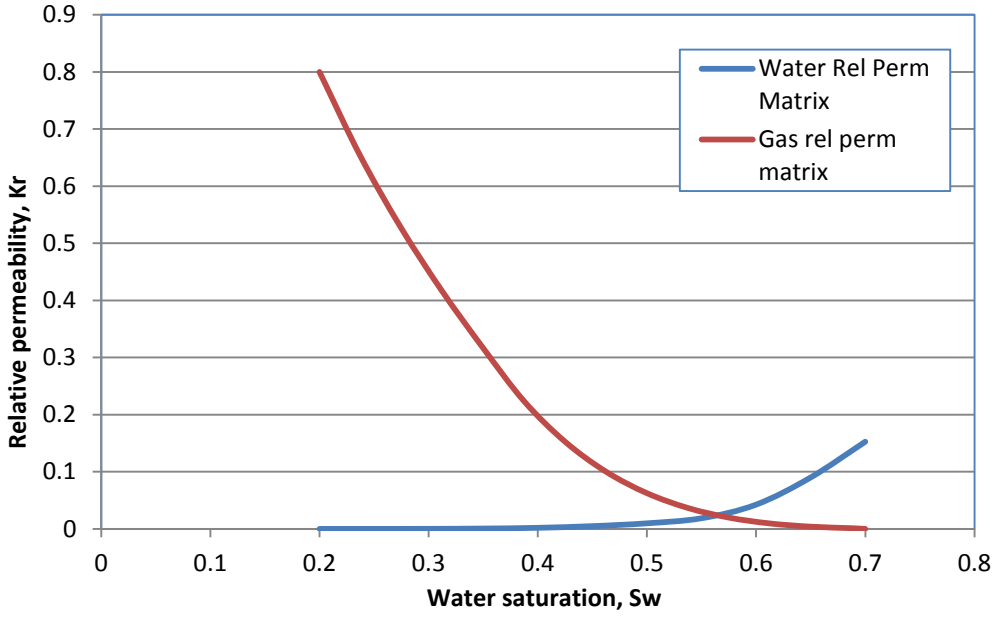

Figure 3.2: Matrix Relative Permeability Curves

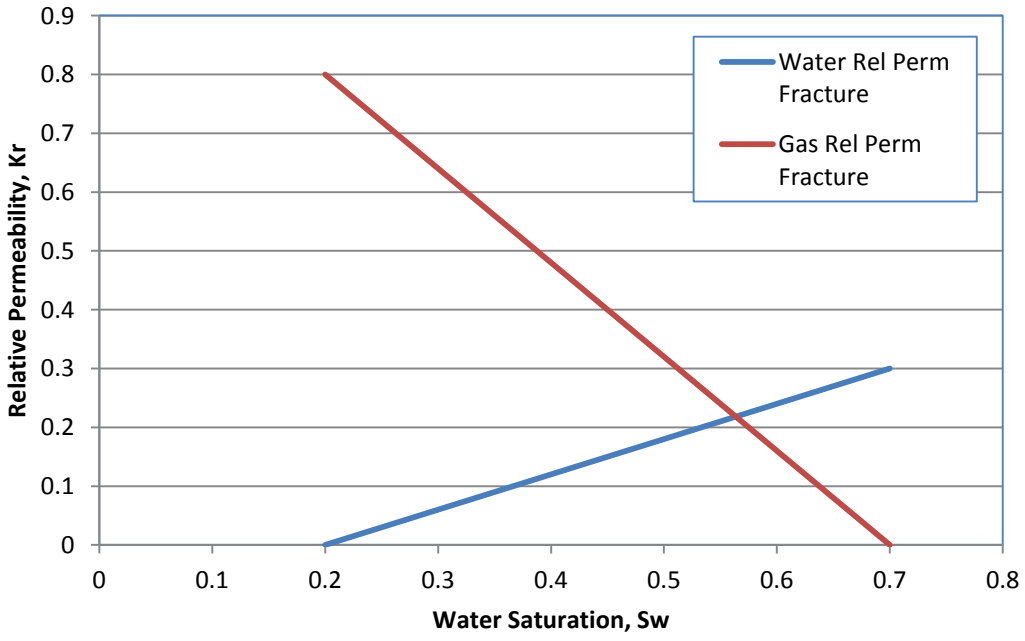

Figure 3.3: Fracture Relative Permeability Curves

3.3 RESULTS

This section shows the variation of saturation in the matrix near the fracture face and in the fracture itself. It gives an indication of how much and where the water loading is taking place. Saturation is monitored and represented both by using saturation maps of fracture and matrix as well as plotted vs. time. We first look at the base case performance of a water gas system.

3.3.1. Base Case

The base case scenario studies a reservoir at residual water saturation ($S_w = 0.2$), a flowing bottomhole pressure of 4500 psi and a shut in wait time of 29 days after the fracturing (slick water injection) process is over (30 days before production is initiated). At the end of a 500 day period, the cumulative gas recovery is 70.7 MMcf and the cumulative water recovery is 279 bbl. This means that out of the 1000 bbl. of frac water pumped only 28 % is recovered back. The remaining 72% is still trapped, either in the matrix or in the fracture itself. Figure 3.4 below indicates the variation of water saturation at the top and bottom of the fracture over time (measured at two specific points). Note that by the 500 day time step the water saturation in the entire fracture reduces to a residual level. However, the water saturation inside the matrix (0.1 ft from fracture face) is still in decline at the end of the 500th day (Figure 3.5). Figure 3.6 shows the saturation maps of fracture surrounded by matrix and the variation in water saturation over time. The well bore passes through the symmetrical center of the fracture and goes into the plane of view.

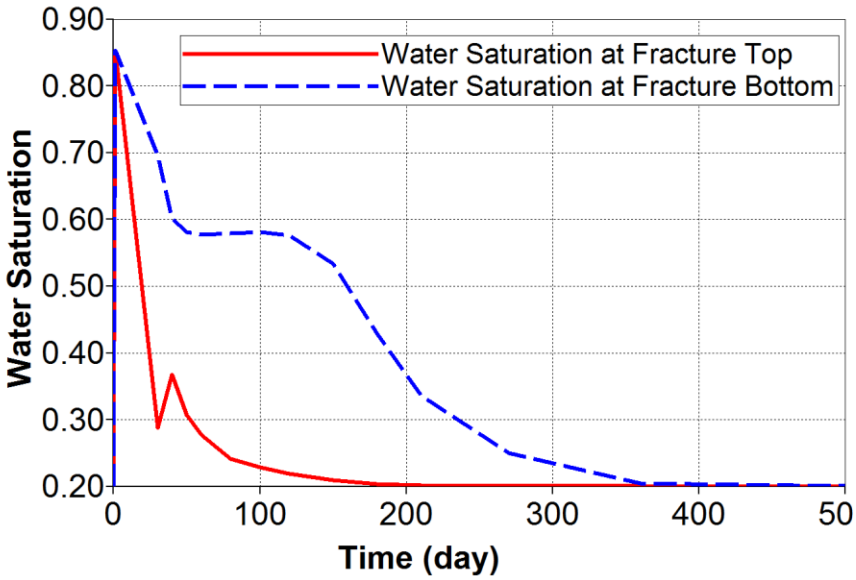

Figure 3.4: Variation of water saturation inside fracture over time

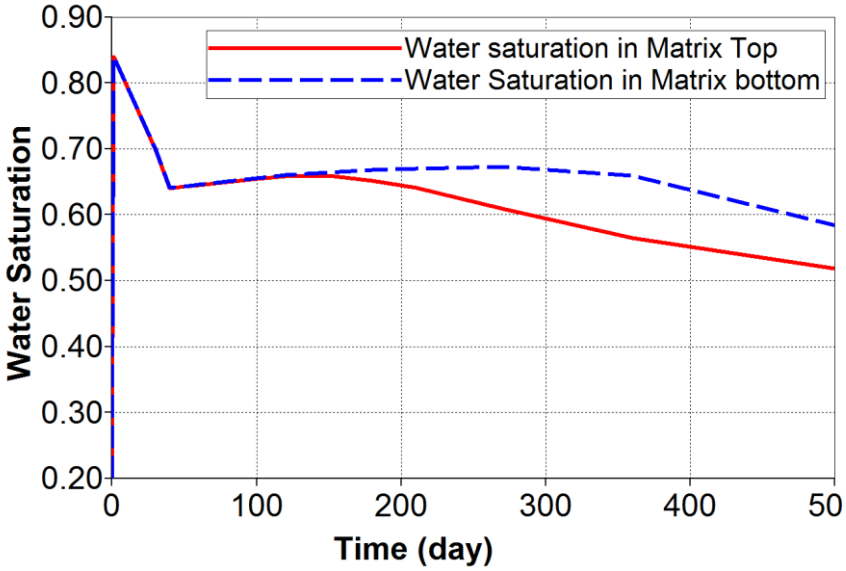

Figure 3.5: Variation of water saturation inside matrix 0.1 ft. from fracture face with time

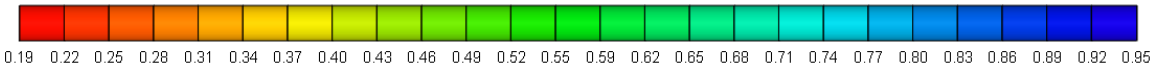

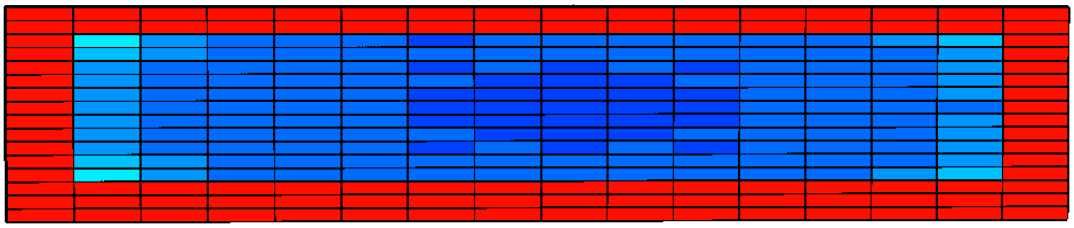

Water saturation inside fracture after 1 day (end of fracture treatment)

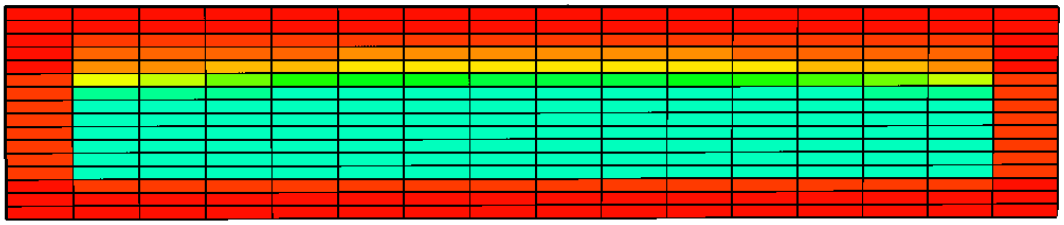

Water saturation inside fracture after 30 days (beginning of production, end of shut-in)

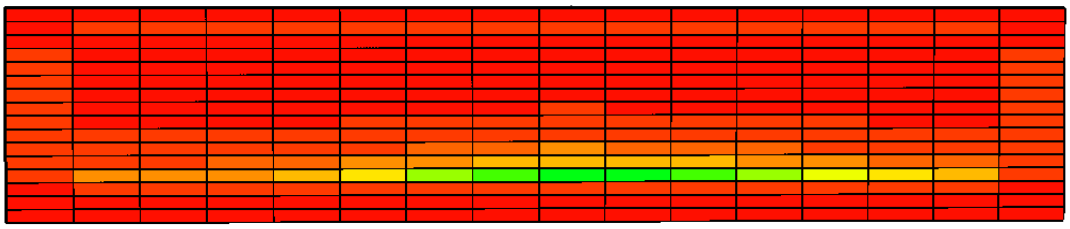

Water saturation inside fracture after 210 days

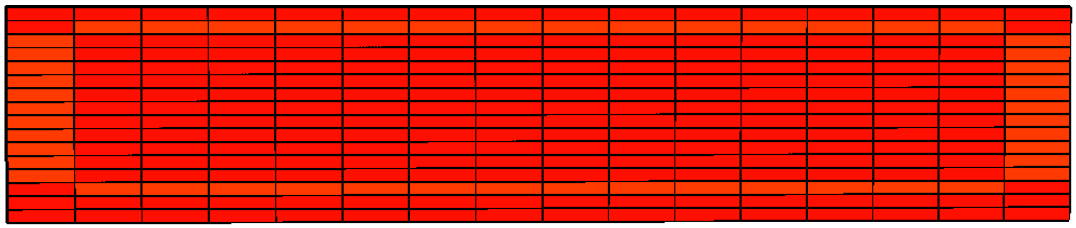

Water saturation inside fracture after 500 days (end of production)

Figure 3.6: Water saturation maps (Base Case)

3.3.2. Liquid Loading Under Different Drawdowns

To study the effect of drawdown on liquid loading within the fracture, we tested two scenarios: one with a higher drawdown (lower P_{wf} = 2500 psi) and other with lower drawdown (higher P_{wf} = 5500 psi). Figure 3.7 and 3.8 show the variation of saturation in fracture and matrix over time for higher drawdown case. Figure 3.9 show the respective saturation maps. Figure 3.10-3.12 show the variations for the low drawdown scenario.

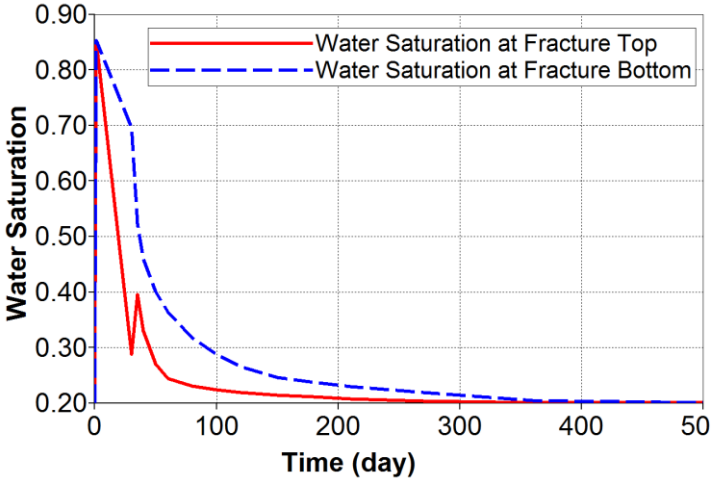

Figure 3.7: Variation of water saturation inside fracture over time (high drawdown)

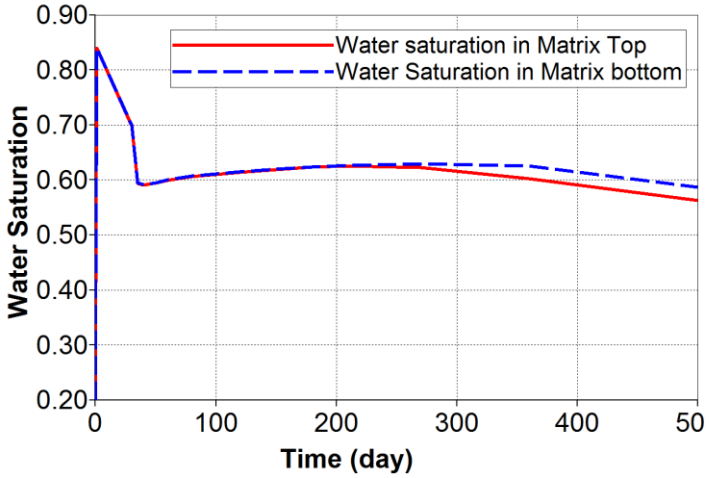

Figure 3.8: Variation of water saturation inside matrix 0.1 ft. from fracture face with time (high drawdown)

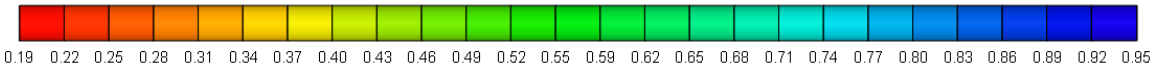

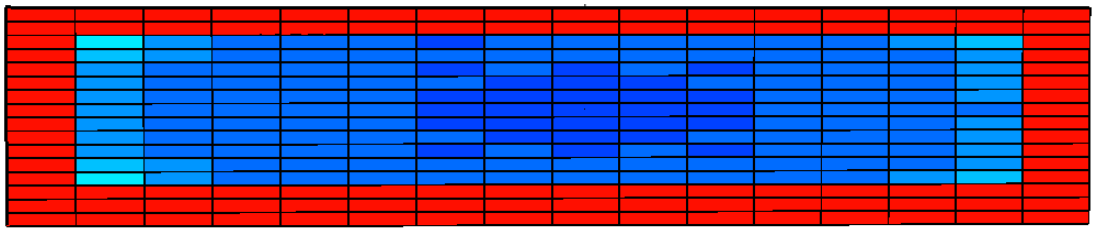

Water saturation inside fracture after 1 day (end of fracture treatment)

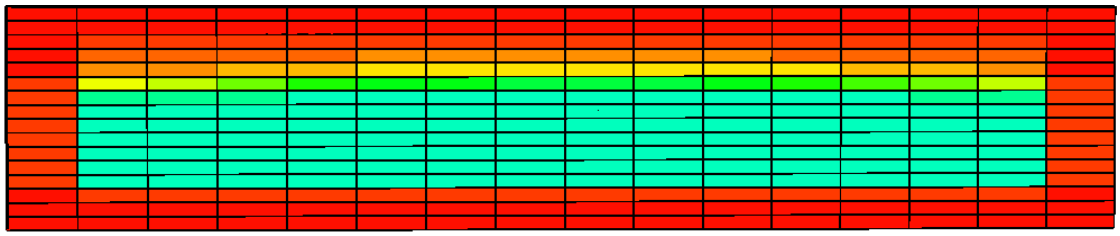

Water saturation inside fracture after 30 days (beginning of production, end of shut-in)

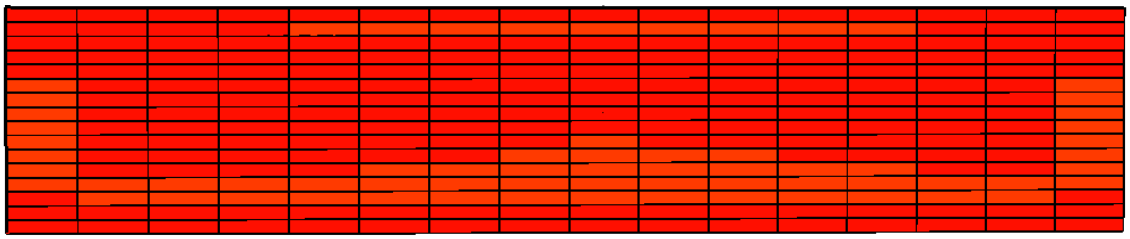

Water saturation inside fracture after 210 days

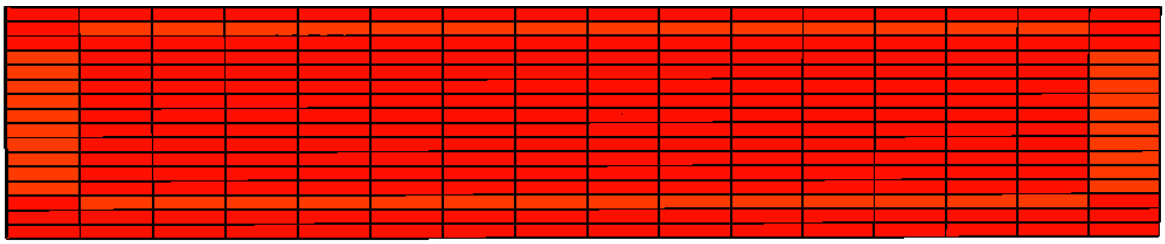

Water saturation inside fracture after 500 days (end of production)

Figure 3.9: Water saturation maps (High Drawdown)

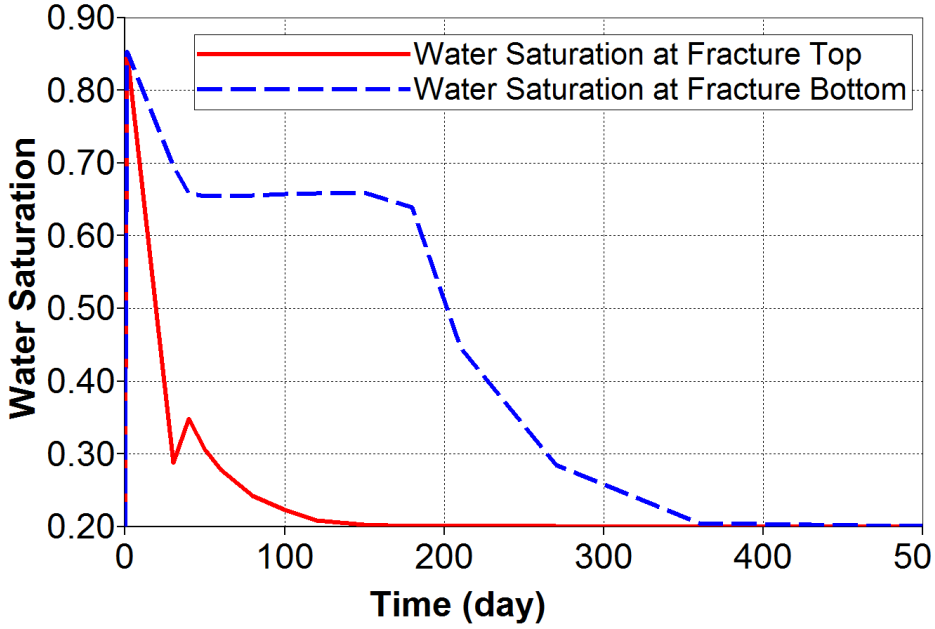

Figure 3.10: Variation of water saturation inside fracture over time (low drawdown)

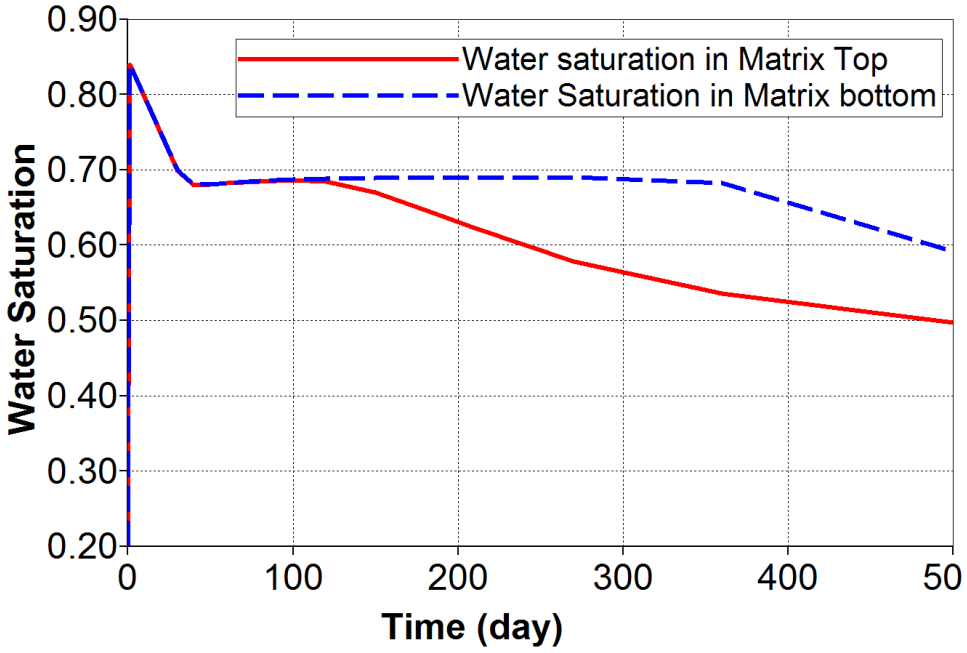

Figure 3.11: Variation of water saturation inside matrix 0.1 ft. from fracture face with time (low drawdown)

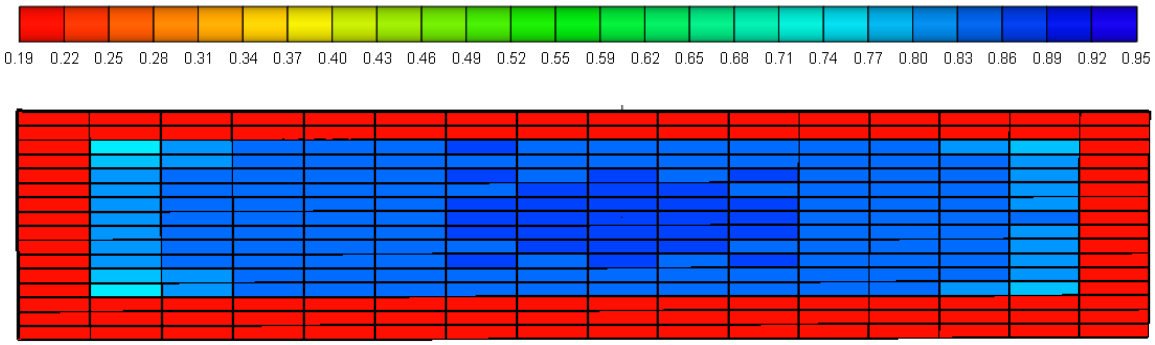

Water saturation inside fracture after 1 day (end of fracture treatment)

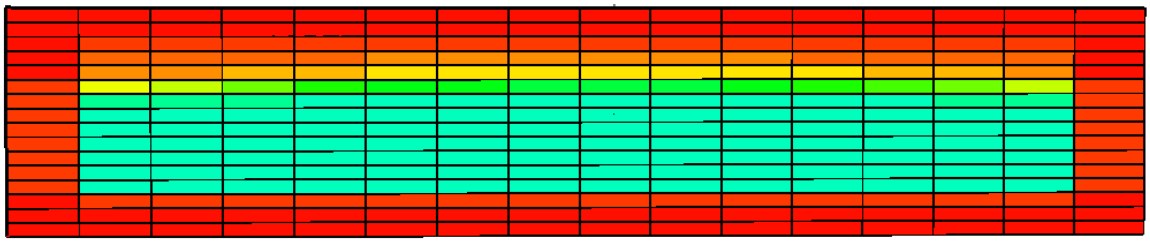

Water saturation inside fracture after 30 days (beginning of production, end of shut-in)

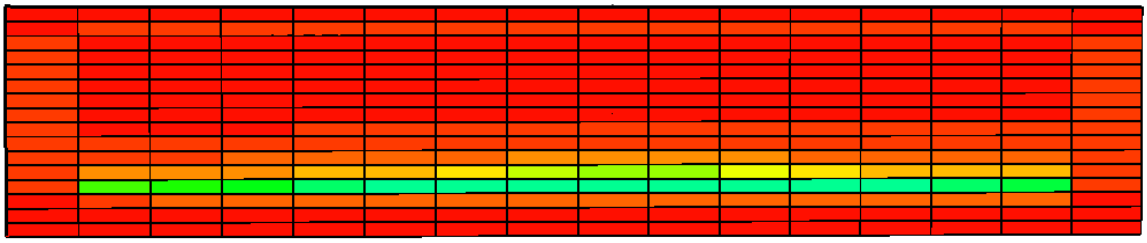

Water saturation inside fracture after 210 days

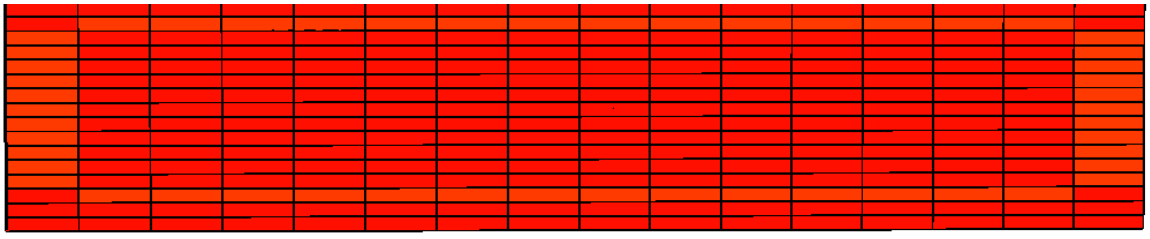

Water saturation inside fracture after 500 days (end of production)

Figure 3.12: Water saturation maps (Low Drawdown)

3.3.3. Liquid Loading for Different Matrix Permeabilities

In line with the conceptual understanding of the system, matrix permeability will have a key impact on the amount of liquid loading. This is because the matrix permeability has a first order control on the gas velocity which is ultimately responsible for overcoming the liquid loading in the fracture. Therefore, higher matrix permeability is expected to show faster cleanup as compared to low permeability. The results for higher matrix permeability of 10 µD and lower permeability of 0.1 µD are presented in Figures 3.13-3.15 and 3.16-3.18 respectively.

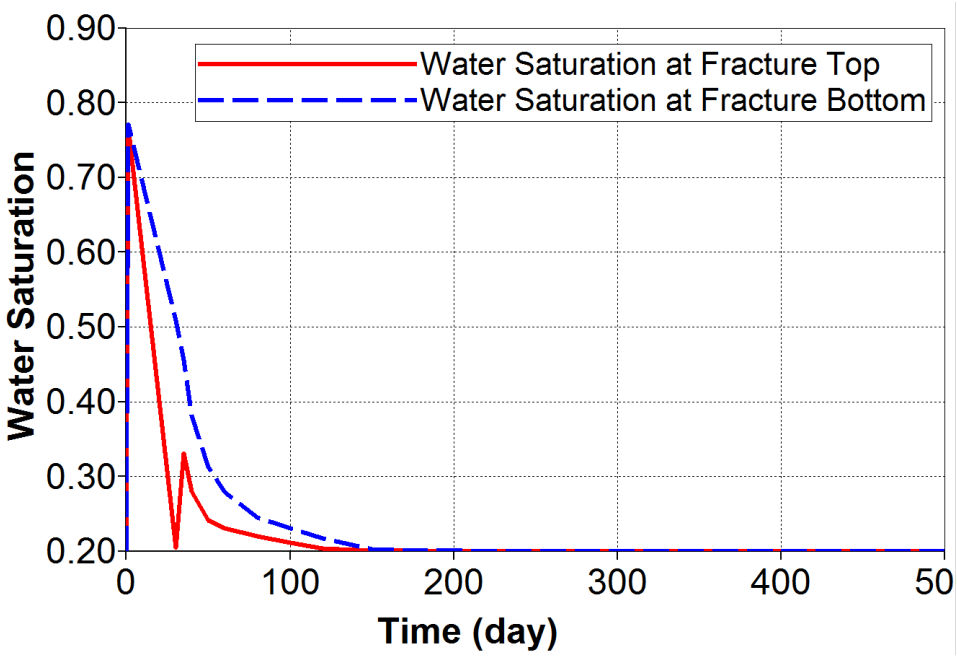

Figure 3.13: Variation of water saturation inside fracture over time (High Km)

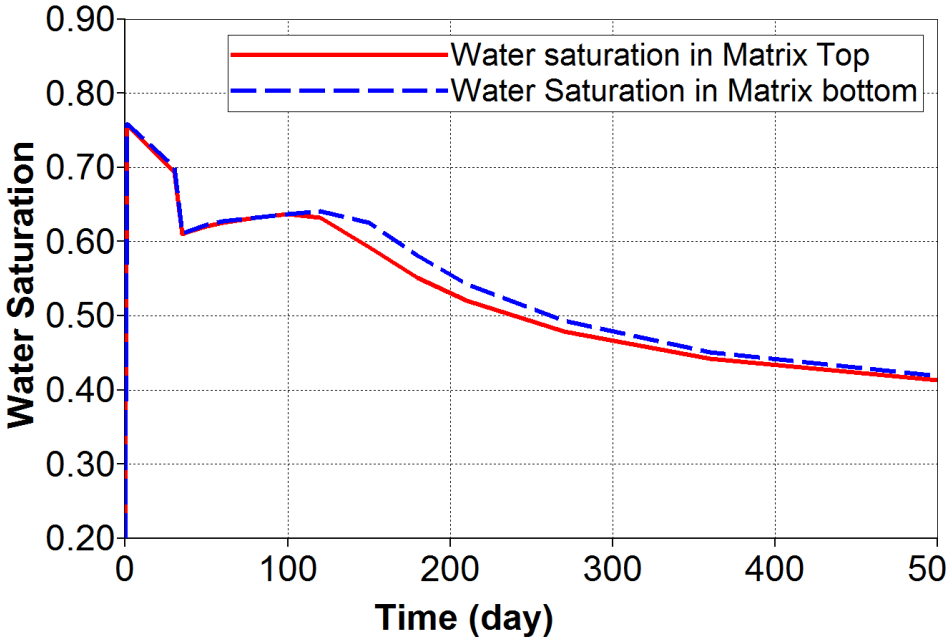

Figure 3.14: Variation of water saturation inside matrix 0.1 ft. from fracture face with time (High Km)

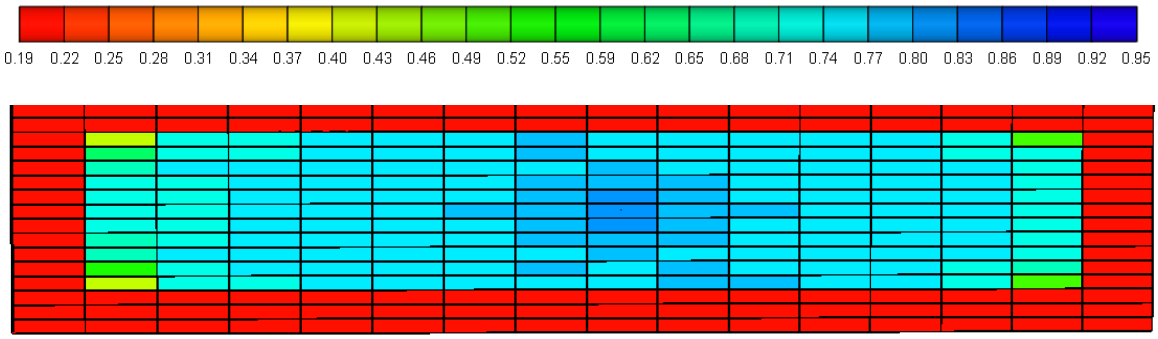

Water saturation inside fracture after 1 day (end of fracture treatment)

Figure 3.15: Water saturation maps (High Km)

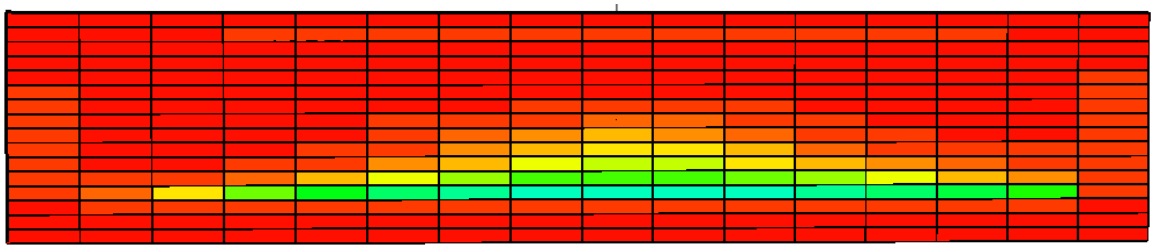

Water saturation inside fracture after 30 days (beginning of production, end of shut-in)

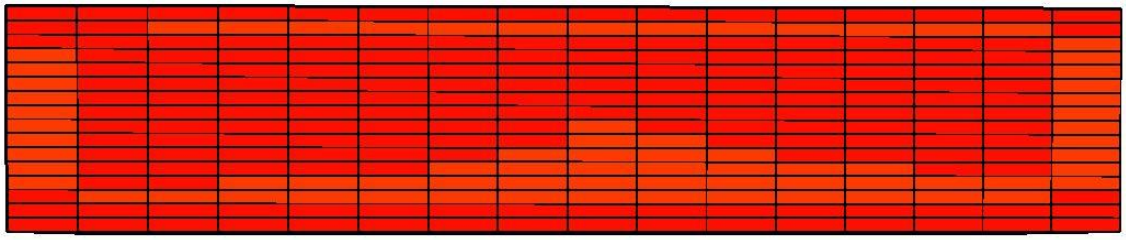

Water saturation inside fracture after 100 days

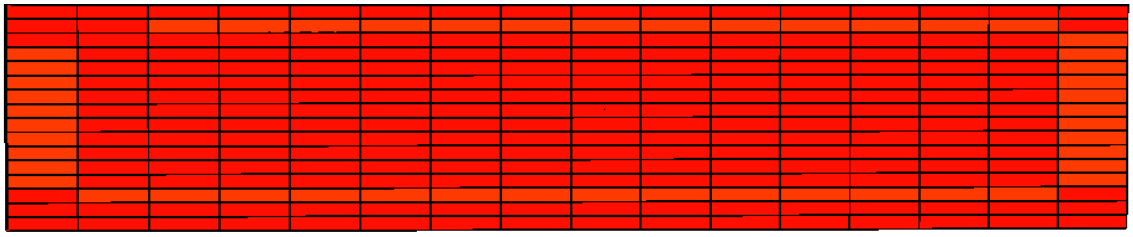

Water saturation inside fracture after 500 days (end of production)

Figure 3.15: Water saturation maps (High Km)- Continued

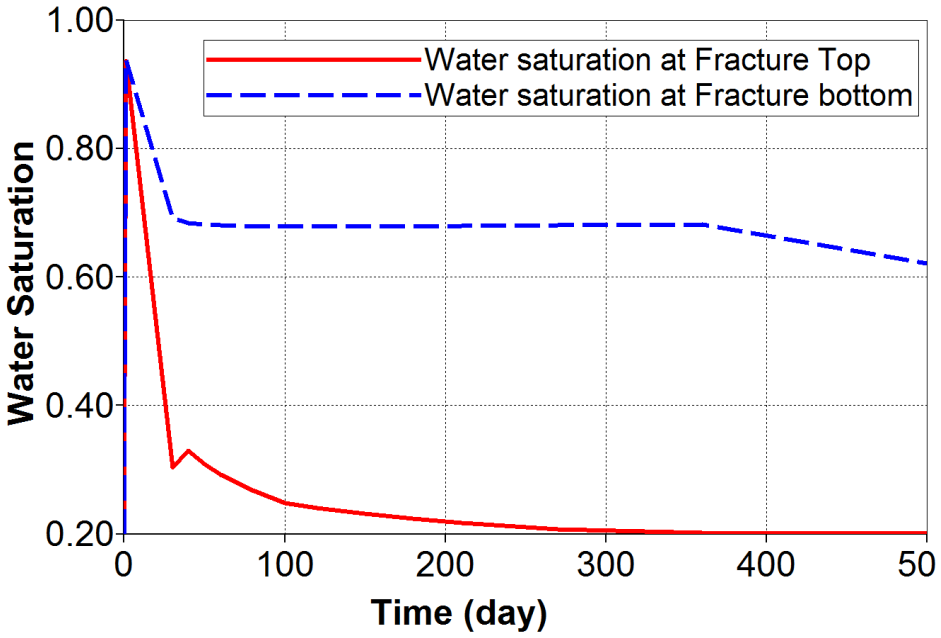

Figure 3.16: Variation of water saturation inside fracture over time (Low K_{mat})

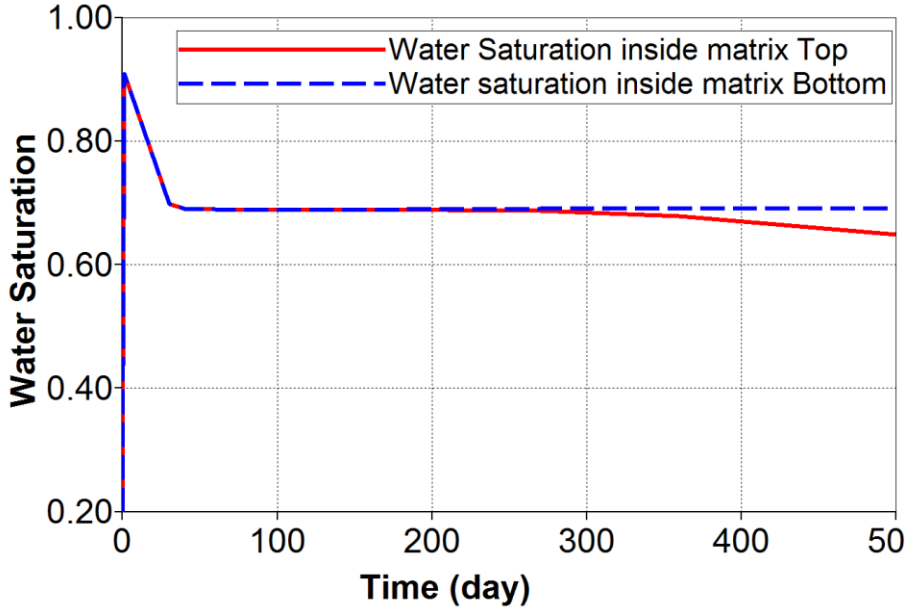

Figure 3.17: Variation of water saturation inside matrix 0.1 ft. from fracture face with time (Low K_{mat})

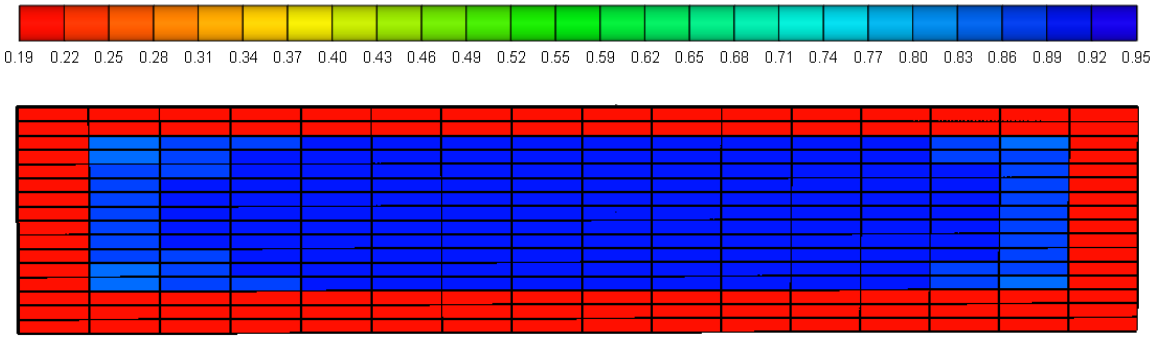

Water saturation inside fracture after 1 day (end of fracture treatment)

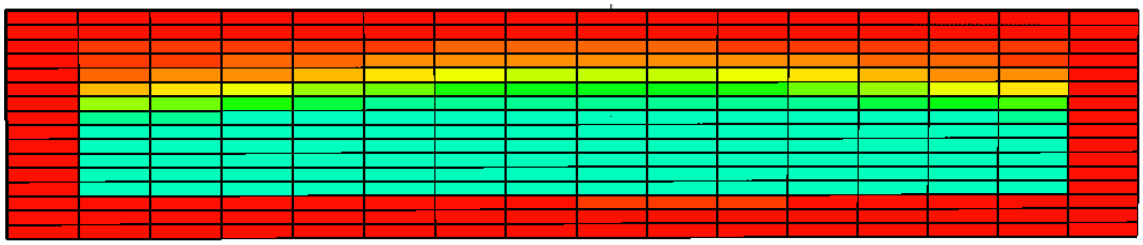

Water saturation inside fracture after 30 days (beginning of production, end of shut-in)

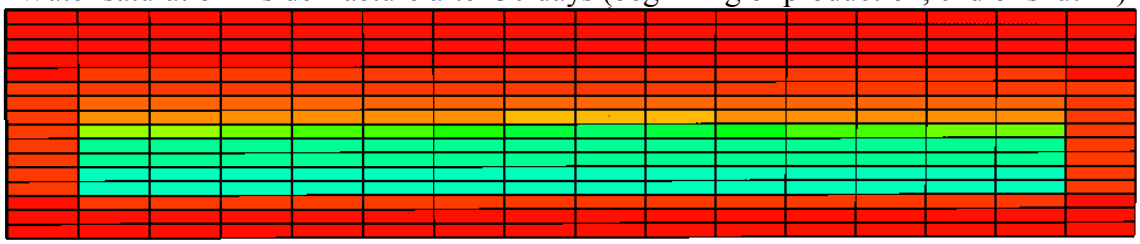

Water saturation inside fracture after 210 days

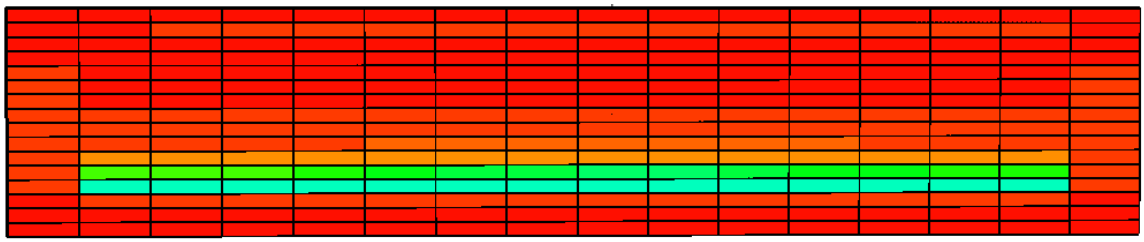

Water saturation inside fracture after 500 days (end of production)

Figure 3.18: Water saturation maps (Low Kmat)

3.3.4. Liquid Loading for Different Fracture Permeabilities

Conventional understanding of fluid flow within fractures stipulates that high fracture conductivity is a beneficial characteristic from the perspective of gas production. Here two fracture permeabilities are compared with the base case: higher fracture permeability of 20 D and lower fracture permeability of 0.2 D. Fracture permeability is essentially the permeability of the proppant pack that is assumed to be evenly distributed in the fracture volume. The results for frac fluid cleanup from the fracture and the matrix for the high frac permeability case are shown in Figures 3.19-3.21. The results for low frac permeability case are shown in Figures 3.22-3.24.

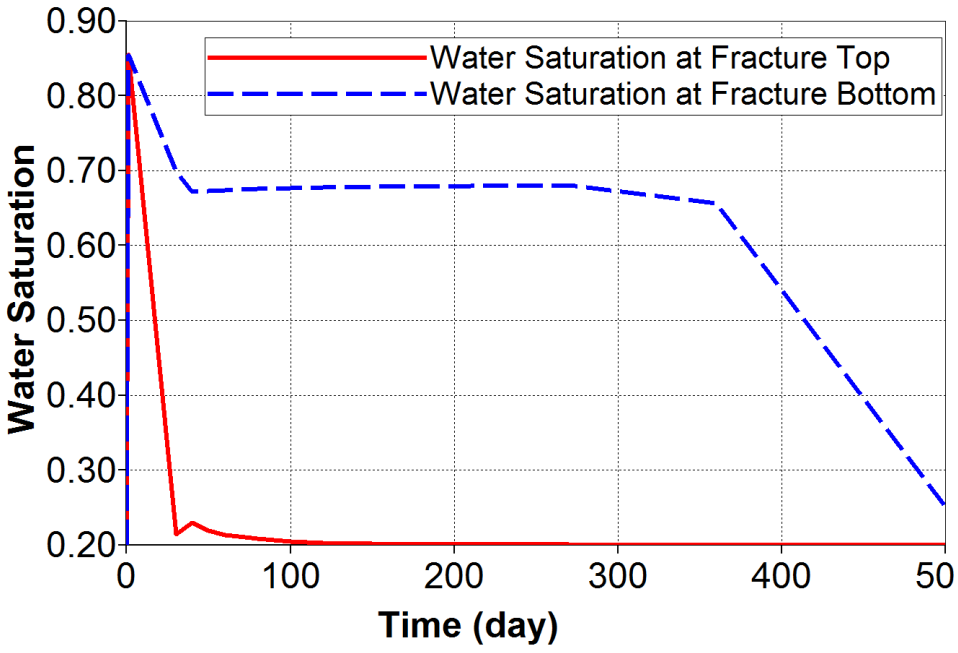

Figure 3.19: Variation of water saturation inside fracture over time (High K_{frac})

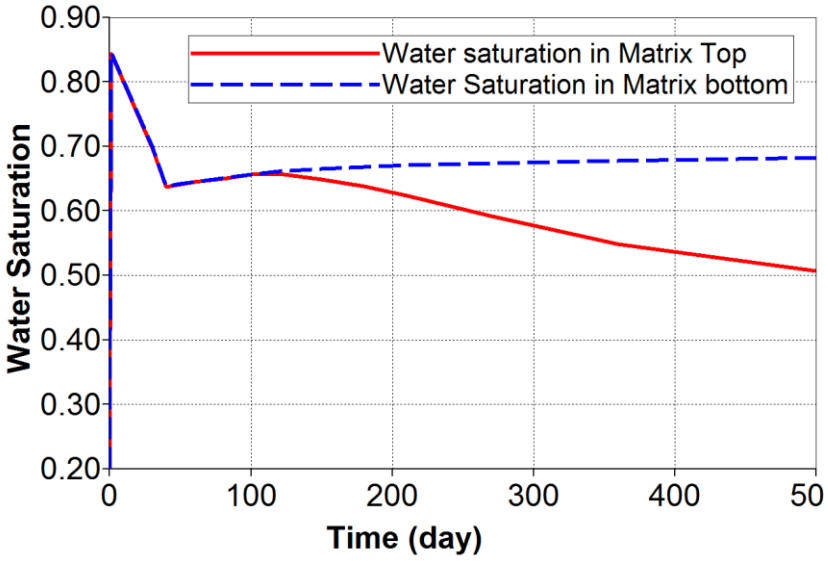

Figure 3.20: Variation of water saturation inside matrix 0.1 ft. from fracture face with time (High K_{frac})

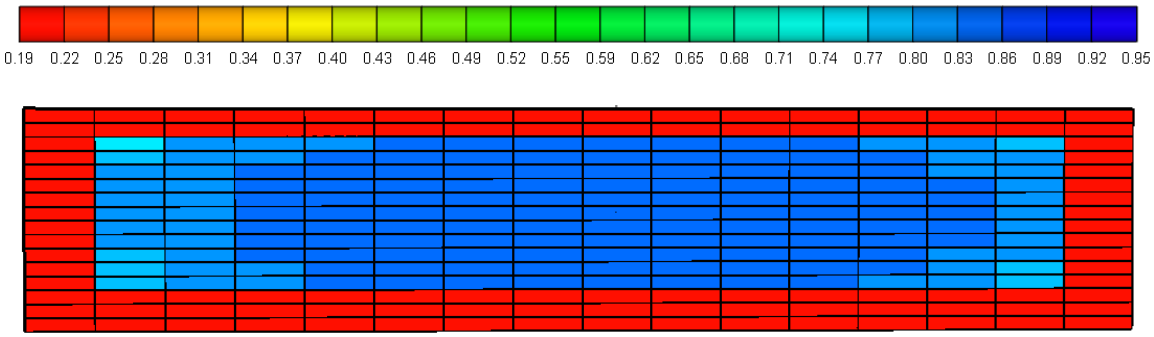

Water saturation inside fracture after 1 day (end of fracture treatment)

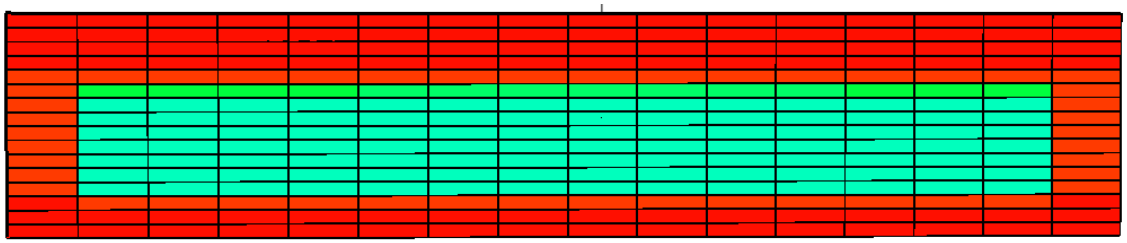

Water saturation inside fracture after 30 days (beginning of production, end of shut-in)

Figure 3.21: Water saturation maps (High Kfrac)

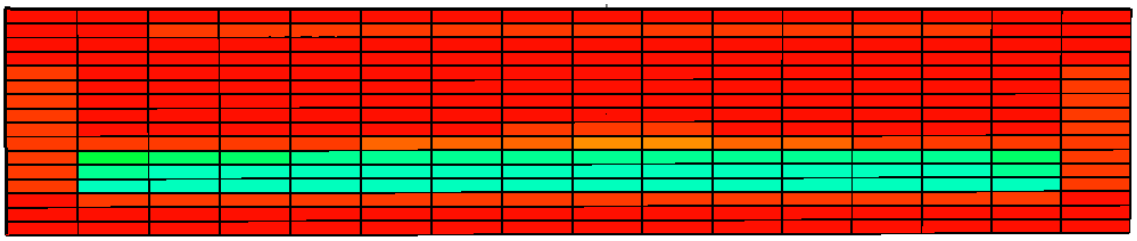

Water saturation inside fracture after 210 days

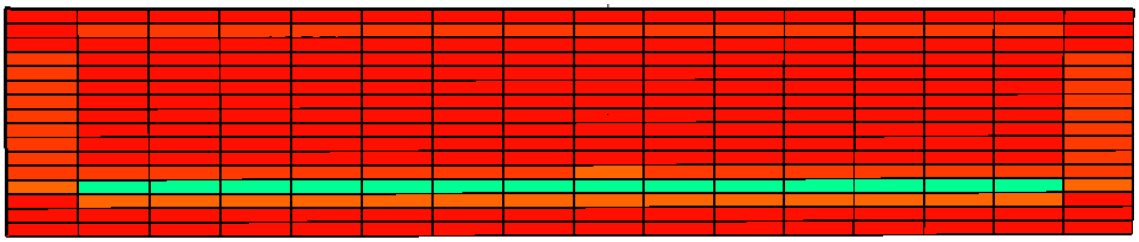

Water saturation inside fracture after 500 days (end of production)

Figure 3.21: Water saturation maps (High Kfrac)- Continued

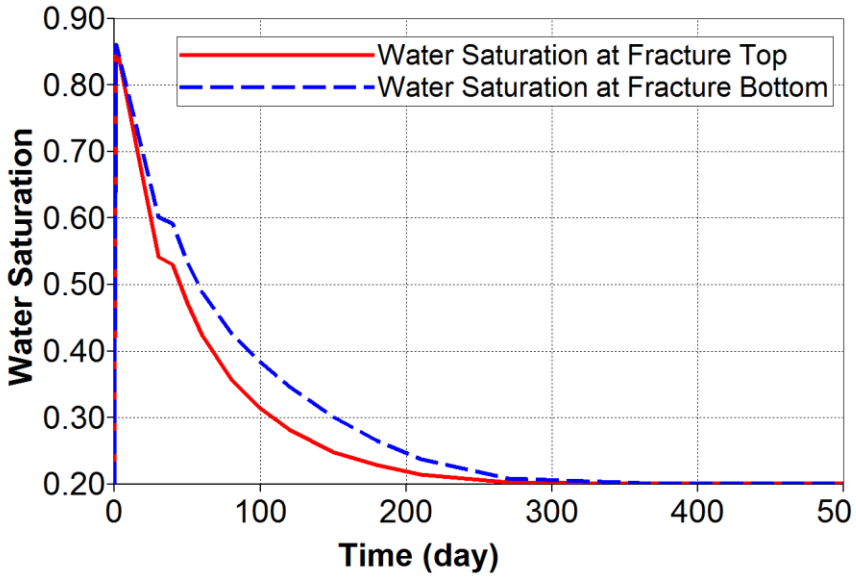

Figure 3.22: Variation of water saturation inside fracture over time (Low K_{frac})

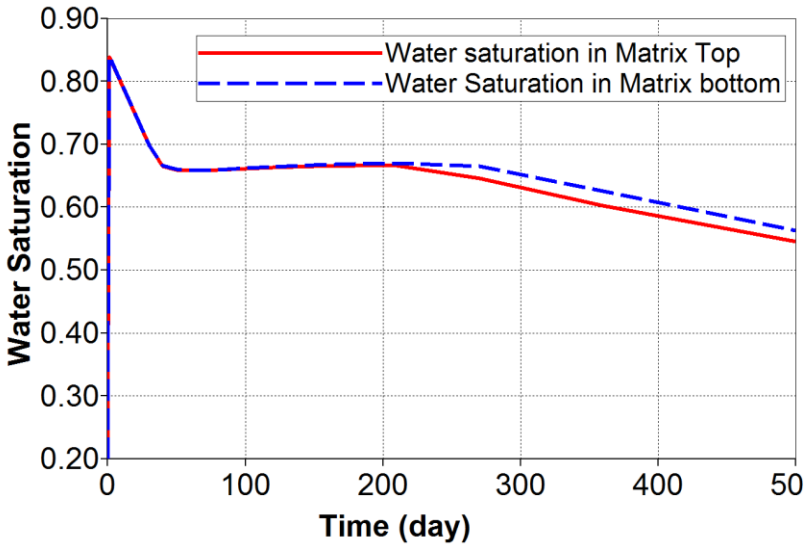

Figure 3.23: Variation of water saturation inside matrix 0.1 ft. from fracture face with time (Low K_{frac})

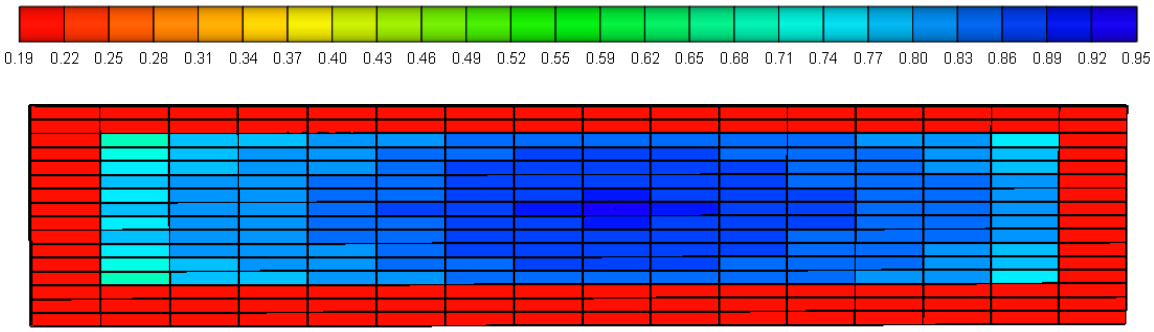

Water saturation inside fracture after 1 day (end of fracture treatment)

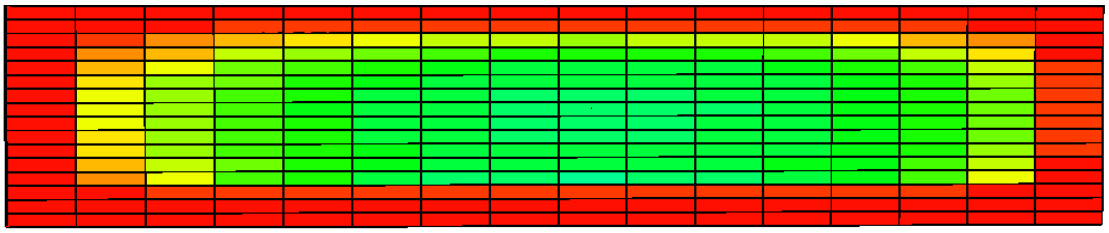

Water saturation inside fracture after 30 days (beginning of production, end of shut-in)

Figure 3.24: Water saturation maps (Low Kfrac)

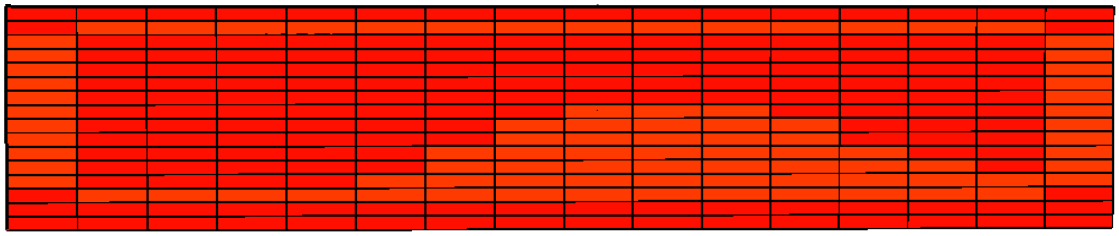

Water saturation inside fracture after 210 days

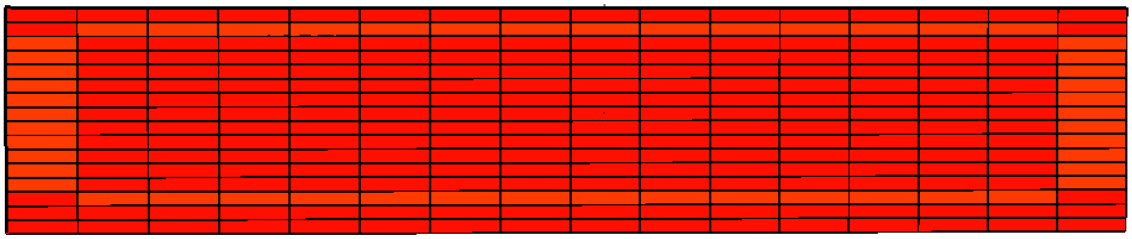

Water saturation inside fracture after 500 days (end of production)

Figure 3.24: Water saturation maps (Low Kfrac) - Continued

3.3.5. Liquid Loading for Different Fracture Heights

Fracture height is an important parameter for analyzing the completion quality. Higher fracture height means more reservoir contact and a higher surface area for gas flow. Higher surface area also leads to more liquid trapping on the fracture face. In this analysis, two different fracture height scenarios were compared against the base: Taller fractures covering 90 ft. out of 100 ft. reservoir thickness and shorter fractures covering only 35 ft. of out 100. Same amount of frac-water is injected. The liquid cleanup profiles are shown below. Figures 3.25-3.27 correspond to the taller fracture case whereas Figures 3.28-3.30 relate to the shorter fracture case.

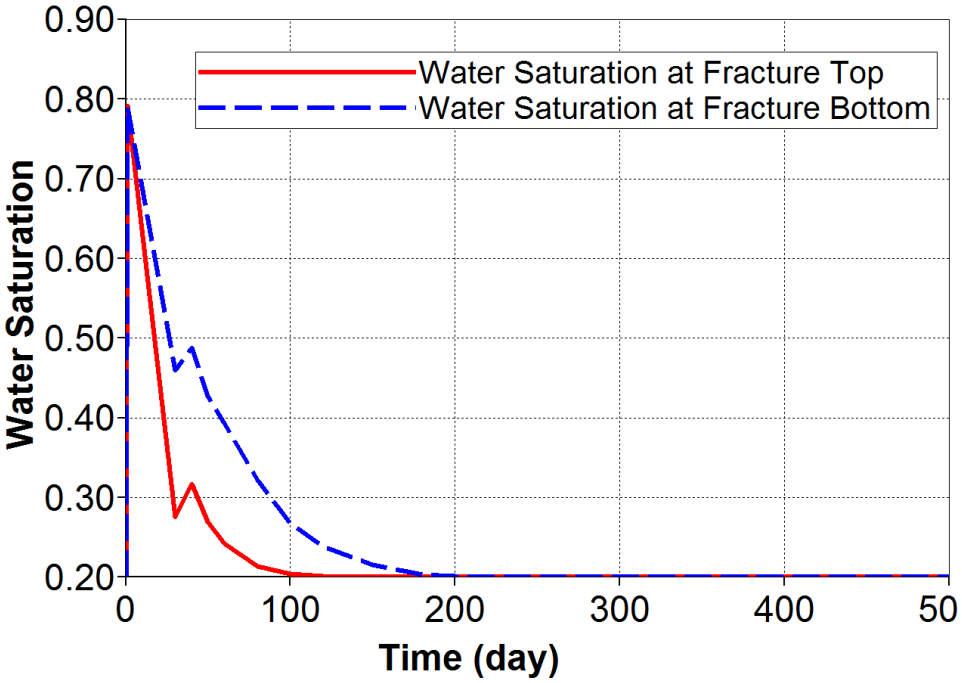

Figure 3.25: Variation of water saturation inside fracture over time (Taller Frac)

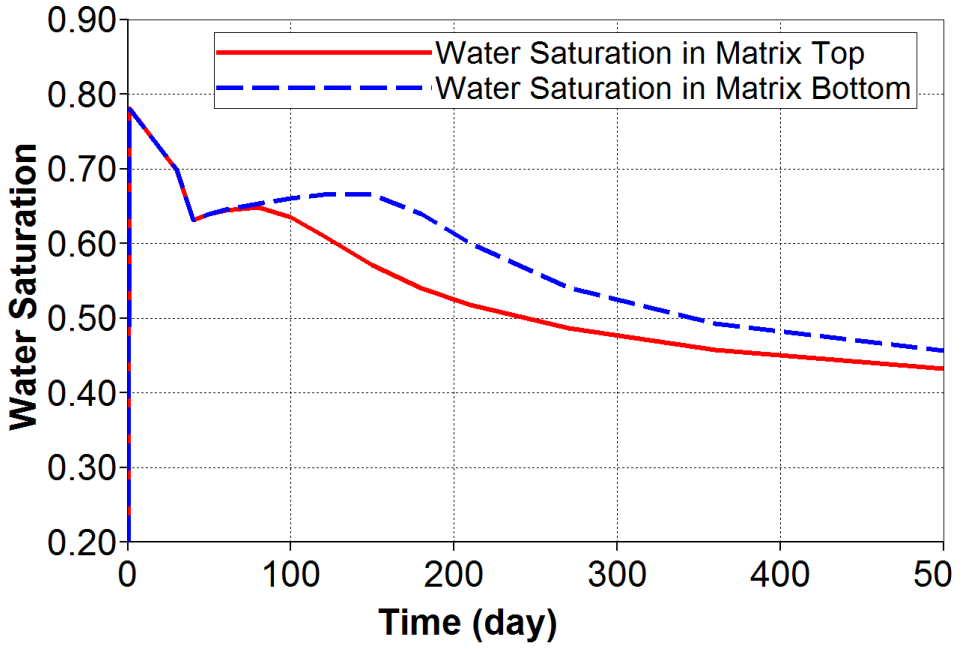

Figure 3.26: Variation of water saturation inside matrix 0.1 ft. from fracture face with time (Taller Frac)

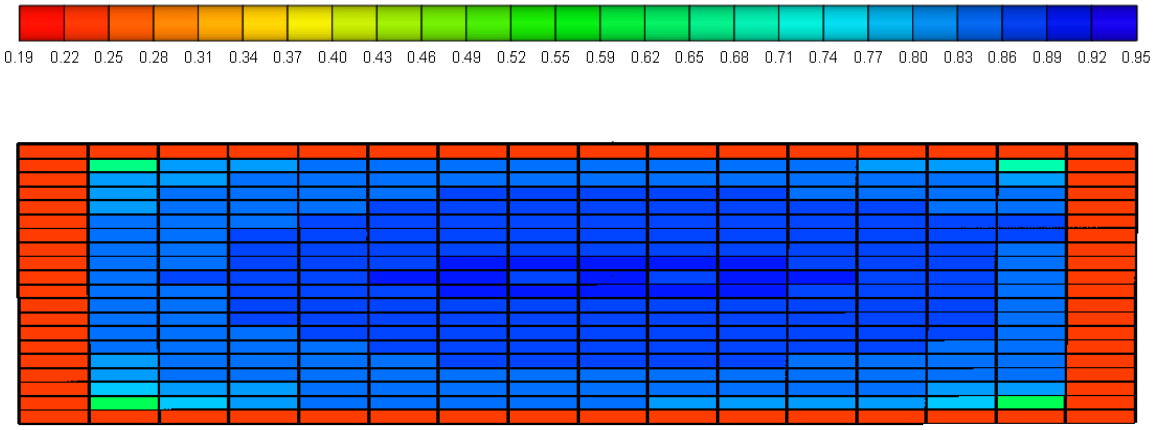

Water saturation inside fracture after 1 day (end of fracture treatment)

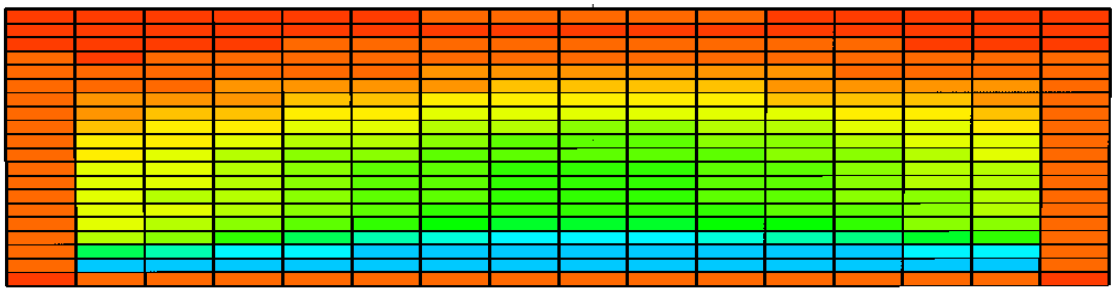

Water saturation inside fracture after 30 days (beginning of production, end of shut-in)

Water saturation inside fracture after 150 days

Figure 3.27: Water saturation maps (Taller Frac)

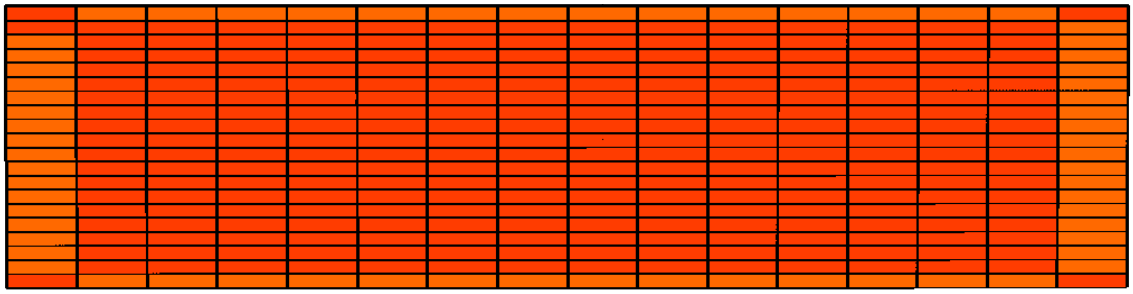

Water saturation inside fracture after 500 days (end of production)

Figure 3.27: Water saturation maps (Taller Frac) - Continued

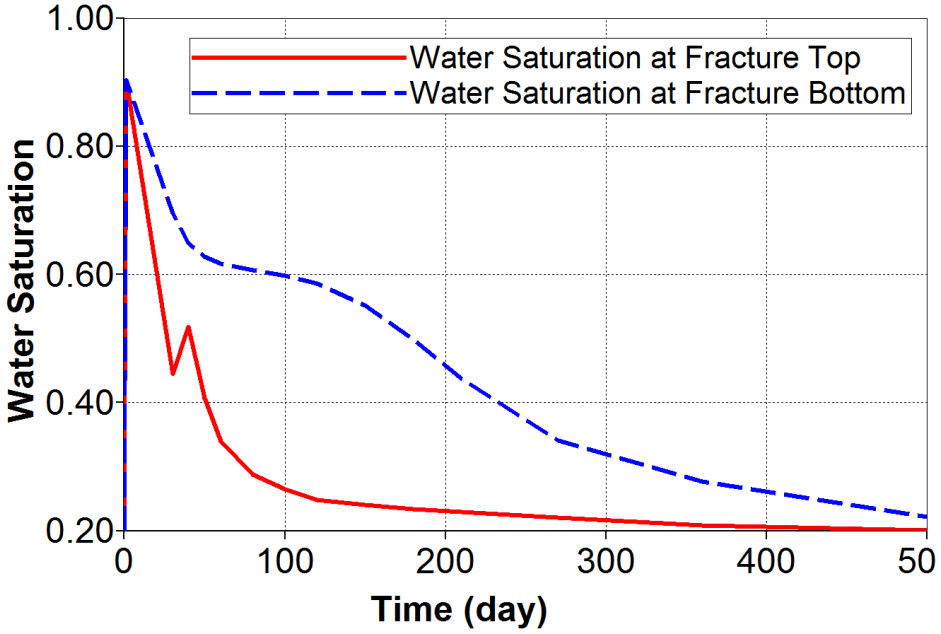

Figure 3.28: Variation of water saturation inside fracture over time (Shorter Frac)

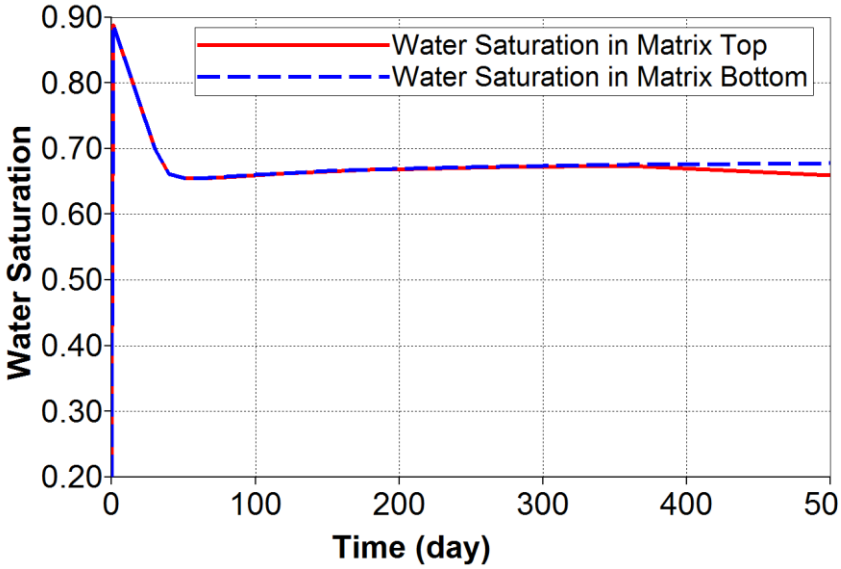

Figure 3.29: Variation of water saturation inside matrix 0.1 ft. from fracture face with time (Shorter Frac)

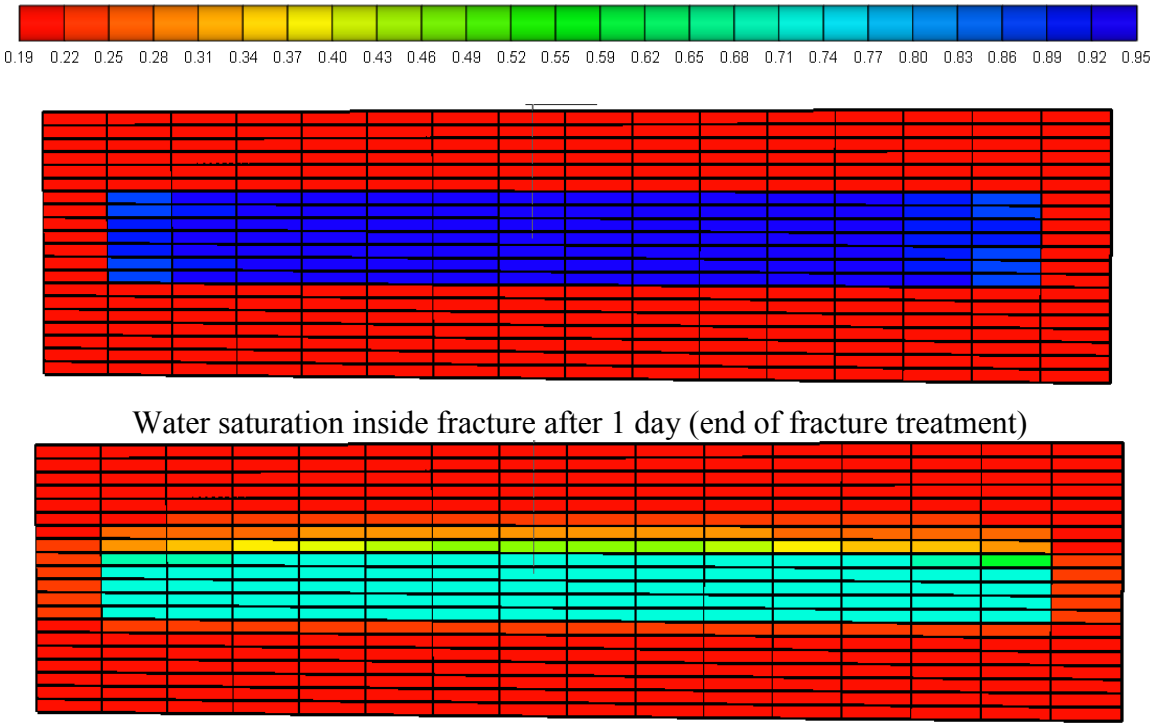

Water saturation inside fracture after 1 day (end of fracture treatment)

Water saturation inside fracture after 30 days (beginning of production, end of shut-in)

Figure 3.30: Water saturation maps (Shorter Frac)

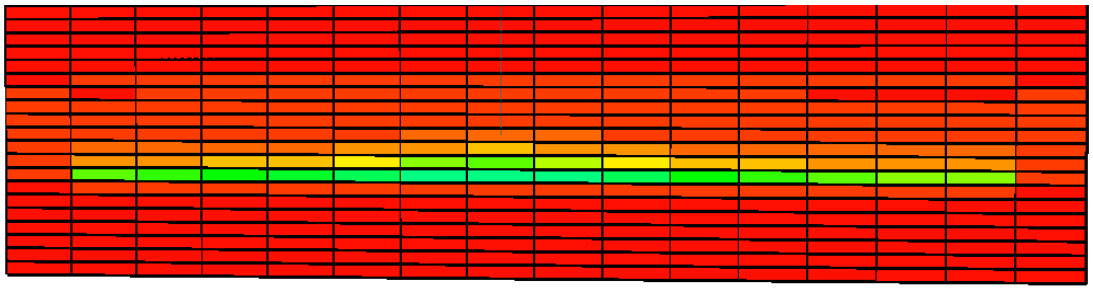

Water saturation inside fracture after 210 days

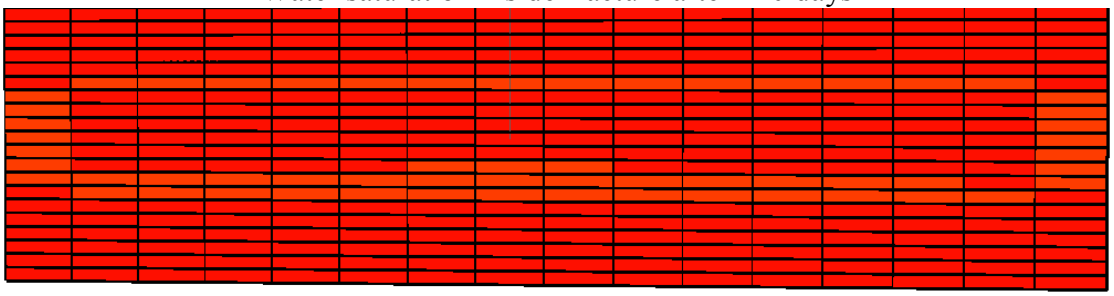

Water saturation inside fracture after 500 days (end of production)

Figure 3.30: Water saturation maps (Shorter Frac)- continued

3.3.6. Liquid Loading After Different Shut-In Times

Some field studies have indicated that keeping the well shut-in for a longer duration leads to better productivities when the well is put on production. One of the possible reasons is water imbibition away from the frac face, which will lead to higher gas relative permeability and therefore, higher gas rates. To investigate this effect, two scenarios with higher (89 days) and lower (2 days) shut-in time were studied. Figures 3.31-3.36 show the cleanup in the two respective cases. Equal production period of 470 days is provided.

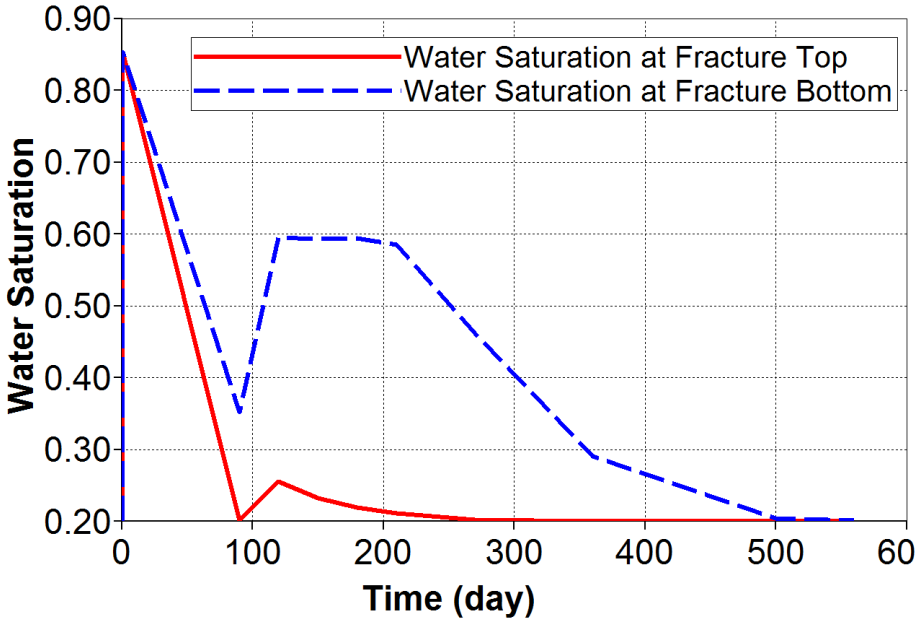

Figure 3.31: Variation of water saturation inside fracture over time (89 day shutin)

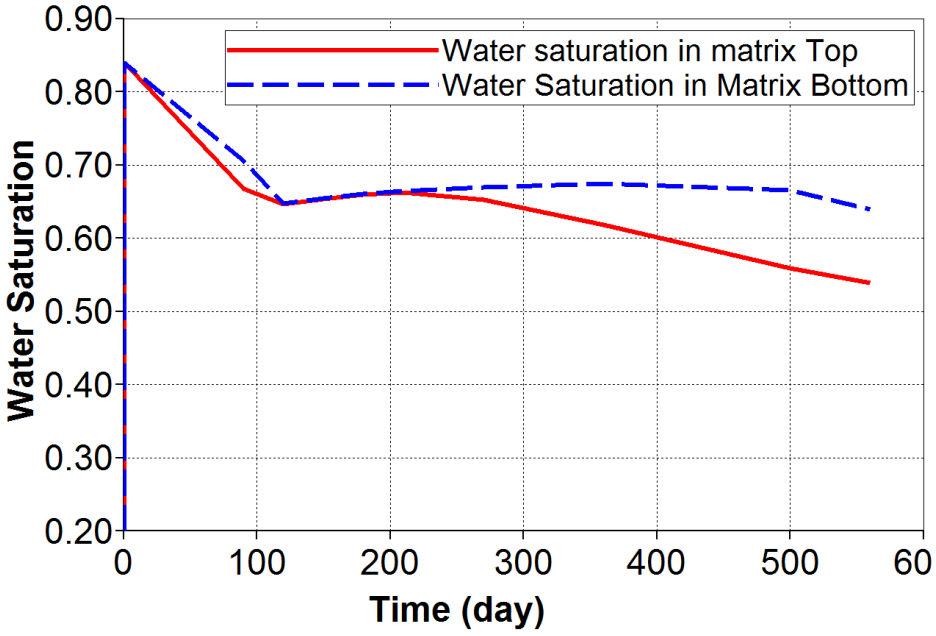

Figure 3.32: Variation of water saturation inside matrix 0.1 ft. from fracture face with time (89 day shutin)

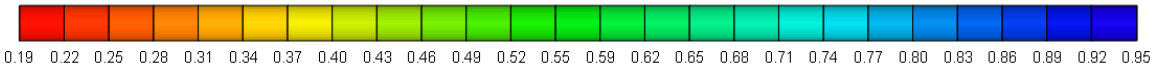

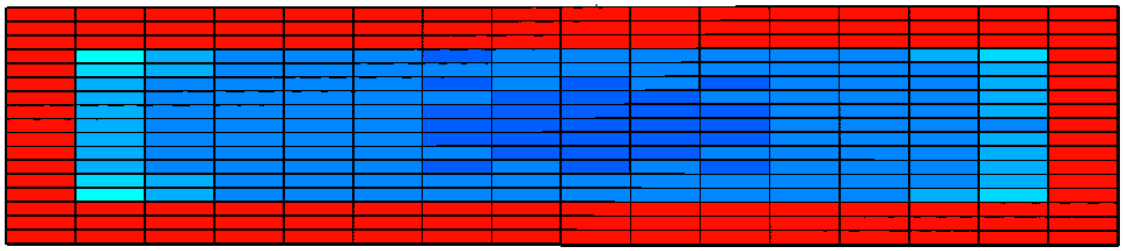

Water saturation inside fracture after 1 day (end of fracture treatment)

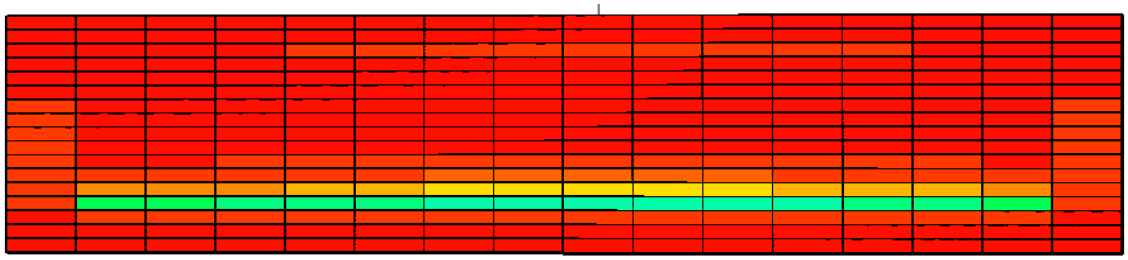

Water saturation inside fracture after 90 days (beginning of production, end of shut-in)

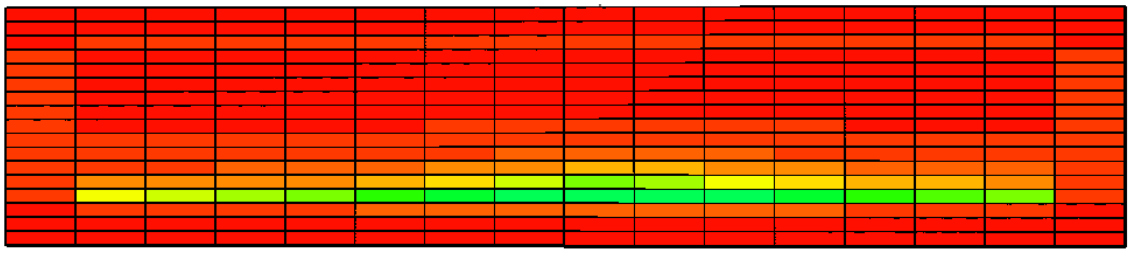

Water saturation inside fracture after 270 days

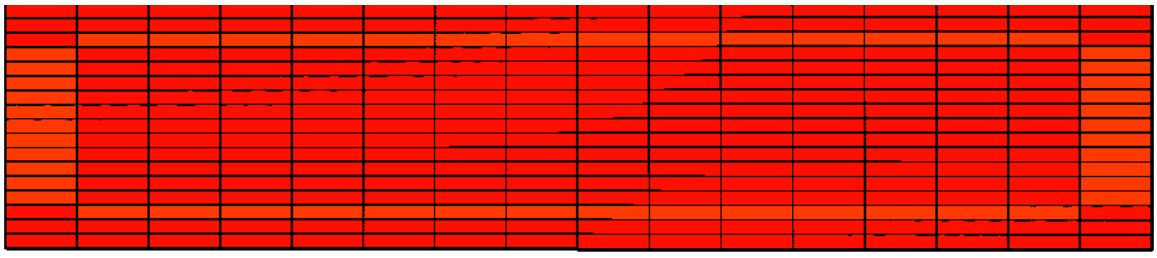

Water saturation inside fracture after 560 days (end of production)

Figure 3.33: Water saturation maps (89 days shut-in)

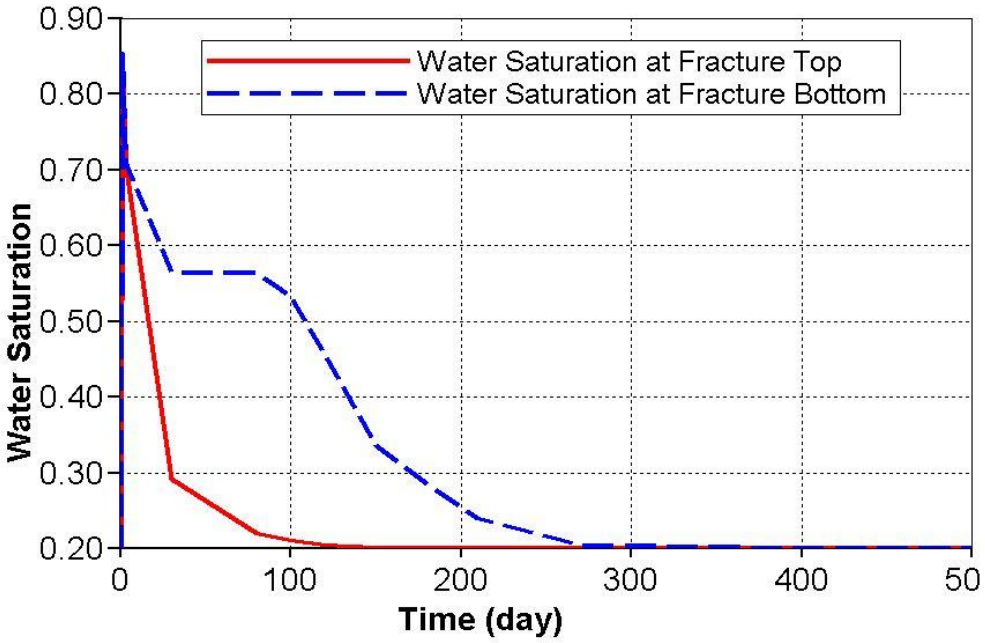

Figure 3.34: Variation of water saturation inside fracture over time (2 days shutin)

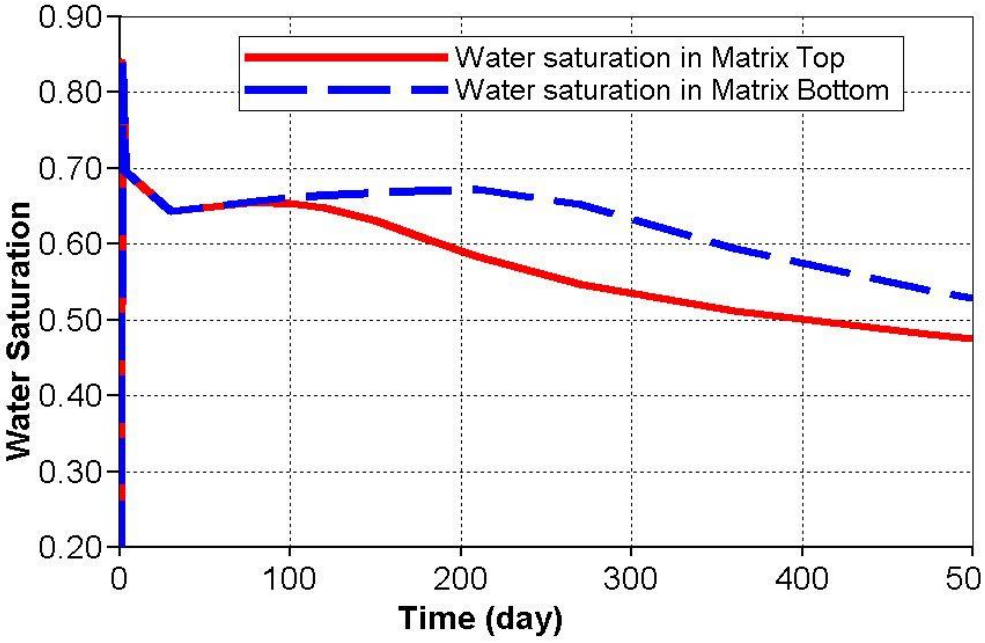

Figure 3.35: Variation of water saturation inside matrix 0.1 ft. from fracture face with time (2 days shutin)

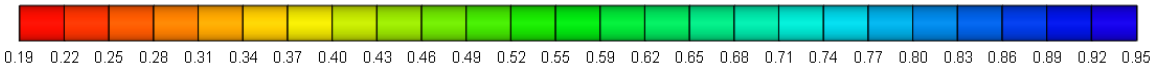

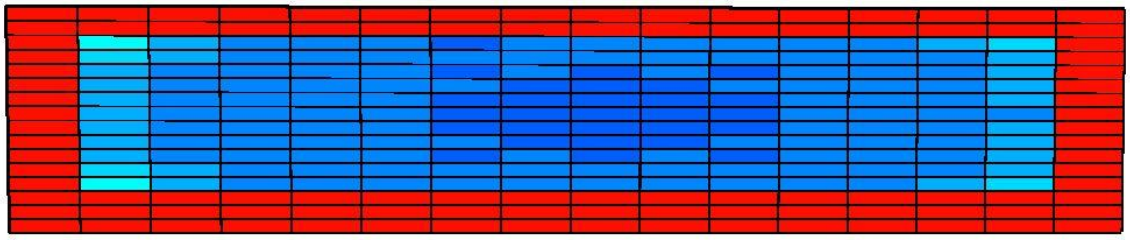

Water saturation inside fracture after 1 day (end of fracture treatment)

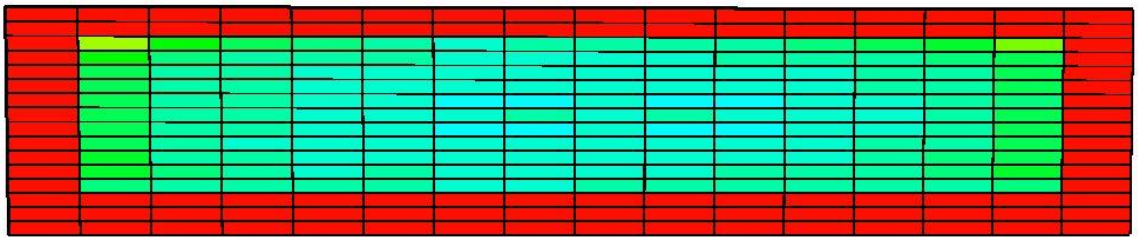

Water saturation inside fracture after 3 days (beginning of production, end of shut-in)

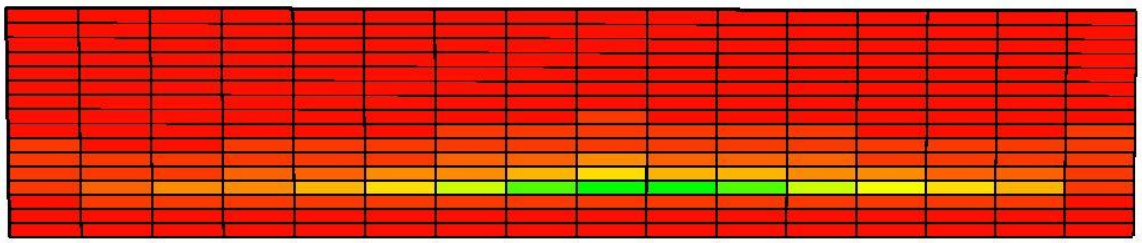

Water saturation inside fracture after 150 days

Water saturation inside fracture after 473 days (end of production)

Figure 3.36: Water saturation maps (2 days shut-in)

3.4. DISCUSSION AND INTERPRETATION

3.4.1. Base Case

There are a couple of interesting things to be observed from figures 3.4-3.6. Since the well is kept shut-in until the 30th day and the reservoir is water wet, the water saturation inside the fracture keeps declining until the 30th day because of imbibition into the matrix. As soon as the production is initiated, water flows into the fracture from the formation due to which the saturation first increases and then declines. Continued production leads to cleanup of water that is present inside the fracture. The bottom of the fracture does not cleanup for a while. As soon as the velocity is large enough to lift the water out of the fracture, the bottom starts cleaning up.

Also note the matrix (near the fracture face) does not start cleaning up until the fracture is cleaned up completely. This is because the two zones are in equilibrium and if there is water inside the fracture, the matrix will keep imbibing from it. As soon as there is no more water to imbibe, the drawdown will produce the water into the wellbore albeit at a very low rate due to its very low relative permeability. In reality, other mechanisms such as evaporation or velocity dependent relative permeability modification may lead to better matrix cleanup. Those possibilities are investigated in later chapters. This counter-current imbibition is highly dependent on the wettability nature of the matrix.

3.4.2. Effect of Drawdown

In the higher drawdown scenario, the cumulative gas and water produced are 131.2 MMcf and 401.5 bbl. (40.1 %). As expected, higher drawdown leads to better cleanup and higher cumulative gas. The figures indicate that the fracture cleans up both at the top and bottom of the fracture by the 400th day even though there is a considerable amount of water trapped at the fracture face. Water doesn't accumulate at the bottom of the fracture because the higher drawdown leads to high gas velocities which continuously push the frac water to the wellbore. However, for the lower drawdown case the cumulative gas and water recovery reduces to 33.9 MMcf and 165.5 bbl. (16.5 %). The effect of drawdown on productivity ($PI = Q/(P_{res} - P_{well})$) is shown below:

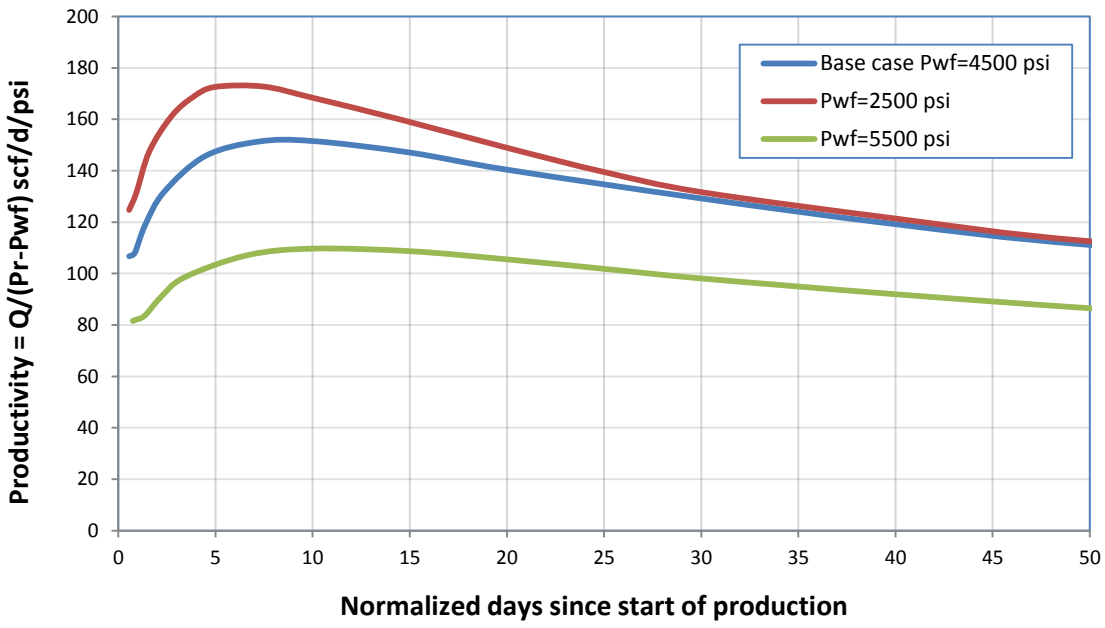

Figure 3.37: Effect of drawdown on gas productivity

3.4.3. Effect of Matrix Permeability

In the case of higher matrix permeability, the cumulative gas and water recovery were 219.7 MMcf and 276 bbl (27.6 %). Considering the high matrix permeability, the gas velocity in the fracture is also high and, therefore, the cleanup of the bottom of the fracture is relatively quick compared to the base case. It's important to note that even though water recovery is essentially the same as in the base case the cumulative gas recovered is almost 3 times as much. Lower water recovery could be explained by deeper invasion of water during fracturing.

Figures 3.16-3.18 show that when the matrix permeability is reduced, there is a considerable amount of water present at the bottom of the fracture even after 1 year of production (the top cleans up by 300^{th} day). Considering that drawdown is still the same as the base case, this accumulation of water can be explained by the lower gas velocity in the fracture. When the matrix permeability is reduced, not only does the flow of gas become more constrained but the capillary blocking of water increases. This leads to a lower gas flow rate which is unable to lift the water from the bottom of the fracture as it is less than the critical lift velocity. The cumulative gas production in this gas is 7.5 MMcf and the cumulative water recovery is 154.2 bbl. (15.4 %). It is evident that water is not only trapped in the matrix but also in the fracture.

The impact on gas productivity is shown in Figure 3.38 below. The productivity here is normalized with respect to the matrix permeability. It shows that for higher matrix permeability the peak gas productivity is achieved earlier than for lower permeability

case, possibly due to faster cleanup. Lower peak for Km=10 μD as compared to Km= 1μD shows that there is a non-linear dependence between matrix permeability and productivity.

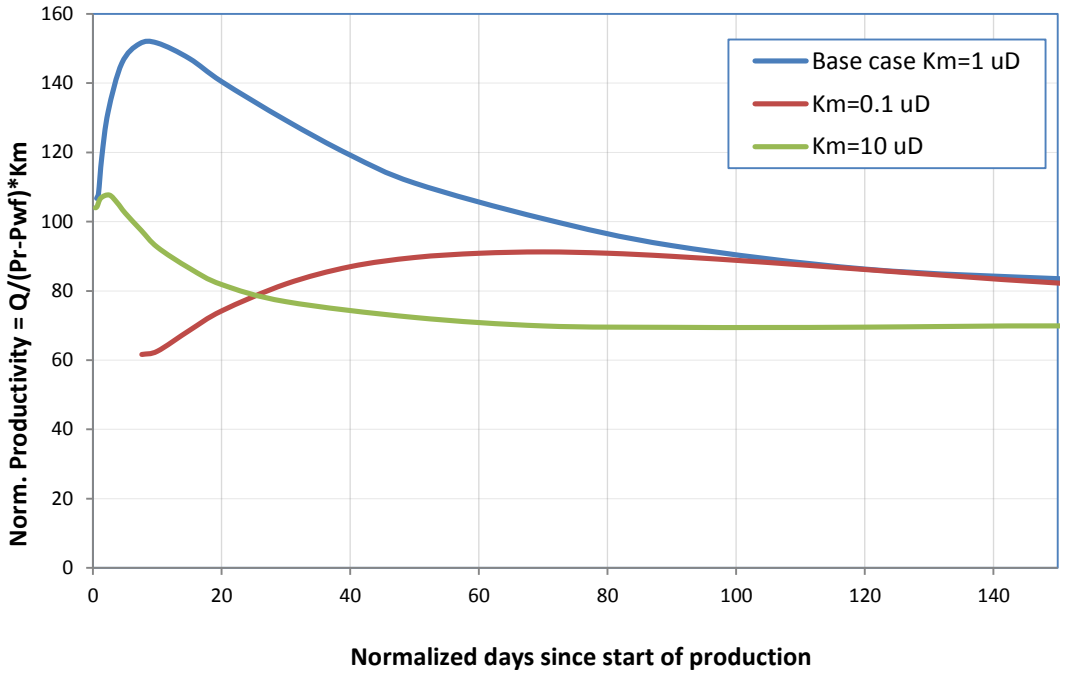

Figure 3.38: Effect of matrix permeability on gas productivity

3.4.4. Effect of Fracture Permeability

Figures 3.19-3.21 show that for the higher fracture permeability case, the liquid at the top of the fracture is cleaned up fairly quickly. This is because gravity, assisted by higher permeability, pulls the fluid down rather easily, so this liquid is either produced or deposited at the bottom of the fracture. The cleanup of the bottom of the fracture is slow until approximately the 375th day and then picks up. The water saturation in the matrix

adjacent to the fracture face bottom remains consistently high throughout the measured period. However, the matrix near the fracture top starts cleaning up as soon as that portion in the fracture cleans up. This indicates that gas flow is primarily occurring from the top part of the fracture where the liquid from fracture face has been removed. The cumulative gas and water recoveries in this scenario are 70.27 MMcf and 245.8 bbl (24.5%) respectively. Since the reservoir conditions were not altered, the gas recovery is almost the same as the base case.

When a lower fracture permeability of 0.2 D is considered, the cumulative gas and water recoveries are 64.3 MMcf and 249.4 bbl. (24.9 %) respectively. As Figures 3.22-3.24 show, the fracture cleans up by the 300th day both at the top and the bottom of the fracture. This is because water produced from the matrix doesn't accumulate at the fracture bottom due to high fracture permeability. Cleanup is governed by drawdown and is, therefore, uniform at the top and bottom.

The effect of cleanup on gas productivity is shown in Figure 3.39 below. It is interesting to note that even though there is liquid loading at bottom of fracture for higher fracture permeability case, the peak productivity is higher and faster than the lower frac permeability case. This is due to faster and more complete cleanup of fracture top. The top of fracture and adjoining matrix volume provide a zone of high gas relative permeability due to lower water saturation.

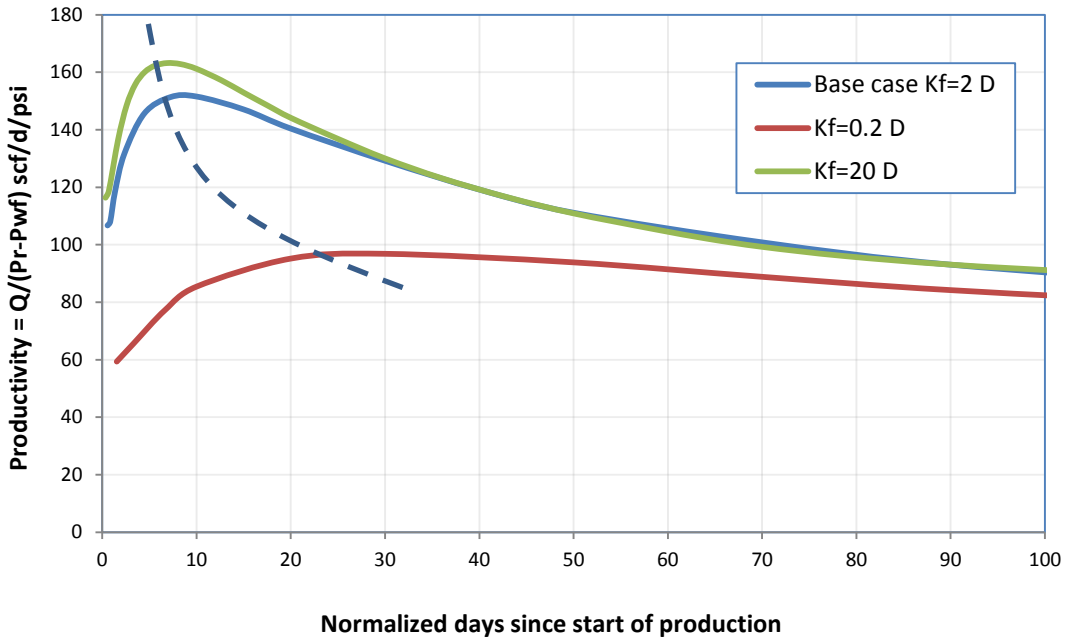

Figure 3.39: Effect of fracture permeability on gas productivity

3.4.5. Effect of Fracture Height

In the base case, the fracture vertical extent (top to bottom) is considered to be 55 ft. in a reservoir with a net pay of 100 ft. If the vertical extent is increased to 90 ft., the cleanup profile is as shown in Figures 3.27-3.29. It is interesting to note that there is no liquid loading at the bottom of the fracture and the cleanup inside the fracture is much faster than in the base case. The cumulative gas and water recovered in this case are 108.8 MMscf and 190.5 bbl. (19.5%) respectively. The higher gas cumulative can be attributed to a higher surface area of the fracture leading to more reservoir contact. In addition, as the fracture volume and surface area increase, the depth of invasion for the

same volume of fluid injected decreases. Less invasion leads to less liquid blocking on the fracture face which leads to a higher gas rate and, therefore, faster fracture cleanup.

When the vertical extent of the fracture (top to bottom) is reduced to 35 ft., the cumulative gas and water recoveries are 41.5 MMSCF and 306.5 bbl. (30.65%). It is evident that fracture cleanup takes a considerably longer time in this case which also affects matrix cleanup near the fracture face. Gas recovery and fracture cleanup suffer because a shorter fracture means a lower surface area and therefore, a higher water saturation which leads to lower gas relative permeability. However with a shorter fracture more water is recovered. Figure 3.40 shows the impact of fracture height on the productivity in the initial flowback period. It shows that reducing the frac height delays peak productivity.

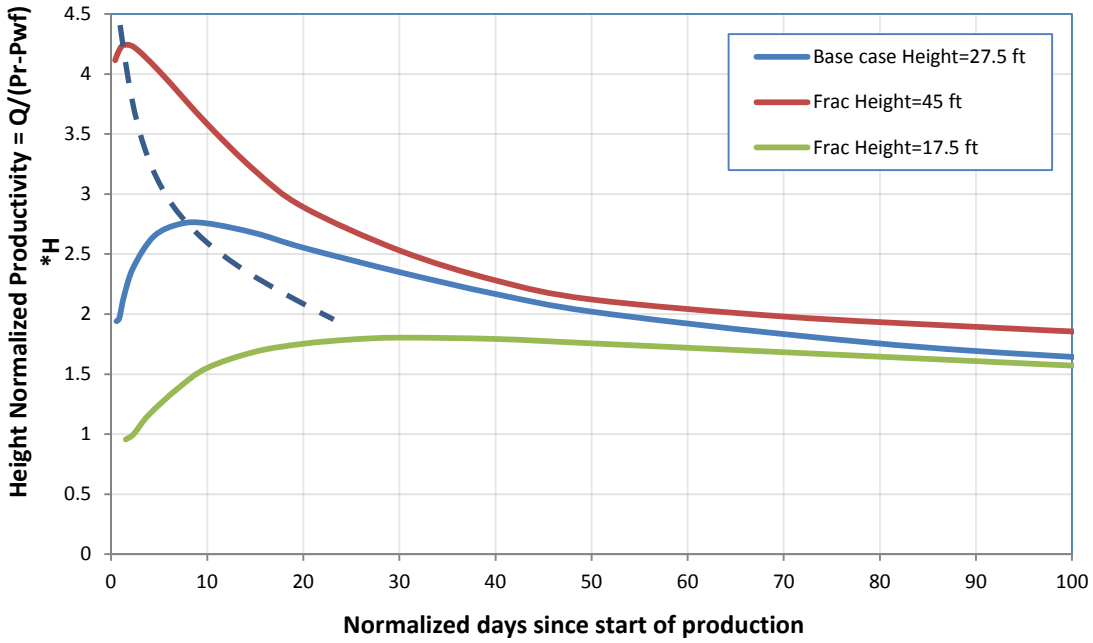

Figure 3.40: Effect of fracture height on gas productivity

3.4.6. Effect of Shut-in time

In the case of a higher well shut-in time of 89 days after fracturing, the cumulative gas and water recoveries are 67.5 MMscf and 173.95 bbl. (17.4%). However, for the shorter shut-in scenario, the cumulative gas and water recoveries were 73.6 MMscf and 375.8 bbl. respectively. The low water recovery for the longer shut-in case can be attributed to deeper imbibition of water over time. Faster cleanup of mobile water from the matrix may also be responsible for the higher cumulative gas production observed here. Although some field studies have shown benefits from higher shut-in, those results may be attributed to other factors such as cleanup of liquid loaded induced fractures due to matrix imbibition over time or due to relaxation of geo-mechanical stresses in the neighborhood of the fracture which would impact the rock permeability. Figure 3.41 below shows that even though the initial productivity after flow-back starts is higher for 89 days shut-in, the peak productivity is higher for 2 days shut-in case.

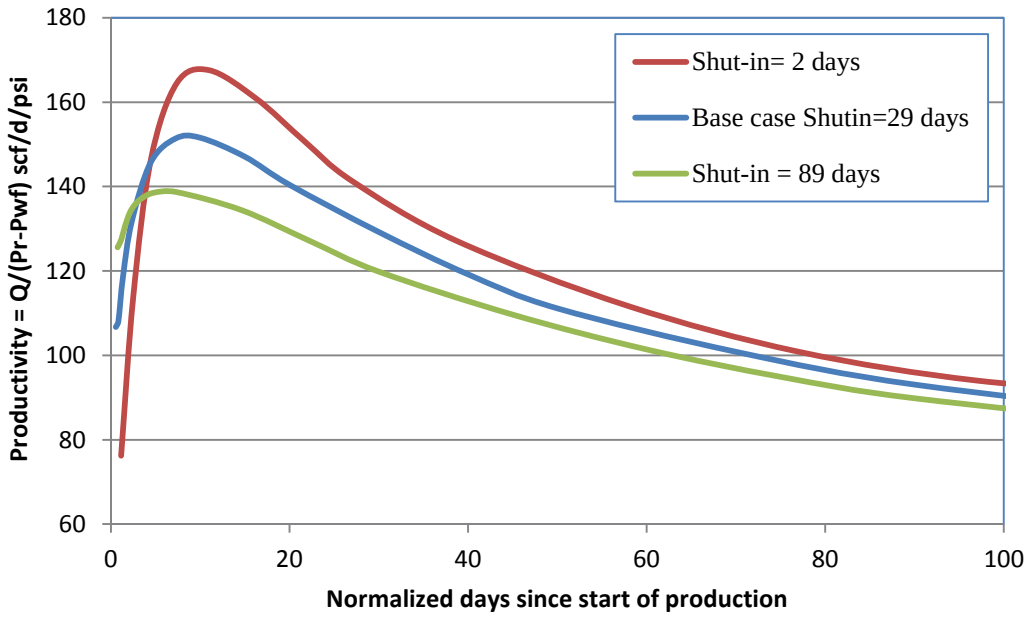

Figure 3.41: Effect of shut-in time on gas productivity

3.5. SUMMARY

This chapter discussed the black oil simulation results for flow back after fracturing operation and identified the scenarios under which there is higher possibility of liquid loading within hydraulic fractures. The results indicate that lower matrix permeability, lower drawdown, higher fracture permeability and lower fracture height lead to higher chances of loading. This loading may affect the total gas production depending on the cleanup of the fracture and the matrix in adjoining areas. However, considering that the lower half of the fracture is possibly the most effectively propped zone, liquid loading in this zone will severely impact gas productivity.

The results have validated the possibility of liquid loading within hydraulic fractures and provide motivation for further detailed compositional modeling of the process including the effects of more mechanisms such as water block cleanup through evaporation and dependence of relative permeability on phase velocity. These effects are studied in the following chapters.

Chapter 4: Flow Back Modeling Using Compositional Simulation

In the previous chapter the problem of fracture cleanup was studied under the assumption that no water is removed by evaporation. In this chapter a compositional simulator is used to study the importance of evaporation and velocity dependent relative permeabilities on frac-water removal from a dry gas reservoir.

4.1 Introduction to GEM

GEM is CMG's advanced equation of state compositional simulator that is used to study the complex compositional and inter-phase interactions of multiphase reservoir fluids during primary and enhanced recovery operations. Complex interactions between reservoir fluids and non-native fluids such as injected water, gas and polymer at reservoir conditions can often make the task of modeling a realistic model difficult. Phenomena such as vaporization and swelling of oil, liquid drop out from gas, viscosity and IFT variation, in addition to miscibility between two fluids can be studied through GEM.

Similar to CMG IMEX, GEM offers Cartesian, cylindrical and variable thickness grids in addition to explicit, fully implicit and adaptive implicit solution modes. In adaptive implicit mode a few blocks are solved fully implicitly whereas the rest are solved explicitly. The adaptive implicit method selects a block's implicitness dynamically during computation. This is very useful in study of coning issues where high rates are observed near wellbore.

GEM uses the Peng-Robinson or the Soave- Redlich-Kwong equations of state to perform the phase change calculations. It uses the proprietary quasi-Newton successive substitution method, QNSS, to solve the nonlinear equations associated with the flash

calculations. Phase stability is tested using Gibbs free energy criteria. GEM can simultaneously perform both the flash and reservoir flow equations at each time step. It offers the capability to specify local variations in rock types and fluid compositions as well as complex reservoir heterogeneity.

Changes in applied stresses during production from a reservoir can have a significant impact on its long term performance. These changes might include plastic deformation, compaction drive in cyclic injection/production strategies, injection induced fracturing, as well as near-well formation failure. GEM implements a geo-mechanical model consisting of three sub-modules for handling the problems referred above. The coupling between the geo-mechanical model and the simulator is done in a modular and explicit fashion. This increases the flexibility and portability of the model, and decreases computational costs.

Similar to IMEX, GEM uses the AIMSOL solver. It has seven distinct keyword groups that are used to specify and simulate the desired scenario. The following order of sections needs to be followed in every simulation deck file:

1. I/O Control
2. Reservoir Description
3. Component Properties
4. Rock-fluid Data
5. Initial Conditions
6. Numerical Methods Control
7. Geo-mechanics Data
8. Well Data and Recurrent Data

4.2 WATER BLOCK CLEANUP THROUGH EVAPORATION

In Mahadevan et al. (2003, 2005), the authors have discussed the evaporative cleanup of water blocks in gas wells. Under this phenomenon, as the saturated gas moves through a low pressure zone it becomes unsaturated and increases its water vapor carrying capacity. Water moves from liquid to vapor phase and is removed along with the gas. Higher volume of gas flow leads to more drying. A simple way to understand the concept is to look at Raoult's Law:

$$\frac{P_{vap}(T)}{P} = \frac{y_{vap}}{x_{liq}}$$

It shows that at a fixed temperature and therefore, a fixed vaporization pressure, when the ambient pressure drops the mole fraction of the fluid in vapor phase goes up. The study by Mahadevan determined two primary effects that operate simultaneously for the cleanup of water blocks: 1) water displacement and 2) evaporation. The effect of evaporation however, dominates only over a long time of production. High drawdown, high temperature and high matrix permeability, along with use of alcohols and fractured wells enhance evaporative cleanup, according to the study. However, the model assumed evaporative cleanup to take place only after a steady-state saturation profile had been established following displacement.

In this study the effect of evaporative cleanup is modeled using CMG GEM™ and is allowed to occur from the beginning of flowback. In GEM, water evaporation can be optionally turned on/off using the *H2O_INLCUDED and *OGW_FLASH *ON keywords. These keywords designate water as one of the components of the

compositional simulation whose phase state will be dictated by the Gibbs free energy. The user can also specify a residual water saturation for evaporation using the *SWR_H2OVAP keyword.

4.3 VELOCITY DEPENDENT RELATIVE PERMEABILITY (VDRP)

Pope et al. (2000) presented a new relative permeability model for accurately modeling gas condensate reservoirs. The study notes that once the near well bore pressure drops below the dew point, condensate starts dropping out of the gas and starts depositing near the wellbore. This increase in condensate (oil phase) saturation leads to a decrease in the gas phase relative permeability. Even lean fluids have been reported to cause considerable damage. Most of the time, relative permeability is considered to be a function of only surface tension (capillary trapping). However, to quantitatively model the actual condensate saturation and its impact on gas relative permeability, one must model more detailed physics behind the process. Brownell and Katz (1947) among others, postulated that residual oil saturation (and thus relative permeability) will be a function of the viscous forces (trying to displace oil) and the capillary forces (trying to keep it in the pores). Since the viscous forces are proportional to the velocity of the displacing fluid or the pressure gradient causing this displacement, a capillary number was introduced to represent the ratio of the viscous and capillary forces:

$$N_{c_l} = \frac{|\vec{\vec{k}} \cdot \vec{\nabla} \Phi_l|}{\sigma_{ll'}}$$

In this equation, *l* is the displaced phase and *l'* is the displacing phase.

It was also noted that in some cases buoyancy forces contribute significantly to the forces acting on the trapped phase. To include its effect, Bond number was introduced in the model. It is defined as the ratio of buoyancy related forces to the capillary forces and is calculated as:

$$N_{B_l} = \frac{kg(\rho_{l'} - \rho_l)}{\sigma_{ll'}}$$

Hence to completely account for all the forces that are acting on the trapped phase, Trapping number was introduced and is calculated as a vector sum of the capillary and Bond number :

$$N_{T_l} = \frac{|\vec{\vec{k}} \cdot (\vec{\nabla}\Phi_{l'} + g(\rho_{l'} - \rho_l)\vec{\nabla}D)|}{\sigma_{ll'}}$$

The new model postulates that the residual saturation for phase l is a function of this trapping number and calculates it as:

$$S_{lr} = \min\left(S_l, S_{lr}^{\text{high}} + \frac{S_{lr}^{\text{low}} - S_{lr}^{\text{high}}}{1 + T_l (N_{T_l})^{\tau_l}} \right)$$

The parameters T_l and τ_l are determined by fitting data to experimental data. S_{lr}^{high} is typically zero and refers to the residual saturation for very high displacement velocities or forces. Once the residual saturation is available, end point relative permeability can be calculated using:

$$k_{rl}^0 = k_{rl}^{0\ \text{low}} + \frac{S_{l'r}^{\text{low}} - S_{l'r}}{S_{l'r}^{\text{low}} - S_{l'r}^{\text{high}}} (k_{rl}^{0\ \text{high}} - k_{rl}^{0\ \text{low}})$$

Here, $S_{l'r}$ is the residual saturation of the conjugate phase. For example condensate is conjugate phase for gas. All the parameters with low or high superscript are constants for a given rock and fluid pair.

After obtaining the end point relative permeability, relative permeability variation as a function of saturation is calculated using a Corey-type relative permeability function. A generalized form of the same was developed and is given as:

$$\log k_{rl} = \log k_{rl}^{0} + \log \overline{S_l} + \frac{\log\left(\frac{k_{rl}}{k_{rl}^{0}}\right)^{\text{low}} - \log \overline{S_l}}{1 + T_{l'}(N_{T_l})^{\tau_{l'}}}$$

The normalized saturation in the above equation is calculated as:

$$\overline{S_l} = \frac{S_l - S_{lr}}{1 - \sum_{l=1}^{n_p} S_{lr}}$$

Here, n_p is the number of phases present, S_l is the saturation and S_{lr} is the residual saturation of that phase.

The benefit of the model lies in the fact that only reference relative permeability curve of each phase at low trapping number and residual saturations as function of trapping number are need to get the condensate and gas relative permeability for wide range of trapping numbers using only T_l and τ_l .

The application of this model to field studies has proven that higher viscous forces are able to strip away more condensate from near well bore region and therefore, the gas relative permeability damage is less. The effect of this relative permeability

model on fracture fluid cleanup was investigated in this study using the velocity dependent relative permeability option available in CMG GEM.

The *VELDEPRP keyword is used to activate this relative permeability model and provides two model options with different input requirements. Model 1 can apply this model to all three flowing phases including water whereas Model 2 is only applicable to gas and condensate. Some of the parameters that are required for Model 1 include:

1. **T_g, T_c, T_w :** These are the parameters from the Pope et al. model used to calculate residual phase saturation.

2. **N_{cbc}, N_{cbg}, N_{cbw} :** This is the threshold capillary number for the gas, condensate or water phase. If internally calculated capillary number is less than the threshold then the relative permeability applied is equal to the base relative permeability and there are no capillary number effects.

3. **τ_g , τ_c , τ_w :** These are the τ_l parameters from the Pope et al. model. The default value is one.

4. **S_{rg}^{high}, S_{rc}^{high}, S_{rw}^{high} :** This is the residual phase saturation under high capillary number limit. Generally it is zero.

5. **$k°_{rg}^{high}$, $k°_{rc}^{high}$, $k°_{rw}^{high}$:** These are the end point relative permeabilities for gas, condensate and water phases. Generally these values are 1.

6. **α_g , α_c , α_w :** These are the 'low' exponents used in calculating log k_{rl} from the Pope et al. model.

4.4 SIMULATION MODEL SETUP

This model is used to study the compositional effects such as evaporative cleanup and velocity dependent relative permeability in a dry gas-water system, using GEM 2011. A Cartesian grid with dimensions 50 X 20 X 20 grids is used. A single, bi-wing lateral fracture is placed symmetrically in the center of the grid and modeled using high porosity and permeability. Local grid refinement is utilized for stable computation. The total dimensions of the reservoir model are 600 ft. X 1560 ft. X 100 ft. The dimensions of the fracture are 480 ft. (wide) X 55ft. (high) X 0.1 ft. (thick). The reservoir properties are as specified in Table 4.1.

Property/ Parameter	**Value**
Matrix Permeability	0.1 μD
Fracture Permeability	2 D
Reservoir Thickness	100 ft.
Matrix Porosity	10 %
Fracture Porosity	60 %
Fracture Height	55 ft.
Fracture Thickness	0.1 ft.
Fracture Half Length	240 ft.
Gas-Water Surface tension	40 dyne/cm
Water Density	60 lb/ft^3
Flowing Wellbore pressure	4500 psi
Initial Reservoir Pressure	6500 psi
Initial Water Saturation	0.3
Residual Water Saturation	0.3
Reservoir Temperature	300 F

Table 4.1: Simulation base model properties

The Peng-Robinson equation of state is used to capture the phase behavior of the methane-water system. The phase behavior of this system is shown below in Figure 4.1:

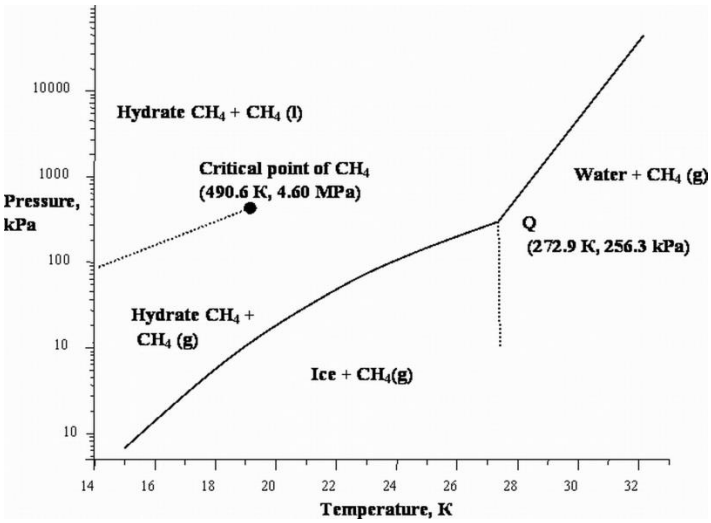

Figure 4.1: Methane-Water P-T diagram

The reservoir conditions chosen here (~45000 kPa and 422 K) are such that water is primarily in the aqueous phase with small mole fractions in the vapor phase. Methane is in the gas phase.

Two sets of relative permeability curves are used, which will be referred to henceforth as Set-1 and Set-2. The parameter values for these sets are given in Tables 4.2 and 4.3 below. The two relative permeability sets are represent two different end point water mobility scenarios. Set-1 offers higher mobility as compared to Set-2. Higher end point water relative permeability is expected to enhance early time frac-water cleanup.

Parameter	Value
Residual water saturation, S_{wr}	0.3
Residual gas saturation, S_{gr}	0.2
(Matrix) Water end point rel-perm, $K_{rw}°$	0.45
(Matrix) Gas end point rel-perm, $K_{rg}°$	1
(Fracture) Water end point rel-perm, $K_{rw}°$	0.7
(Fracture) Gas end point rel-perm, $K_{rg}°$	0.9

Table 4.2: Relative permeability Set-1 properties

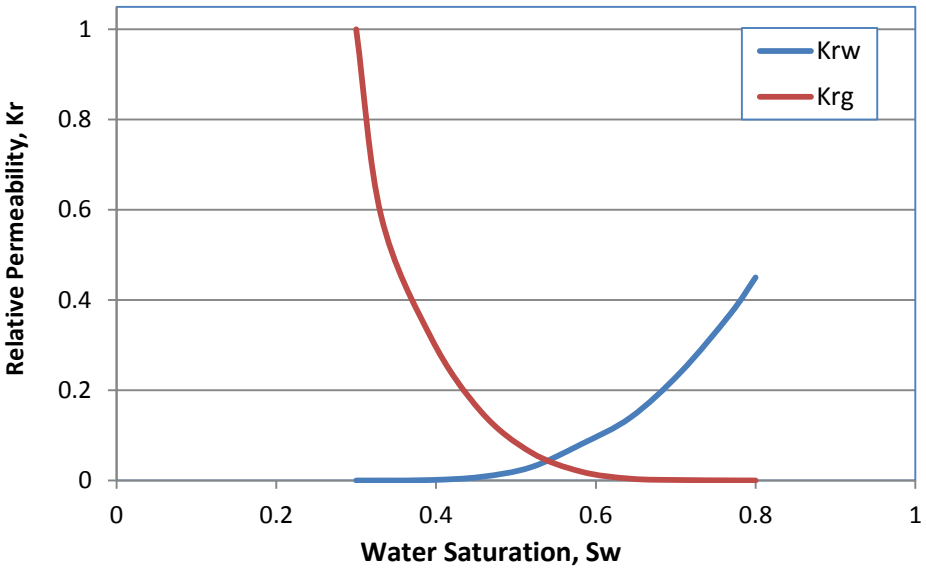

Figure 4.2: Matrix gas-water relative permeability curves, Set-1

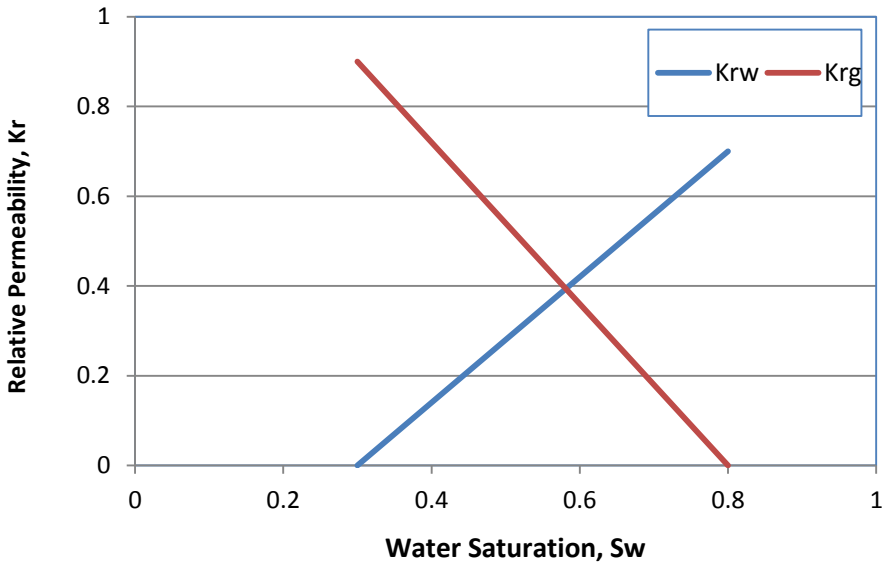

Figure 4.3: Fracture gas-water relative permeability curves, Set-1

The parameter values for Set-2 are shown in Table 4.3 below:

Parameter	Value
Residual water saturation, S_{wr}	0.2
Residual gas saturation, S_{gr}	0.3
(Matrix) Water end point rel-perm, $K_{rw}°$	0.15
(Matrix) Gas end point rel-perm, $K_{rg}°$	0.8
(Fracture) Water end point rel-perm, $K_{rw}°$	0.3
(Fracture) Gas end point rel-perm, $K_{rg}°$	0.8

Table 4.3: Relative permeability Set-2 properties

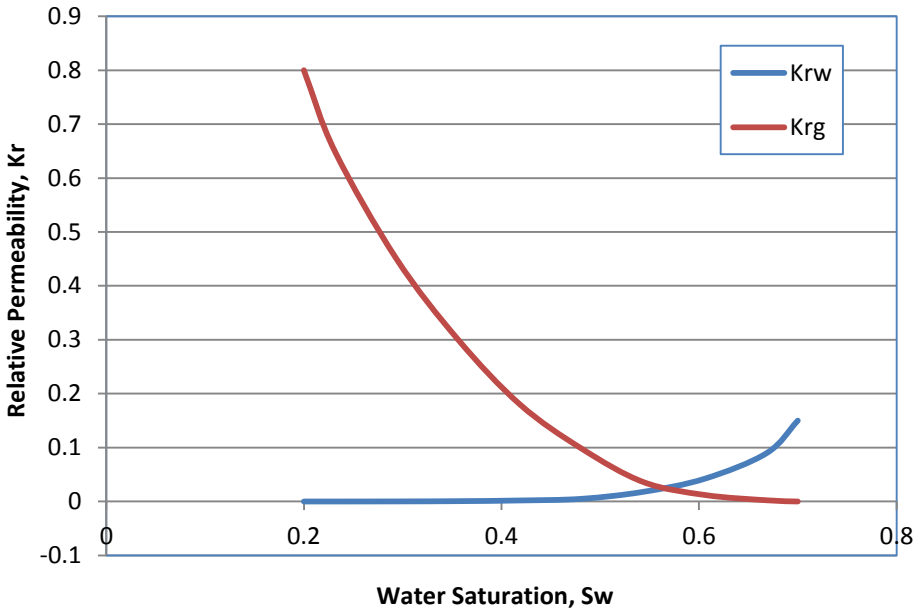

Figure 4.4: Matrix gas-water relative permeability curves, Set-2

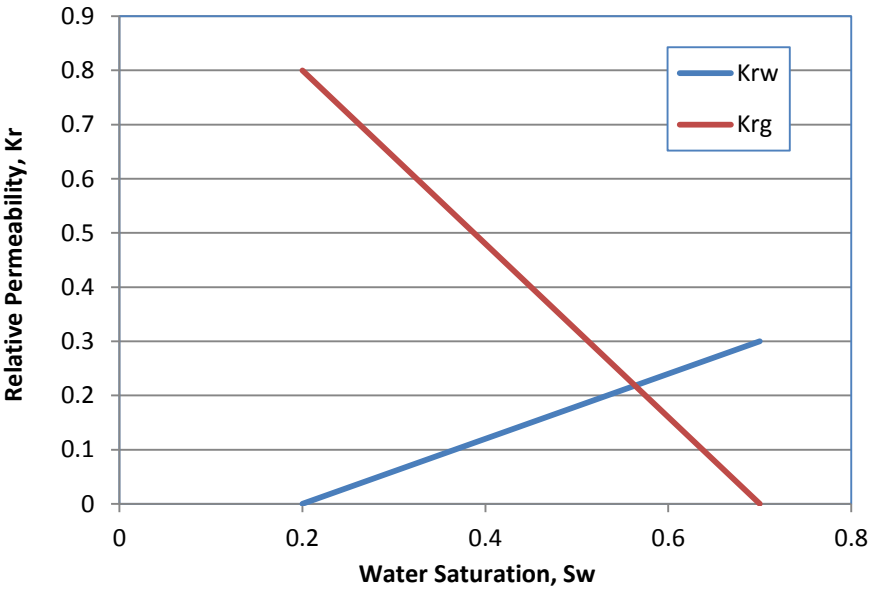

Figure 4.5: Fracture gas-water relative permeability curves, Set-2

Considering extremely low capillary pressures within fractures, straight line relative permeability curves are used as shown in Figures 4.3 and 4.5. For scenarios where the velocity dependent relative permeability model is used, following model parameters are used as per Table 4.4.

Parameter	Value
T_w	250
T_o	3000
T_g	24556
τ_w, τ_o, τ_g	1
S_{rg}^{high}, S_{ro}^{high}, S_{rw}^{high}	0
$k°_{rg}^{high}$, $k°_{ro}^{high}$, $k°_{rw}^{high}$	1
$\alpha_g, \alpha_o, \alpha_w$	4, 2.9, 1
N_{cbo}, N_{cbg}, N_{cbw}	0

Table 4.4: Velocity dependent relative permeability model properties

In the dry gas scenarios as considered in this chapter, there is no condensate dropout.

The simulation setup is similar to the black oil simulation scenarios discussed in the previous chapters. 1000 bbl. of water is injected into the fractured well within 1 day. This is followed by a 29 day shut-in period, and the well is put into production after the 30^{th} day. A constant bottom-hole pressure is applied to put the well on production.

4.5 RESULTS

In the previous chapter, the results indicated a realistic possibility of frac-water build up at the bottom of the fracture. In this chapter, compositional simulation of the same process is performed, which includes the effects of water evaporation and velocity dependent relative permeability. The objective is to observe the extent of additional cleanup possible due to these effects. Water saturation is monitored both inside and near the fracture face to understand the importance of evaporation in liquid removal and wellbore fluid cleanup.

4.5.1. Base Case: No evaporation, No VDRP (Relative perm. Set-1)

In this case, neither water evaporation nor VDRP model is turned on. Water cleanup is purely a displacement process against capillary and gravity forces. The cleanup profiles within the fracture and matrix are shown in Figures 4.6 – 4.8 and indicate that there is considerable fracture bottom loading until 100^{th} day. Even after 500^{th} day of operation, water saturation in fracture is ~ 0.45, which is higher than 0.3, residual water saturation. The cumulative gas recovery is 16.87 MMscf. Fine gridding was applied to the entire fracture volume in order to overcome numerical instabilities.

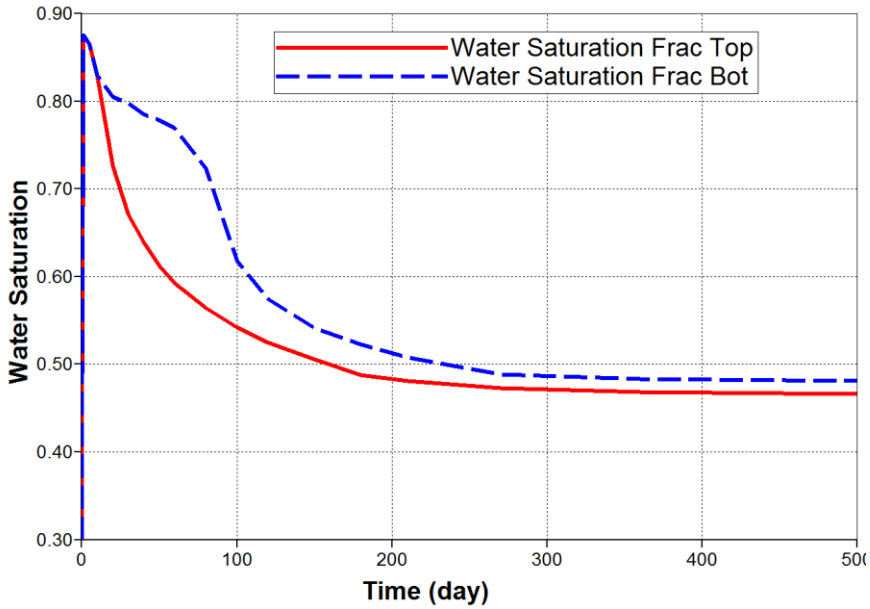

Figure 4.6: Variation of water saturation inside fracture over time
(No evaporation, No VDRP)

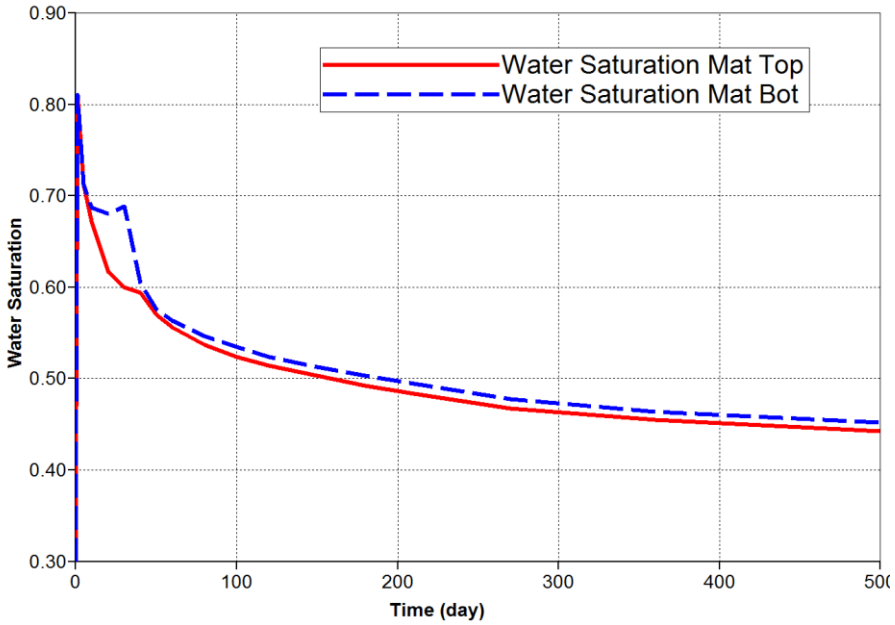

Figure 4.7: Variation of water saturation inside matrix 0.1 ft. from fracture face with time
(No evaporation, No VDRP)

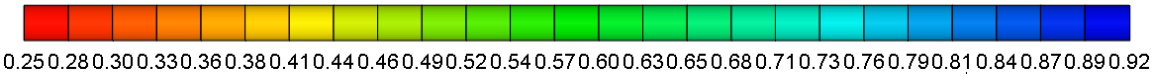

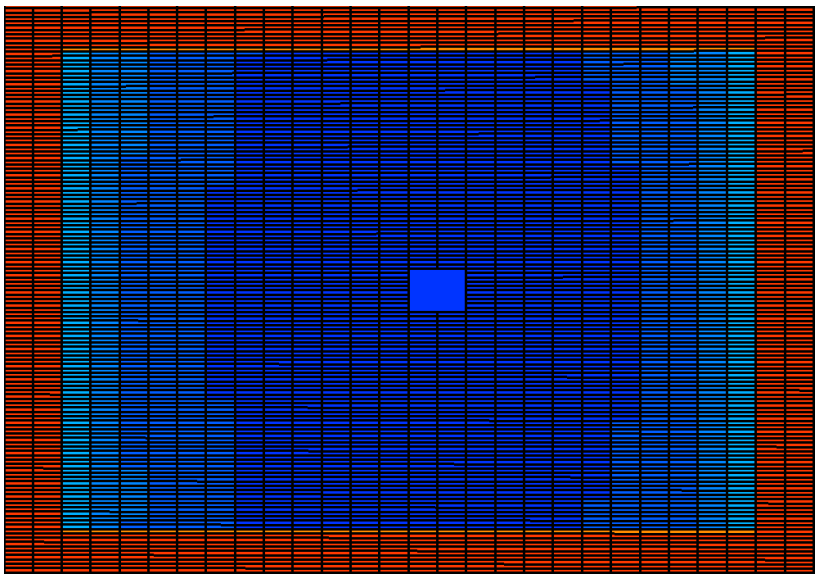

Water saturation inside fracture after 1 day (end of fracture treatment)

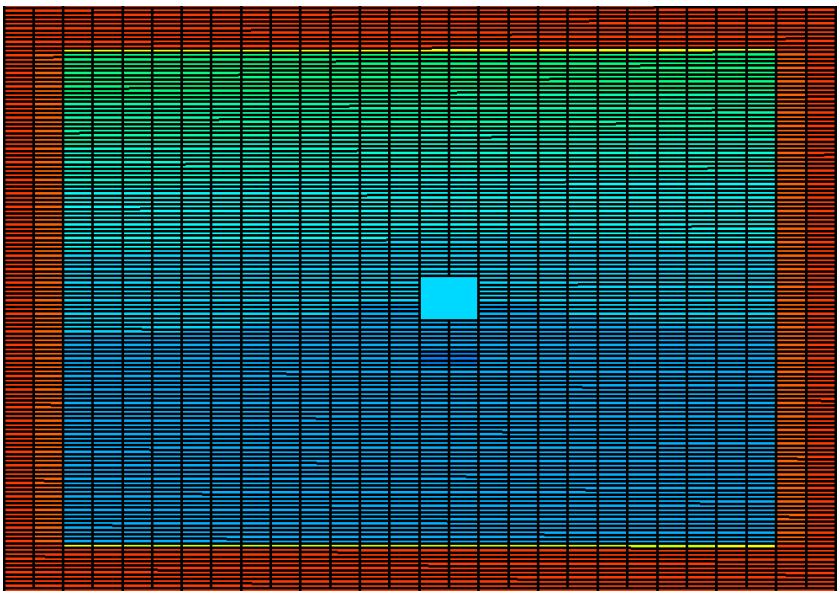

Water saturation inside fracture after 30 days (beginning of production, end of shut-in)

Figure 4.8: Water saturation maps (No evaporation, No VDRP)

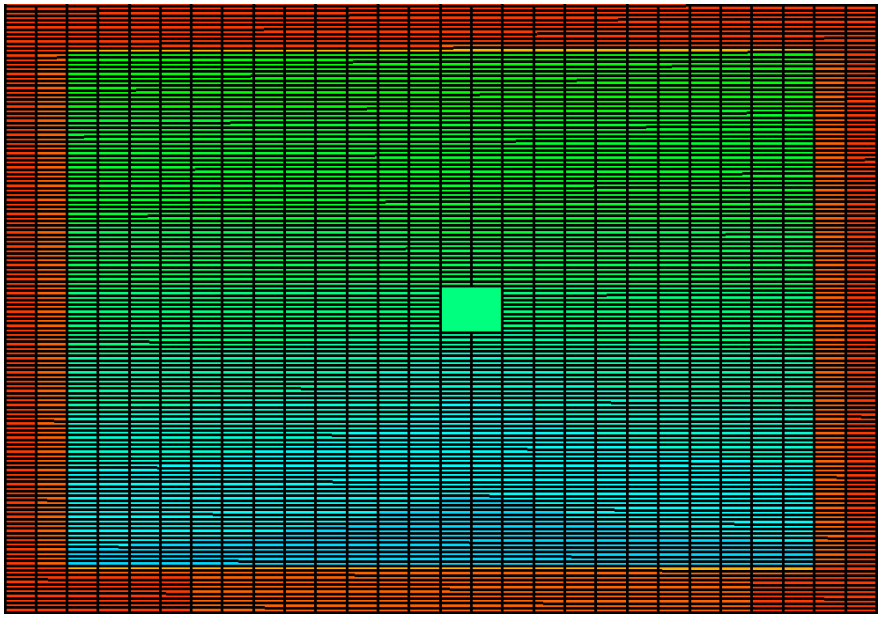

Water saturation inside fracture after 60th day

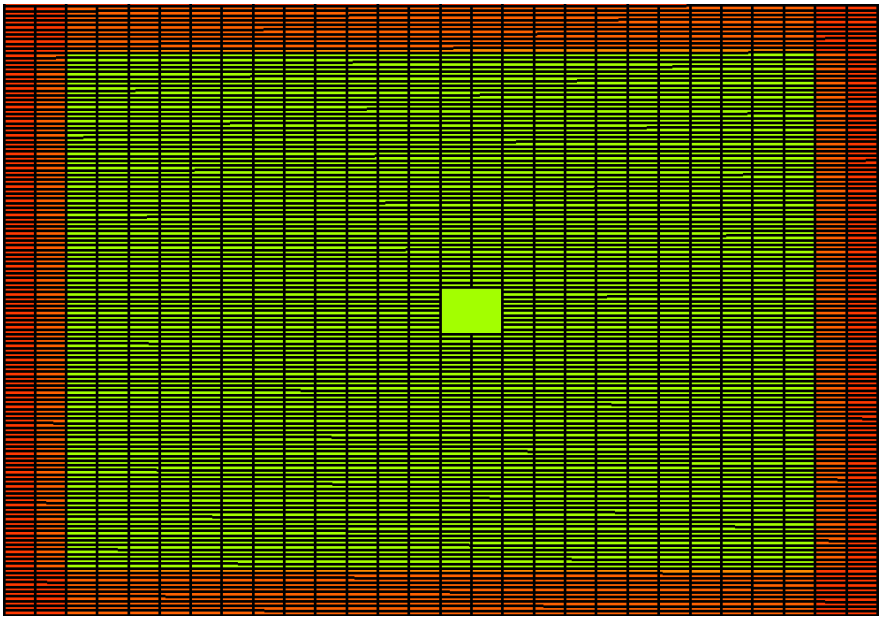

Water saturation inside fracture after 500 days (end of production)

Figure 4.8: Water saturation maps (No evaporation, No VDRP)- Continued

4.5.2. No evaporation, Only VDRP (Relative Permeability Set-1)

In this scenario, evaporation is neglected whereas velocity dependent relative permeability (VDRP) model is enabled. The cumulative gas recovery in this scenario was 18.3 MMscf. after the 500th day of operation. The cleanup profiles within fracture and matrix are shown in Figures 4.9-4.11. Cleanup is much faster as compared to the previous case and the final water saturation in fracture is ~ 0.4, both at top and bottom. This is because VDRP model leads to higher water saturation in fracture as compared to Base case and therefore, allows for faster frac-water cleanup from fracture. This is explained later in the discussions section. Better frac-water cleanup leads to higher cumulative gas recovery.

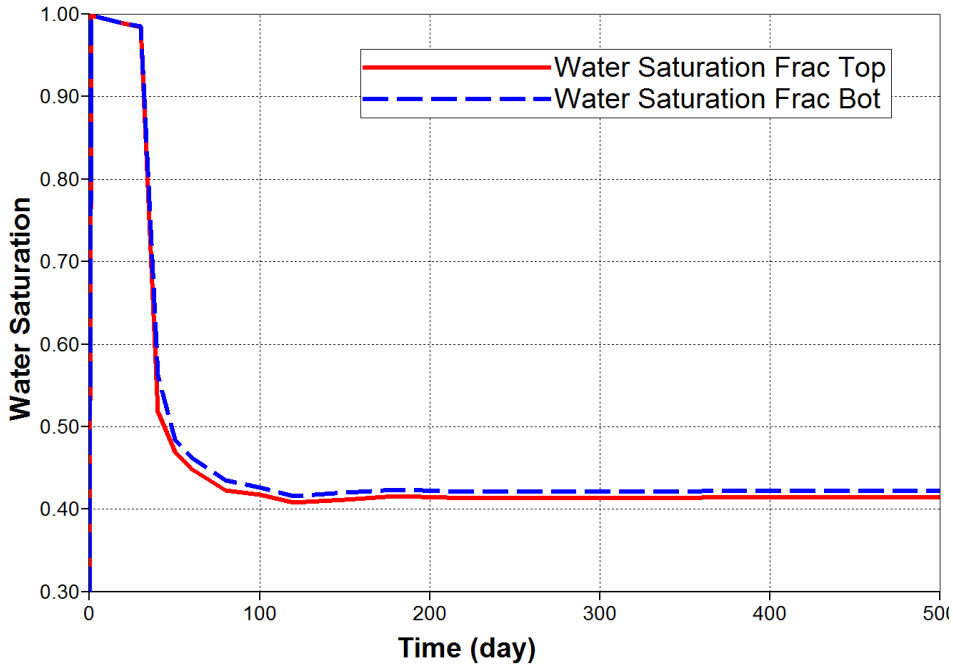

Figure 4.9: Variation of water saturation inside fracture over time (No evaporation, Only VDRP)

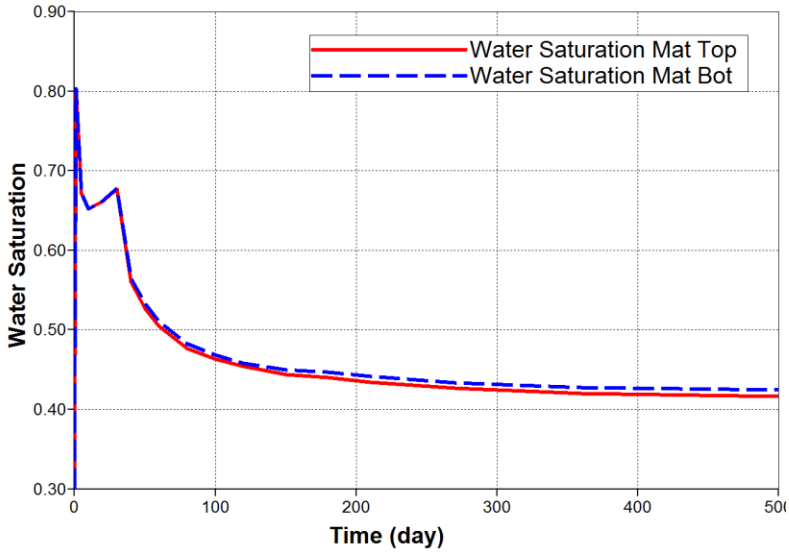

Figure 4.10: Variation of water saturation inside matrix 0.1 ft. from fracture face with time (No evaporation, Only VDRP)

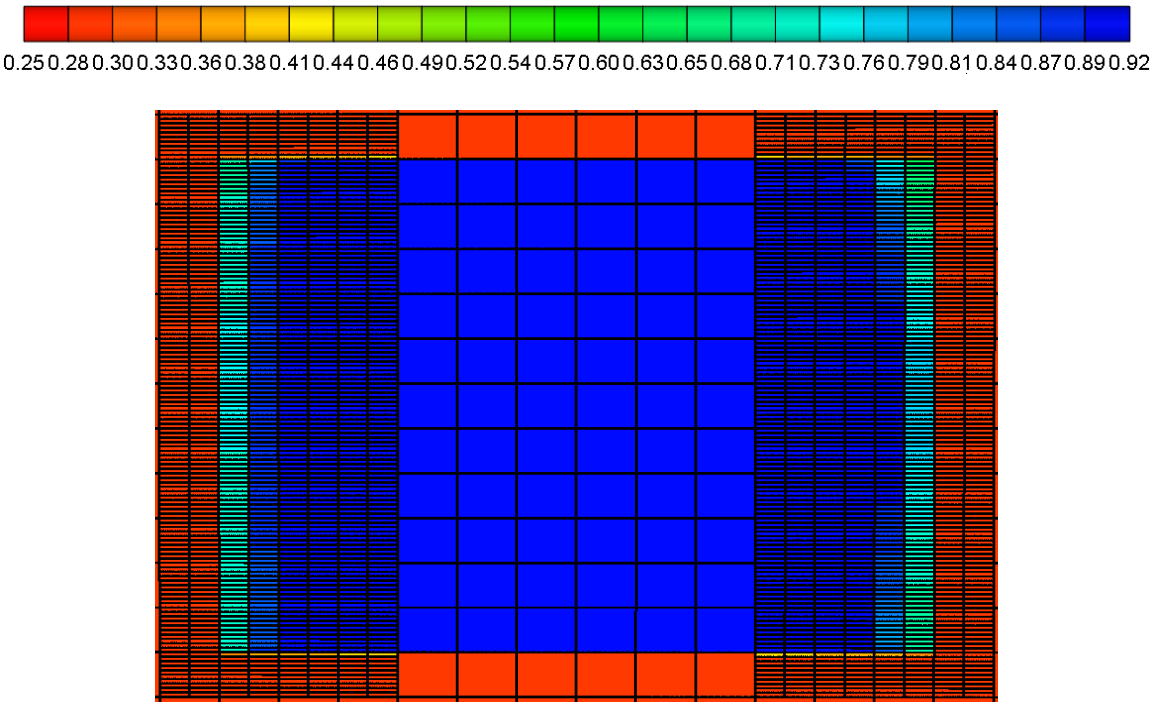

Water saturation inside fracture after 1 day (end of fracture treatment)

Figure 4.11: Water saturation maps (No evaporation, Only VDRP)

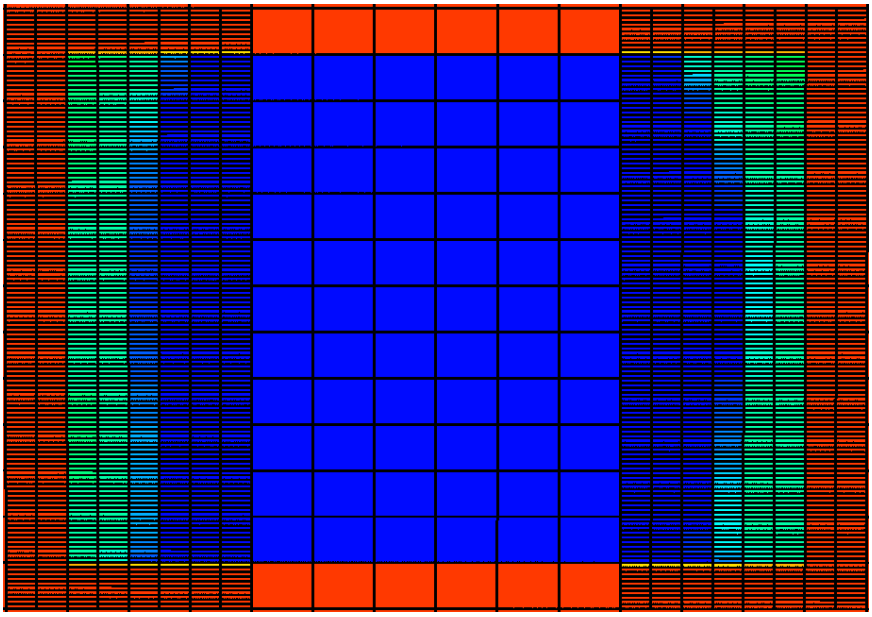

Water saturation inside fracture after 30 days (beginning of production, end of shut-in)

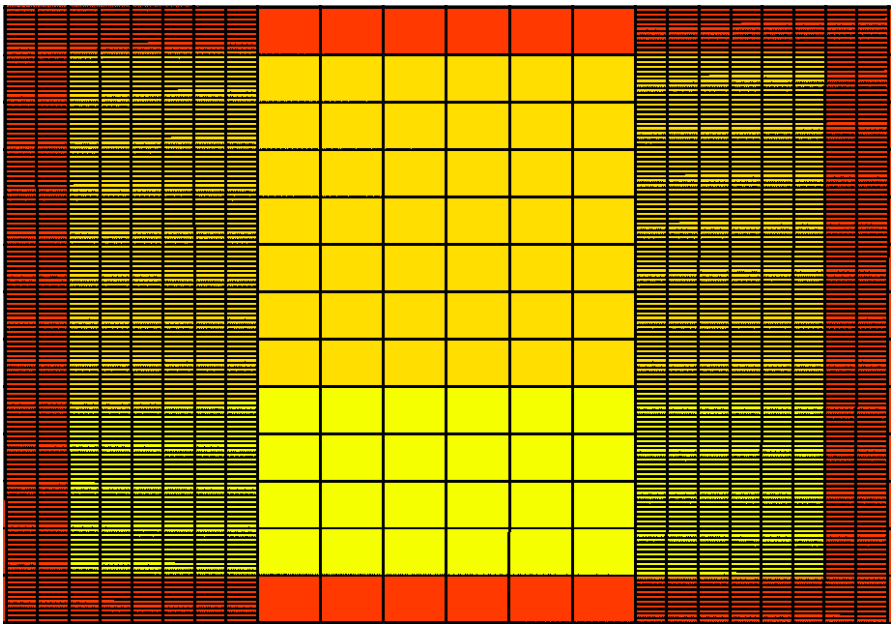

Water saturation inside fracture after 80 days

Figure 4.11: Water saturation maps (No evaporation, Only VDRP)- Continued

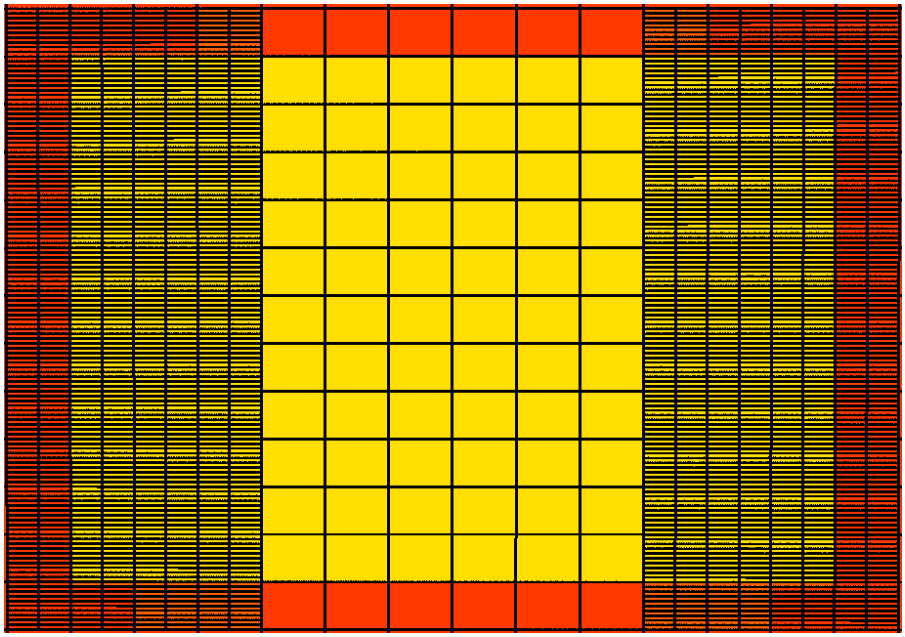

Water saturation inside fracture after 500 days (end of production)

Figure 4.11: Water saturation maps (No evaporation, Only VDRP)- Continued

4.5.3. Only evaporation, No VDRP (Relative Permeability Set-1)

When the VDRP option is turned off and only water evaporation model is turned on, the cumulative gas recovery is 17.4 MMscf. The cleanup profiles are as shown in Figures 4.12-4.14 and indicate that there is more cleanup with evaporation as compared to base case. However, this cleanup is not as rapid as due to VDRP effect. It is a long term, gradual effect and if the simulation is allowed to continue for longer duration then more clean-up is expected. Better frac-water cleanup as compared to base case leads to higher cumulative gas produced.

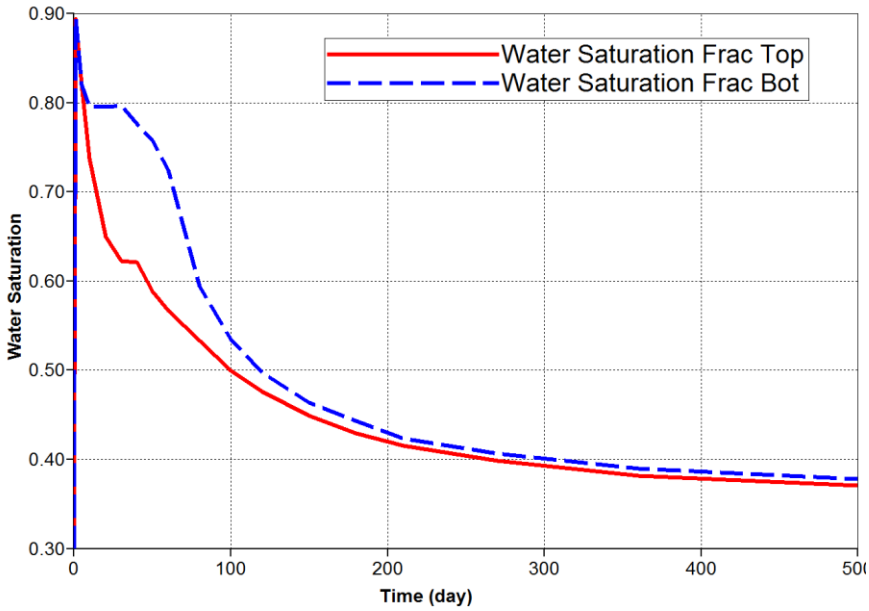

Figure 4.12: Variation of water saturation inside fracture over time (Only evaporation, No VDRP)

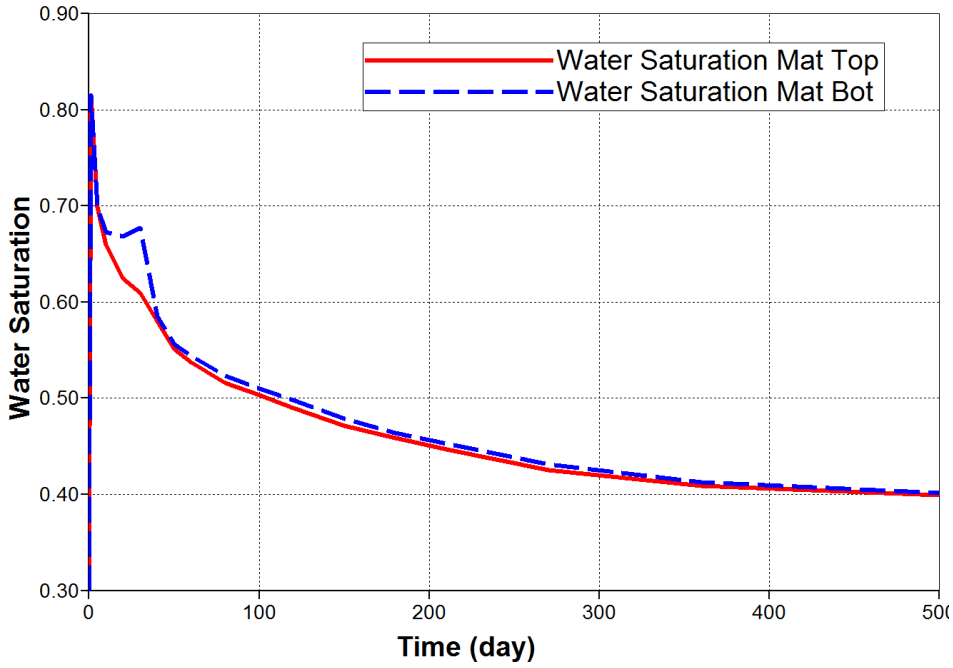

Figure 4.13: Variation of water saturation inside matrix 0.1 ft. from fracture face with time (Only evaporation, No VDRP)

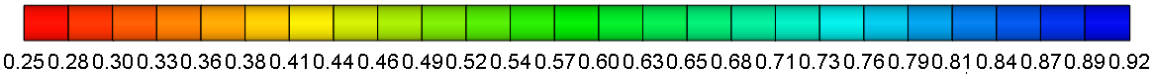

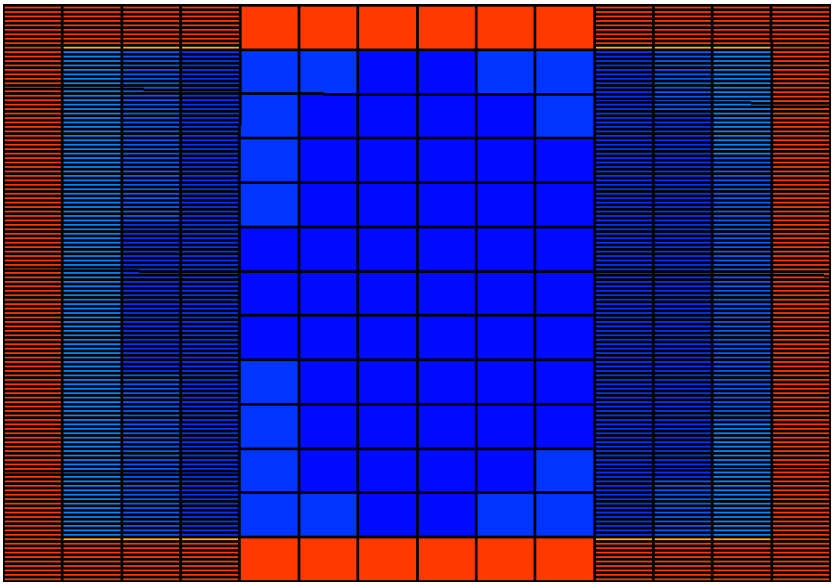

Water saturation inside fracture after 1 day (end of fracture treatment)

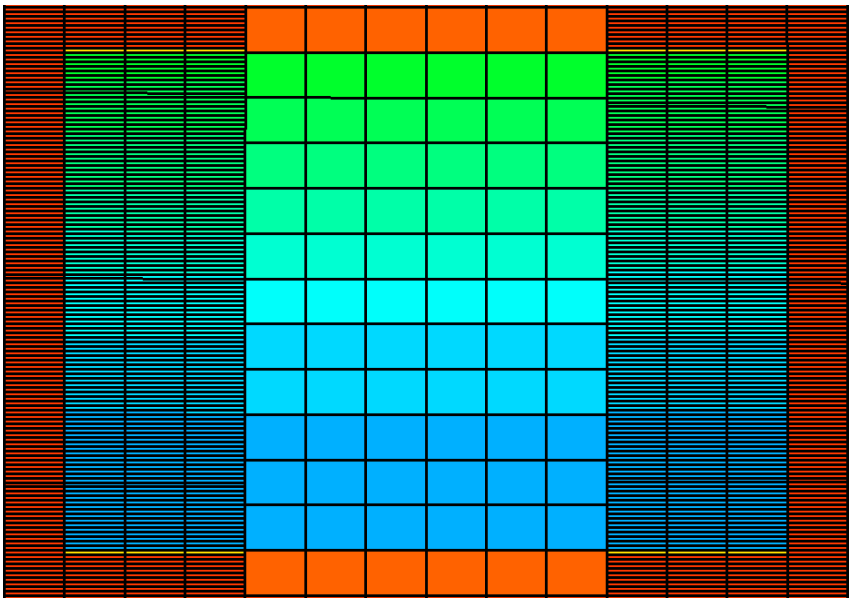

Water saturation inside fracture after 30 days (beginning of production, end of shut-in)

Figure 4.14: Water saturation maps (Only evaporation, No VDRP)

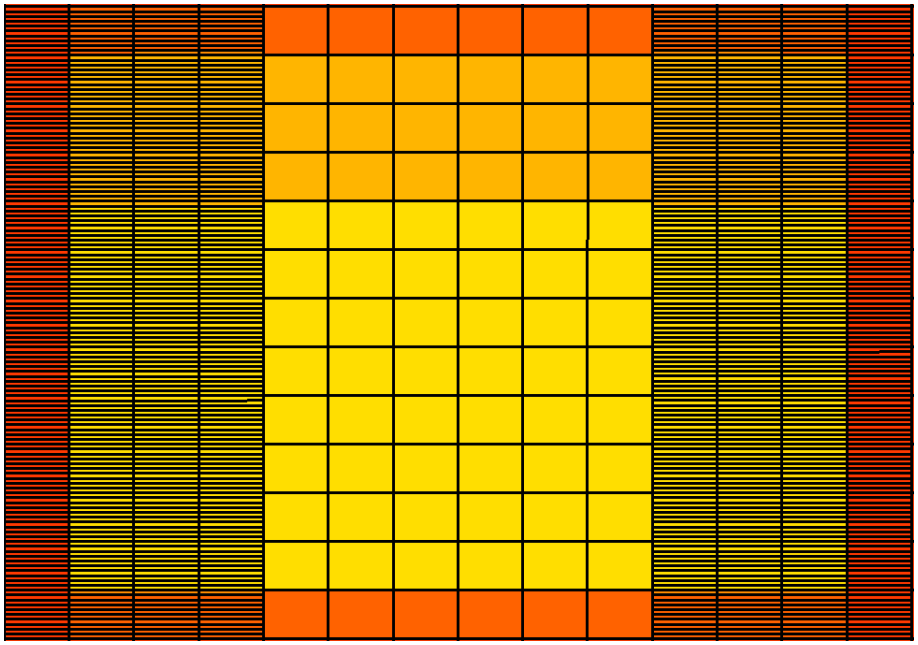

Water saturation inside fracture after 360 days

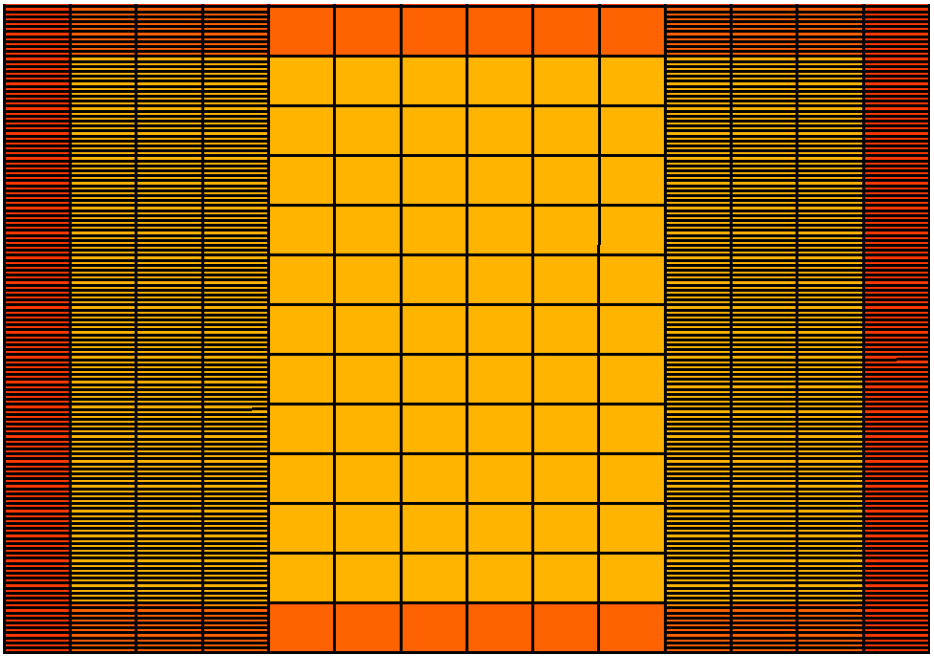

Water saturation inside fracture after 500 days (end of production)

Figure 4.14: Water saturation maps (Only evaporation, No VDRP)- Continued

4.5.4. Both evaporation and VDRP (Relative Permeability Set-1)

When both evaporation and VDRP effects are effective, the cleanup profiles within the fracture and in matrix near the fracture face are shown in Figures 4.15-4.17. As expected, combining the effects of evaporation and VDRP leads to a much faster and effective frac-water clean-up as compared to earlier cases. The terminal saturation in fracture after 500th day is ~0.35 which is lower than that from the base case or any of the effects acting alone. Also, top and bottom of the fracture don't indicate significant saturation differential indicating gravity effect is overcome.

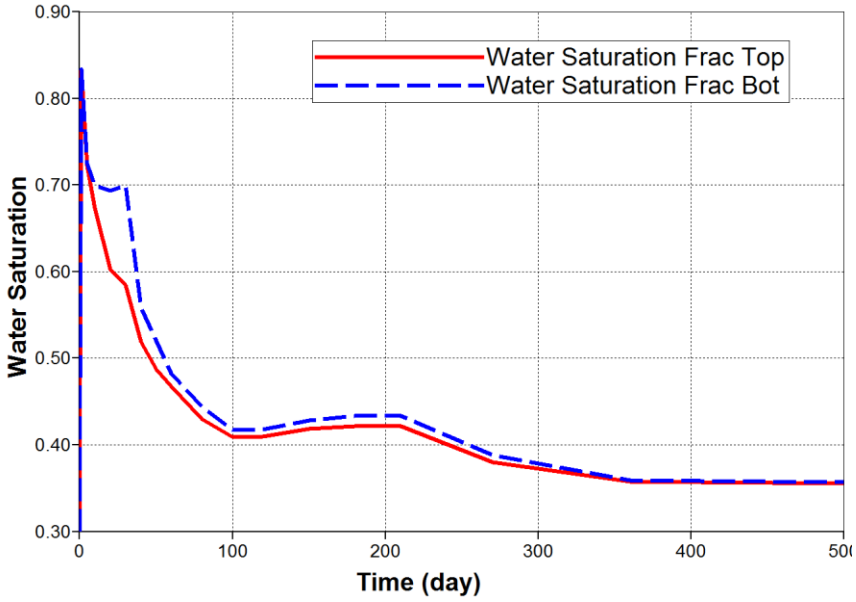

Figure 4.15: Variation of water saturation inside fracture over time (VDRP+Evaporation)

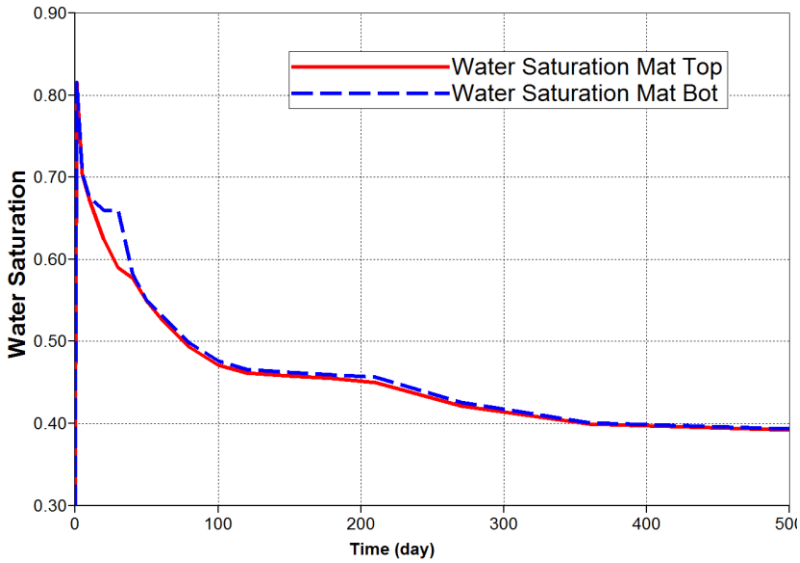

Figure 4.16: Variation of water saturation inside matrix 0.1 ft. from fracture face with time (VDRP+Evaporation)

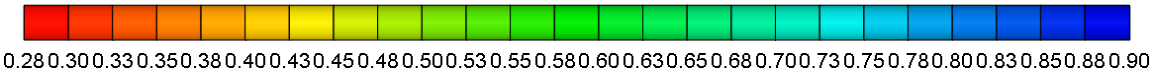

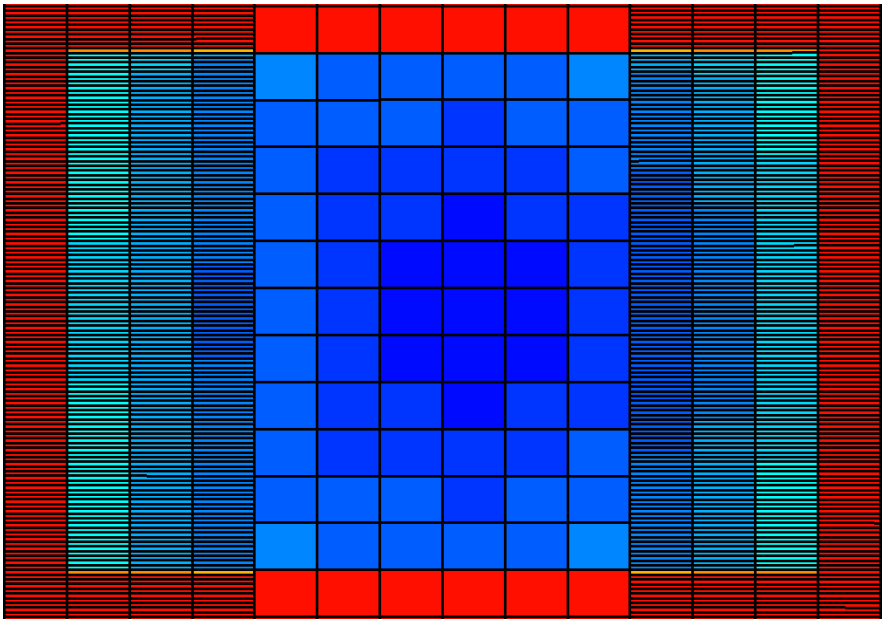

Water saturation inside fracture after 1 day (end of fracture treatment)

Figure 4.17: Water saturation maps (VDRP+Evaporation)

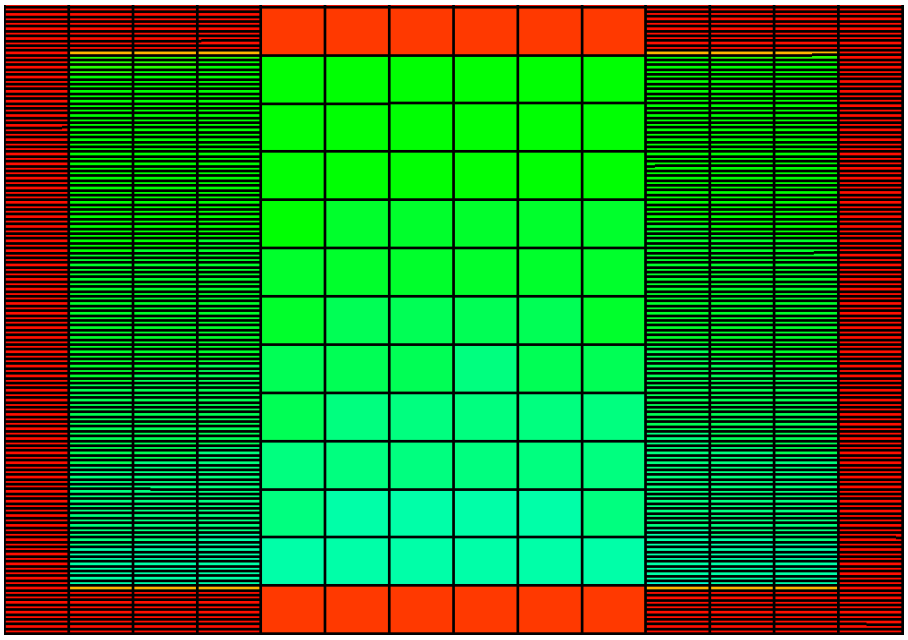

Water saturation inside fracture after 30 days (beginning of production, end of shut-in)

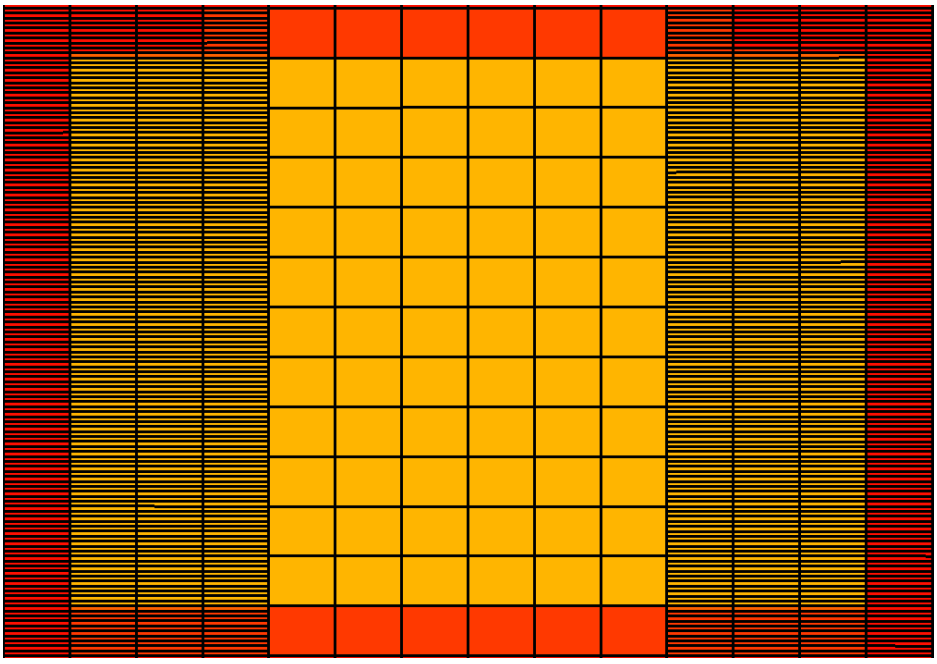

Water saturation inside fracture after 270 days

Figure 4.17: Water saturation maps (VDRP+Evaporation) - Continued

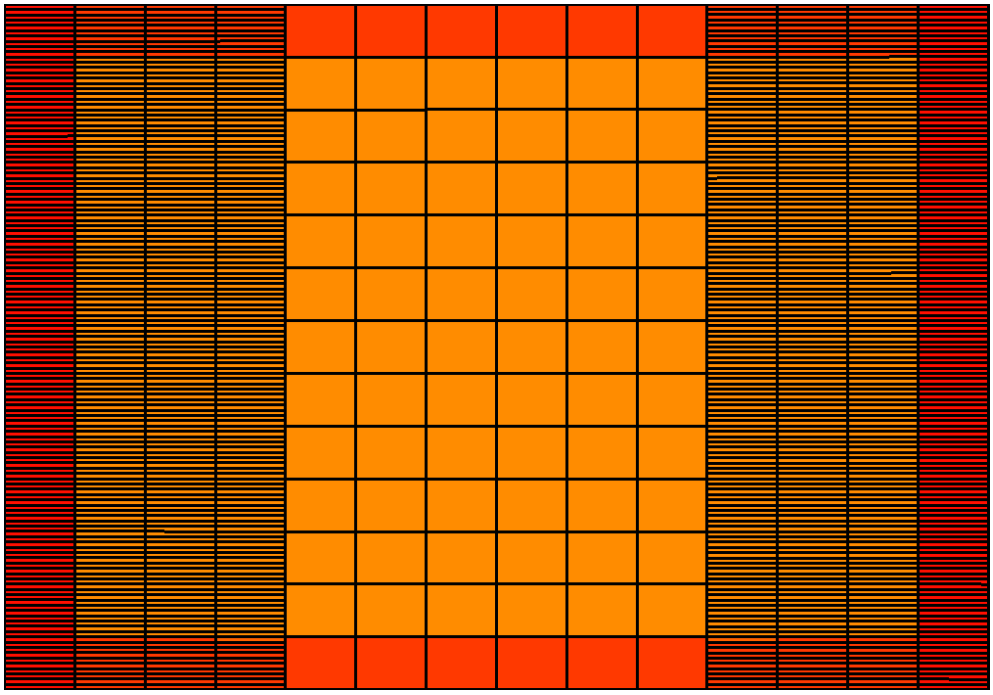

Water saturation inside fracture after 500 days (end of production)

Figure 4.17: Water saturation maps (VDRP+Evaporation) - Continued

4.5.5. Base Case: No evaporation, No VDRP (Relative perm. Set-2)

With Set-2 relative permeability curves, the initial (and residual) water saturation is 0.2 and the end point relative permeability for water is 0.15. The cleanup profiles within the fracture and the matrix are shown in Figures 4.18-4.20. The cumulative gas recovery after 500th day was 16.79 MMScf. Since end point relative permeability for water is lower than in Set-1, Set-2 corresponds to lower water mobility scenario. The results indicate slower initial frac-water cleanup as compared to Set-1. However cumulative gas recovery is not significantly different.

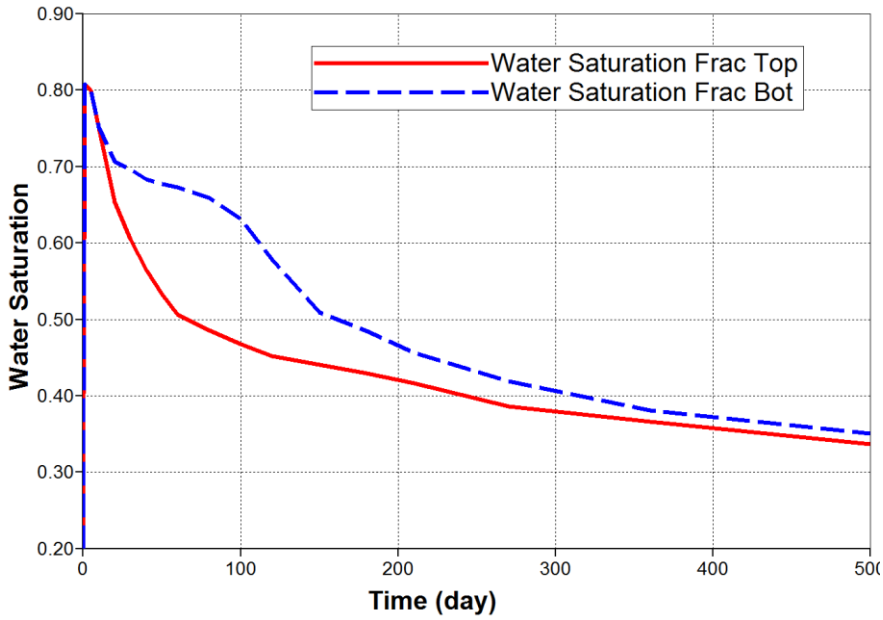

Figure 4.18: Variation of water saturation inside fracture over time (No evaporation, No VDRP)

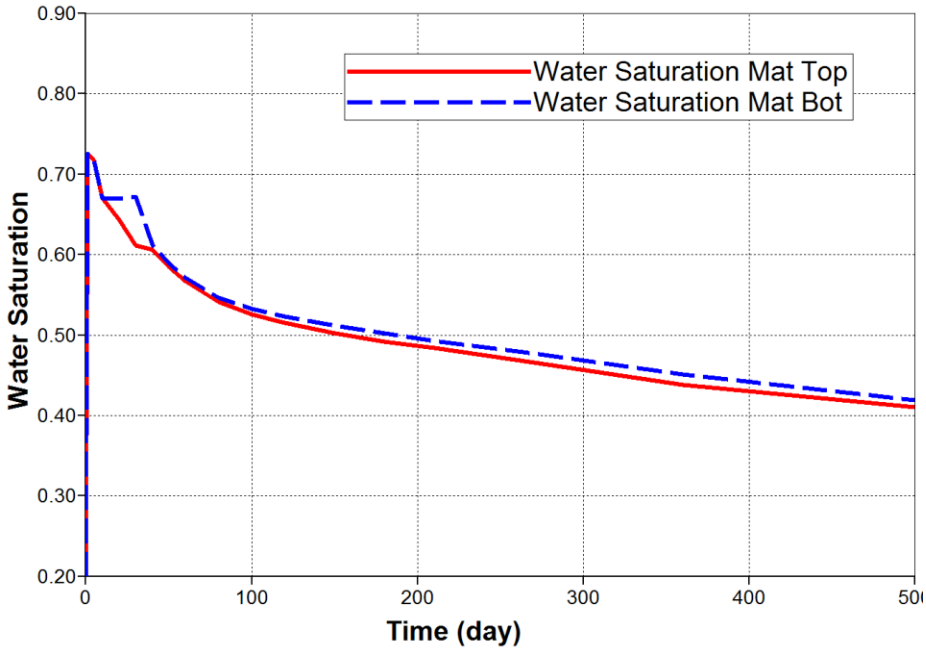

Figure 4.19: Variation of water saturation inside matrix 0.1 ft. from fracture face with time (No evaporation, No VDRP)

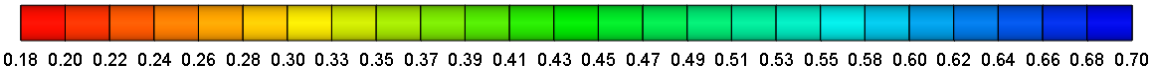

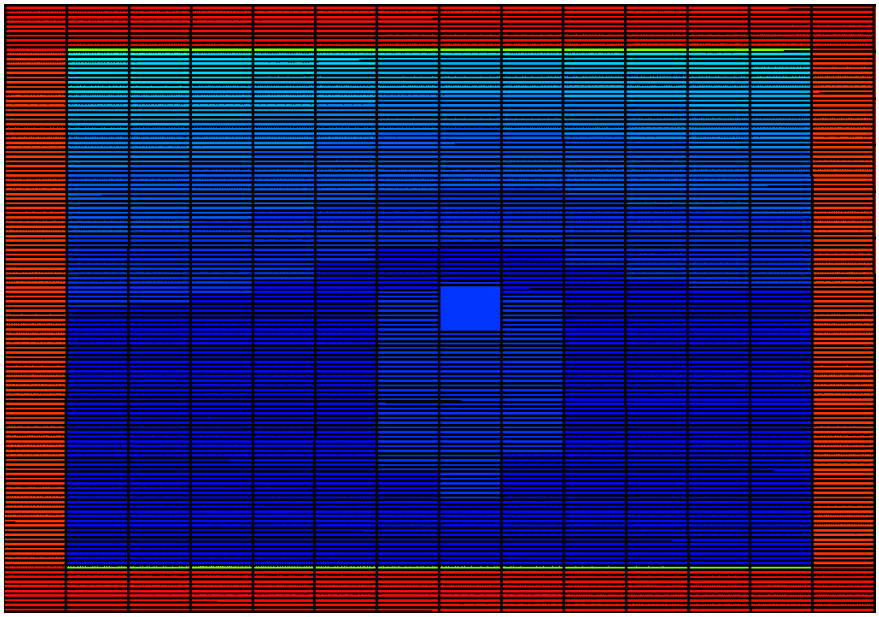

Water saturation inside fracture after 30 days (beginning of production, end of shut-in)

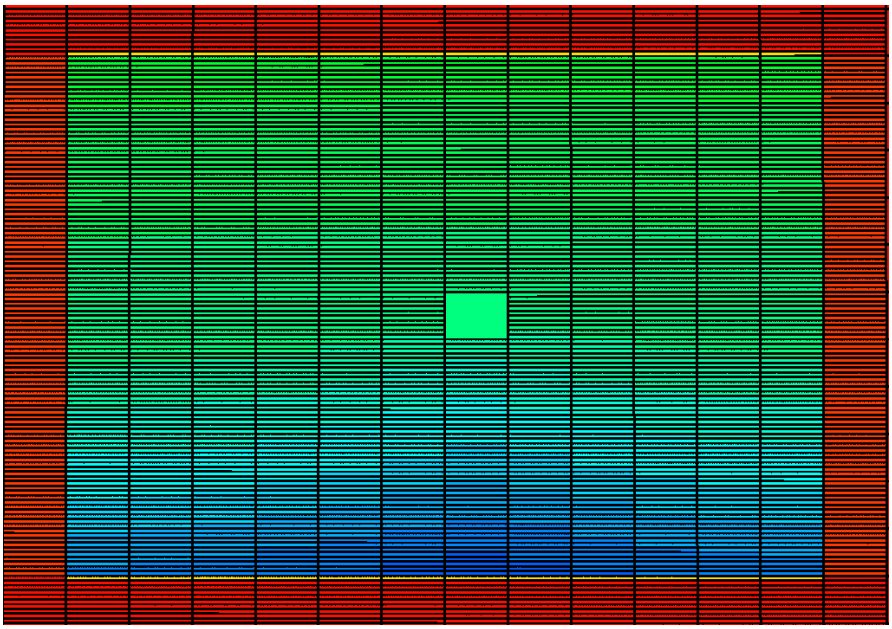

Water saturation inside fracture after 100th day

Figure 4.20: Water saturation maps (No evaporation, No VDRP)

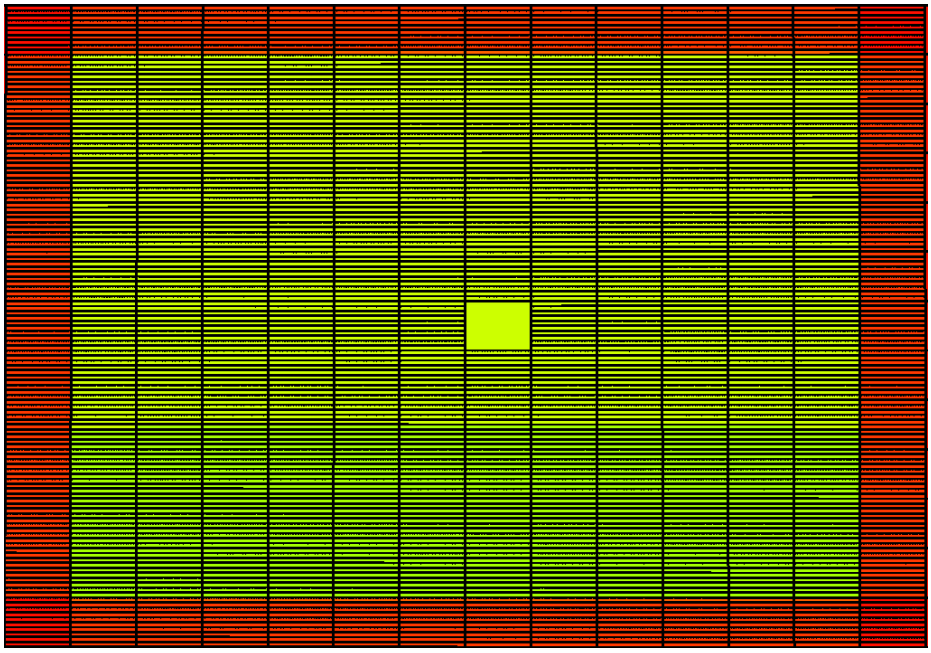

Water saturation inside fracture after 500 days (end of production)

Figure 4.20: Water saturation maps (No evaporation, No VDRP) - Continued

4.5.6. No evaporation, Only VDRP (Relative Permeability Set-2)

In this scenario, evaporation is neglected whereas velocity dependent relative permeability (VDRP) model is enabled. The cumulative gas recovery in this scenario was 17.32 MMscf after 500th day of operation. The cleanup profiles within fracture and matrix are shown in Figures 4.21-4.23. The cumulative gas recovery is higher than in the base case for the same relative permeability set. This is because water saturation in fracture after pumping is higher than in base case. This allows faster frac-water removal after production is initiated. (More details in discussion section)

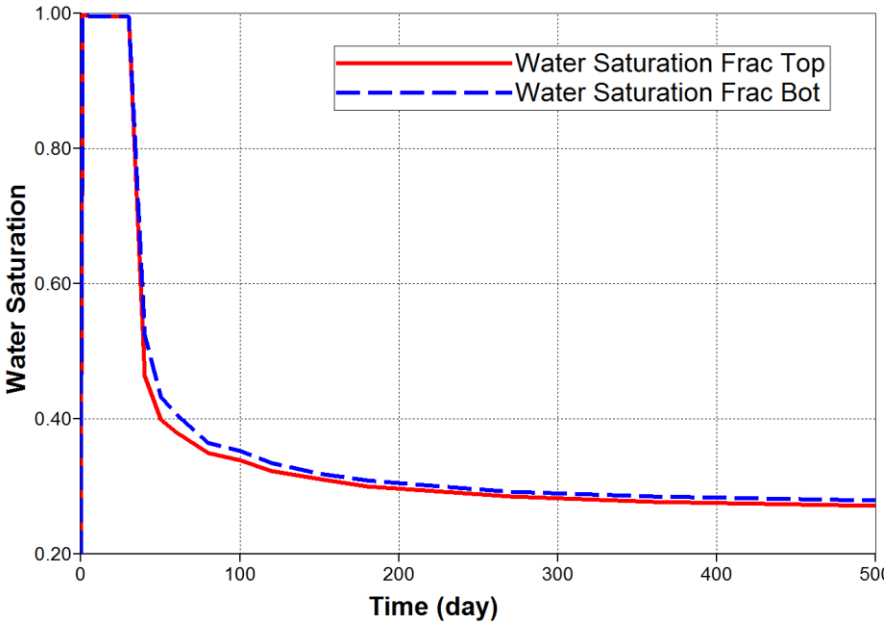

Figure 4.21: Variation of water saturation inside fracture over time (No evaporation, Only VDRP)

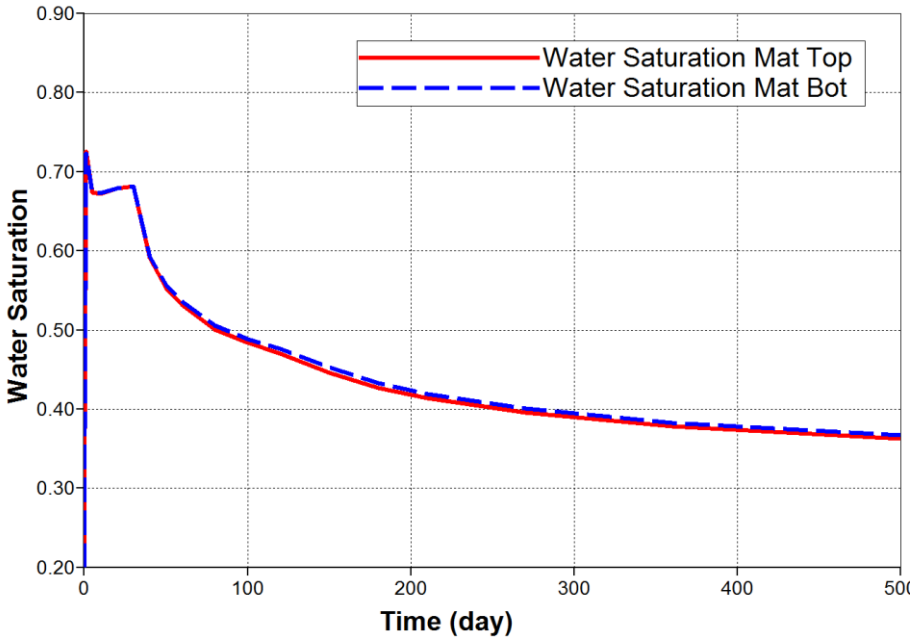

Figure 4.22: Variation of water saturation inside matrix 0.1 ft. from fracture face with time (No evaporation, Only VDRP)

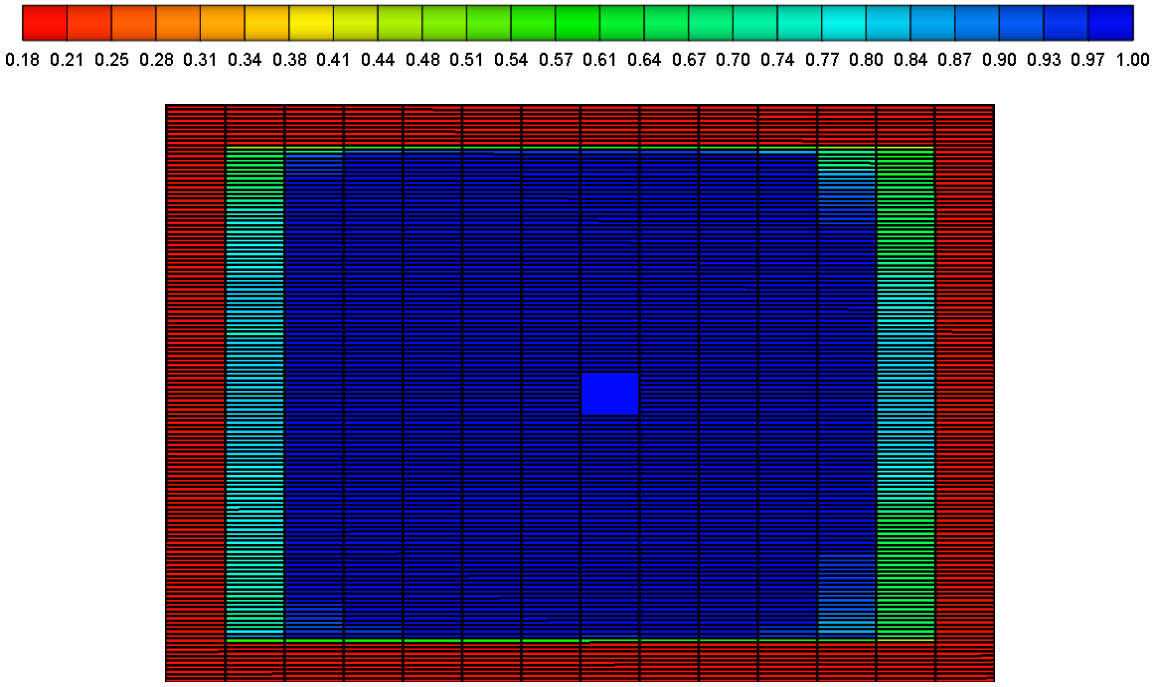

Water saturation inside fracture after 30th day (end of shutin)

Water saturation inside fracture after 100th day

Figure 4.23: Water saturation maps (No evaporation, Only VDRP)

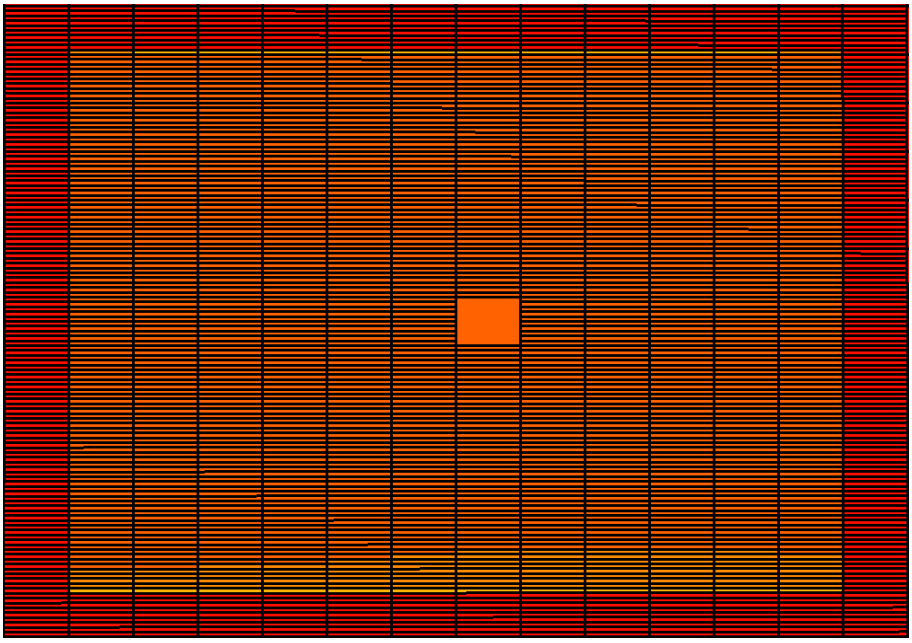

Water saturation inside fracture after 500 days (end of production)

Figure 4.23: Water saturation maps (No evaporation, Only VDRP) - continued

4.5.7. Only evaporation, No VDRP (Relative Permeability Set-2)

When only water evaporation model is turned on, the cumulative gas recovery was 17.98 MMscf. The cleanup profiles are as shown in Figures 4.24- 4.26. It can be observed that evaporative cleanup provides enhanced cleanup as compared with base case and therefore, leads to higher gas recovery.

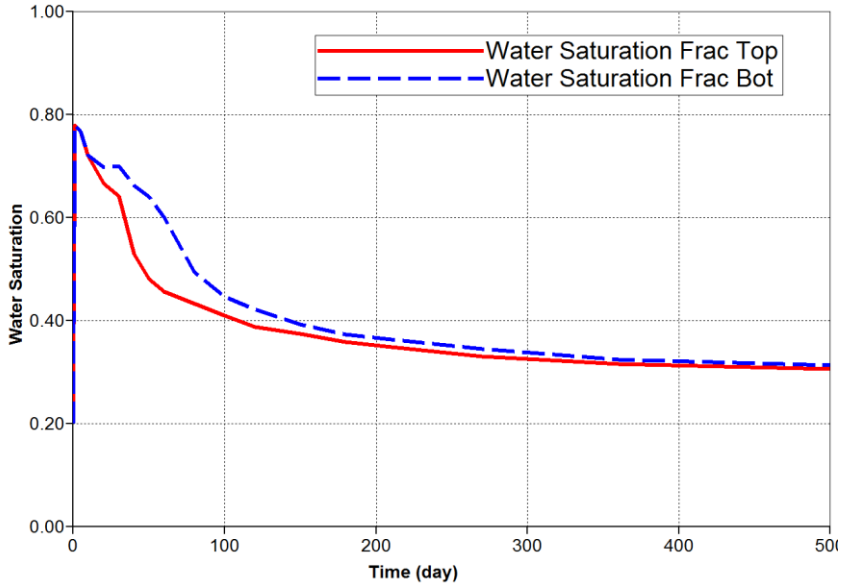

Figure 4.24: Variation of water saturation inside fracture over time (Only evaporation, No VDRP)

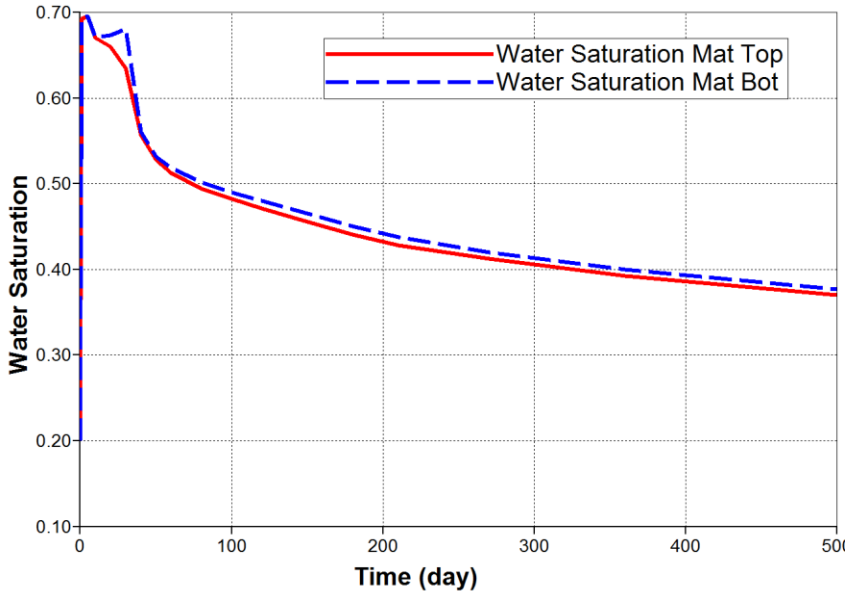

Figure 4.25: Variation of water saturation inside matrix 0.1 ft. from fracture face with time (Only evaporation, No VDRP)

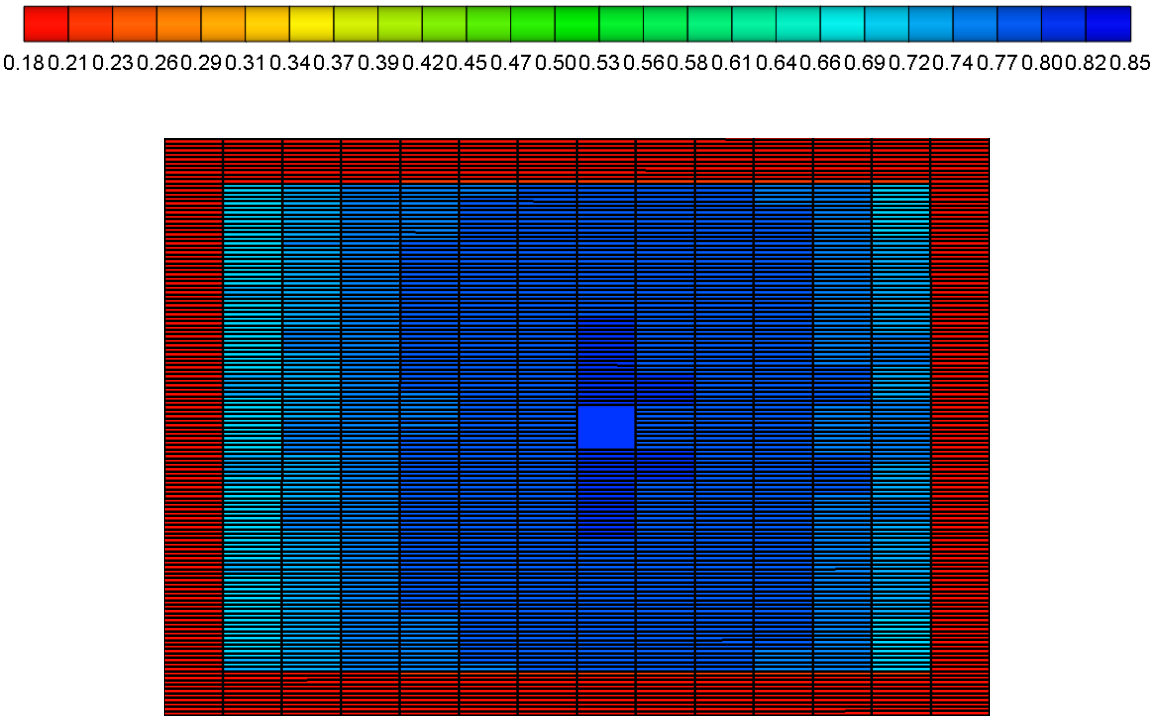

Water saturation inside fracture after 1 day (end of fracture treatment)

Water saturation inside fracture after 30 days (beginning of production, end of shut-in)

Figure 4.26: Water saturation maps (Only evaporation, No VDRP)

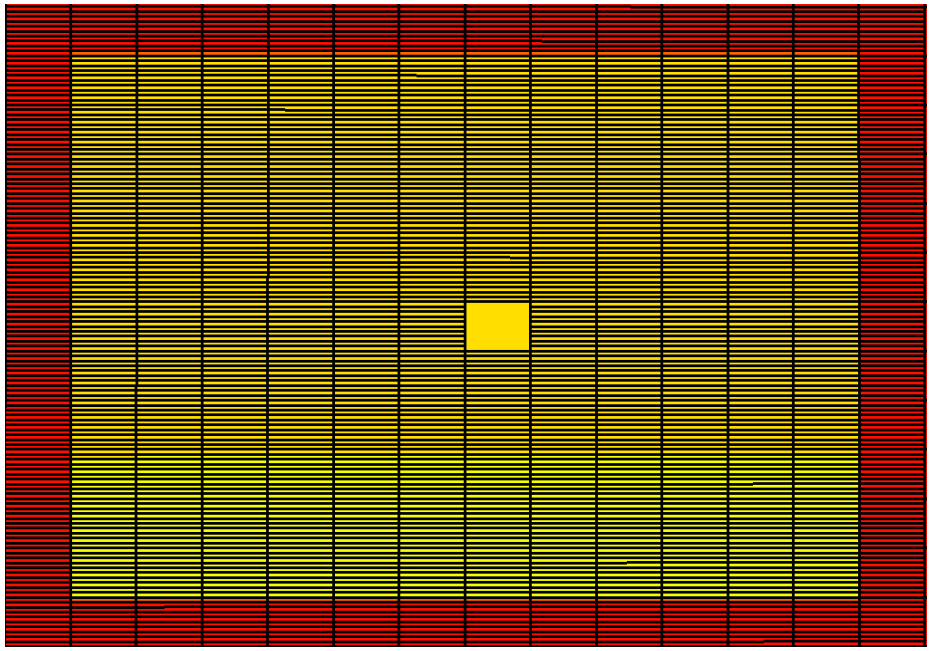

Water saturation inside fracture after 360 days

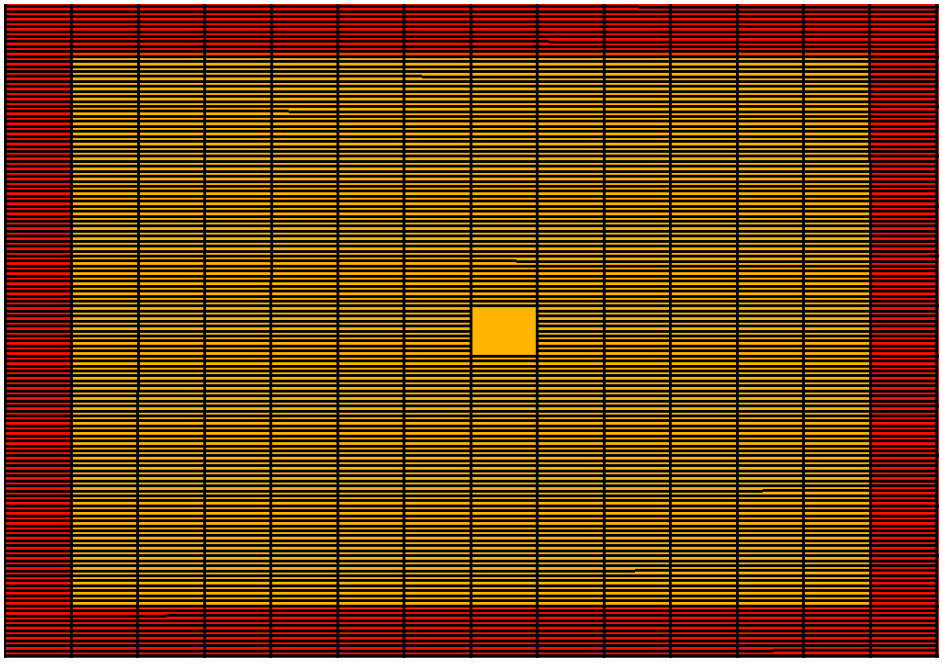

Water saturation inside fracture after 500 days (end of production)

Figure 4.26: Water saturation maps (Only evaporation, No VDRP) - Continued

4.5.8. Both evaporation and VDRP (Relative Permeability Set-2)

When both evaporation and VDRP effects are effective, the cumulative gas recovery by the end of 500th day was 18.53 MMscf. The cleanup profiles within the fracture and in the matrix near the fracture face are shown in Figures 4.27-4.29. The results clearly show that including the two effects significantly improves the cleanup process. No liquid segregation is observed at the fracture bottom during production. However, the water saturation inside fracture after 500th day of production is still above the residual saturation.

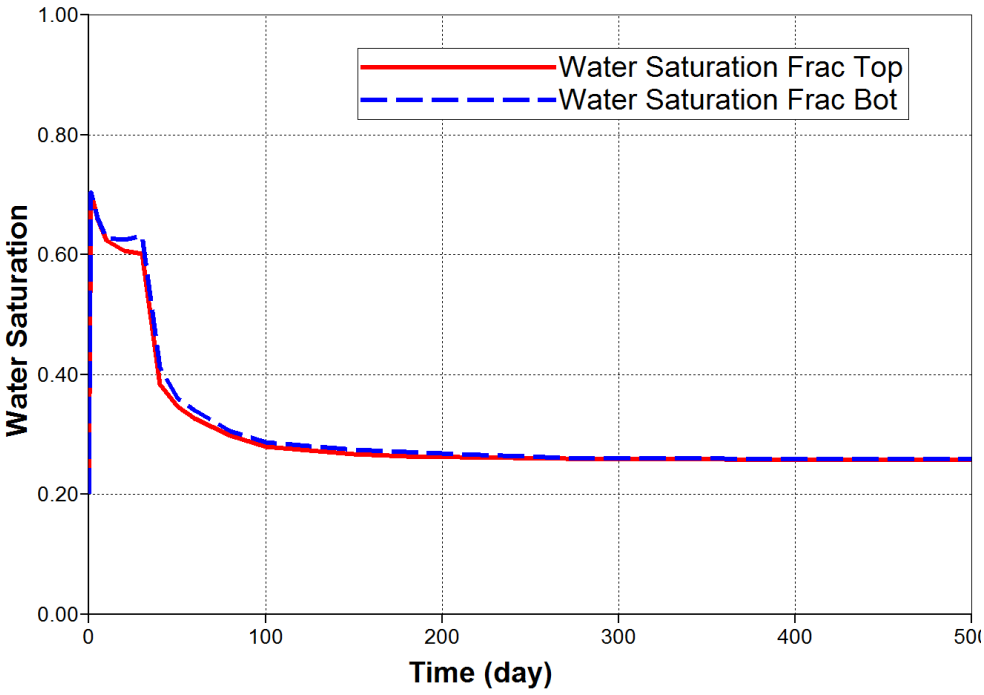

Figure 4.27: Variation of water saturation inside fracture over time (VDRP+Evaporation)

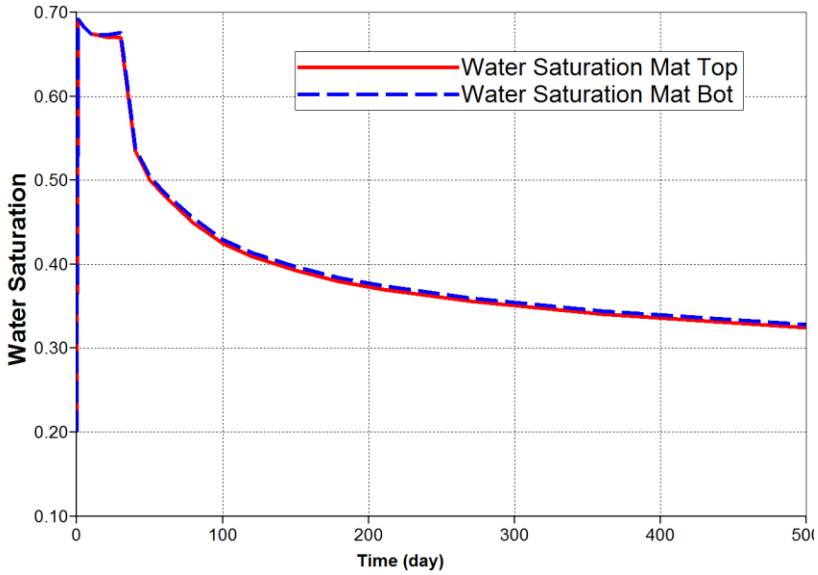

Figure 4.28: Variation of water saturation inside matrix 0.1 ft. from fracture face with time (VDRP+Evaporation)

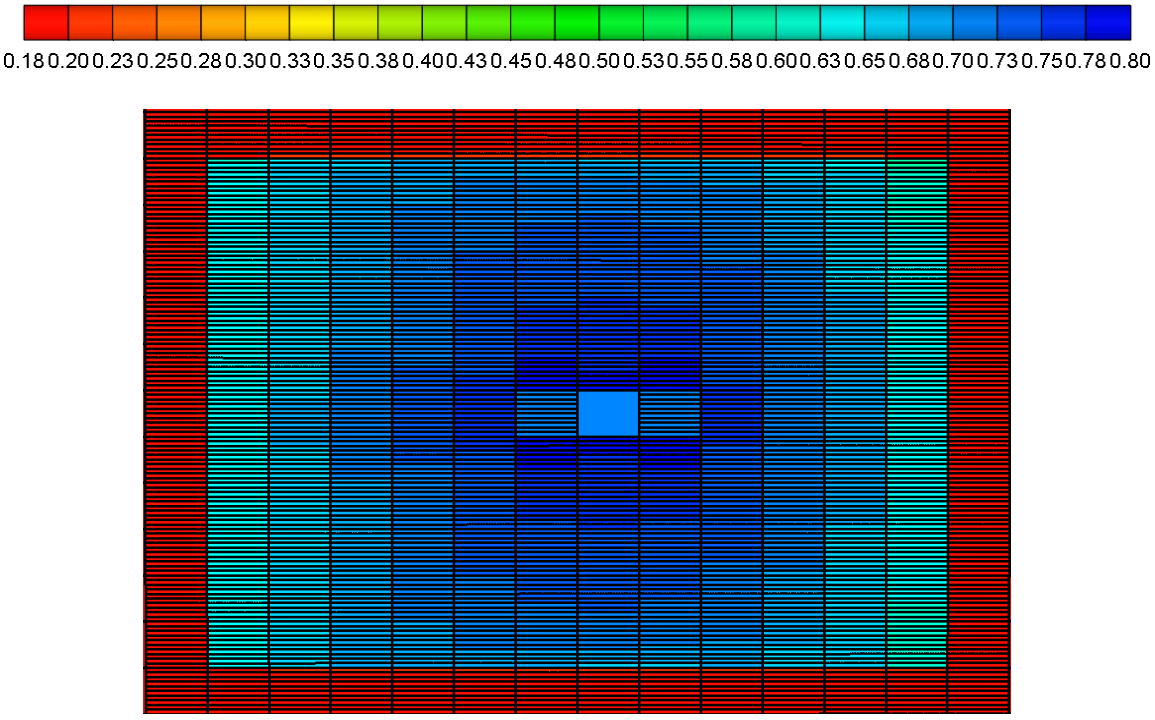

Water saturation inside fracture after 1 day (end of fracture treatment)

Figure 4.29: Water saturation maps (VDRP+Evaporation)

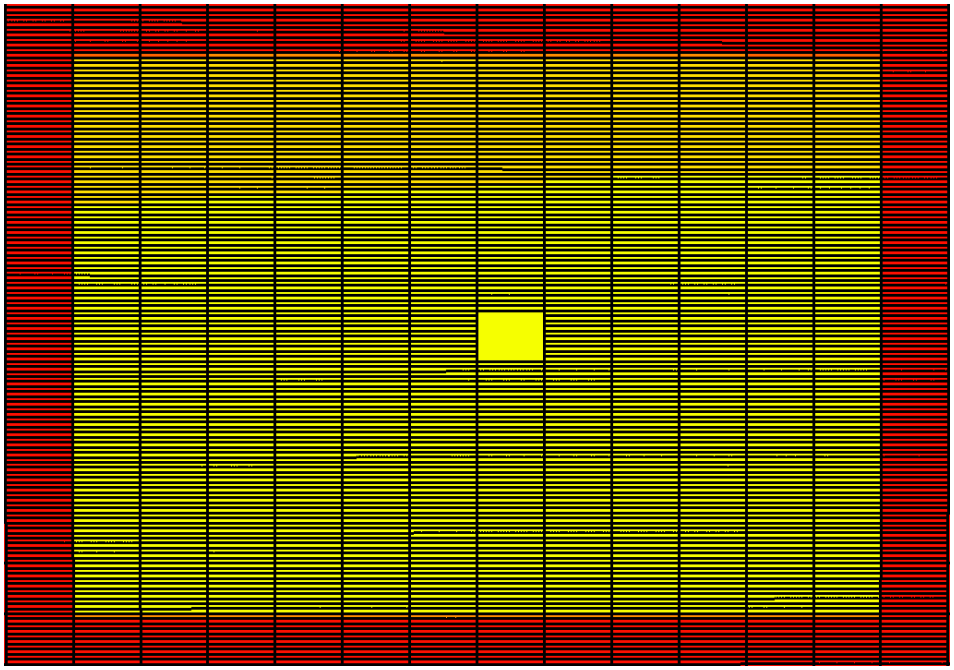

Water saturation inside fracture after 60th day

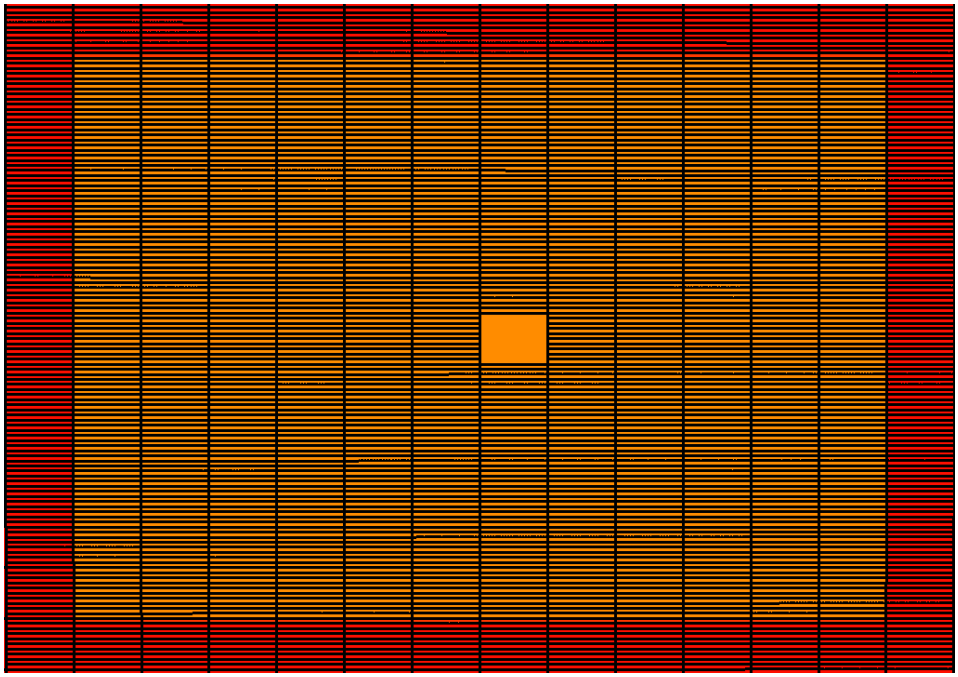

Water saturation inside fracture after 500 days (end of production)

Figure 4.29: Water saturation maps (VDRP+Evaporation) - Continued

4.6. DISCUSSIONS

The above simulations have shown the impact of VDRP and evaporation models on fracture and fracture face cleanup. They also provide the basis for analysis of impact of each set of relative permeability on the cumulative gas production in a given time.

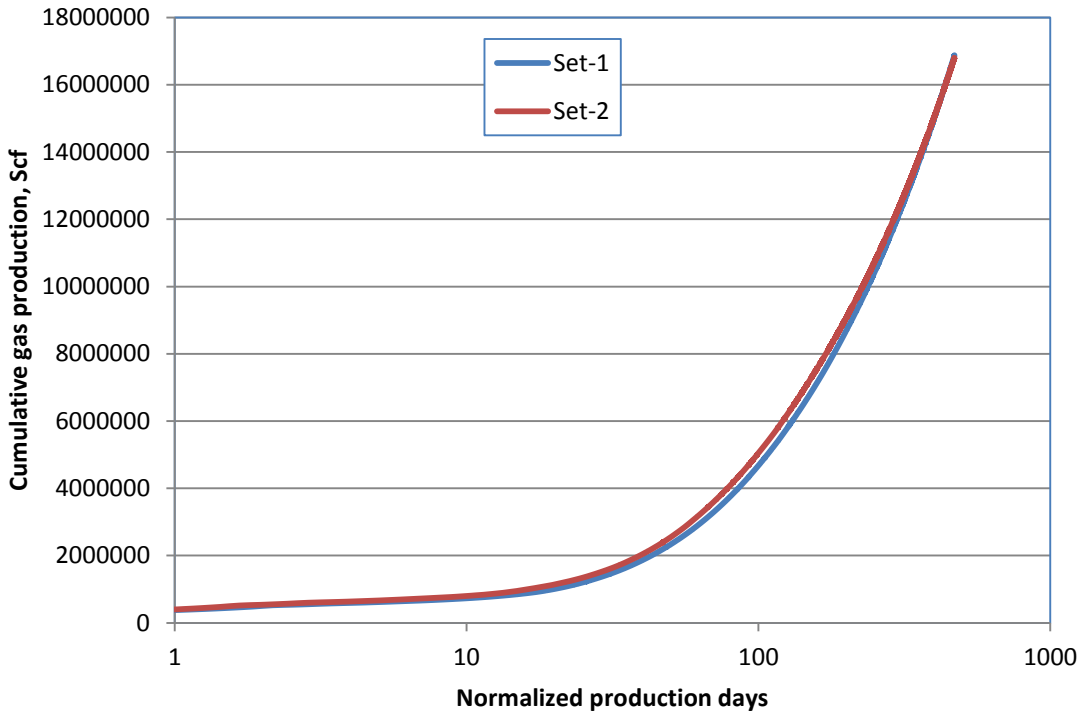

Figure 4.30: Effect of rel-perm on cumulative gas production with no VDRP and no evaporation

Figure 4.30 shows that the gas production is slow initially and then speeds up. This can be attributed to the frac-water cleanup and its impact on gas productivity, as seen in the previous chapter. Sets 1 and 2 provide similar cleanup and gas recovery when neither of the evaporation or velocity dependent relative permeability (VDRP) models is active. Figure 4.31 shows that enabling only VDRP model leads to delayed gas

breakthrough. This is because during injection, water is the displacing phase while gas is the displaced phase. VDRP leads to reduced residual saturation for the displaced phase (gas), which leads to higher water saturation in the near/ within fracture zone when VDRP is turned ON than when it's not. This is shown in the following Figures 4.32 and 4.33. Figure 4.32 shows that water saturation within the fracture (block 25,10,10) at the end of shut-in is 0.99 whereas gas saturation is only 0.01. This leads to zero gas relative permeability within the fracture and therefore, only water is produced initially. Once gas saturation increases and it becomes mobile then gas starts flowing to the perforations. However, when VDRP is OFF (Figure 4.33), the initial gas relative permeability in the fracture is non-zero and therefore gas breakthrough is instantaneous.

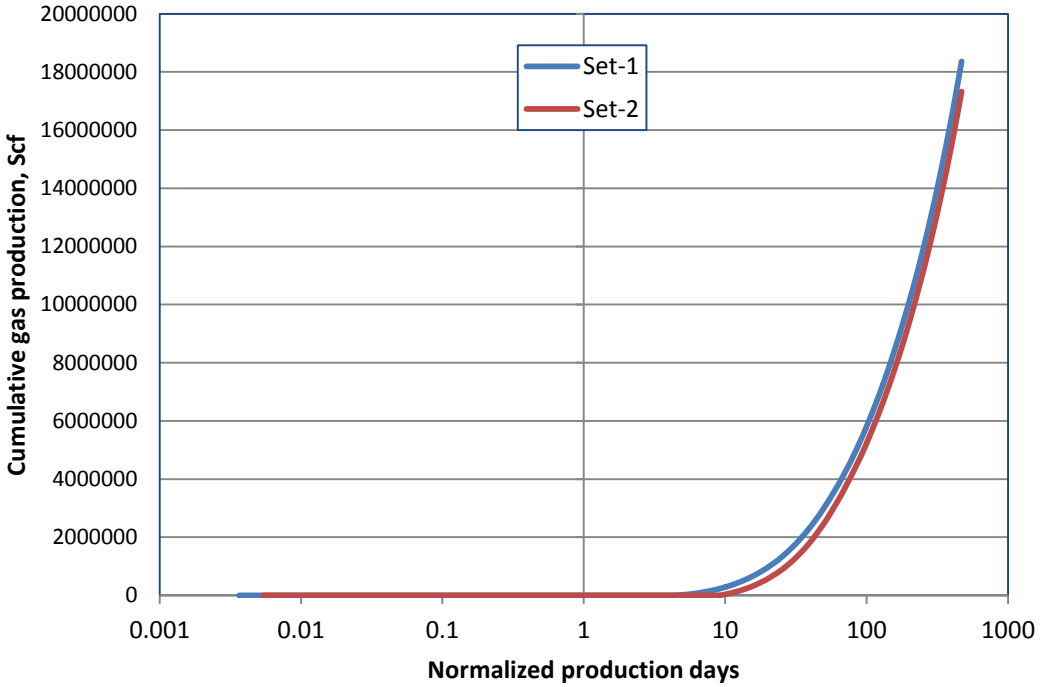

Figure 4.31: Effect of rel-perm on cumulative gas production with only VDRP active

Figure 4.32: Water-Gas saturation near fracture after shut-in (VDRP active)

Figure 4.33: Water-Gas saturation near fracture after shut-in (VDRP OFF)

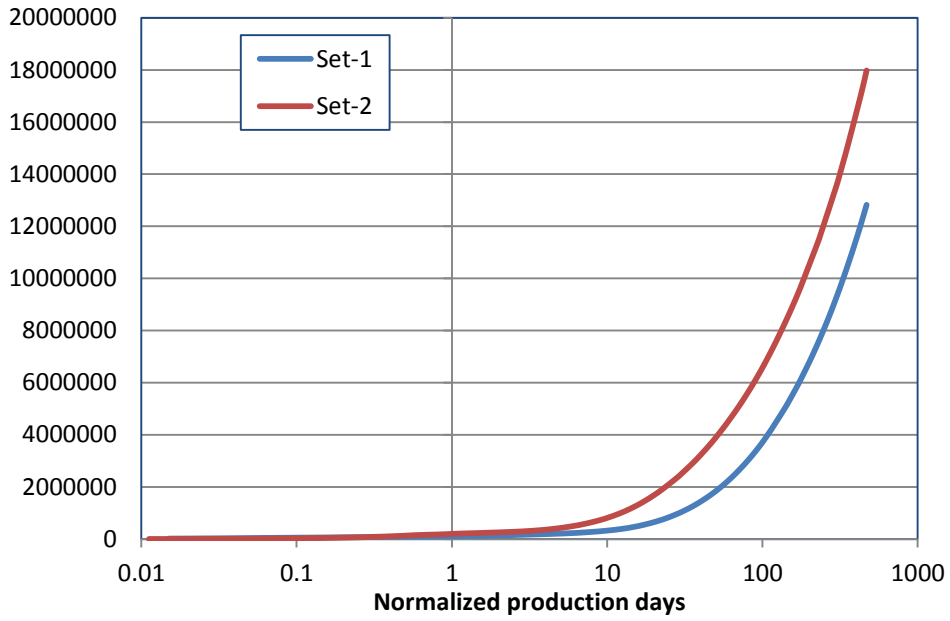

Figure 4.34: Effect of rel-perm on cumulative gas production with only evaporation active

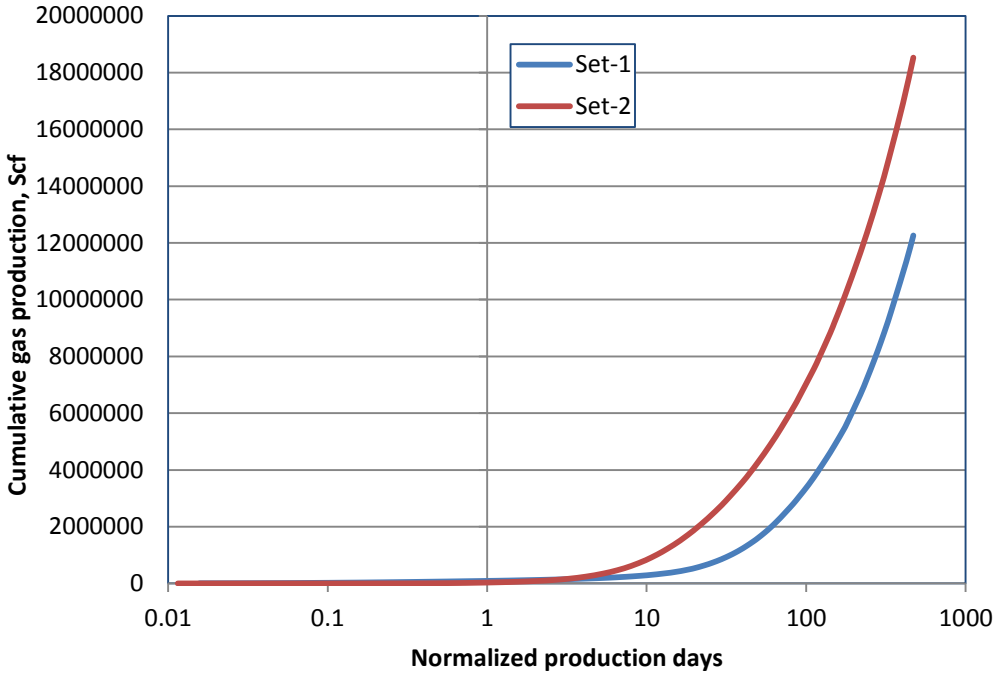

Figure 4.35: Effect of rel-perm on cumulative gas production with both VDRP and evaporation active

Figure 4.34 shows gas production when only evaporation model is active. Compared with Figure 4.30, it is evident that evaporation assists in the frac-water cleanup and therefore, leads to higher gas recovery for both relative permeability sets. Since the amount of evaporative cleanup is dependent on the drawdown applied and amount of gas flowing through, Set-2 provides higher cumulative recovery. Finally, Figure 4.35 shows the production profile under the combined effects of VDRP and water evaporation model. Figure 4.36 indicates that evaporation is more significant that VDRP for the overall cleanup and performance under the operating conditions and the low matrix permeability.

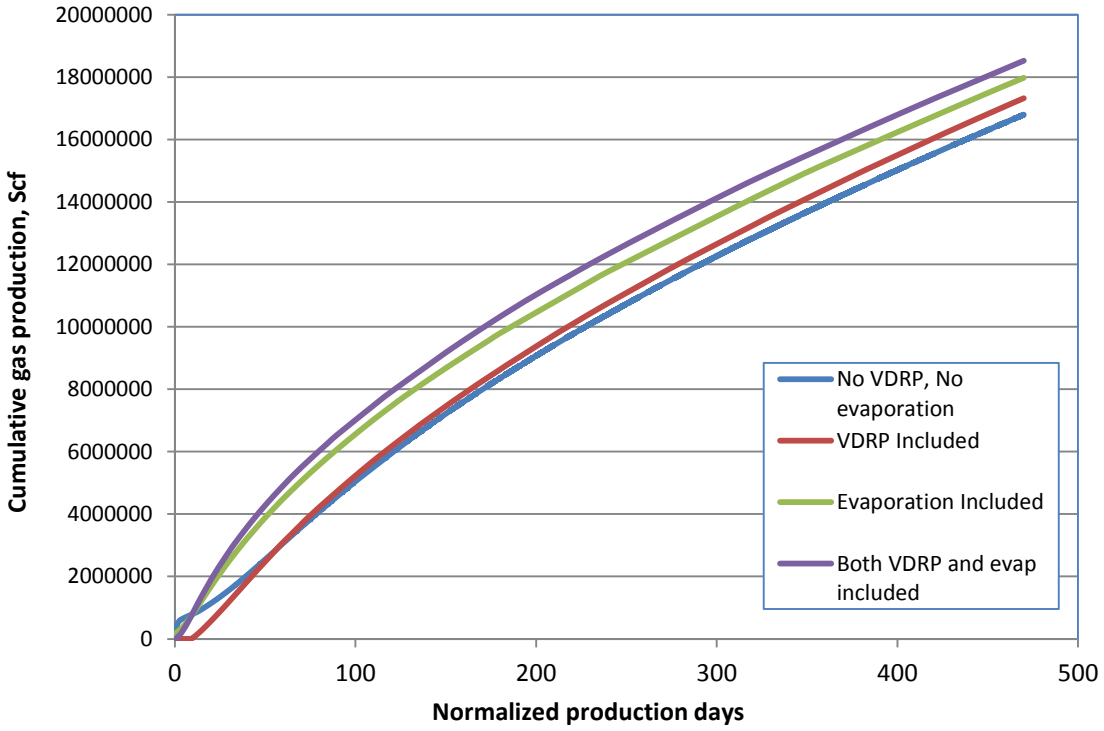

Figure 4.36: Effect of evaporation and VDRP models on cumulative gas recovery (Set-2)

4.7. SUMMARY

This chapter's results have shown that even after considering more realistic reservoir effects such as the evaporation of water and velocity dependent relative permeability, one can still observe early time liquid loading within the fracture. Figure 4.36 demonstrates how the cumulative gas recovery is improved due to inclusion of evaporation and velocity dependent relative permeability models. CMG GEM 2011 doesn't provide the capability to quantify the barrels of water removed in the vapor phase after the OGW flash used in evaporation model. Inclusion of that information will further enhance the quantitative estimation of amount of frac-water recovered.

As seen in Chapter 3, the severity of the liquid loading within fracture will be higher for lower drawdown, lower matrix permeability and higher surface tension between the fluids. Higher drawdown will support both evaporation as well as capillary de-saturation due to VDRP. This will lead to more efficient cleanup of frac-water and lead to productivity enhancement.

What effect will drawdown have on the production from 'liquids rich' gas reservoirs? This question is explored in next chapter where liquid loading in fractures is studied for lean and rich gas condensate reservoirs.

Chapter 5: Three Phase Flow Back Compositional Simulation

5.1 INTRODUCTION

In previous chapters, we have looked at the various factors that may impact the loading of frac-water inside the hydraulic fracture or on the fracture face in the matrix. It was noted that low drawdown in low permeability formations may exacerbate the problem. In order to minimize such liquid trapping within the fracture, drawdown must be maximized as per the surface, well bore and reservoir constraints to achieve the highest possible fluid recovery. However, when dealing with gas condensate reservoirs there may be additional constraints.

In a gas condensate reservoir, once the reservoir pressure falls below the dew point, liquid starts dropping out of the gas. This introduces a third phase into the scenario and further damages the gas relative permeability due to increased liquid saturation. Hence for optimal recovery from liquid rich tight gas/shale reservoirs, understanding the phase behavior of the fluids is extremely important. A higher drawdown may not yield proportionately higher gas production and or improve the fracture cleanup over lower drawdown. This understanding can lead to significant cost savings.

In this chapter, three phase compositional reservoir simulation is employed to study the fracture cleanup process for a lean and a rich gas condensate reservoir under different scenarios. It is imperative to study not only the cleanup of water but also the condensate (oil) that condenses into the fracture or matrix face. These simulations include velocity dependent relative permeability model (Pope et al.) and evaporation of water due to pressure drop during flow back.

5.2 SIMULATION MODEL

A Cartesian grid with dimensions 50 X 20 X 20 grids is used to define the reservoir. A single, bi-wing lateral fracture is placed symmetrically in the center of the grid and modeled using high porosity and permeability. Local grid refinement is utilized for stable computation, near fracture face and within the fracture. The total dimensions of the reservoir model are 600 ft. X 1560 ft. X 100 ft. The dimensions of the fracture are 480 ft. (wide) X 55ft. (high) X 0.1 ft. (thick). The reservoir properties are as specified in Table 5.1.

Property/ Parameter	**Value**
Matrix Permeability	0.1 μD
Fracture Permeability	2 D
Reservoir Thickness	100 ft.
Matrix Porosity	10 %
Fracture Porosity	60 %
Fracture Height	55 ft.
Fracture Thickness	0.1 ft.
Fracture Half Length	240 ft.
Gas-Water Surface tension	40 dyne/cm
Water Density	60 lb/ft^3
Flowing Wellbore pressure	4000 psi
Initial Reservoir Pressure	6500 psi
Initial Water Saturation	0.3
Residual Water Saturation	0.3
Reservoir Temperature	300 F

Table 5.1: Simulation model properties

Three sets of relative permeability curves were simulated corresponding to low, medium and high water end point relative permeability or mobility. These will be referred to as Set 1, 2 and 3 respectively. The properties for the three relative permeability sets are shown below.

Parameter	Value
Residual water saturation, S_{wr}	0.3
Residual gas saturation, S_{gr}	0.3
Residual oil saturation, S_{or}	0.2
(Matrix) Water end point rel-perm, $K_{rw}°$	0.2
(Matrix) Gas end point rel-perm, $K_{rg}°$	1
(Fracture) Water end point rel-perm, $K_{rw}°$	0.4
(Fracture) Gas end point rel-perm, $K_{rg}°$	0.9

Table 5.2: Relative permeability Set-1 properties

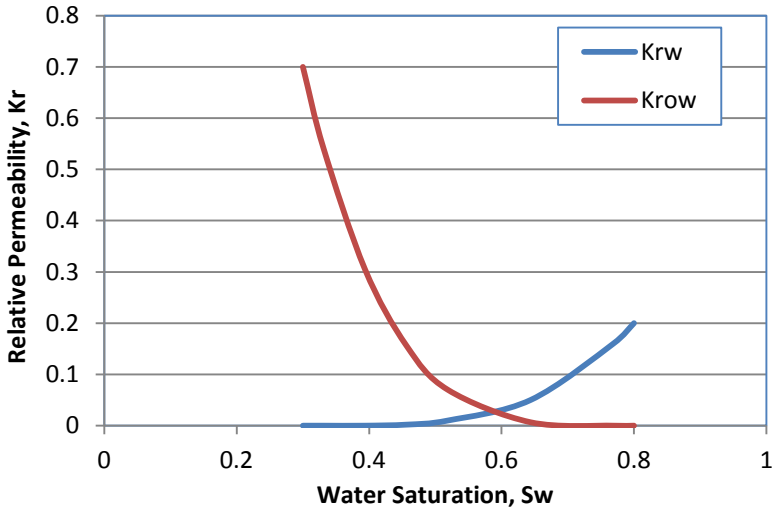

Figure 5.1: Matrix oil-water rel-perm (Set-1)

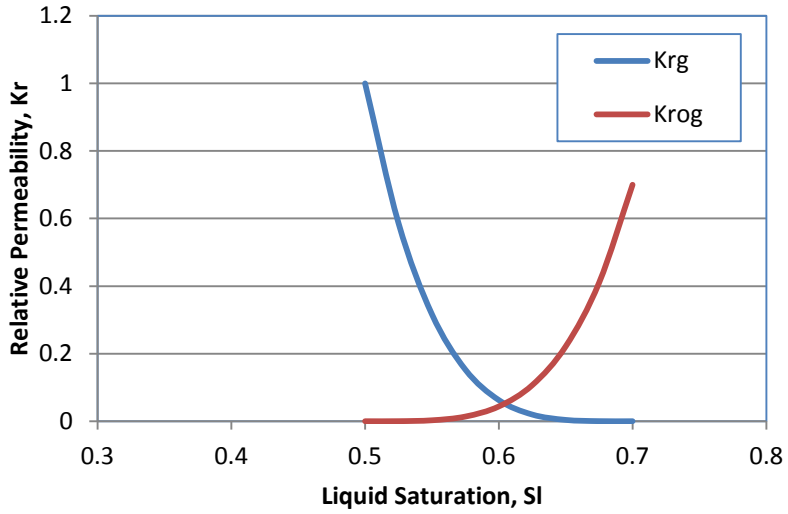

Figure 5.2: Matrix liquid-gas rel-perm (Set-1)

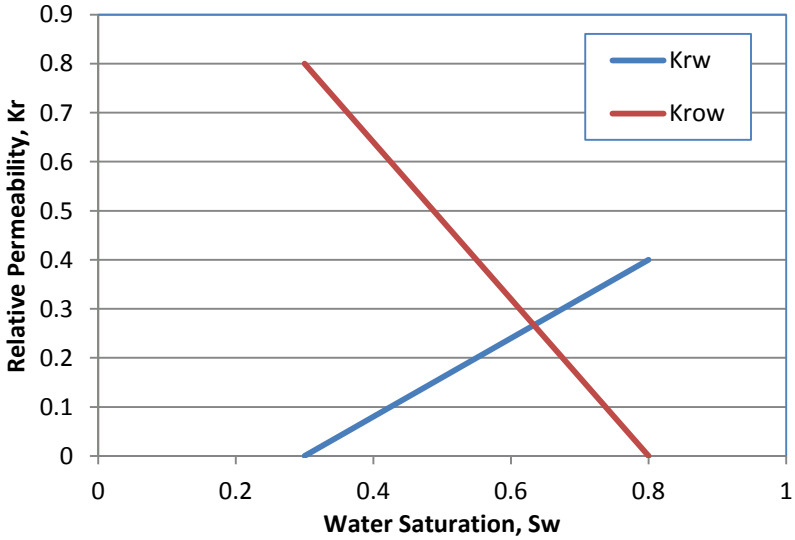

Figure 5.3: Fracture oil-water rel-perm (Set-1)

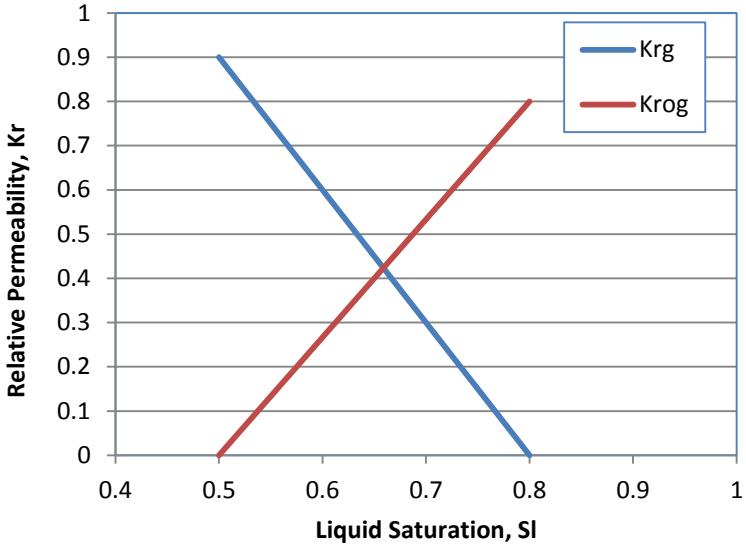

Figure 5.4: Fracture liquid-gas rel-perm (Set-1)

Parameter	Value
Residual water saturation, S_{wr}	0.3
Residual gas saturation, S_{gr}	0.3
Residual oil saturation, S_{or}	0.2
(Matrix) Water end point rel-perm, $K_{rw}°$	0.45
(Matrix) Gas end point rel-perm, $K_{rg}°$	1
(Fracture) Water end point rel-perm, $K_{rw}°$	0.7
(Fracture) Gas end point rel-perm, $K_{rg}°$	0.9

Table 5.3: Relative permeability Set-2 properties

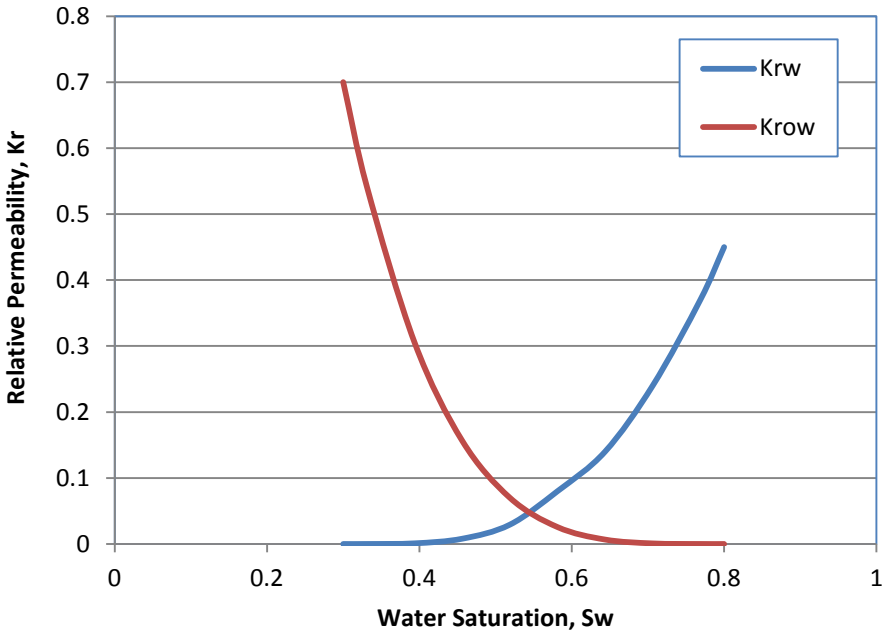

Figure 5.5: Matrix oil-water rel-perm (Set-2)

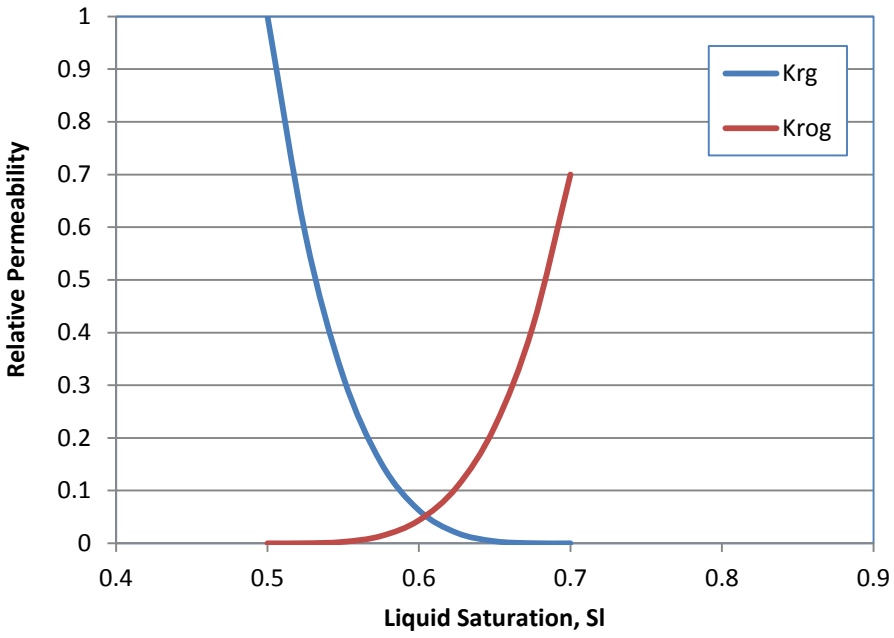

Figure 5.6: Matrix liquid-gas rel-perm (Set-2)

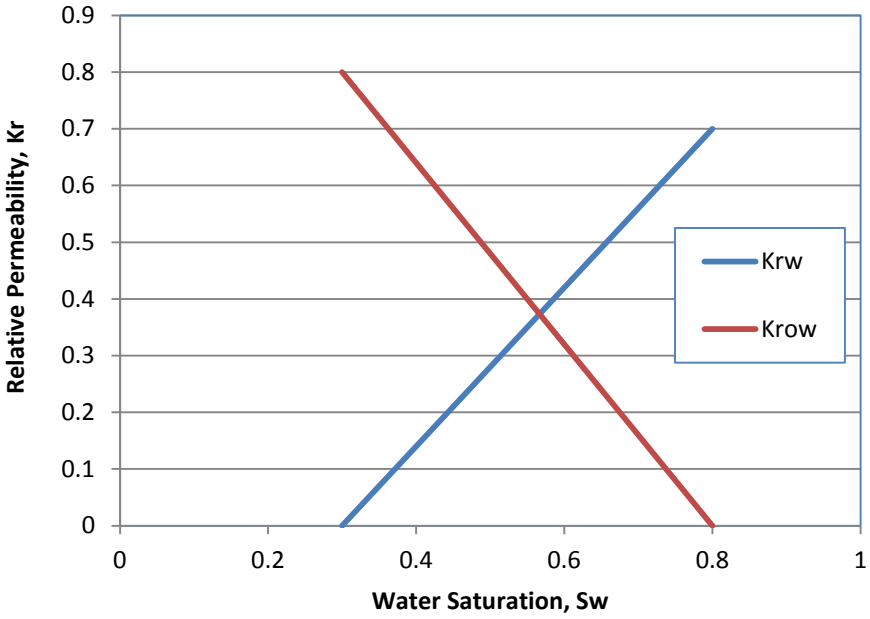

Figure 5.7: Fracture oil-water rel-perm (Set-2)

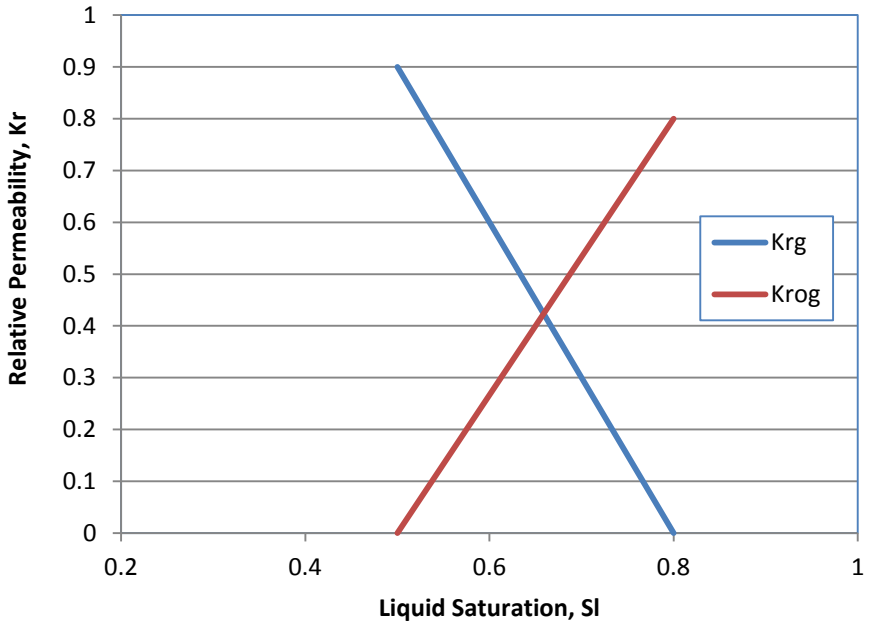

Figure 5.8: Fracture liquid-gas rel-perm (Set-2)

Parameter	Value
Residual water saturation, S_{wr}	0.3
Residual gas saturation, S_{gr}	0.3
Residual oil saturation, S_{or}	0.2
(Matrix) Water end point rel-perm, $K_{rw}°$	0.8
(Matrix) Gas end point rel-perm, $K_{rg}°$	1
(Fracture) Water end point rel-perm, $K_{rw}°$	0.7
(Fracture) Gas end point rel-perm, $K_{rg}°$	0.9

Table 5.4: Relative permeability Set-3 properties

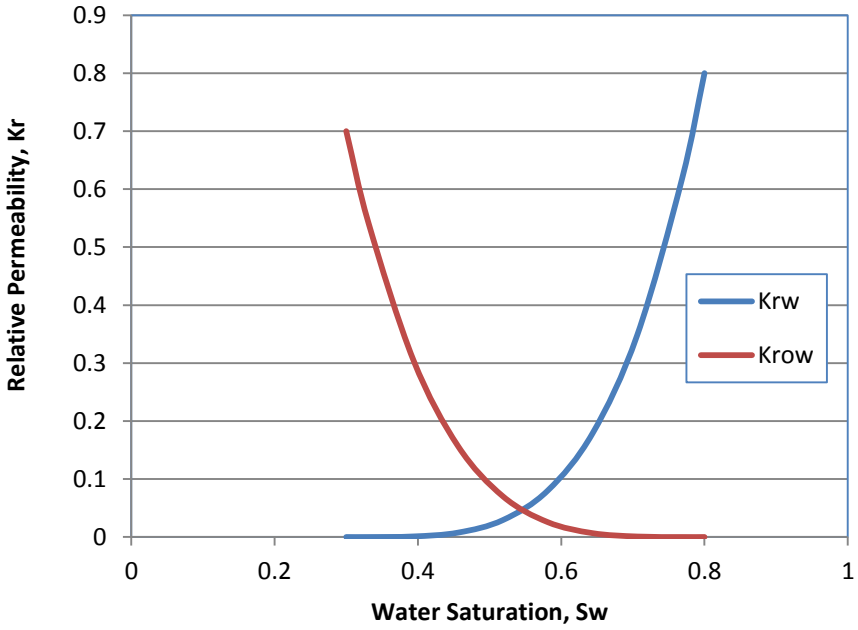

Figure 5.9: Matrix oil-water rel-perm (Set-3)

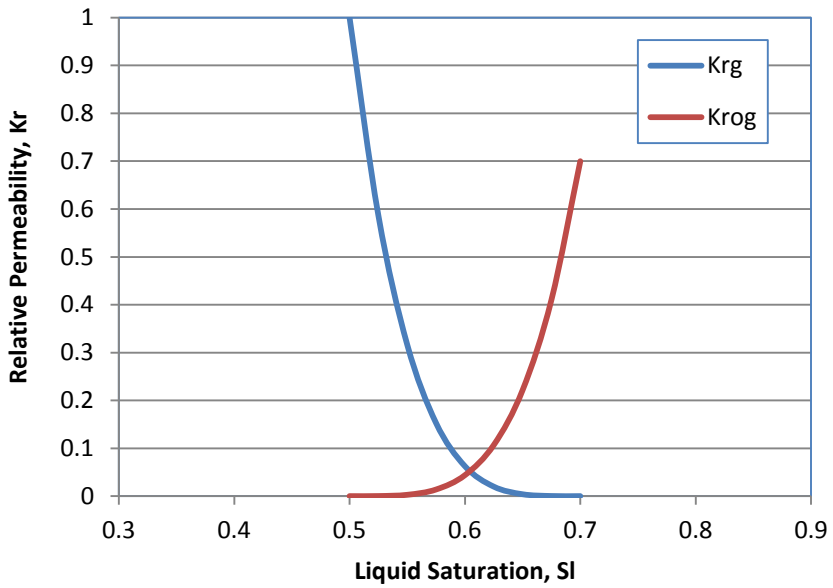

Figure 5.10: Matrix liquid-gas rel-perm (Set-3)

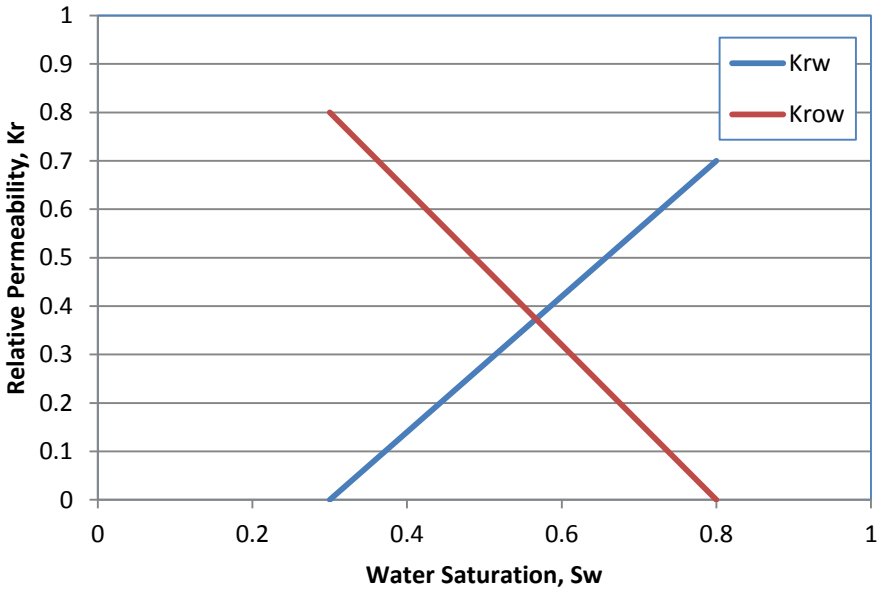

Figure 5.11: Fracture oil-water rel-perm (Set-3)

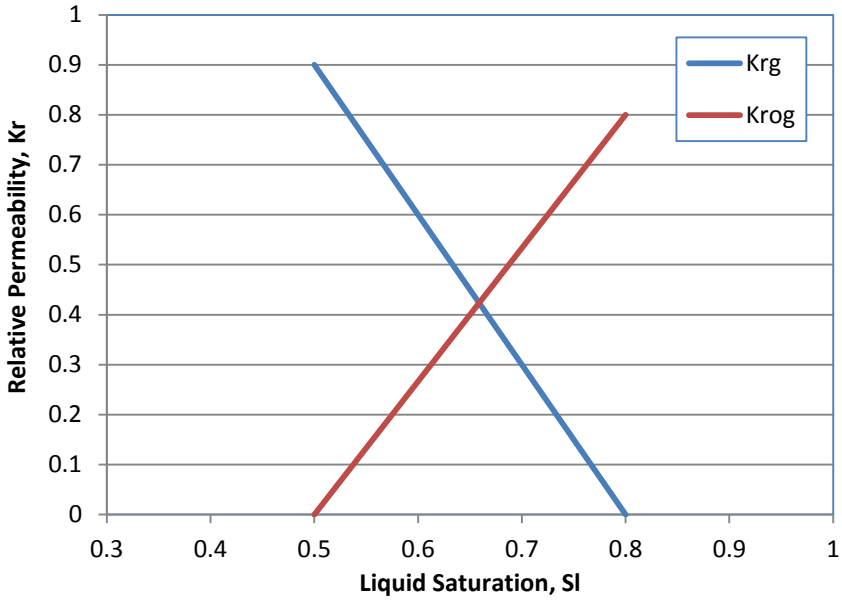

Figure 5.12: Fracture liquid-gas rel-perm (Set-3)

Stone 2 model is used to obtain the oil end point relative permeability (K_{ro}) for the three phase flow simulation from the two phase K_{row} and K_{rog}. All three sets have the same K_{row} and K_{rog} variation. The ternary diagrams for matrix and fracture are presented below.

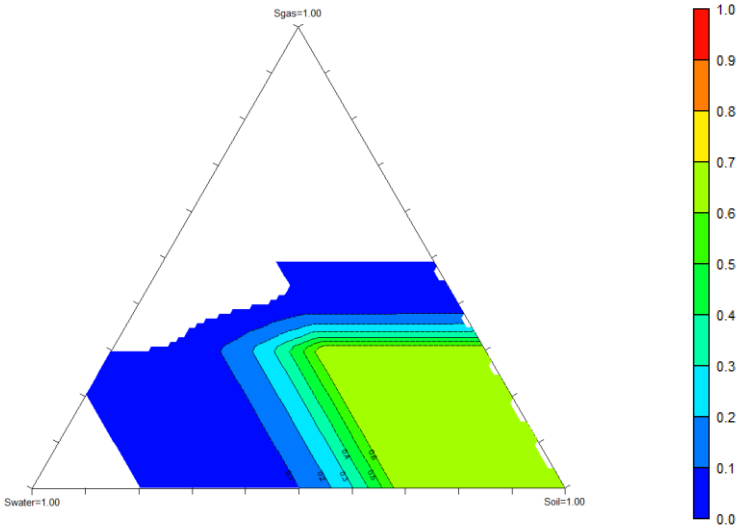

Figure 5.13: Kro values for Matrix from Stone 2 model

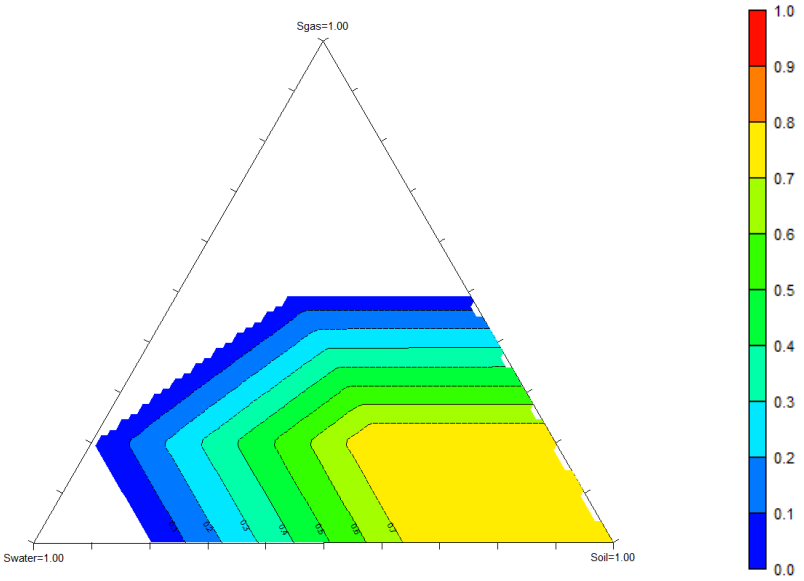

Figure 5.14: Kro values for Fracture from Stone 2 model

For the velocity dependent relative permeability model, Table 4.4 (previous chapter) provides the parameter values.

This study uses two gas condensate compositions: first is a rich condensate with high liquid content and the second is a lean gas condensate. The Peng-Robinson equation of state is used to model the behavior of the reservoir fluid. CMG provides WINPROP™ as a tool to model the PVT behavior for different hydrocarbon compositions. It allows for selecting pre-defined library components, defining custom components or lumping of various hydrocarbon fractions to characterize the fluid's PVT behavior. Accurate PVT modeling of a condensate reservoir is essential because the fluid's phase behavior can have significant impact on the productivity.

The composition and binary interaction coefficients used for the rich condensate fluid are given in Table 5.5 and 5.6. (Mohan, 2005)

Components	Mol Frac	Pc (atm)	Tc (K)	Acentric Factor	Mol Wt.	Vc (l/mol)	Parachor
N2	0.0283	33.5	126.2	0.04	28.013	0.0895	41
CO2	0.0613	72.8	304.2	0.225	44.01	0.094	78
CH4	0.4625	45.4	190.6	0.008	16.043	0.099	77
C2-3	0.1624	45.03	337.91	0.1253	35.82	0.172327	102.3429
C4-6	0.1439	34.6	461.72	0.2348	69.2	0.296256	197.7143
C7P1	0.10069	19.9	508.82	0.3319	109.33	0.550326	312.3714
C7P2	0.03944	14.42	814.39	0.5931	210.23	1.112666	600.6571
C7P3	0.00148	8.48	1096.89	1.0344	424.84	2.150231	1213.829

Table 5.5: Rich condensate fluid composition and PR-EOS parameters

	N2	C02	CH4	C2-3	C4-6	C7P1	C7P2	C7P3
N2	0							
CO2	0	0						
CH4	-0.05	0.05	0					
C2-3	-0.05	0.05	0	0				
C4-6	-0.05	0.05	0	0	0			
C7P1	-0.05	0.05	0	0	0	0		
C7P2	-0.05	0.05	0	0	0	0	0	
C7P3	-0.05	0.05	0	0	0	0	0	0

Table 5.6: Rich condensate fluid binary interaction coefficients

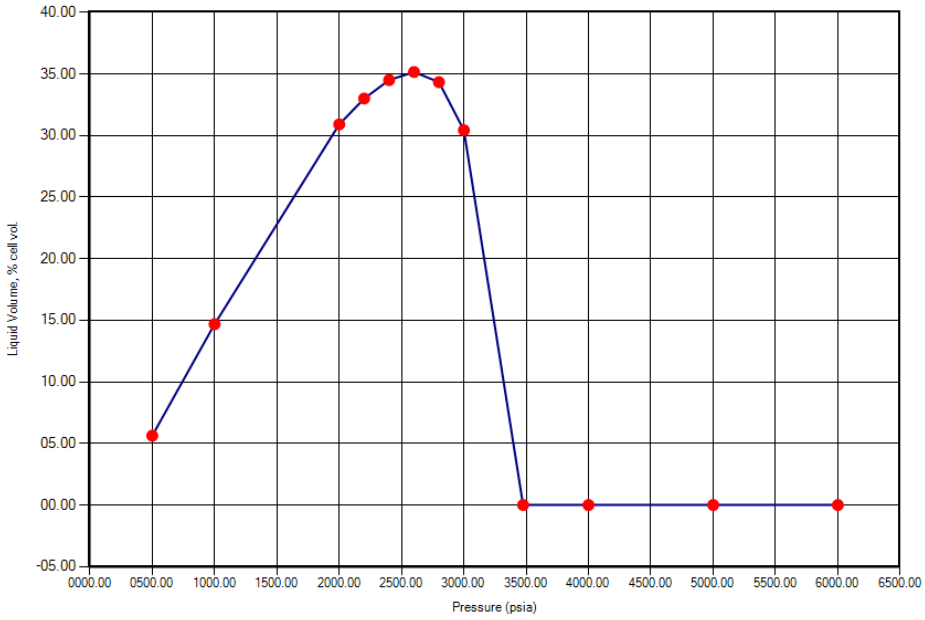

Figure 5.15: Liquid drop out for rich condensate
(Constant Composition Expansion)

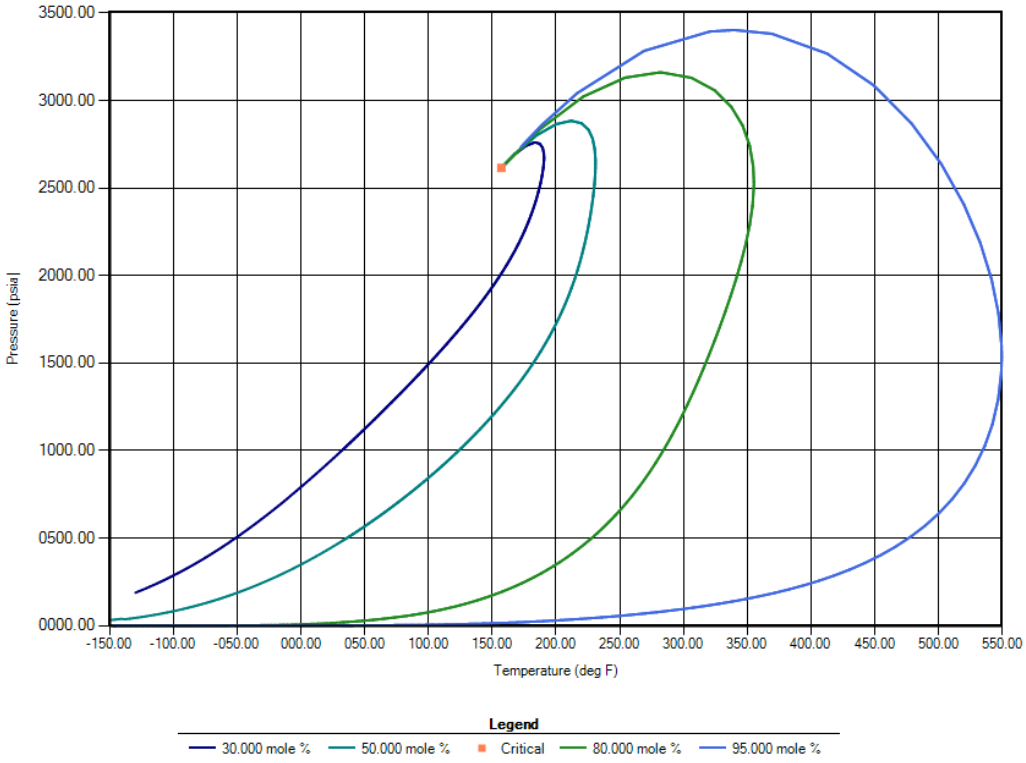

Figure 5.16: P-T diagram for rich condensate

Figures 5.15 and 5.16 indicate the high value of maximum liquid drop out (~0.35) and the dew point pressure of approximately 3470 psi.

The composition, PR-EOS parameters and binary interaction coefficients for the lean condensate are shown in Tables 5.7 and 5.8. Figure 5.17 and 5.18 show the simulated phase behavior for this fluid under reservoir conditions.

Components	**Mol frac**	**Pc (atm)**	**Tc (K)**	**Acentric Factor**	**Mol Wt.**	**Vc (l/mol)**	**Parachor**
CO2	5.3	72.8	304.2	0.23	44.01	0.094	78
N2	0.09	33.5	126.2	0.04	28.013	0.0895	41
CH4	80.54	45.4	190.6	0.01	16.043	0.099	77
C2H6	5.6	48.2	305.4	0.1	30.07	0.148	108
C3H8	3.34	41.9	369.8	0.15	44.097	0.203	150.3
IC4	0.8	36	408.1	0.18	58.124	0.263	181.5
NC4	0.83	37.5	425.2	0.19	58.124	0.255	189.9
C5-C6	1.23	38.87	480.1	0.23	74.64	0.275	217.4307
C7-C8	0.8	30.82	585.8	0.32	102.69	0.3887	297.0892
C9-C11	0.703	25.12	652.2	0.48	136.5	0.5136	388.5041
C12-C15	0.445	20.21	699.7	0.51	183.85	0.6757	508.0737
C16+	0.322	14.72	836.2	0.7	280.59	0.974	721.6981

Table 5.7: Lean condensate fluid composition and PR-EOS parameters

	CO2	N2	CH4	C2H6	C3H8	IC4	NC4	C5-C6	C7-C8	C9-C11	C12-C15	C16+
CO2	0											
N2	-0.02	0										
CH4	0.103	0.031	0									
C2H6	0.13	0.042	0	0								
C3H8	-0.02	0.091	0	0	0							
IC4	0.103	0.095	0	0	0	0						
NC4	0.13	0.095	0	0	0	0	0					
C5-C6	0.15	0.12	0	0	0	0	0	0				
C7-C8	0.15	0.12	0	0	0	0	0	0	0			
C9-C11	0.15	0.12	0	0	0	0	0	0	0	0		
C12-C15	0.15	0.12	0	0	0	0	0	0	0	0	0	
C16+	0.15	0.12	0	0	0	0	0	0	0	0	0	0

Table 5.8: Lean condensate fluid binary interaction coefficients

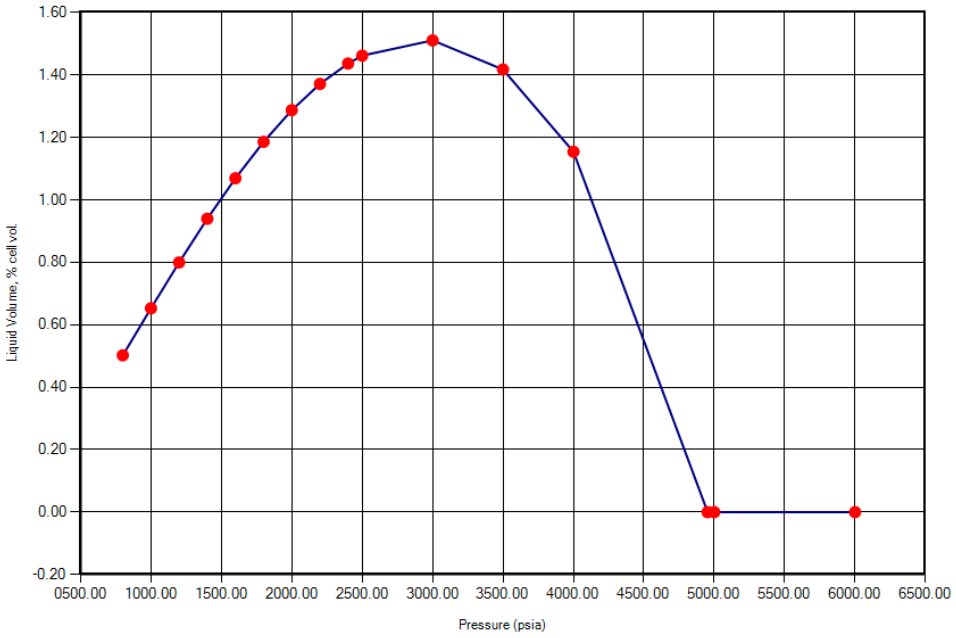

Figure 5.17: Liquid drop out for lean condensate
(Constant Composition Expansion)

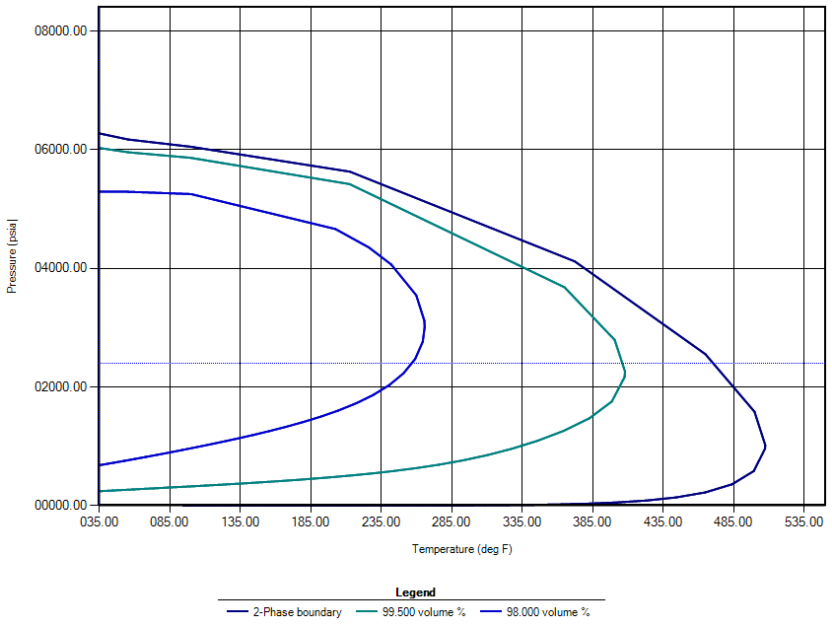

Figure 5.18: P-T diagram for lean condensate

5.3 RESULTS

Earlier studies have already looked at condensate buildup in the near wellbore region. This study differs in that it aims to study condensate buildup within the fracture as a whole, especially at the top and bottom. As more gas passes through the near wellbore region, more condensate is deposited which leads to higher oil saturation. This oil saturation can be greater than the maximum drop-out observed in CCE experiment. The following results show frac-water and oil saturations measured in two specific grid blocks at the top and bottom of fracture/ matrix above the wellbore. Water evaporation and velocity dependent relative permeability models are active during these simulations.

5.3.1. Lean Condensate – Base case (Relative Permeability Set -1)

As Figure 5.17 indicates, the maximum liquid drop out from the lean gas (as per CCE) is only approximately 1.5%. The dew point is ~4950 psi. In the base case, the applied bottom-hole pressure for flowback is 4000 psi. Since the pressure is below dew point, condensate drop out is expected. The observed variation of oil and water saturation within fracture and matrix is shown in Figures 5.19-5.24. It can be seen that initially the fracture cleans up very rapidly. However, even until 500th day the water saturation in fracture is above the residual level. Matrix cleanup also closely follows fracture cleanup as observed in previous chapters. In addition, no vertical segregation of water is observed inside fracture. Condensate saturation at top and bottom of fracture/ fracture face does go up as production progresses. This is because as more gas passes through low pressure zone, more condensate is deposited.

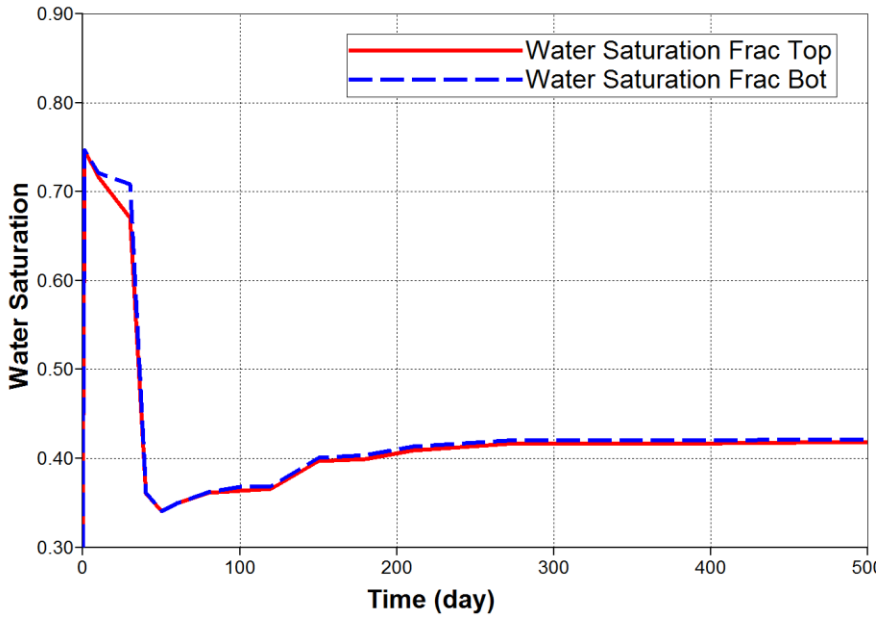

Figure 5.19: Variation of water saturation inside fracture over time (Lean condensate- Base case)

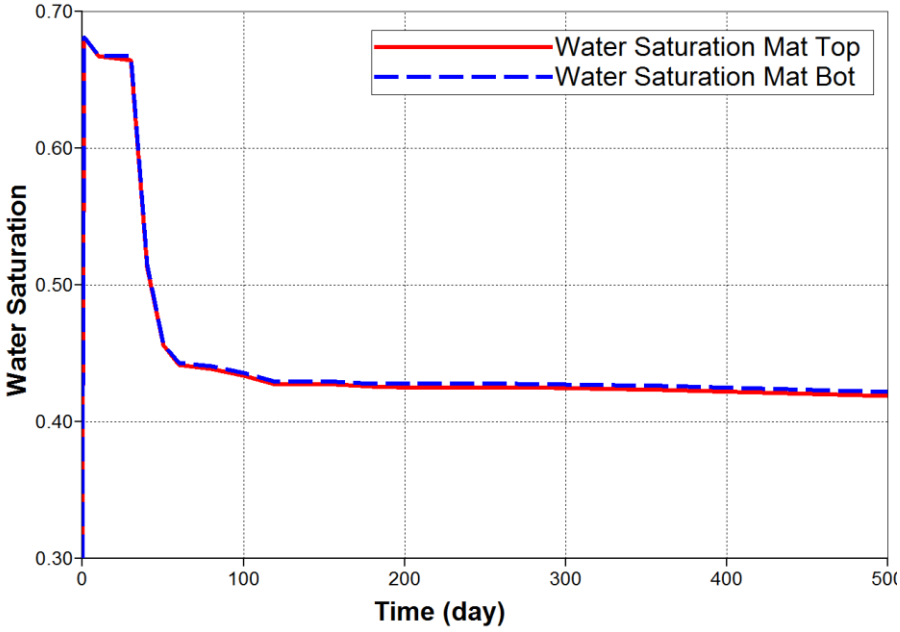

Figure 5.20: Variation of water saturation inside matrix 0.1 ft. from fracture face with time (Lean condensate-Base case)

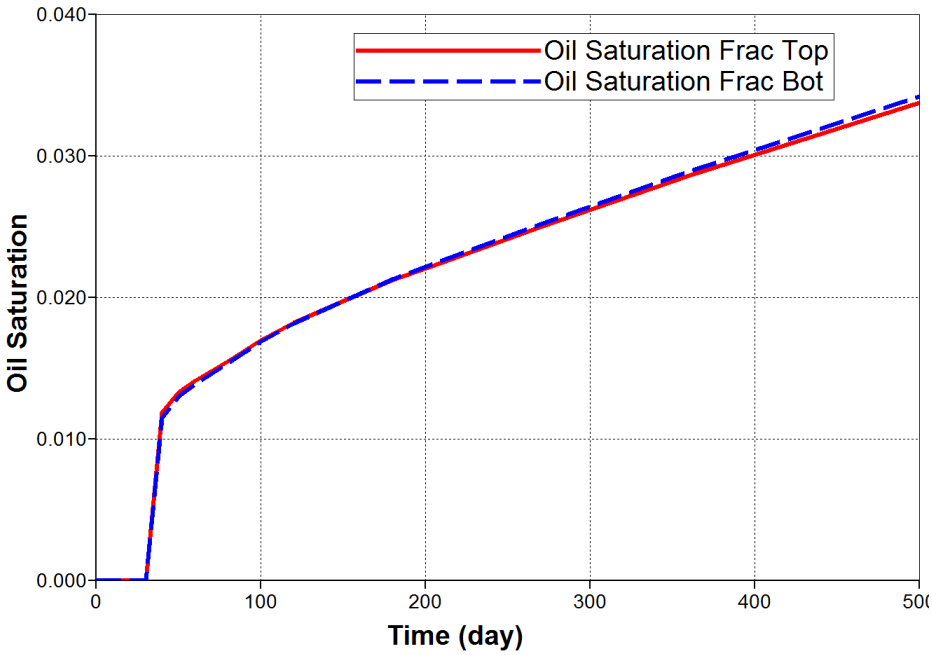

Figure 5.21: Variation of oil (condensate) saturation inside fracture over time (Lean condensate- Base case)

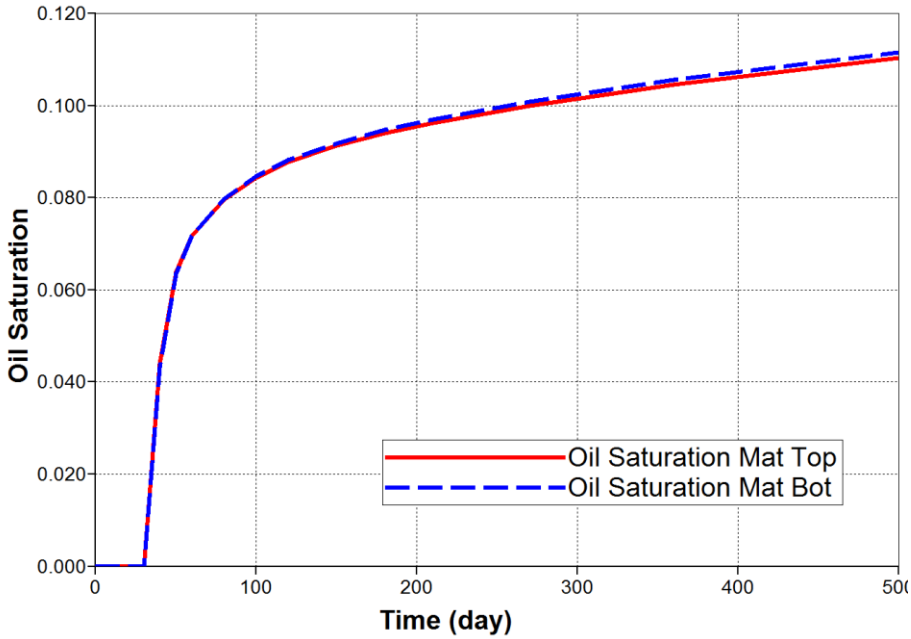

Figure 5.22: Variation of oil (condensate) saturation inside matrix 0.1 ft. from fracture face with time (Lean condensate-Base case)

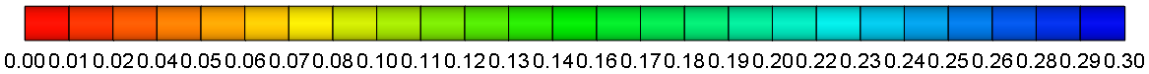

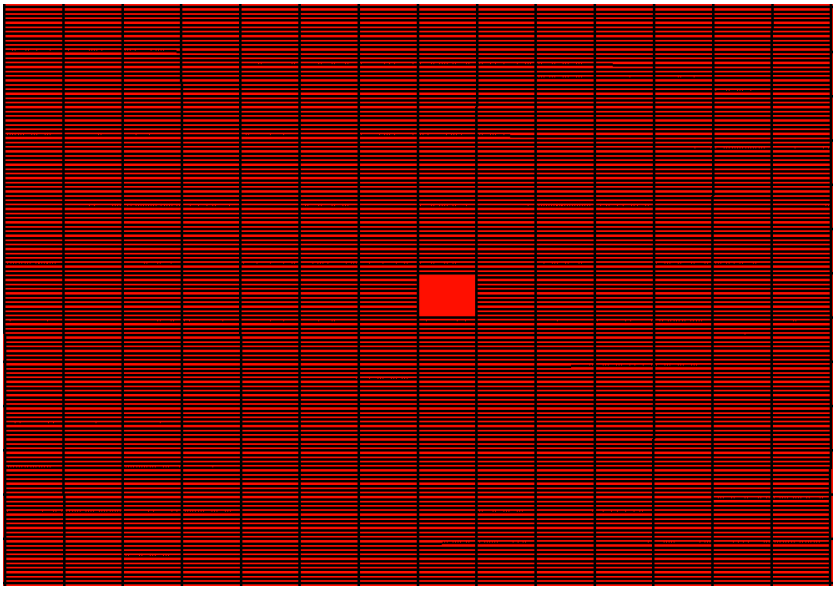

Oil saturation inside fracture after 30 days (end of shut-in period)

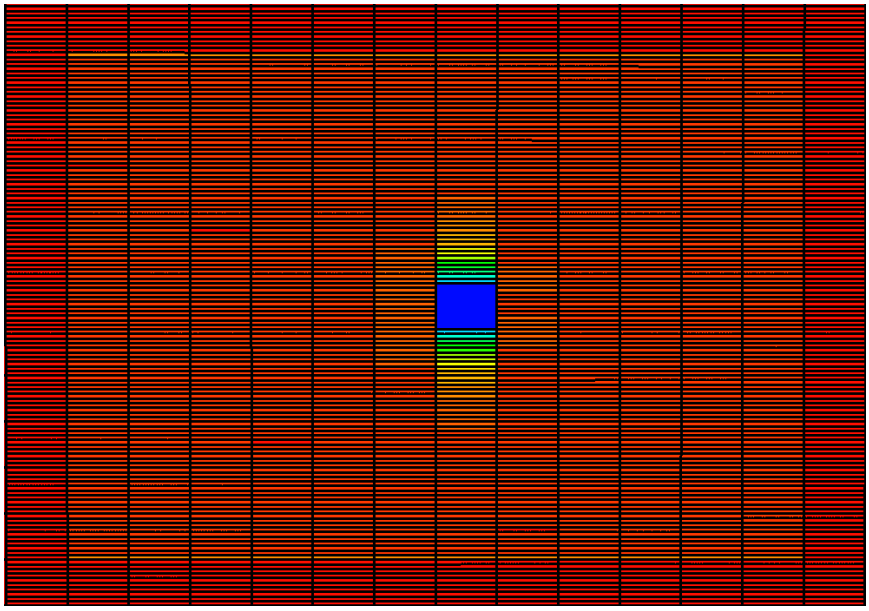

Oil saturation inside fracture after 120th day

Figure 5.23: Oil saturation maps (Lean condensate- Base case)

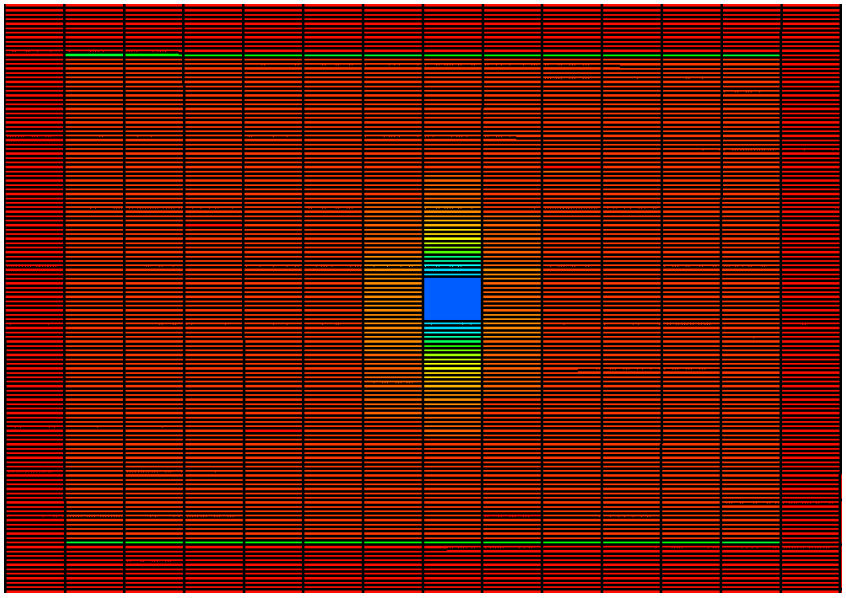

Oil saturation inside fracture after 500th day (end of production)

Figure 5.23: Oil saturation maps (Lean condensate- Base case) - Continued

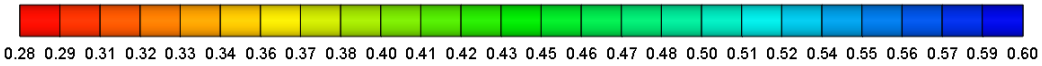

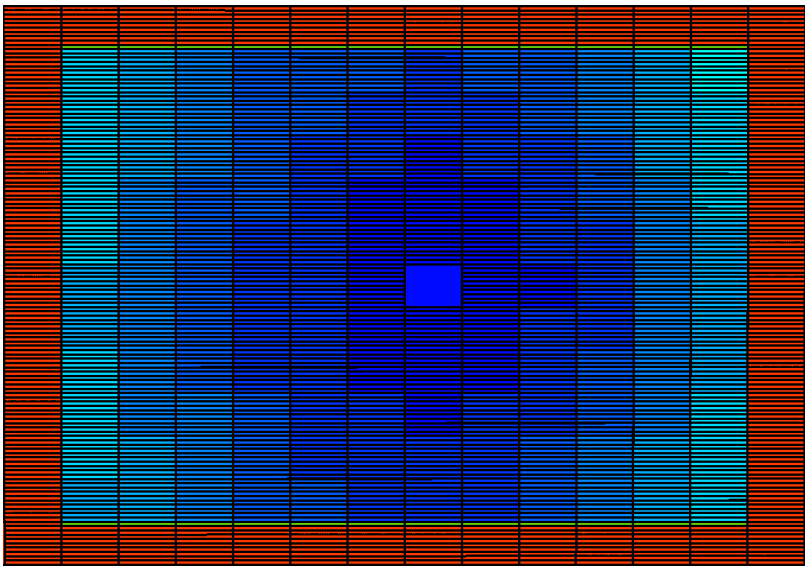

Water saturation inside fracture after 30th day (start of production)

Figure 5.24: Water saturation maps (Lean condensate- Base case)

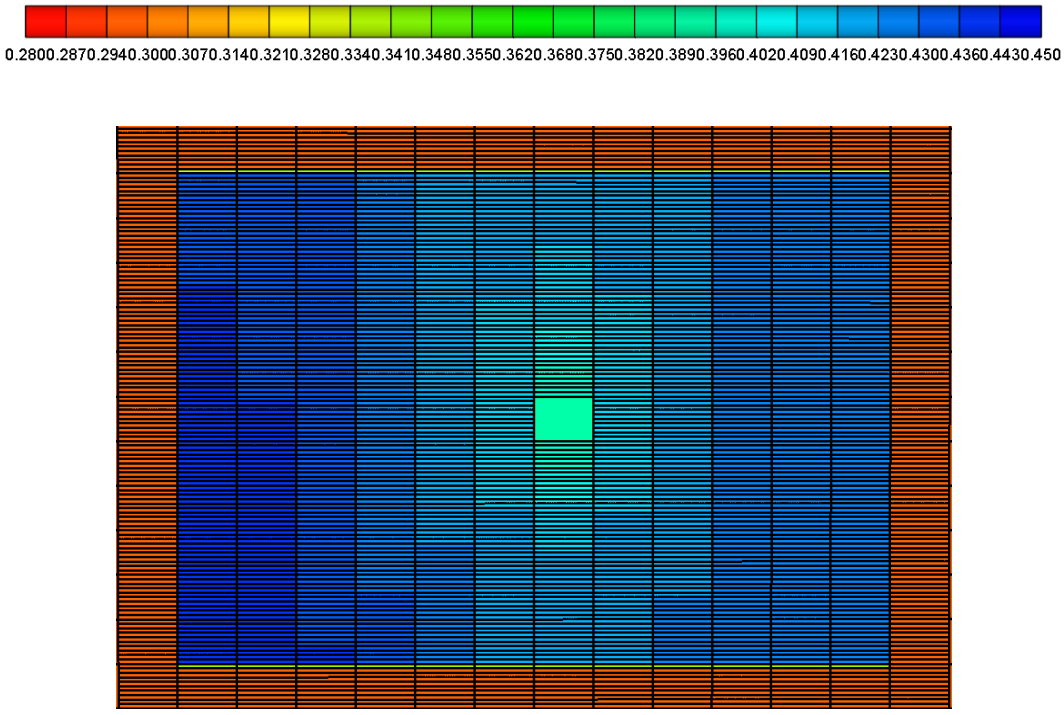

Water saturation inside fracture after 500th day (end of production)

Figure 5.24: Water saturation maps (Lean condensate- Base case)

5.3.2. Lean Condensate – Low drawdown (Relative perm. Set-1)

Increasing the wellbore pressure to 5500 psi reduces the drawdown to 1000 psi. Figure 5.17 suggests that at P_{wf} =5500 psi there would be no liquid drop out from the gas (Figures 5.27-29 indicate zero oil saturation). Lower drawdown will also lead to poorer frac-water cleanup. The cleanup is shown in Figures 5.25-5.30 below. Poorer cleanup impacts the gas production and is discussed later.

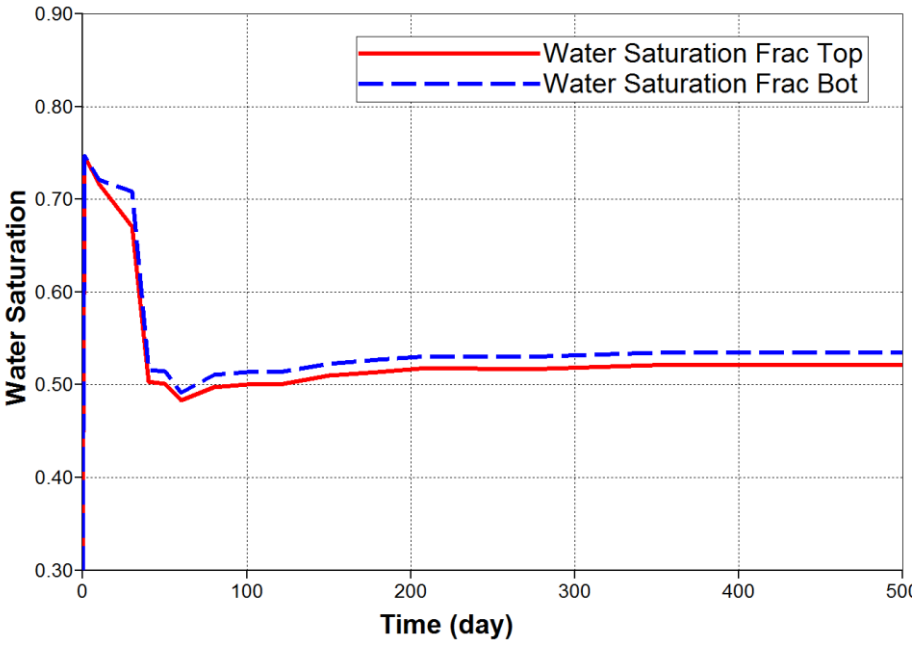

Figure 5.25: Variation of water saturation inside fracture over time (Lean condensate- Low drawdown)

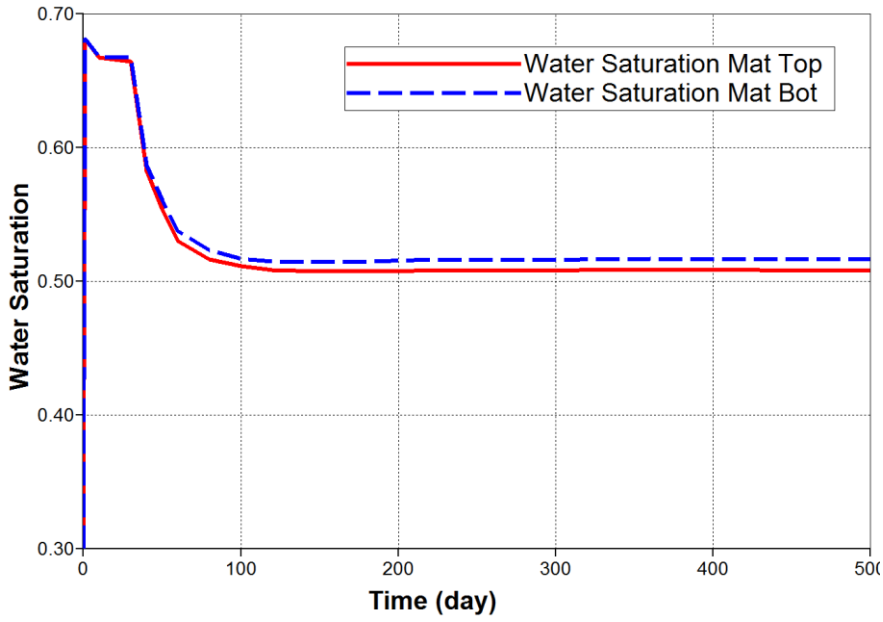

Figure 5.26: Variation of water saturation inside matrix 0.1 ft. from fracture face with time (Lean condensate- Low drawdown)

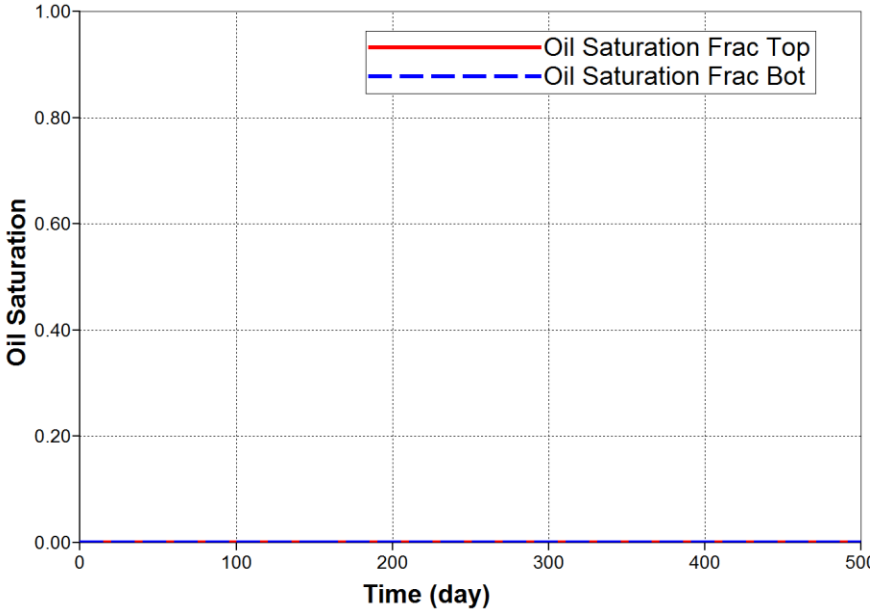

Figure 5.27: Variation of oil saturation inside fracture over time
(Lean condensate- Low drawdown)

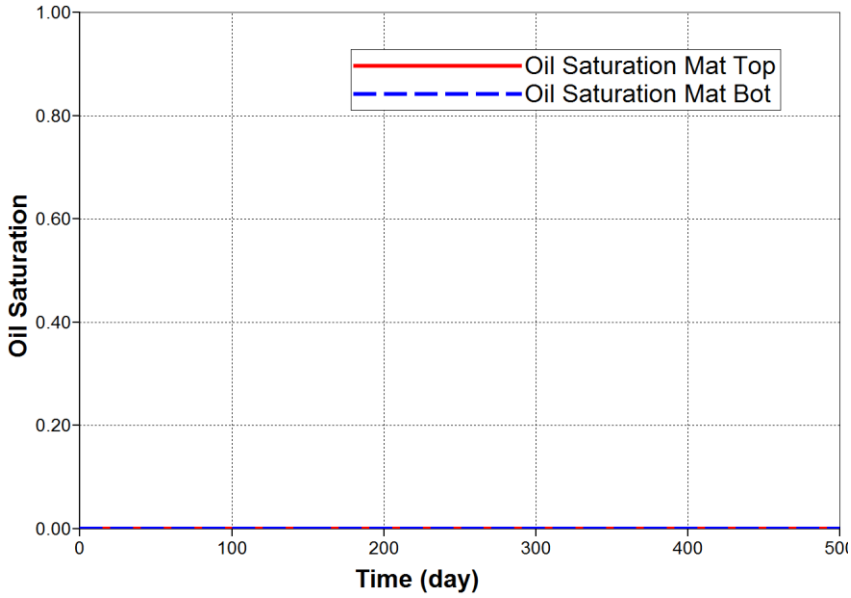

Figure 5.28: Variation of oil saturation inside matrix 0.1 ft. from fracture face with time
(Lean condensate- Low drawdown)

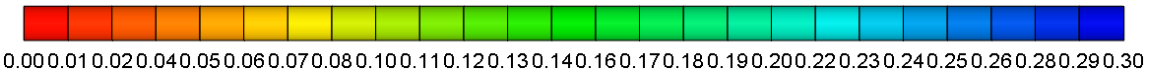

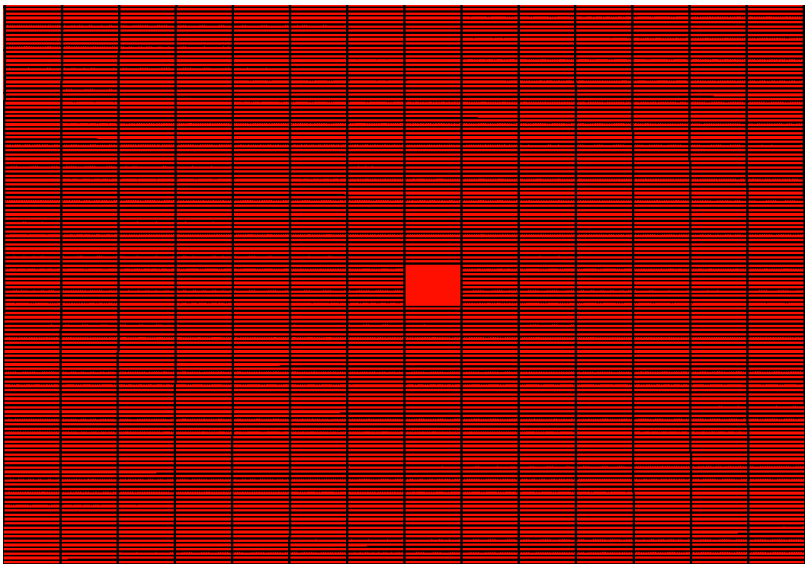

Oil saturation inside fracture after 60th day (30 days after start of production)

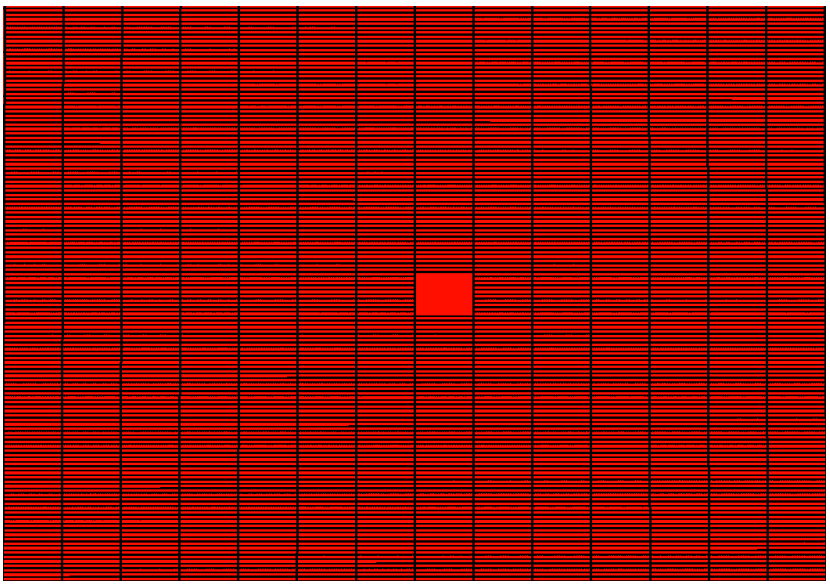

Oil saturation inside fracture after 500th day (end of production)

Figure 5.29: Oil saturation maps (Lean condensate- Low drawdown)

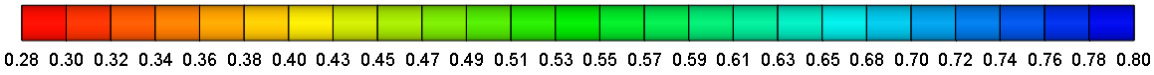

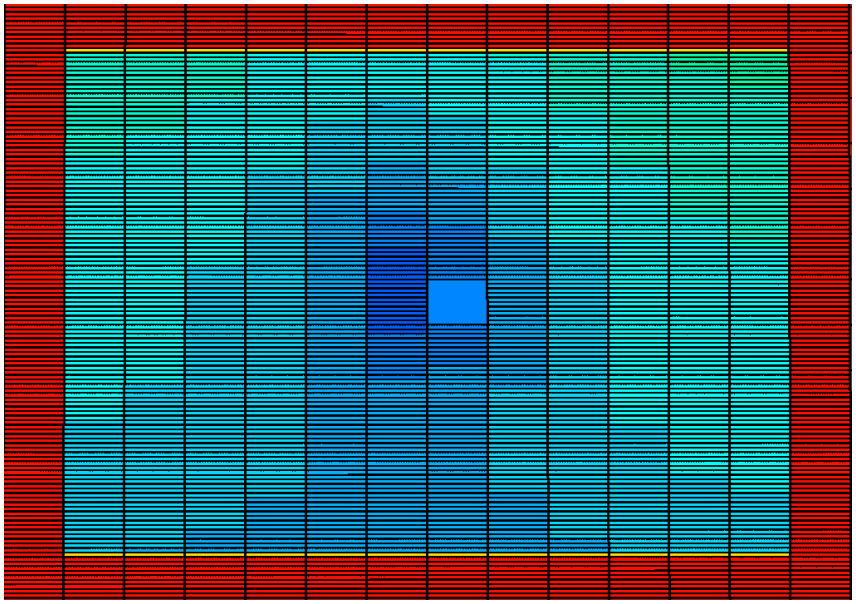

Water saturation inside fracture after 30th day (end of shut-in, start of production)

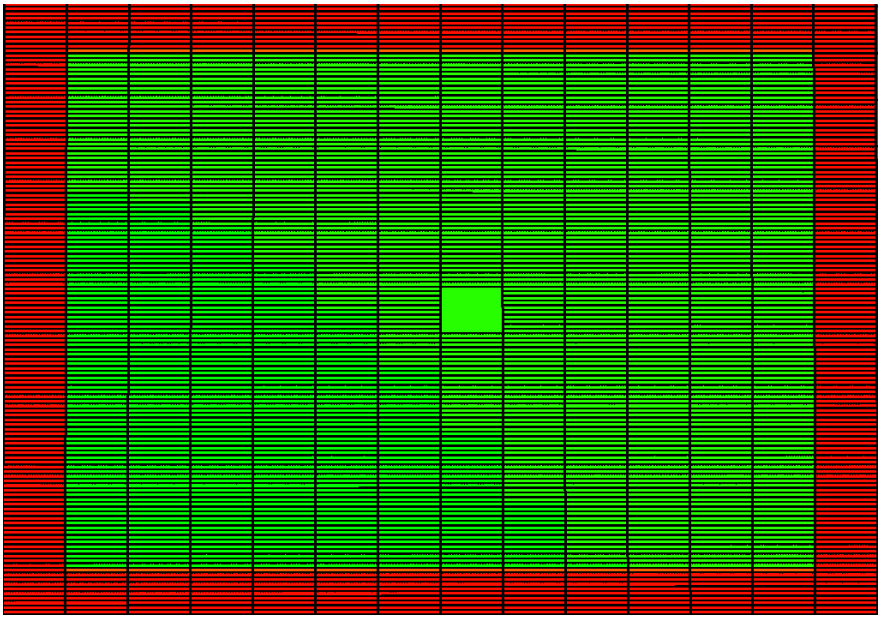

Water saturation inside fracture after 500th day (end of production)

Figure 5.30: Water saturation maps (Lean condensate- Low drawdown)

5.3.3. Lean Condensate – High drawdown (Relative perm. Set-1)

The drawdown is increased to 3500 psi by applying a flowing bottom-hole pressure of 3000 psi. Figure 5.17 shows that the liquid drop-out is maximum at this pressure. Maximum condensate drop out is expected, in addition to more efficient frac-water cleanup from fracture. The results below confirm the same. Water saturation inside the fracture goes down immediately after onset of production due to high initial flow rates. As more water flows from matrix into the fracture and gas velocities decline the water saturation inside the fracture also increases. The oil saturation inside the fracture and on matrix face is higher as per the PVT properties of the gas.

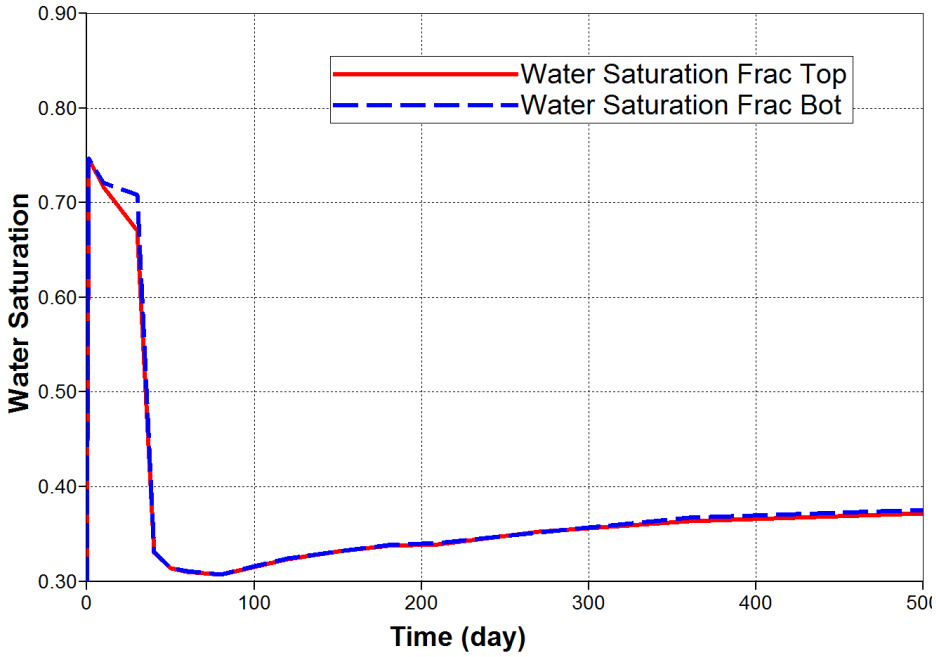

Figure 5.31: Variation of water saturation inside fracture over time (Lean condensate- high drawdown)

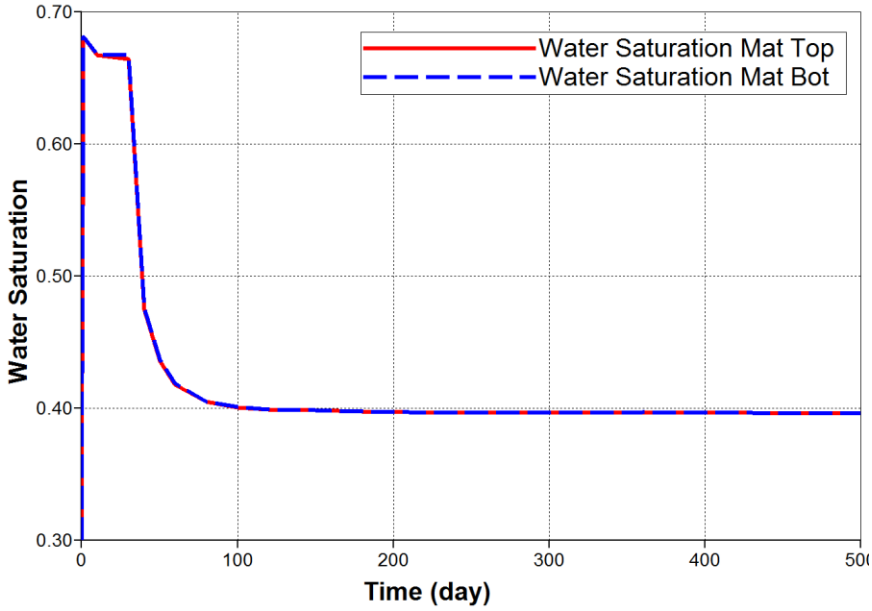

Figure 5.32: Variation of water saturation inside matrix 0.1 ft. from fracture face with time (Lean condensate- High drawdown)

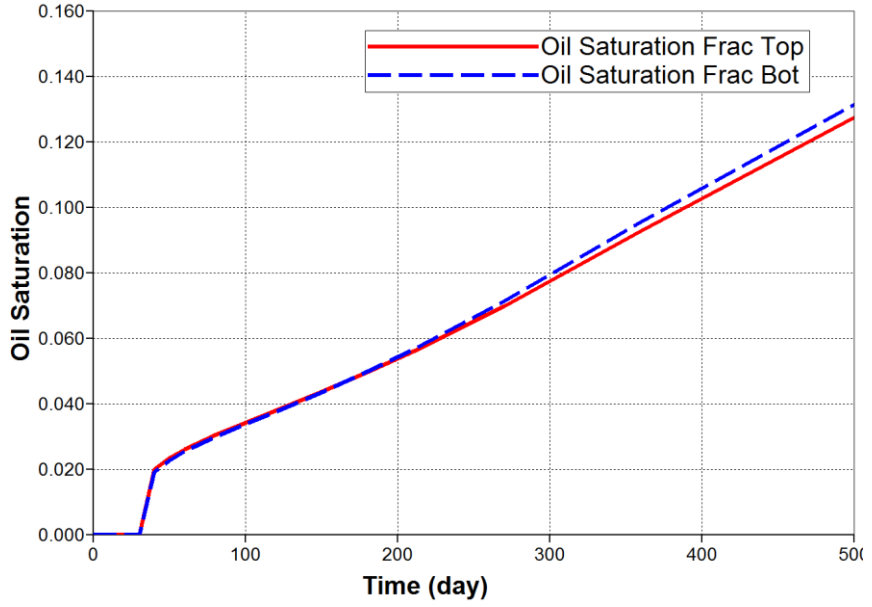

Figure 5.33: Variation of oil saturation inside fracture over time (Lean condensate- High drawdown)

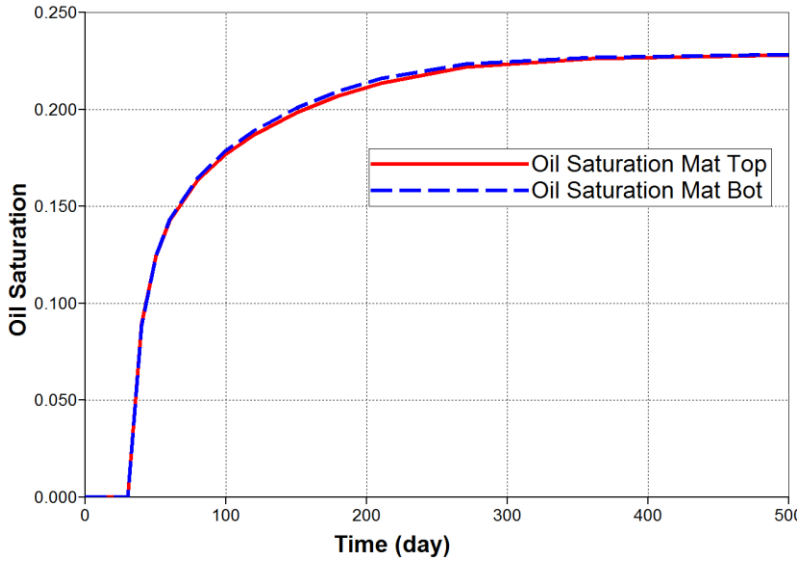

Figure 5.34: Variation of oil saturation inside matrix 0.1 ft. from fracture face with time (Lean condensate- High drawdown)

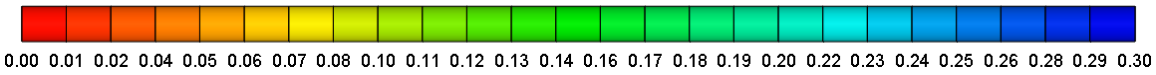

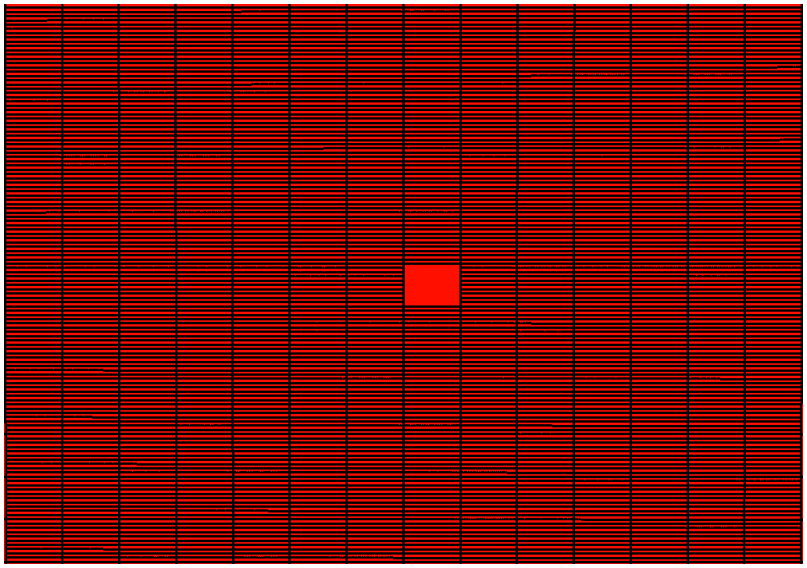

Oil saturation inside fracture after 30th day (end of shut-in, start of production)

Figure 5.35: Oil saturation maps (Lean condensate- High drawdown)

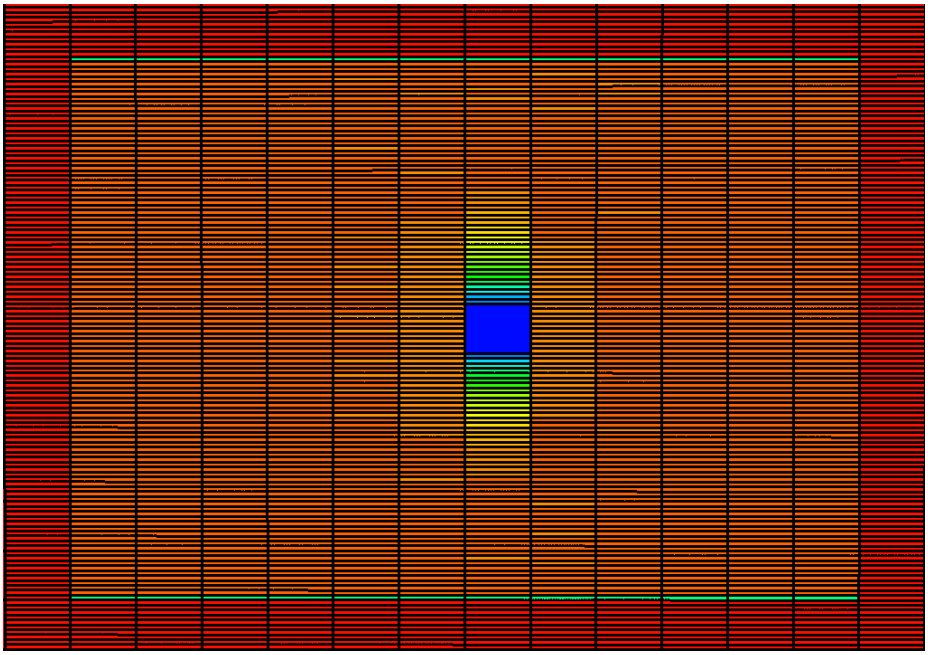

Oil saturation inside fracture after 210th day

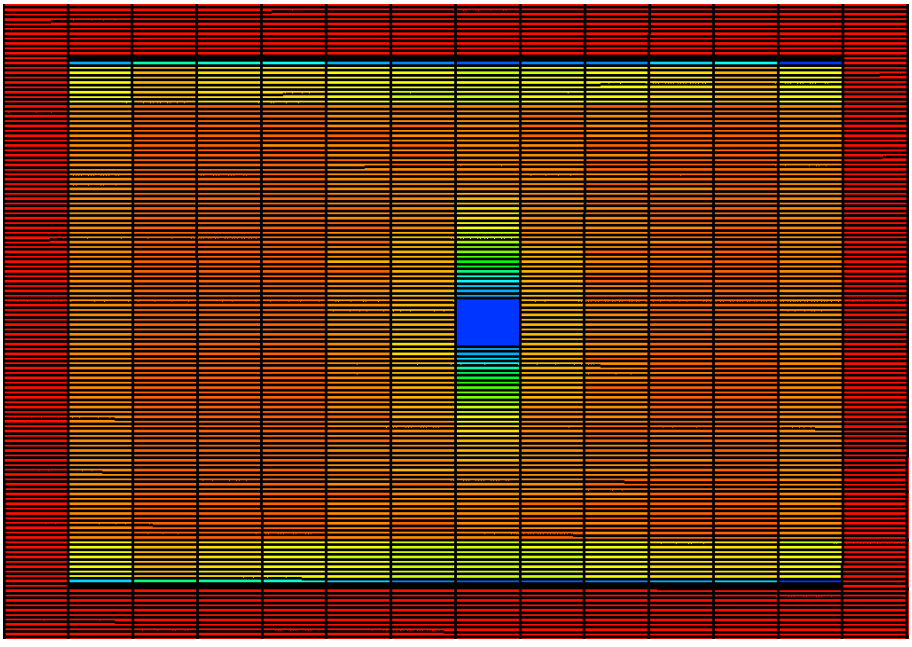

Oil saturation inside fracture after 500th day (end of production)

Figure 5.35: Oil saturation maps (Lean condensate- High drawdown) - Continued

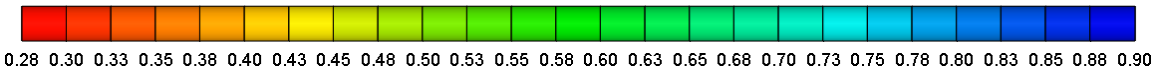

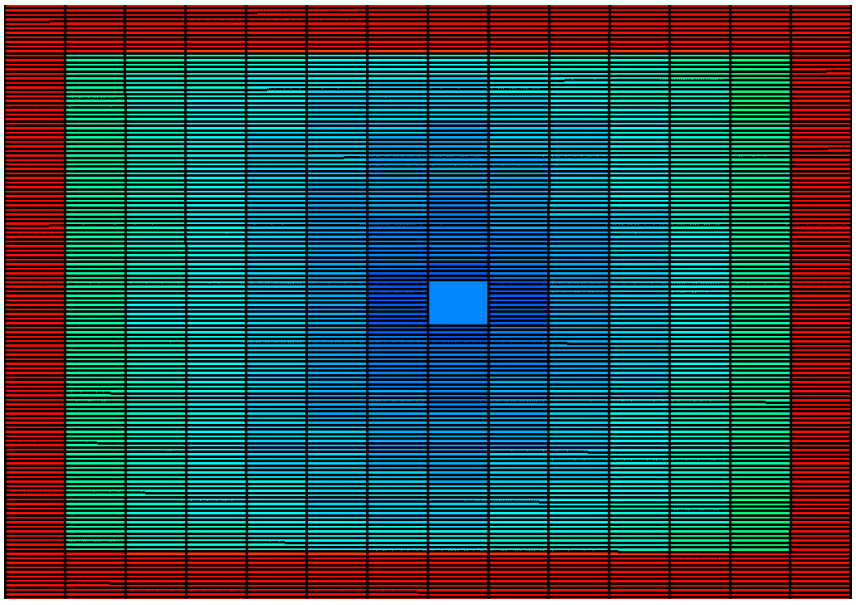

Water saturation inside fracture after 1 day (end of injection)

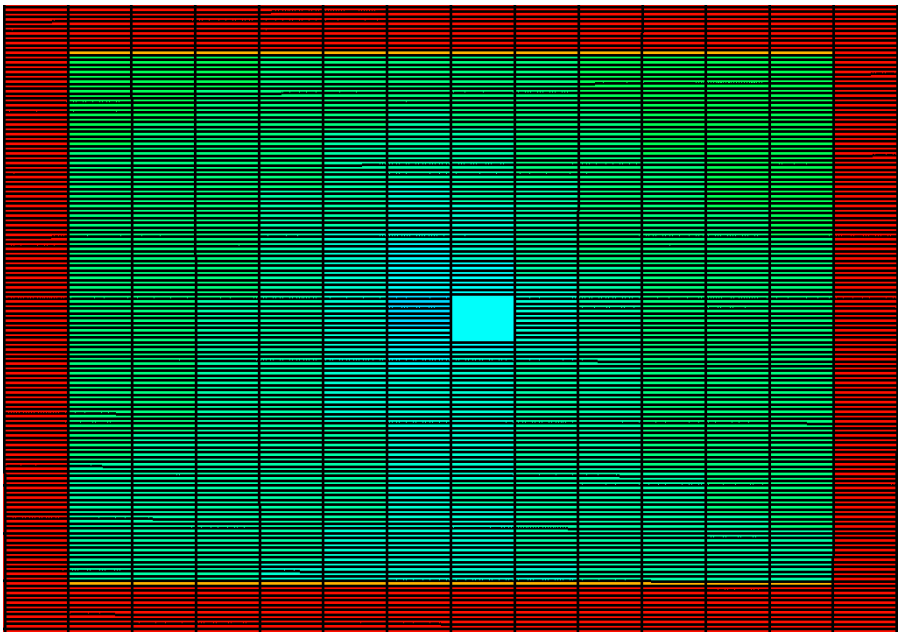

Water saturation inside fracture after 30th day (end of shut-in)

Figure 5.36: Water saturation maps (Lean condensate- High drawdown)

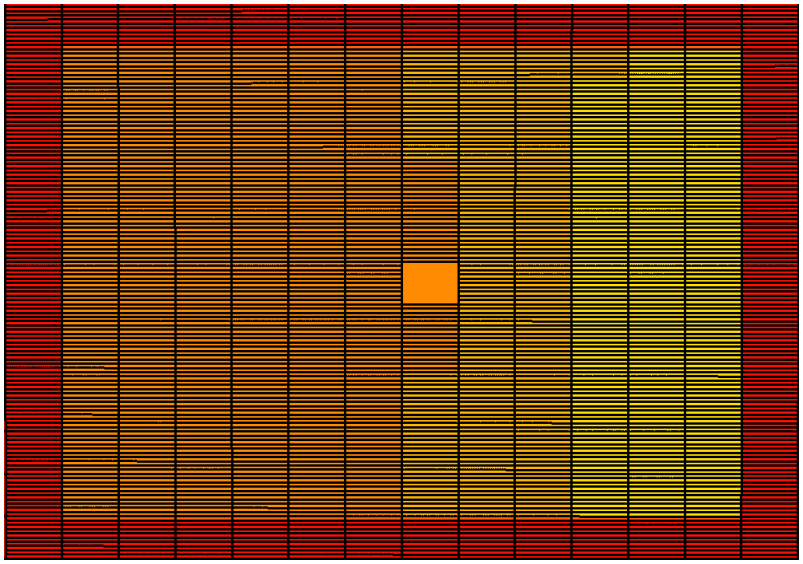

Water saturation inside fracture after 500th day (end of production)

Figure 5.36: Water saturation maps (Lean condensate- High drawdown) - continued

5.3.4. Rich Condensate- Base case (Relative permeability Set-1)

For rich condensate scenarios, a fluid with high condensate content (as shown in Figures 5.15-5.16) is selected. The maximum liquid drop out in CCE is approximately 35% and the dew point is 3470 psi. Considering the high liquid content, larger condensate drop out is expected in the fracture and matrix. This would lead to greater impact on gas relative permeability. In the base case bottom-hole pressure is kept at 3000 psi. The frac water and oil (condensate) cleanup profiles are shown in Figures 5.37-5.42. Results show that water cleanup is uniform at top and bottom. However, even after 500th day of production there is mobile water saturation inside the fracture. There is significant condensate buildup within the fracture and it segregates towards the bottom (Figure 5.41). This will severely impact gas productivity from the bottom half of the fracture. Another point to note is that oil saturations inside fracture and in matrix at fracture face

are different. This is because the water-wet matrix doesn't counter imbibe oil from fracture. The oil saturation in the matrix is only dependent on whether drawdown can overcome capillary forces.

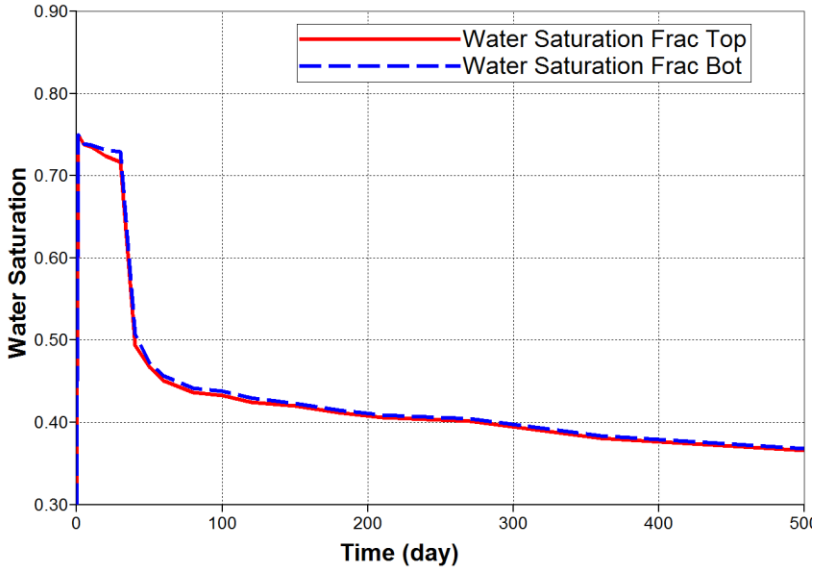

Figure 5.37: Variation of water saturation inside fracture over time (Rich condensate- Base)

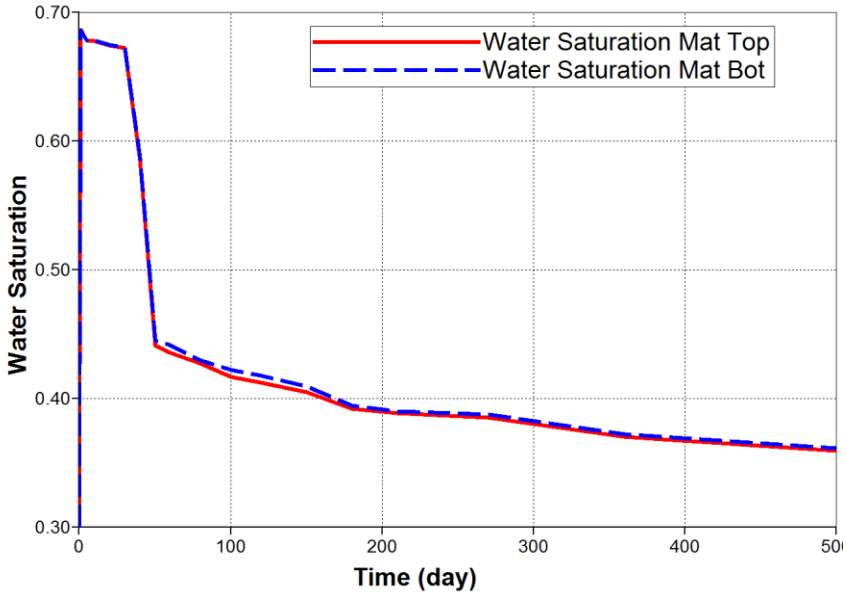

Figure 5.38: Variation of water saturation inside matrix 0.1 ft. from fracture face with time (Rich condensate- Base)

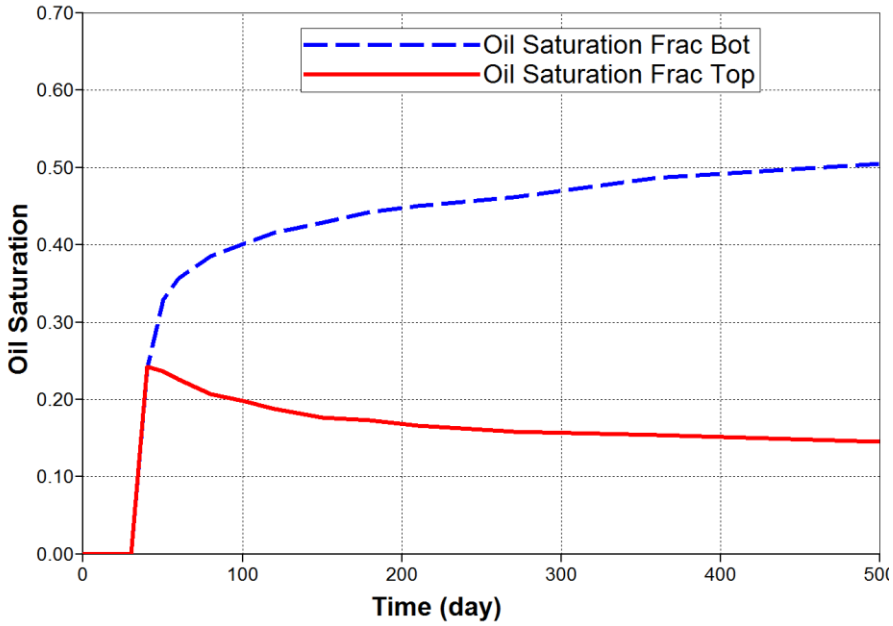

Figure 5.39: Variation of oil saturation inside fracture over time
(Rich condensate- Base)

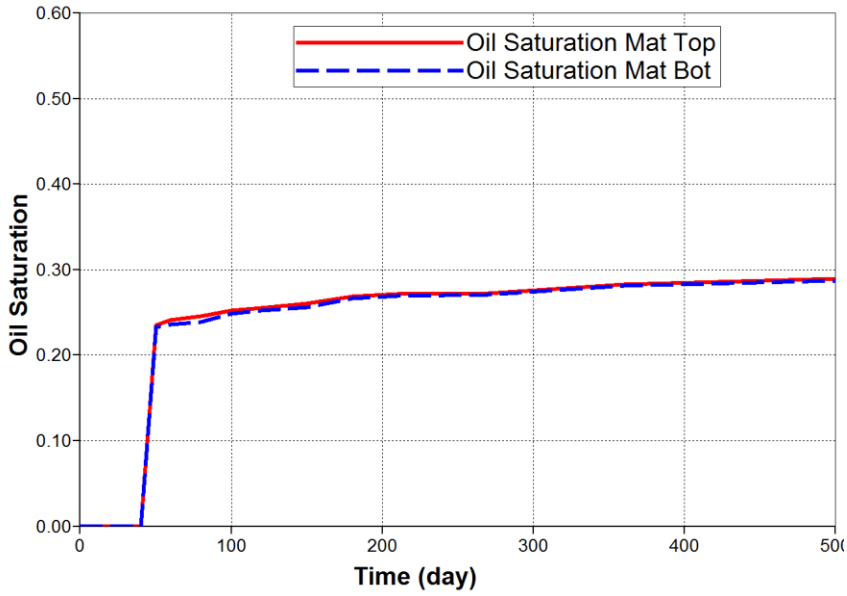

Figure 5.40: Variation of oil saturation inside matrix 0.1 ft. from fracture face with time
(Rich condensate- Base)

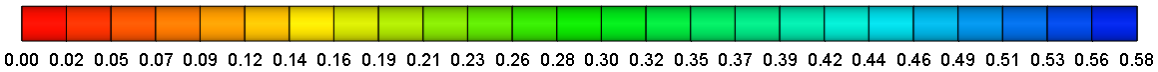

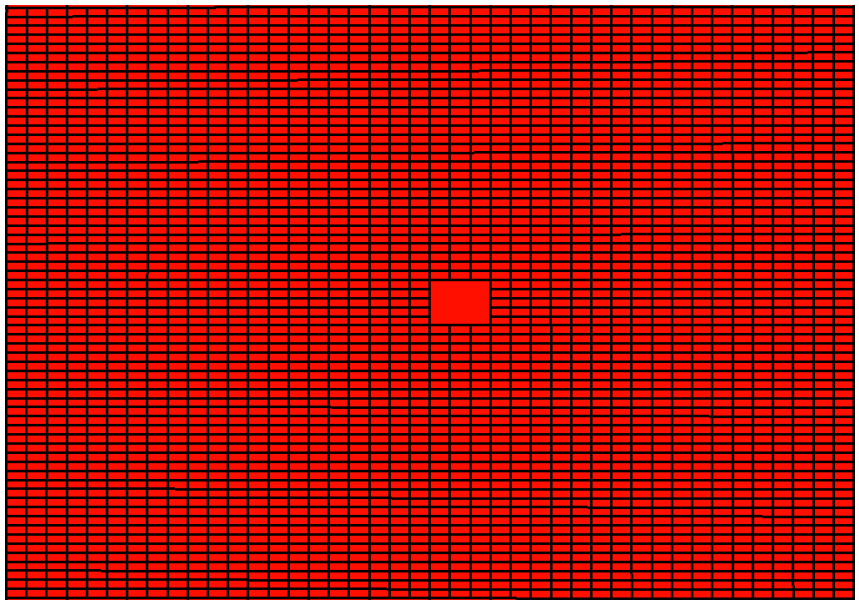

Oil saturation inside fracture after 30th day

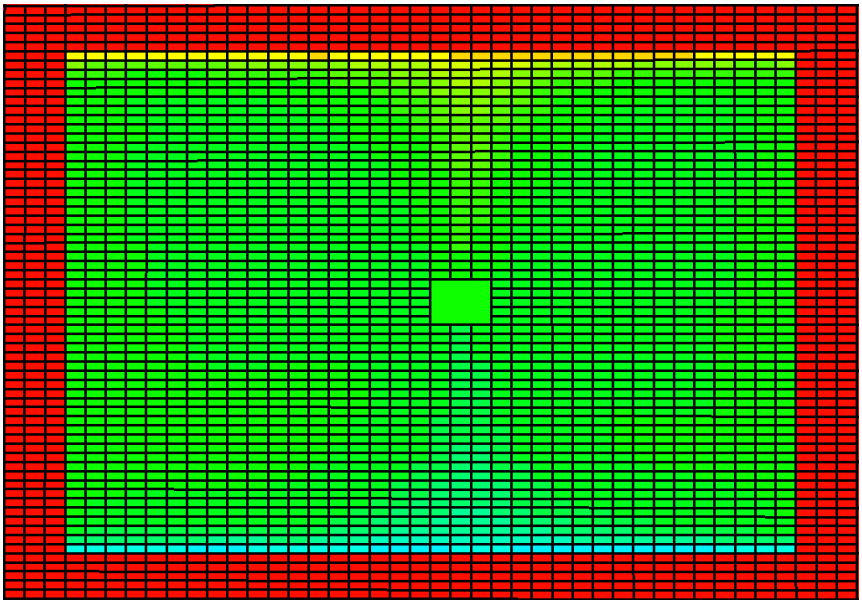

Oil saturation inside fracture after 80th day

Figure 5.41: Oil saturation maps (Rich condensate- Base case)

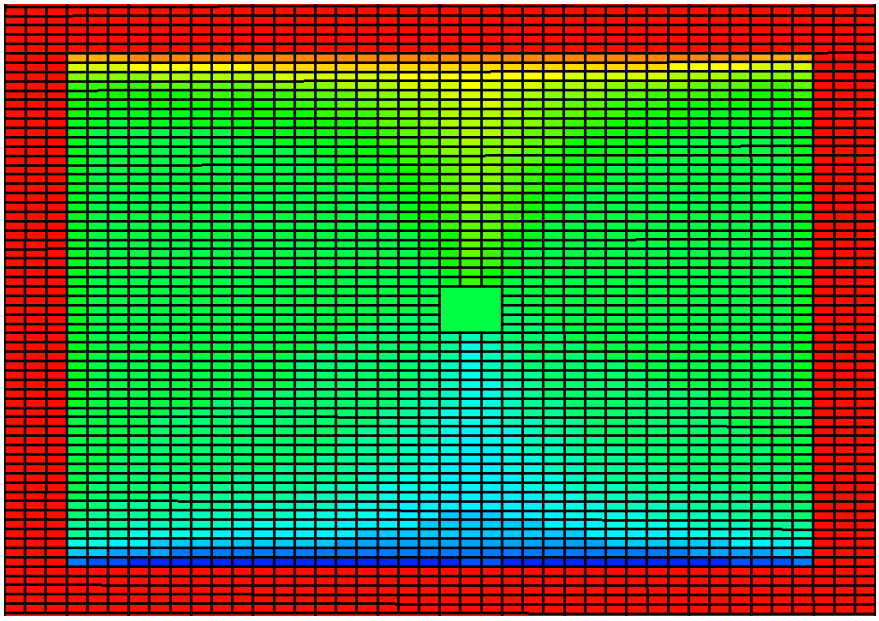

Water saturation inside fracture after 500th day (end of production)

Figure 5.41: Oil saturation maps (Rich condensate- Base case) - Continued

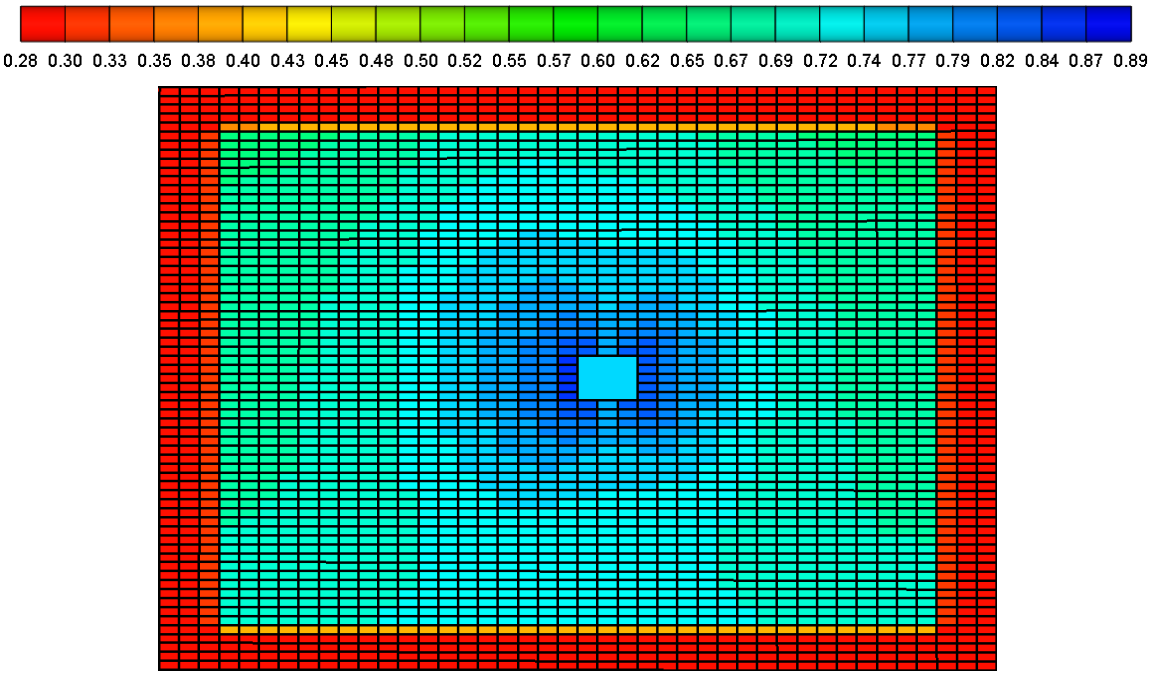

Water saturation inside fracture after 30th day (end of shut-in)

Figure 5.42: Water saturation maps (Rich condensate- Base)

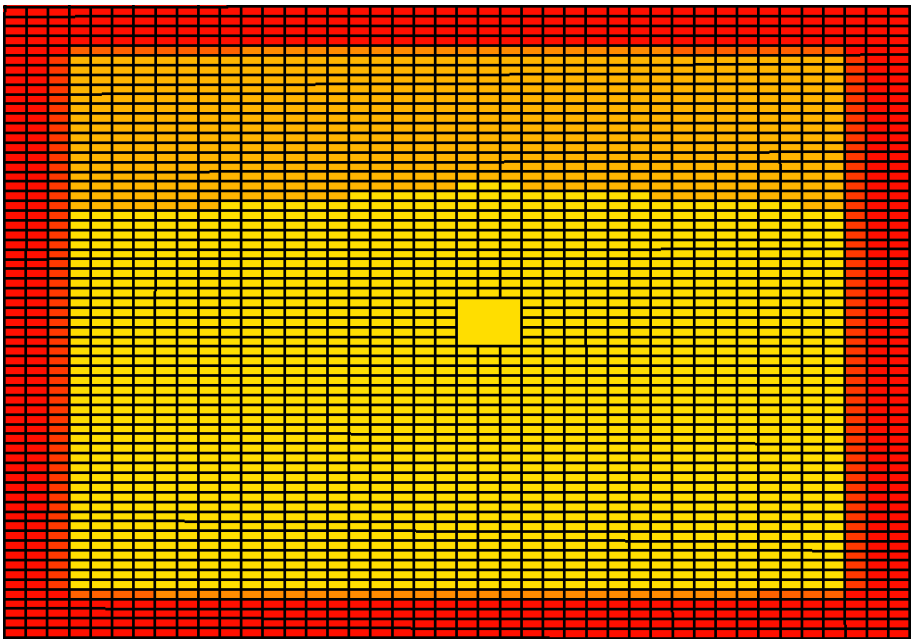

Water saturation inside fracture after 270th day

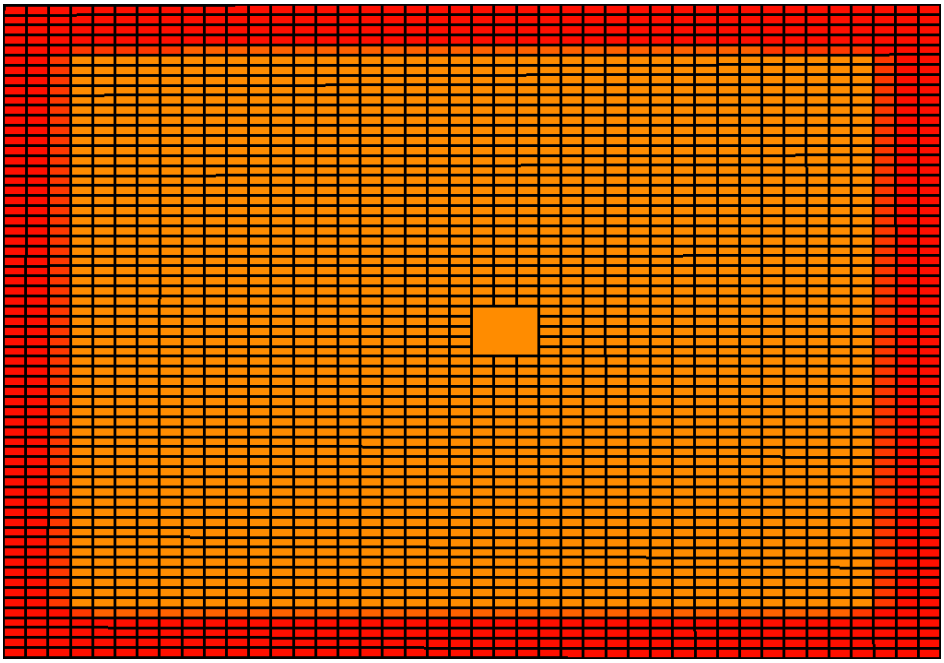

Water saturation inside fracture after 500th day (end of production)

Figure 5.42: Water saturation maps (Rich condensate- Base)- Continued

5.3.5. Rich Condensate – Low drawdown (Relative Perm. Set-1)

To understand the impact of low drawdown on fracture cleanup, a bottom-hole pressure of 5500 psi is applied. No condensate drop-out is expected since wellbore pressure is above dew point. The water and oil cleanup profiles are shown in Figures 5.43-5.48. Low drawdown leads to worse frac-water cleanup from fracture and matrix face as compared to base case.

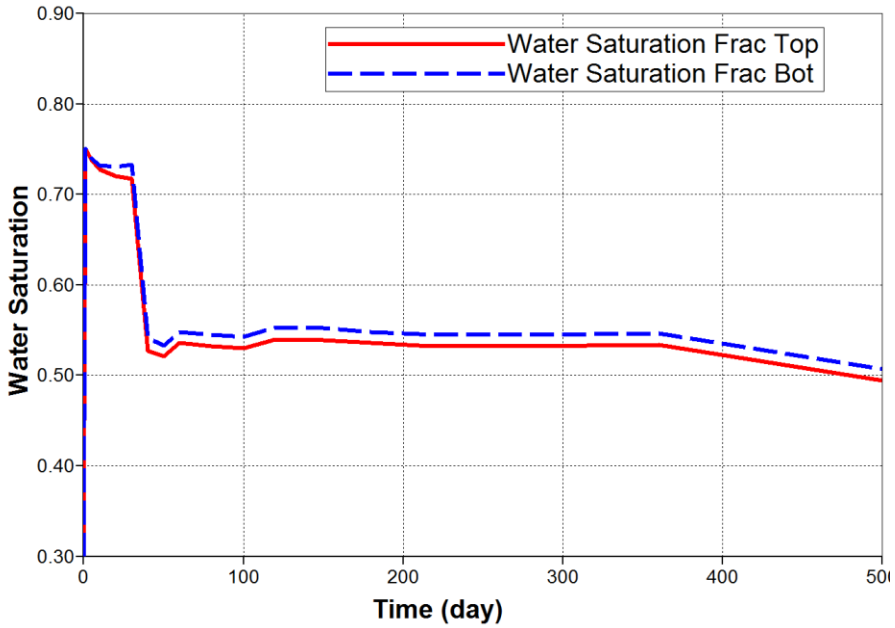

Figure 5.43: Variation of water saturation inside fracture over time (Rich condensate- low drawdown)

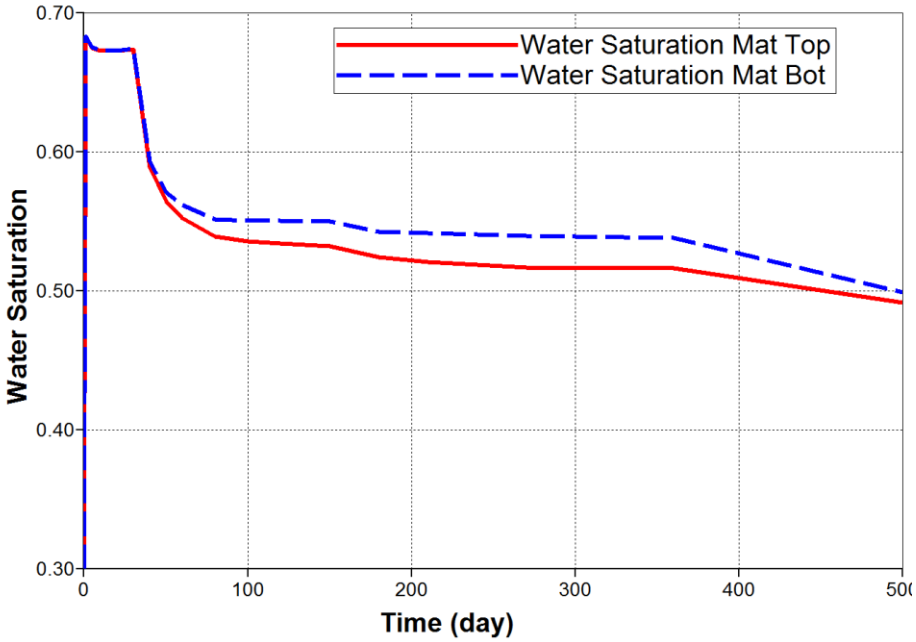

Figure 5.44: Variation of water saturation inside matrix 0.1 ft. from fracture face with time (Rich condensate- Low drawdown)

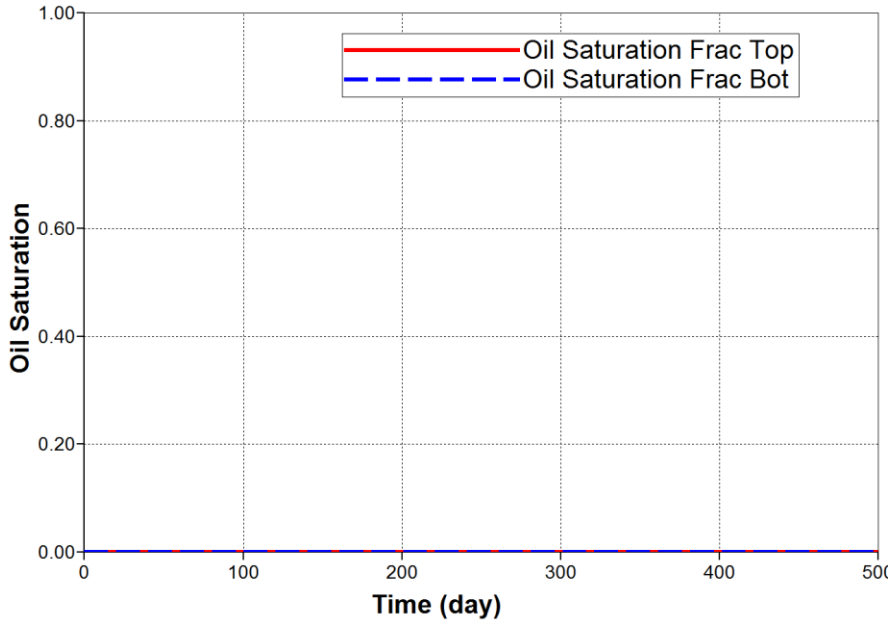

Figure 5.45: Variation of oil saturation inside fracture over time (Rich condensate- low drawdown)

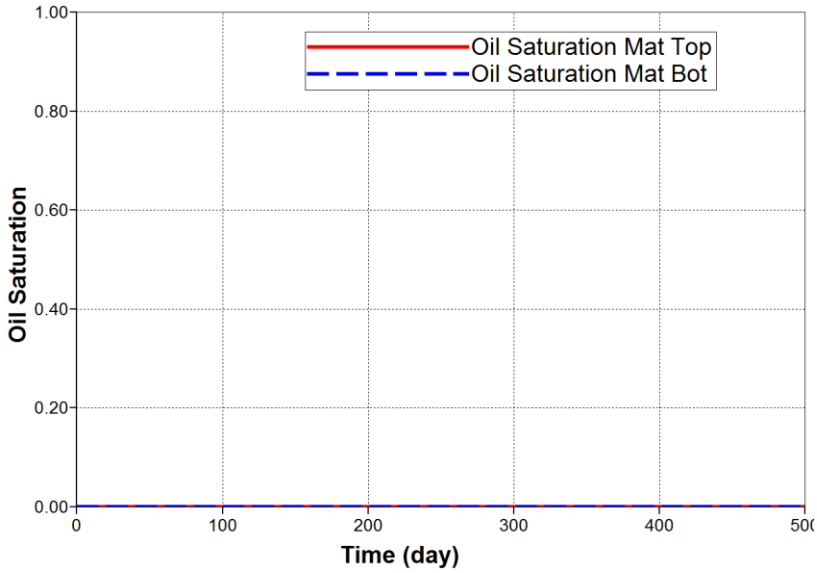

Figure 5.46: Variation of oil saturation inside matrix 0.1 ft. from fracture face with time (Rich condensate- Low drawdown)

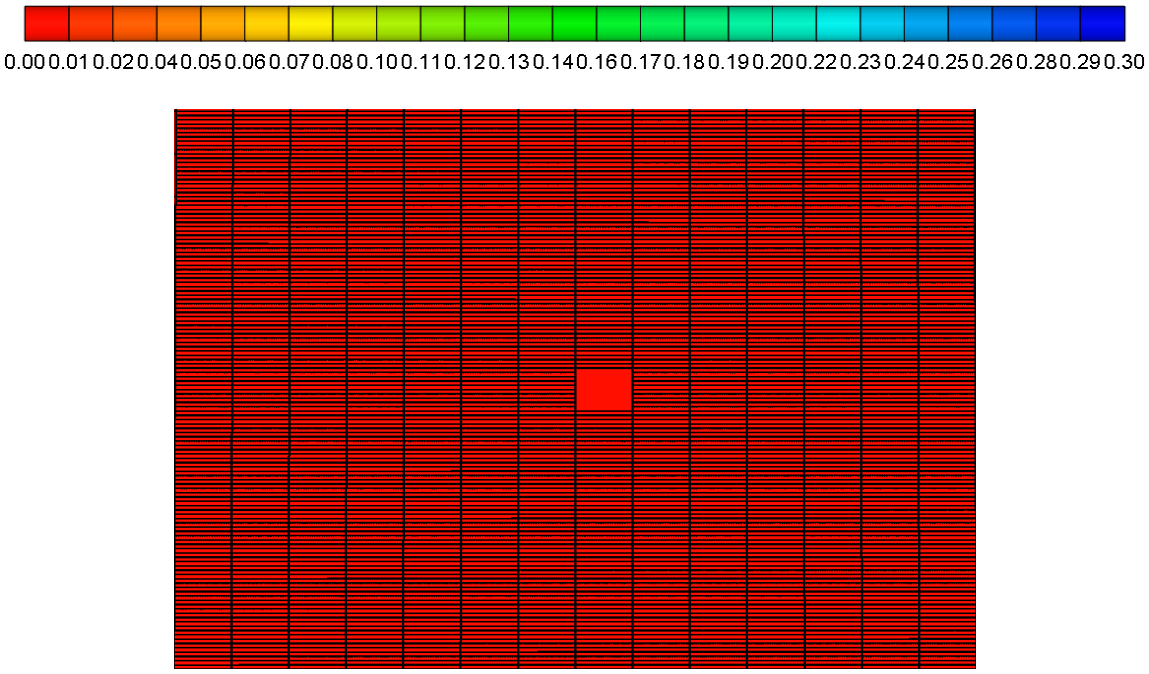

Oil saturation inside fracture after 30th day (end of shut-in, start of production)

Figure 5.47: Oil saturation maps (Rich condensate- Low drawdown)

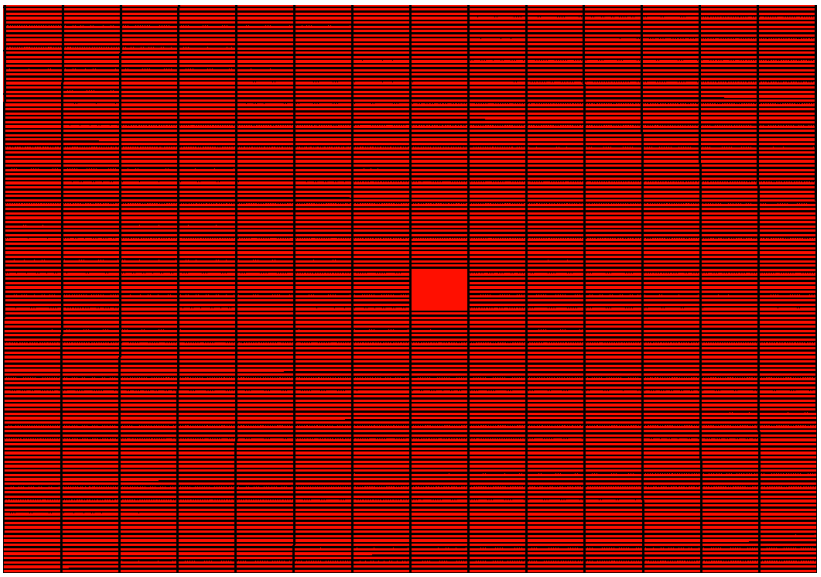

Oil saturation inside fracture after 120th day

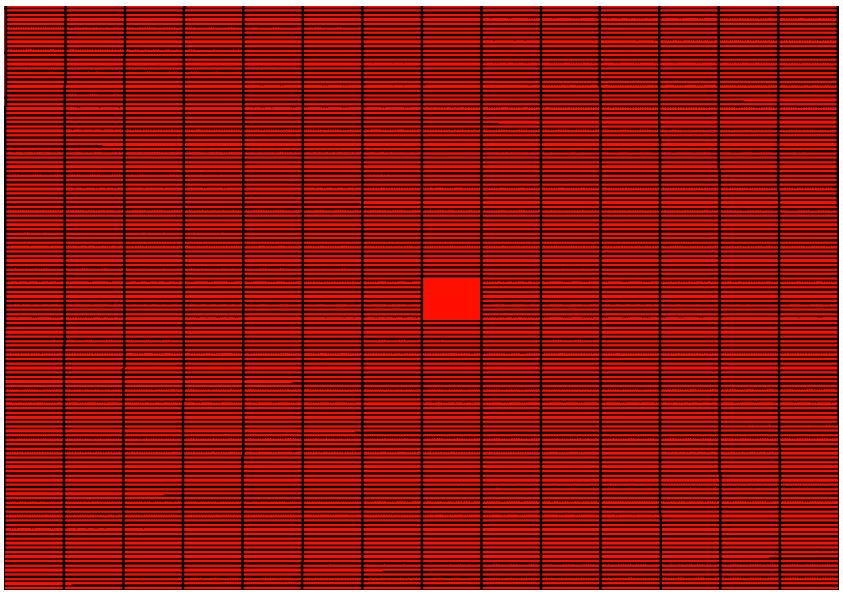

Oil saturation inside fracture after 500th day (end of production)

Figure 5.47: Oil saturation maps (Rich condensate- Low drawdown) – Continued

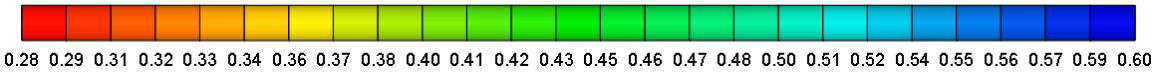

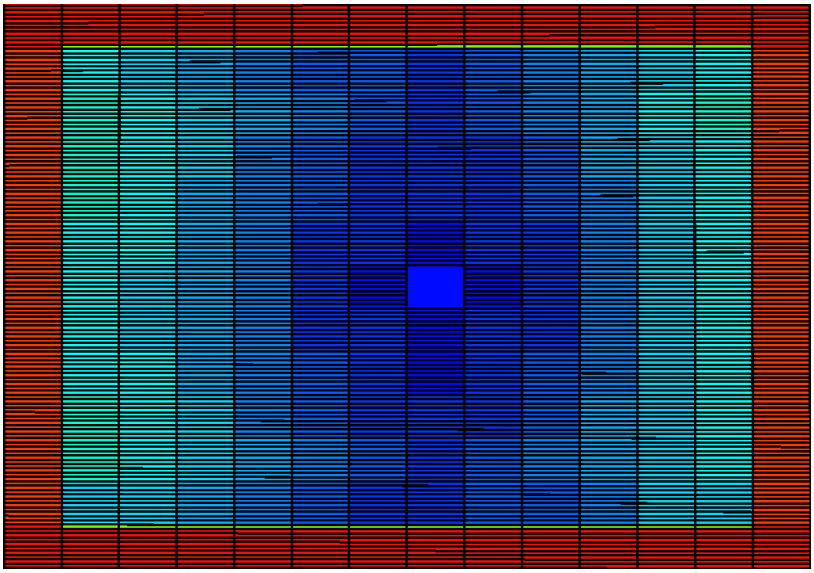

Water saturation inside fracture after 30th day (end of shut-in, start of production)

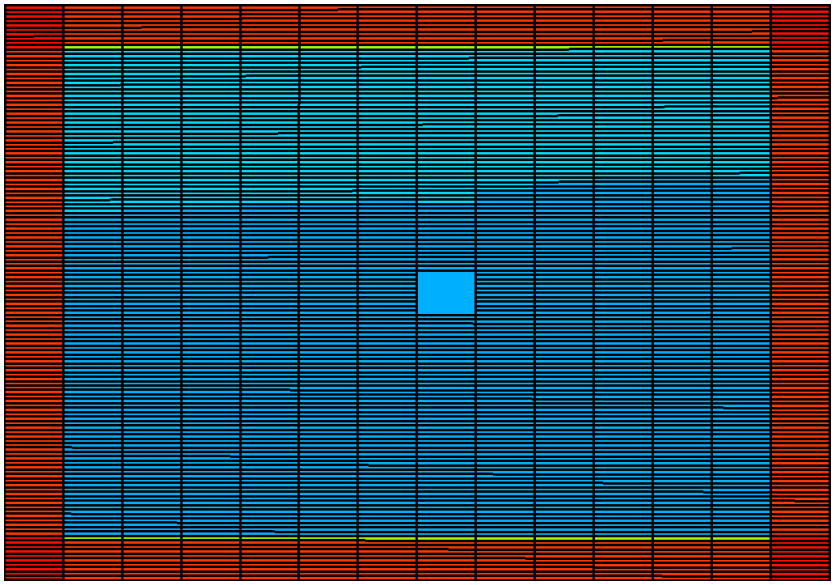

Water saturation inside fracture after 80th day

Figure 5.48: Water saturation maps (Rich condensate- Low drawdown)

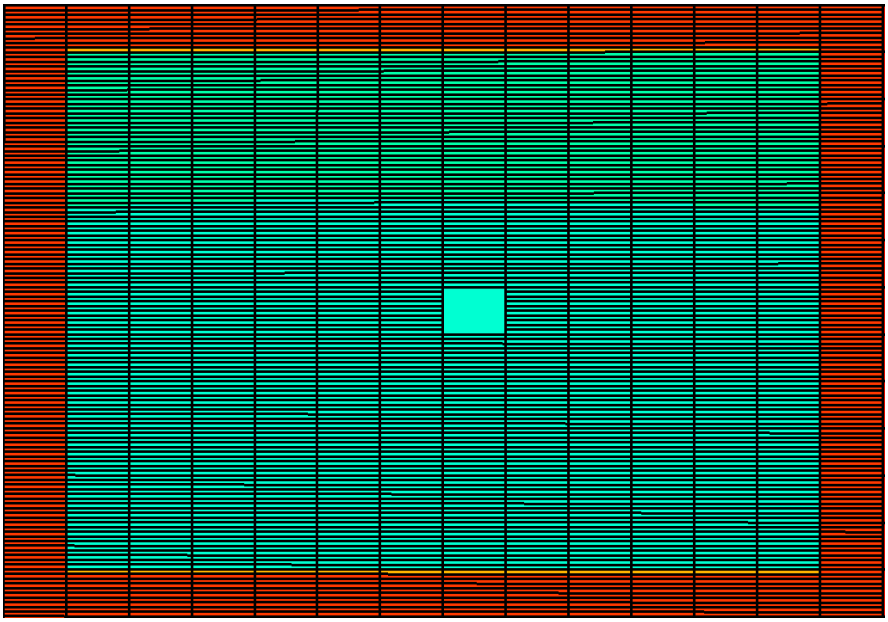

Water saturation inside fracture after 500th day (end of production)

Figure 5.48: Water saturation maps (Rich condensate- Low drawdown) - Continued

5.3.6. Rich Condensate – High drawdown (Relative perm. Set-1)

A bottom-hole pressure of 2500 psi is applied to study cleanup at higher drawdown. Figure 5.15 shows liquid drop out is near maximum at this pressure. The cleanup of fracture and matrix is shown in Figures 5.49-5.54. The important thing to note is the loading of condensate inside the fracture, primarily towards the bottom (Figure 5.53). This is similar to the water loading that was observed in the dry gas scenarios.

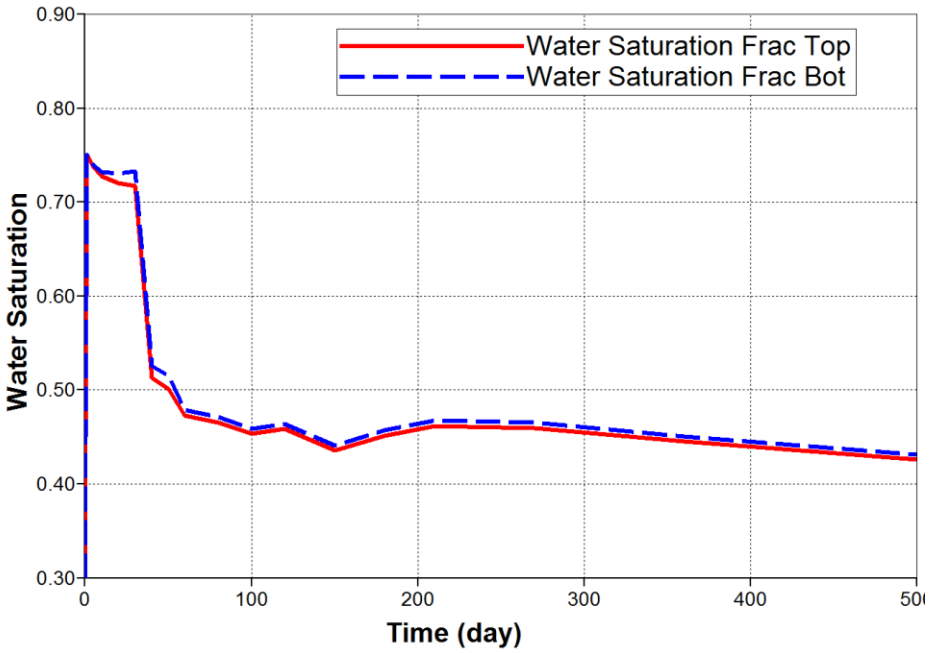

Figure 5.49: Variation of water saturation inside fracture over time (Rich condensate- High drawdown)

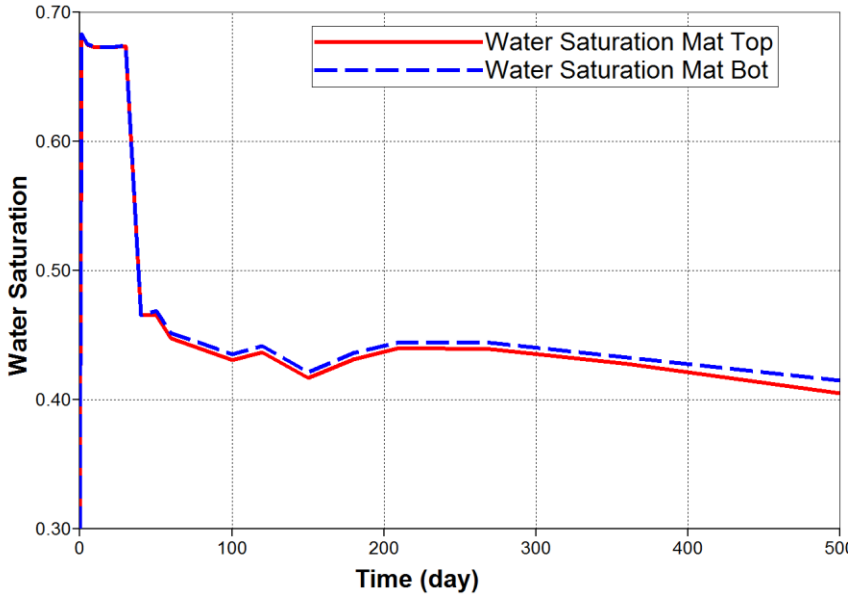

Figure 5.50: Variation of water saturation inside matrix 0.1 ft. from fracture face with time (Rich condensate- High drawdown)

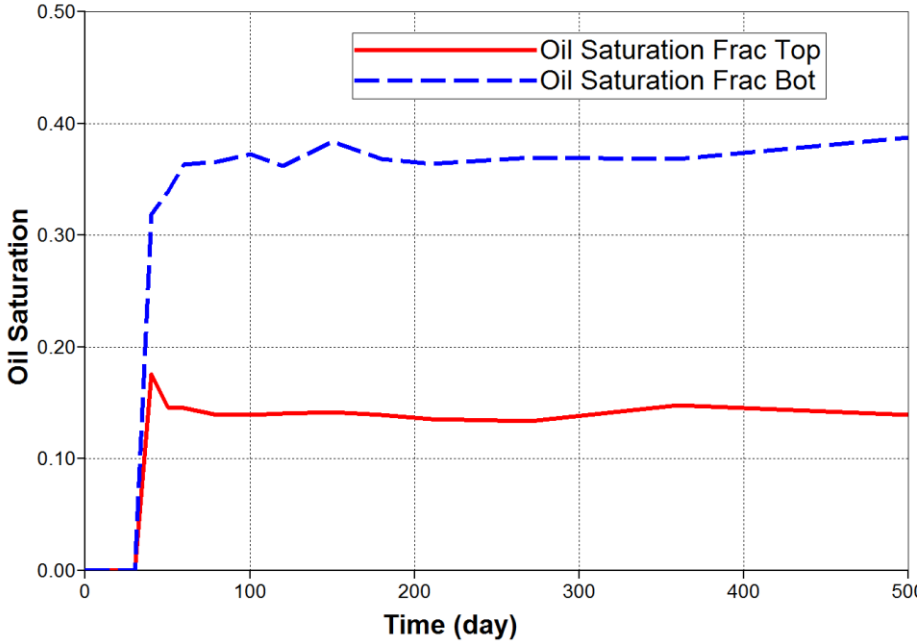

Figure 5.51: Variation of oil saturation inside fracture over time
(Rich condensate- High drawdown)

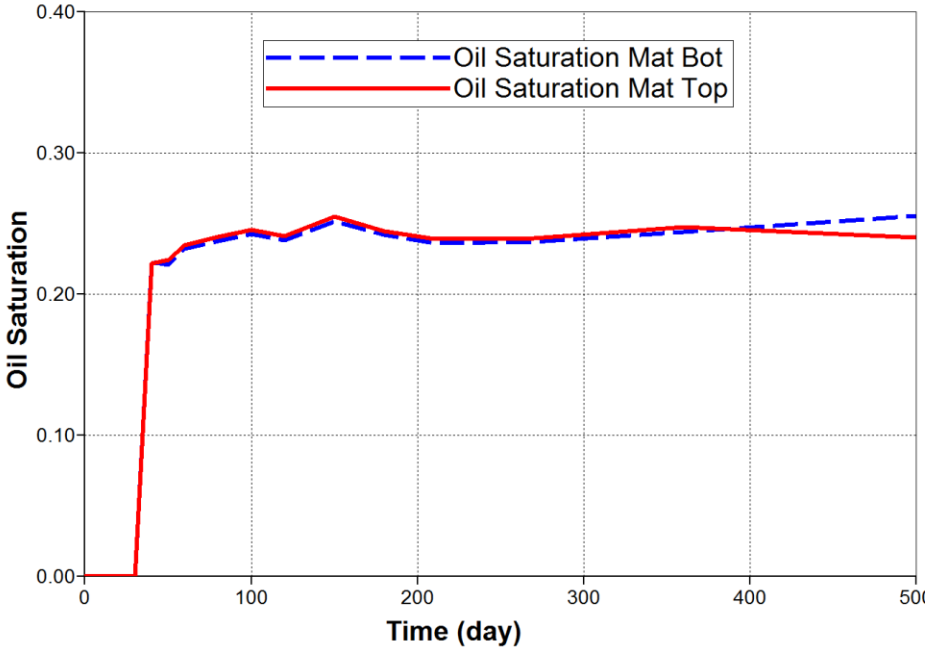

Figure 5.52: Variation of oil saturation inside matrix 0.1 ft. from fracture face with time
(Rich condensate- High drawdown)

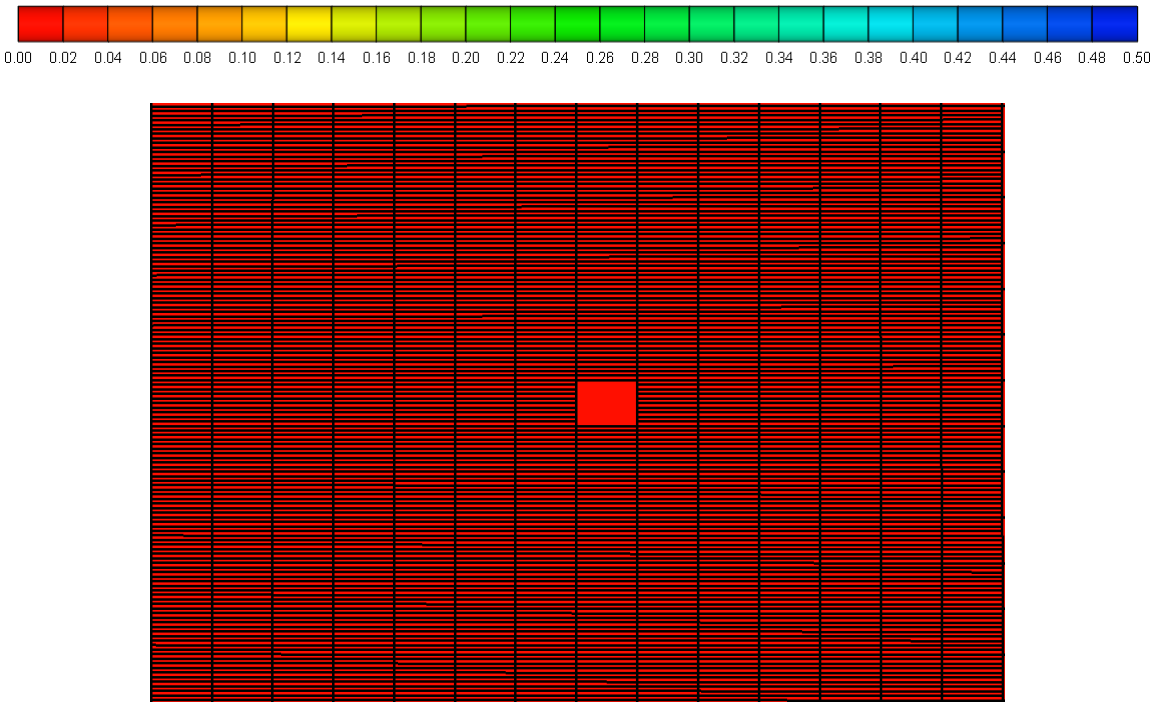

Oil saturation inside fracture after 30th day (end of shut-in, start of production)

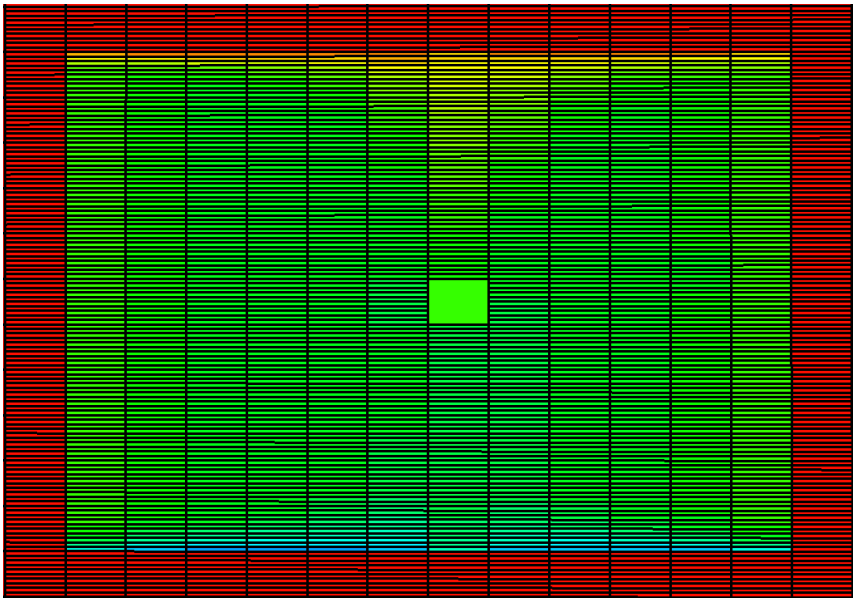

Oil saturation inside fracture after 50th day

Figure 5.53: Oil saturation maps (Rich condensate- High drawdown)

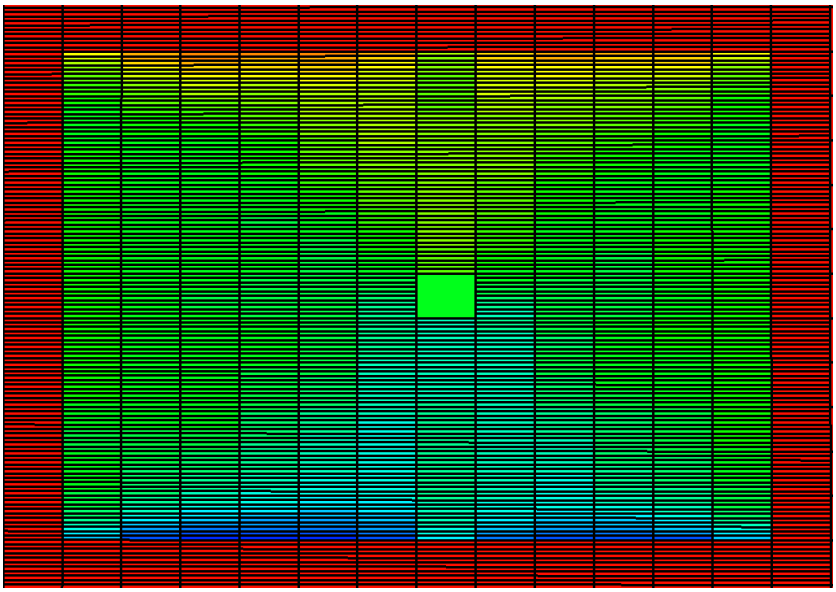

Oil saturation inside fracture after 500th day (end of production)

Figure 5.53: Oil saturation maps (Rich condensate- High drawdown) - Continued

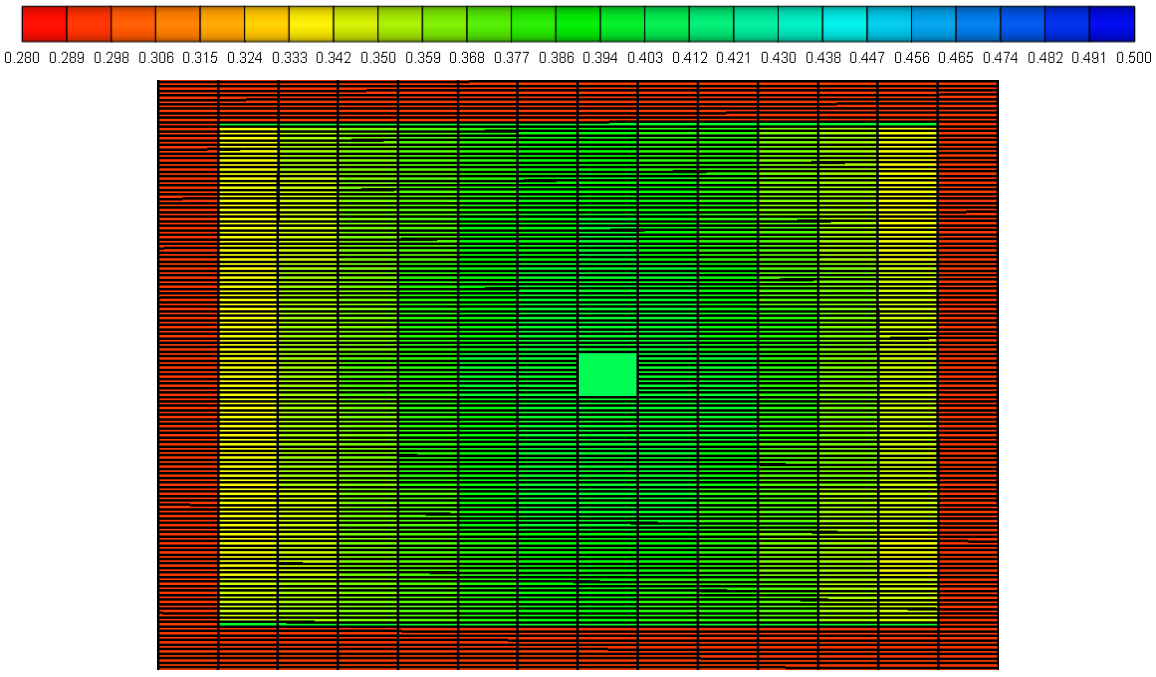

Water saturation inside fracture after 30th day (end of shut-in, start of production)

Figure 5.54: Water saturation maps (Rich condensate- High drawdown)

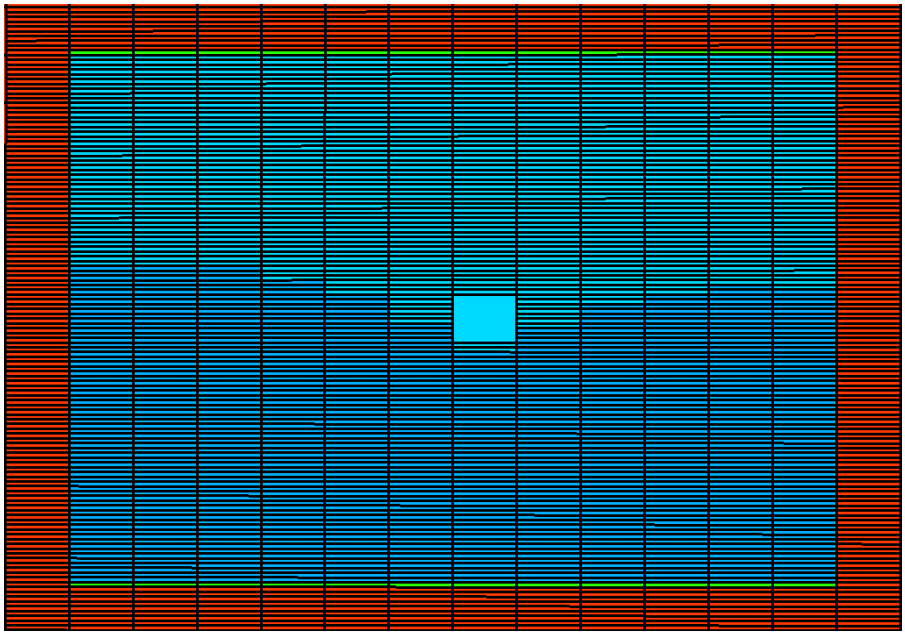

Water saturation inside fracture after 100th day

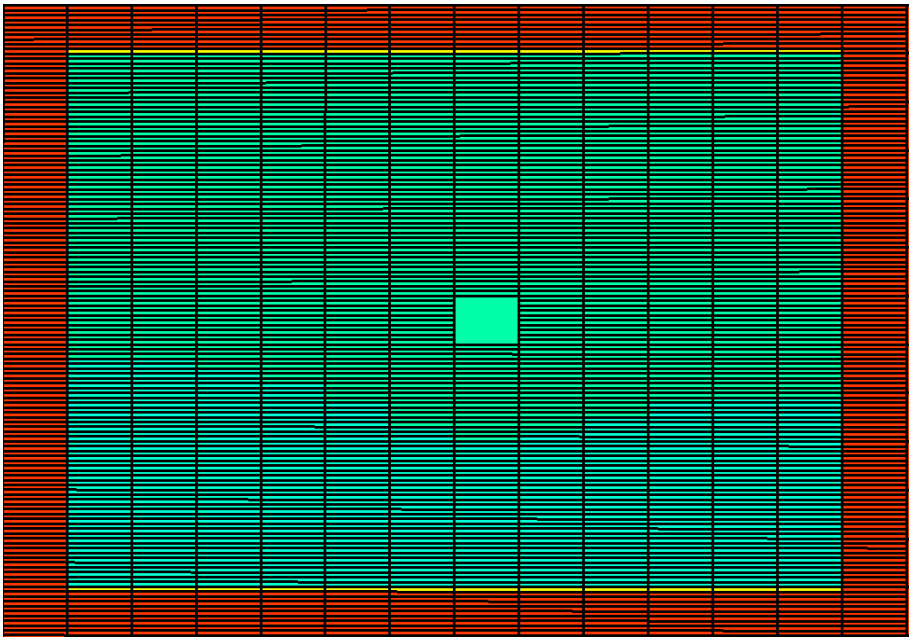

Water saturation inside fracture after 500th day (end of production)

Figure 5.54: Water saturation maps (Rich condensate- High drawdown) - Continued

5.3.7. Lean Condensate – Base case (Relative permeability Set-2)

Set-2 represents the medium water end point relative permeability or mobility case. As the end point relative permeability is higher, early time frac-water cleanup is expected to be somewhat faster. In this scenario bottom-hole pressure of 4000 psi is applied to the lean condensate reservoir. The cleanup of water and oil from the fracture and matrix is shown in the following figures. As observed in Set-1 results, the frac-water initially cleans up quickly from the fracture but later builds up due to flow from matrix.

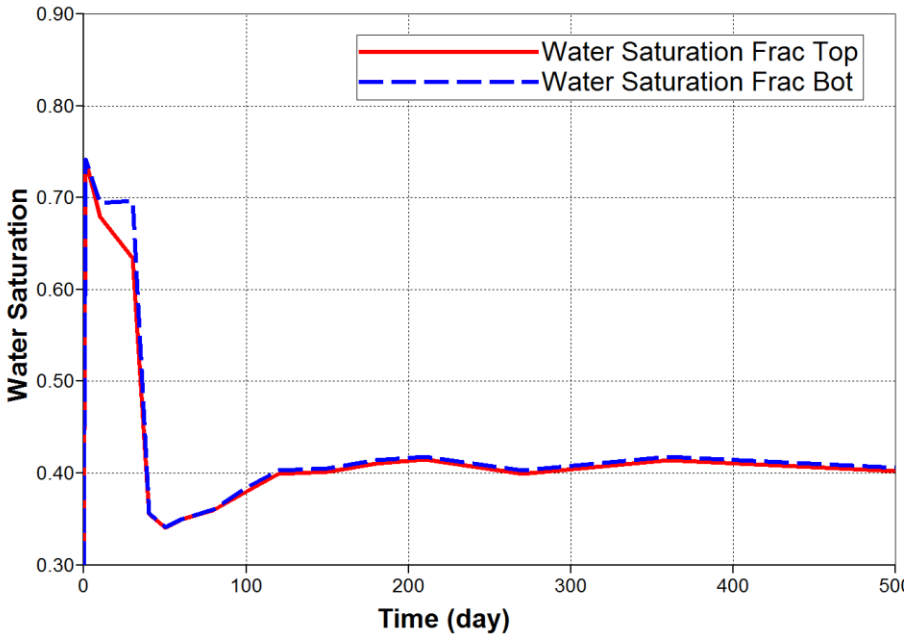

Figure 5.55: Variation of water saturation inside fracture over time (Lean condensate- Base)

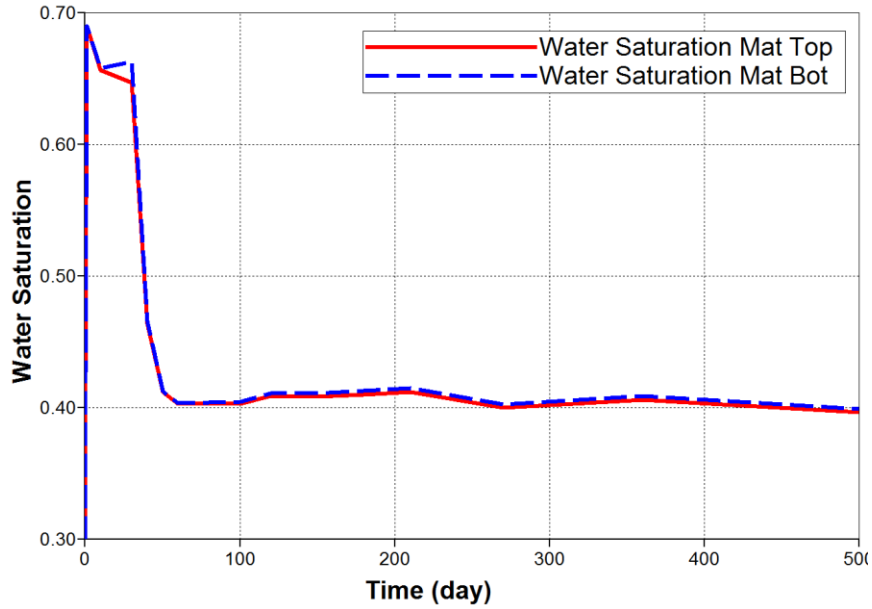

Figure 5.56: Variation of water saturation inside matrix 0.1 ft. from fracture face with time (Lean condensate- Base)

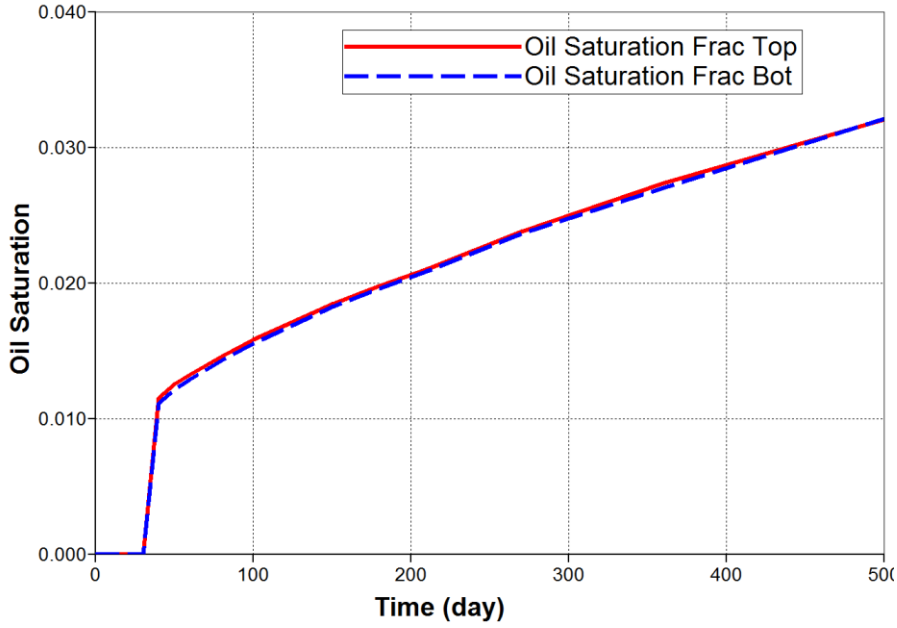

Figure 5.57: Variation of oil saturation inside fracture over time (Lean condensate- Base)

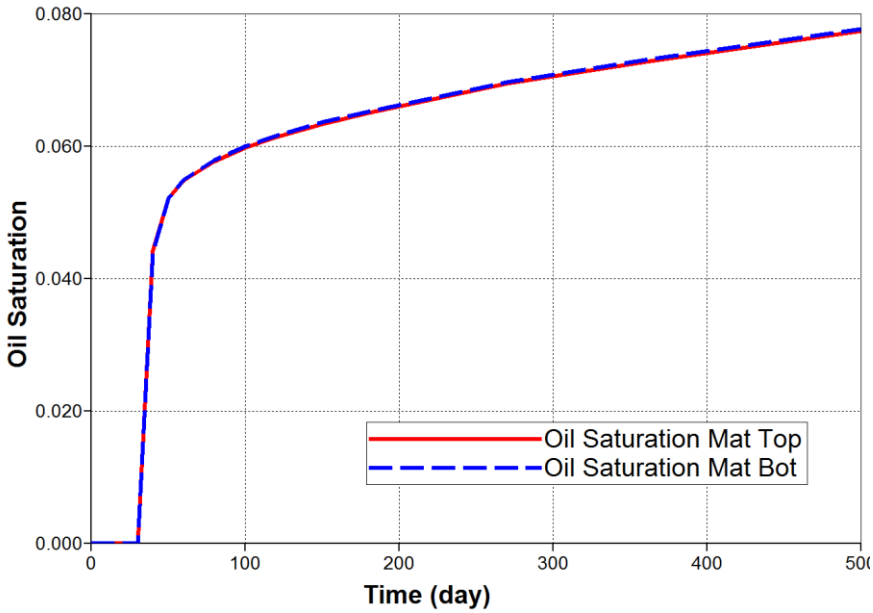

Figure 5.58: Variation of oil saturation inside matrix 0.1 ft. from fracture face with time (Lean condensate- Base)

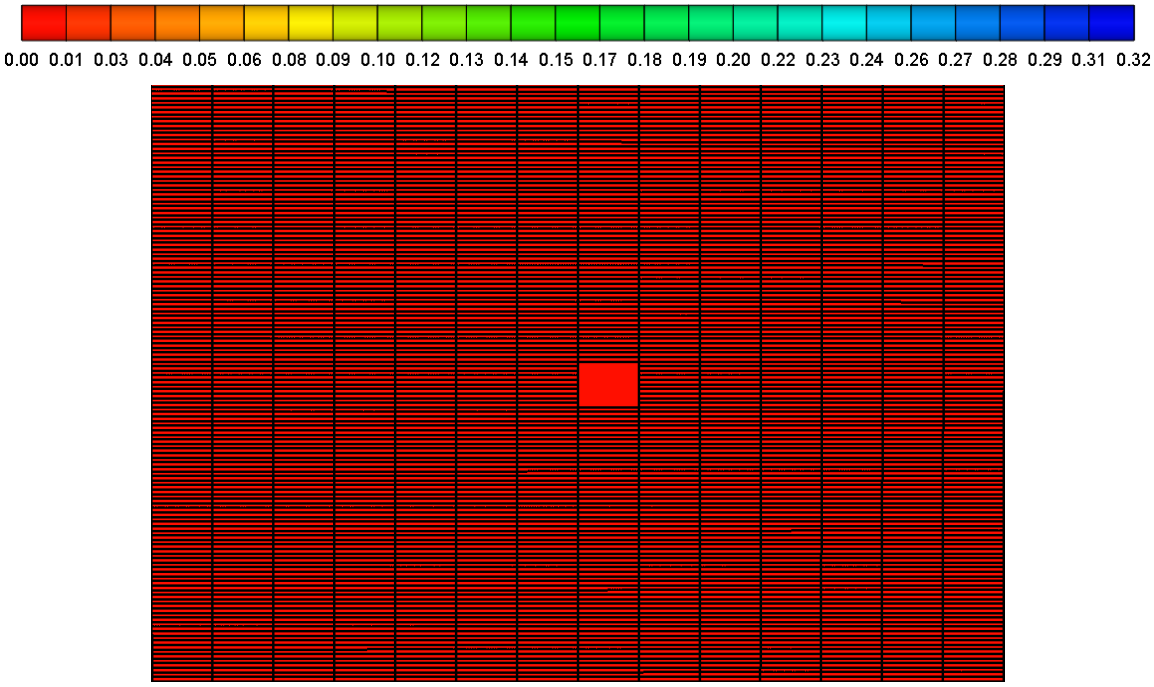

Oil saturation inside fracture after 30th day (end of shut-in)

Figure 5.59: Oil saturation maps (Lean condensate- Base)

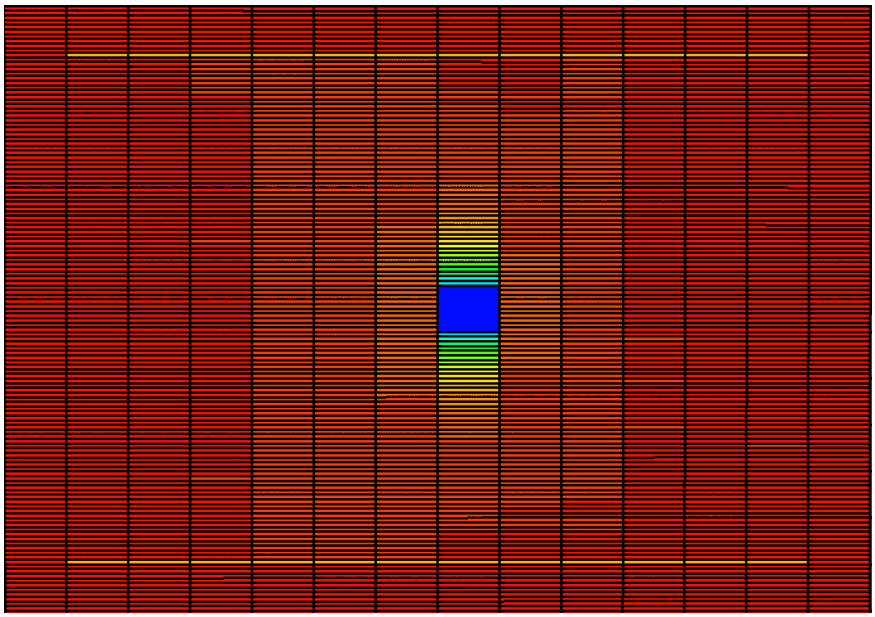

Oil saturation inside fracture after 120th day

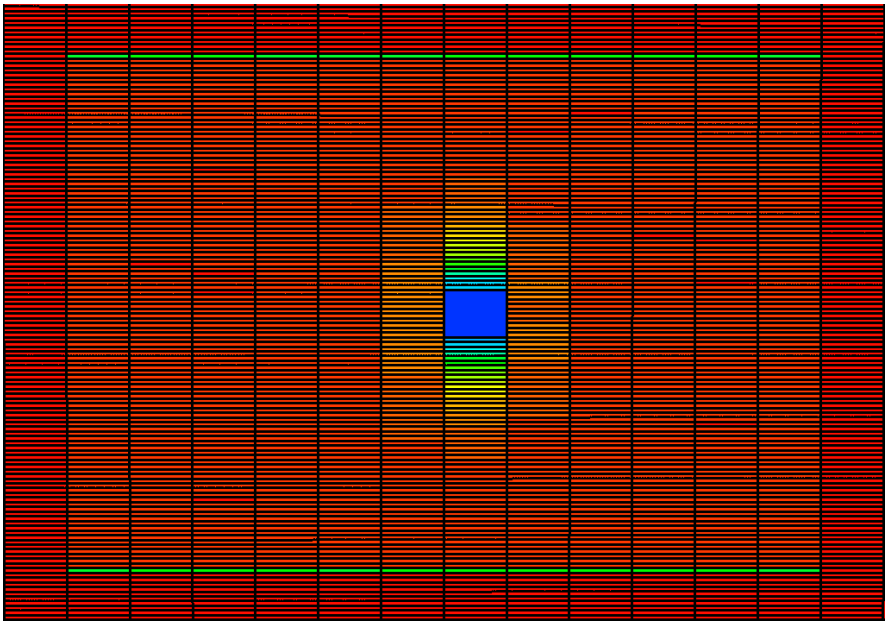

Oil saturation inside fracture after 500th day (end of production)

Figure 5.59: Oil saturation maps (Lean condensate- Base) - Continued

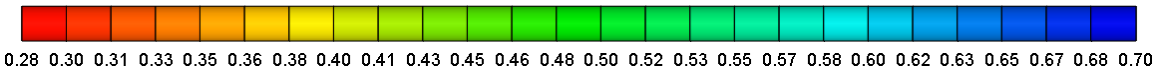

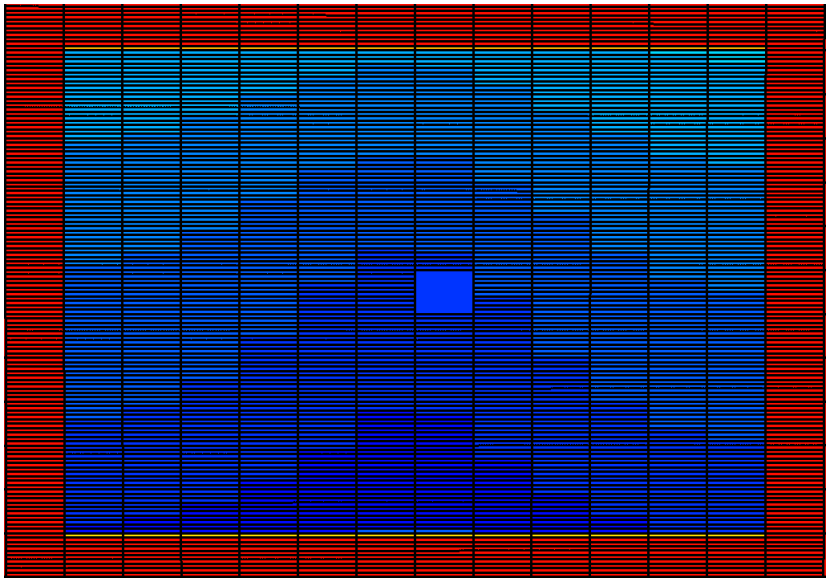

Water saturation inside fracture after 30th day (end of shut-in)

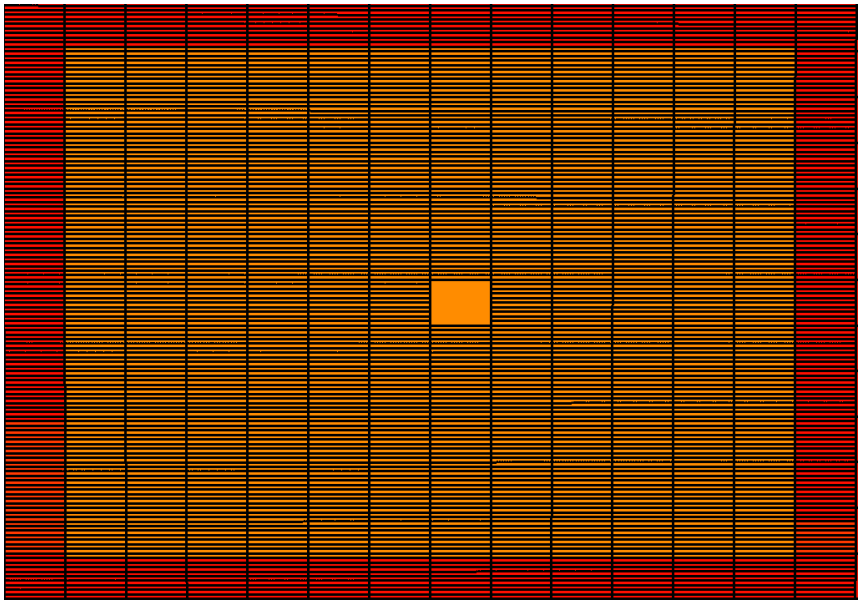

Water saturation inside fracture after 50th day

Figure 5.60: Water saturation maps (Lean condensate- Base)

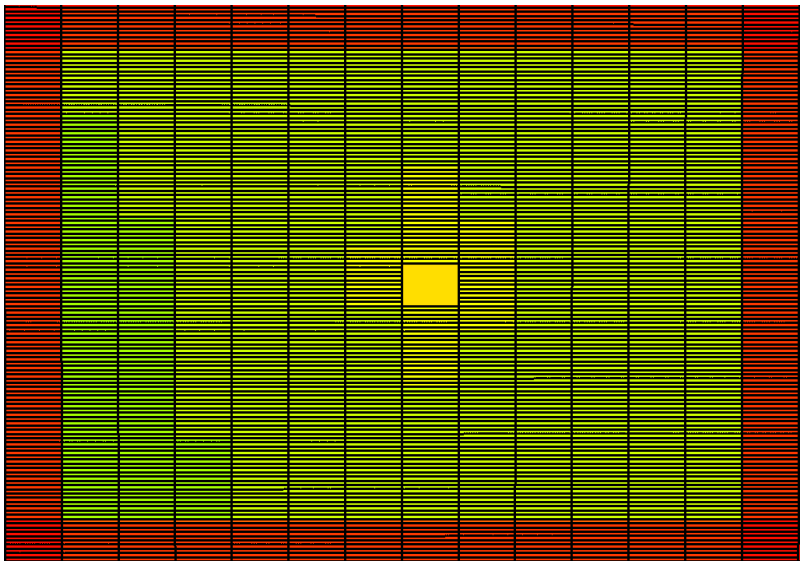

Water saturation inside fracture after 500th day (end of production)

Figure 5.60: Water saturation maps (Lean condensate- Base) - Continued

5.3.8. Lean Condensate – Low drawdown (Relative perm. Set-2)

In this case, the applied bottomhole pressure is 5500 psi which is higher than the dew point of the lean condensate; hence liquid-drop is not expected. Lower drawdown leads to worse frac-water recovery.

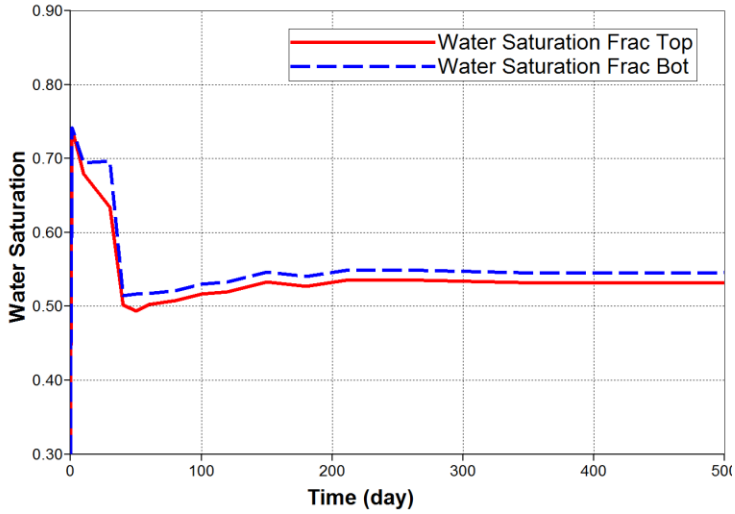

Figure 5.61: Variation of water saturation inside fracture over time (Lean condensate- Low drawdown)

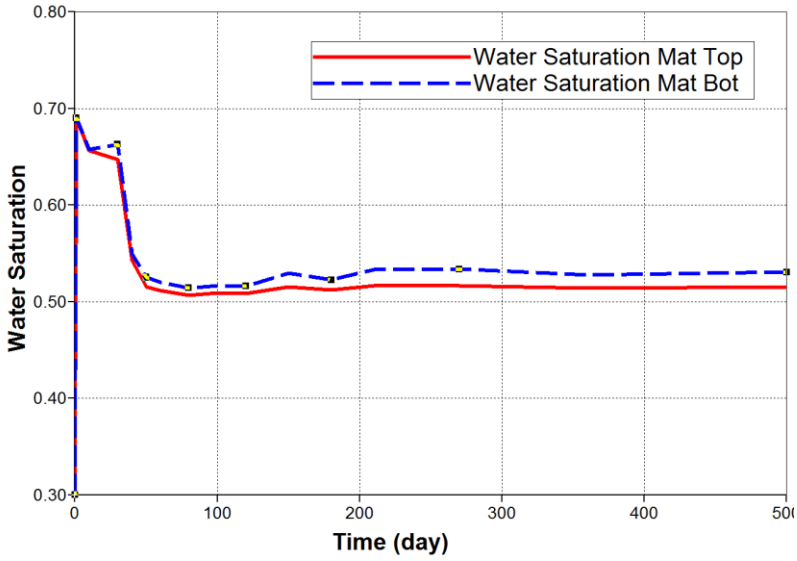

Figure 5.62: Variation of water saturation inside matrix 0.1 ft. from fracture face with time (Lean condensate- Low drawdown)

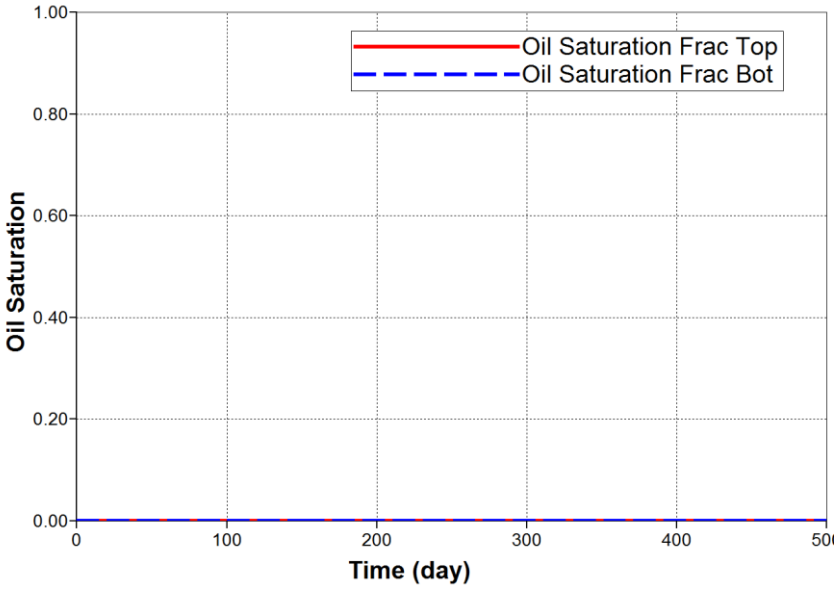

Figure 5.63: Variation of oil saturation inside fracture over time (Lean condensate- Low drawdown)

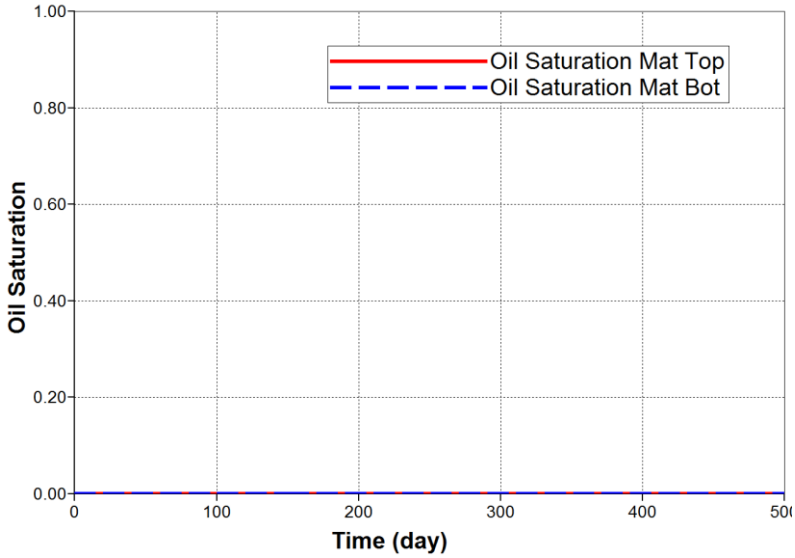

Figure 5.64: Variation of oil saturation inside matrix 0.1 ft. from fracture face with time (Lean condensate- Low drawdown)

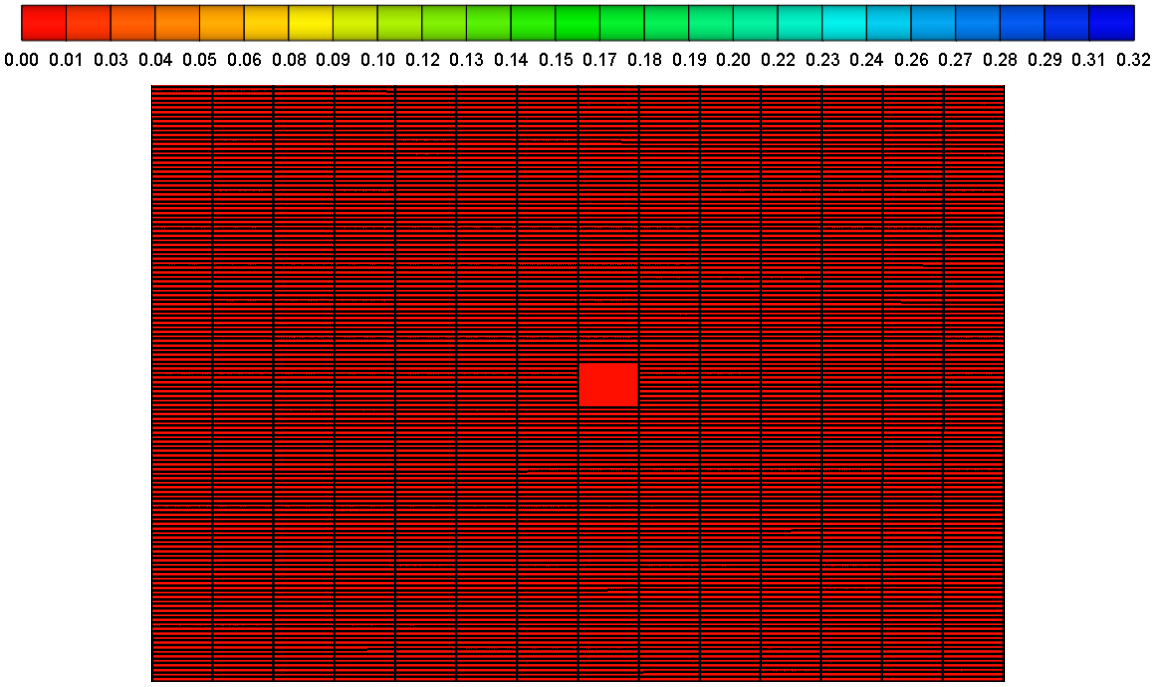

Oil saturation inside fracture after 30th day (end of shut-in)

Figure 5.65: Oil saturation maps (Lean condensate- Low drawdown)

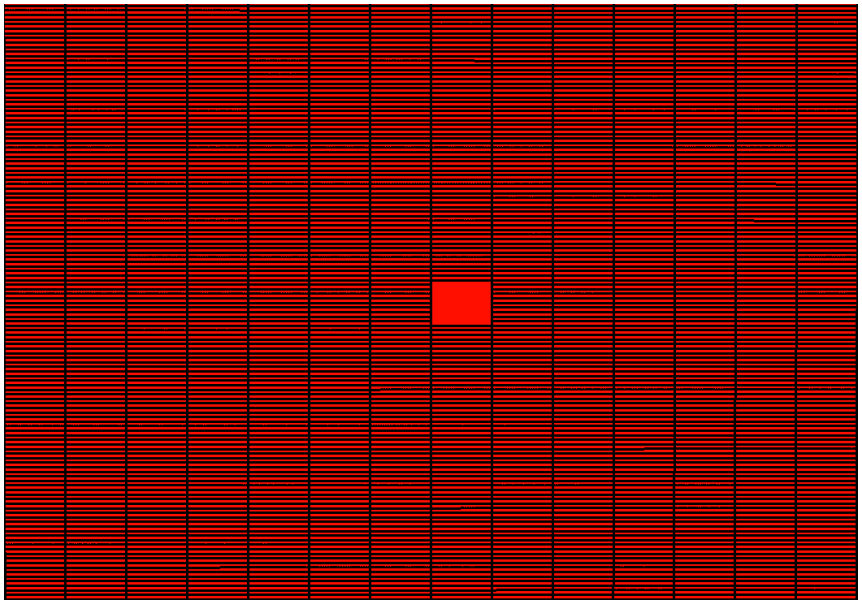

Oil saturation inside fracture after 500th end (end of production)

Figure 5.65: Oil saturation maps (Lean condensate- Low drawdown)- Continued

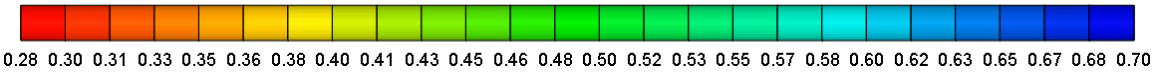

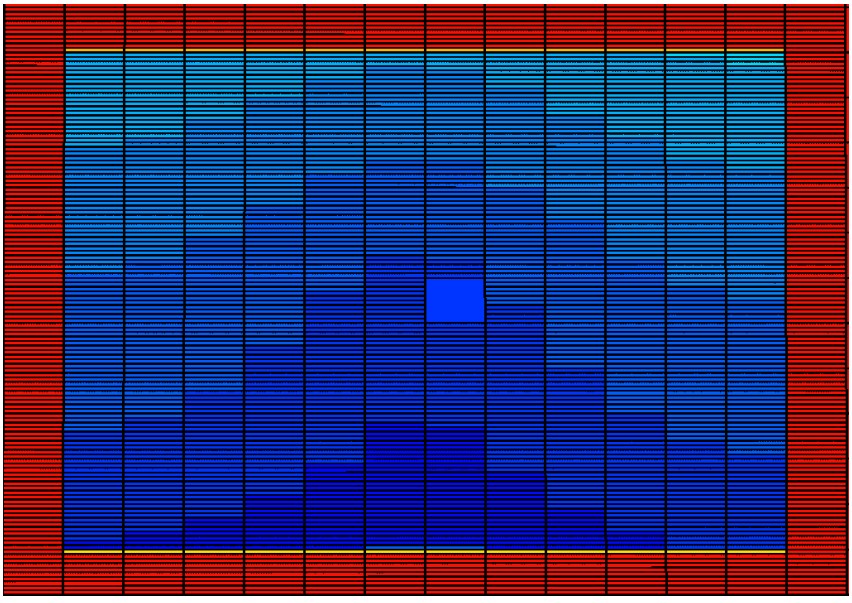

Water saturation inside fracture after 30th day (end of shut-in)

Figure 5.66: Water saturation maps (Lean condensate- Low drawdown)

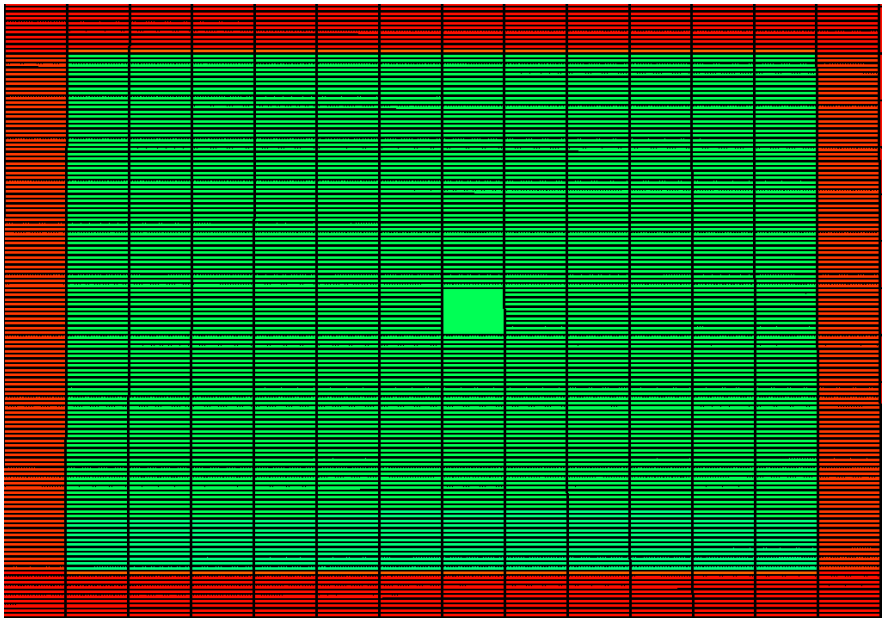

Water saturation inside fracture after 120th day

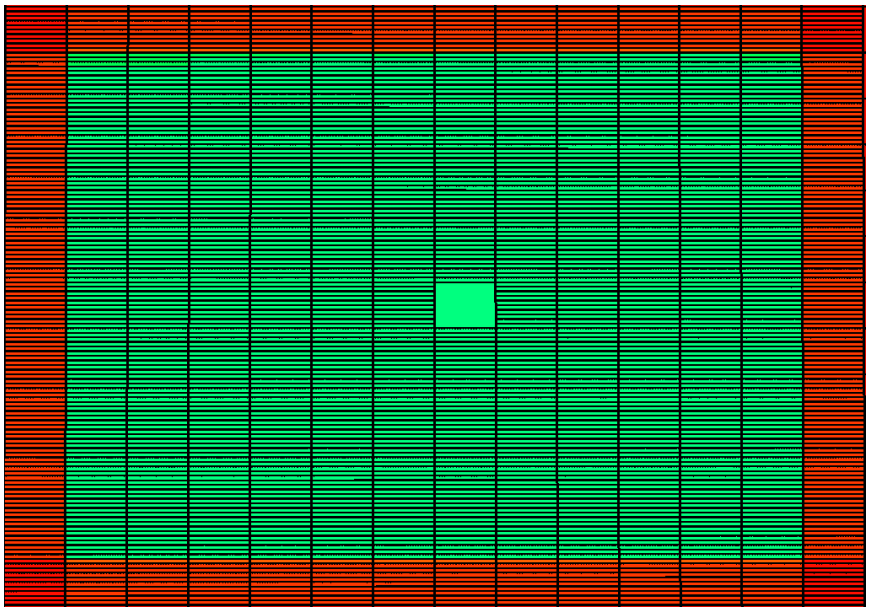

Water saturation inside fracture after 500th end (end of production)

Figure 5.66: Water saturation maps (Lean condensate- Low drawdown) - Continued

5.3.9. Lean Condensate – High drawdown (Relative perm. Set-2)

Wellbore bottom-hole pressure equal to 3000 psi is applied to produce the reservoir at maximum liquid drop out conditions. The corresponding water and oil cleanup profiles are shown below. Significantly better frac-water cleanup is achieved. However, higher oil saturations are observed inside the fracture and on fracture face. The total liquid saturation will determine the gas relative permeability.

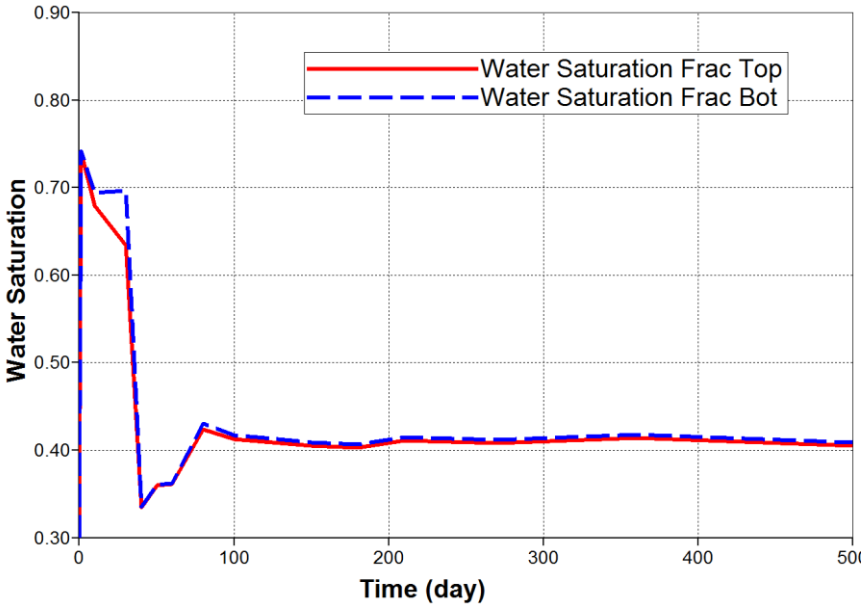

Figure 5.67: Variation of water saturation inside fracture over time (Lean condensate- High drawdown)

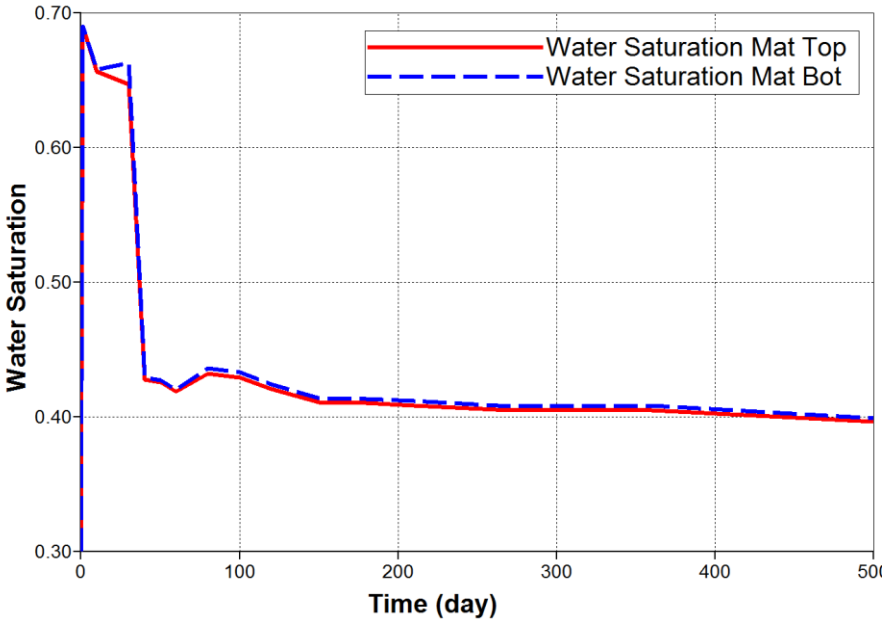

Figure 5.68: Variation of water saturation inside matrix 0.1 ft. from fracture face with time (Lean condensate- High drawdown)

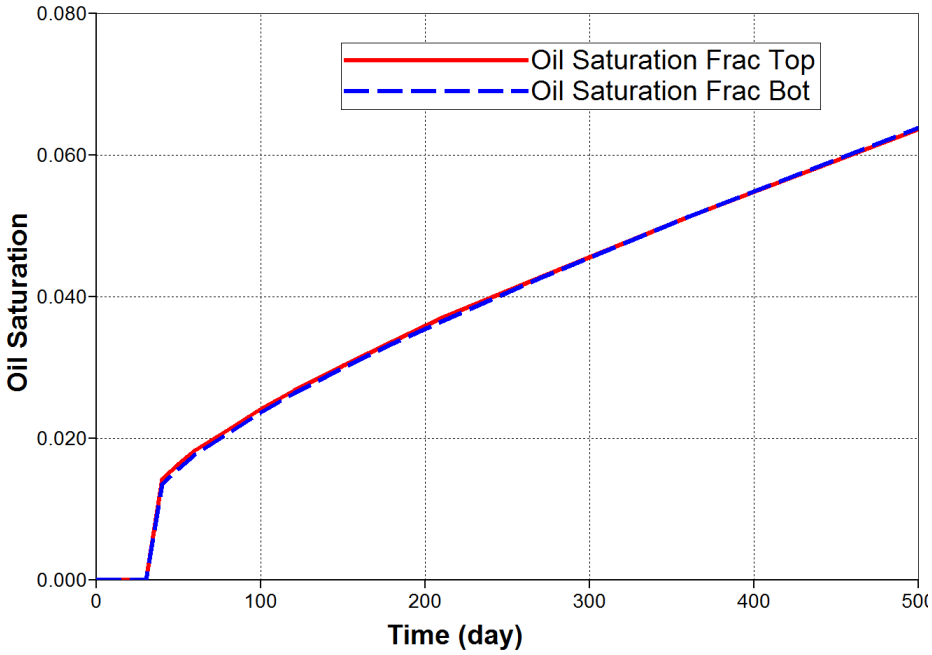

Figure 5.69: Variation of oil saturation inside fracture over time (Lean condensate- High drawdown)

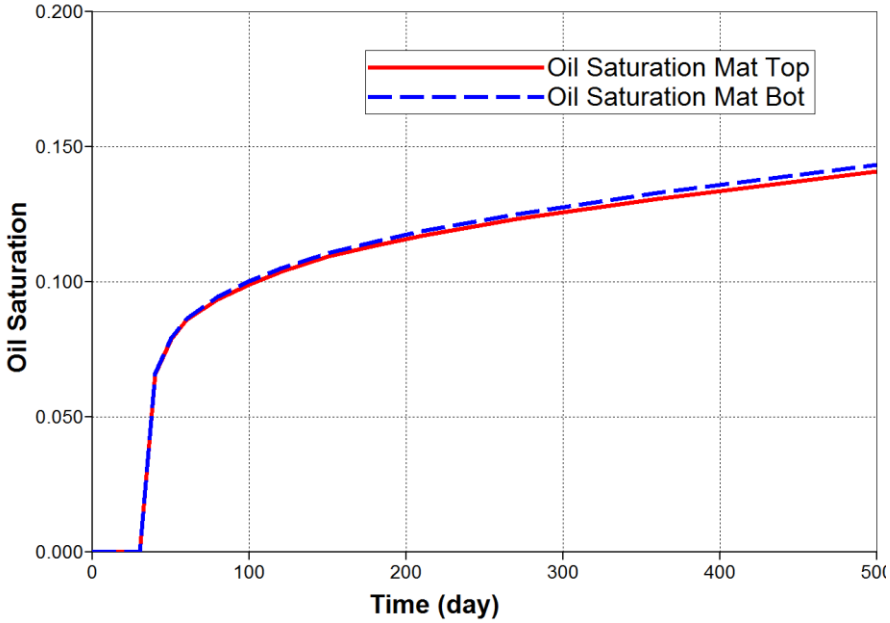

Figure 5.70: Variation of oil saturation inside matrix 0.1 ft. from fracture face with time (Lean condensate- High drawdown)

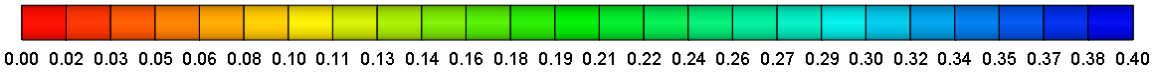

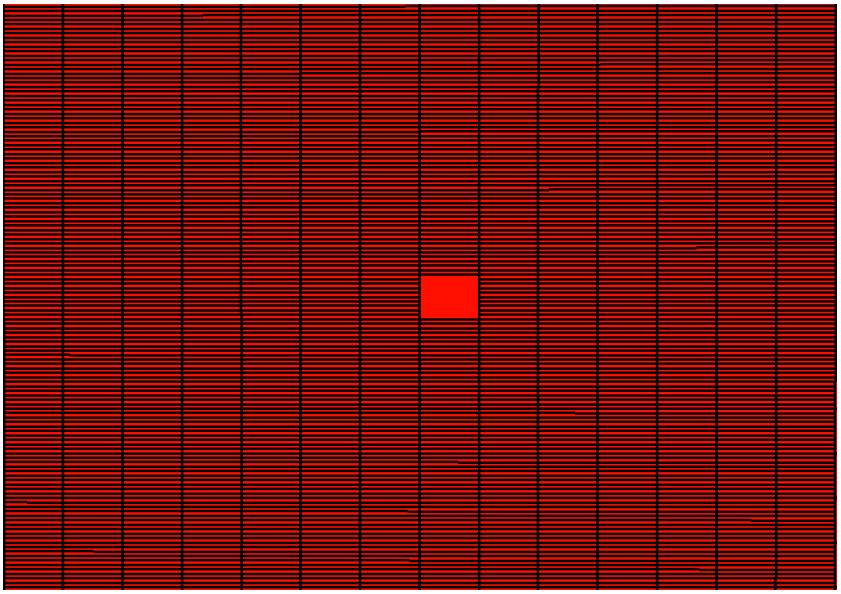

Oil saturation inside fracture after 30th day (end of shut-in)

Figure 5.71: Oil saturation maps (Lean condensate- High drawdown)

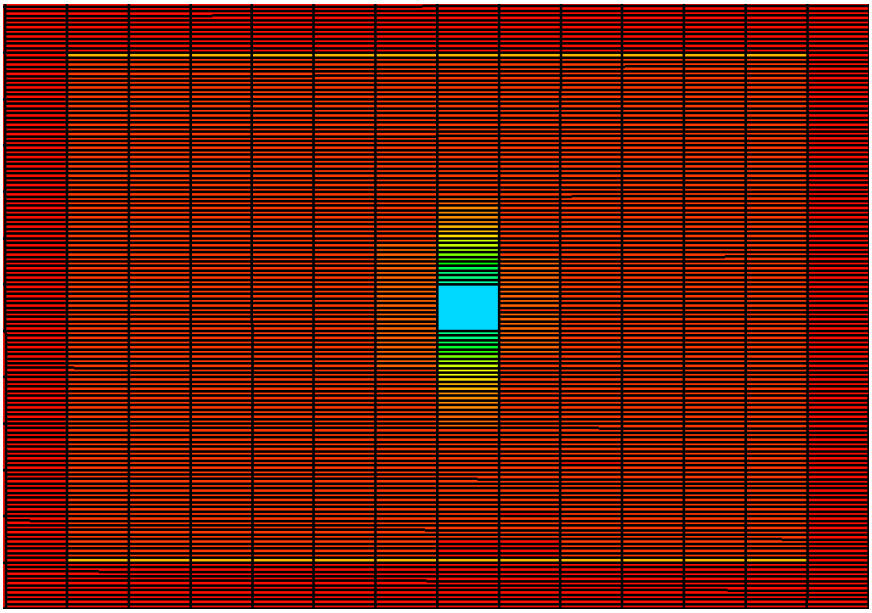

Oil saturation after 100th day

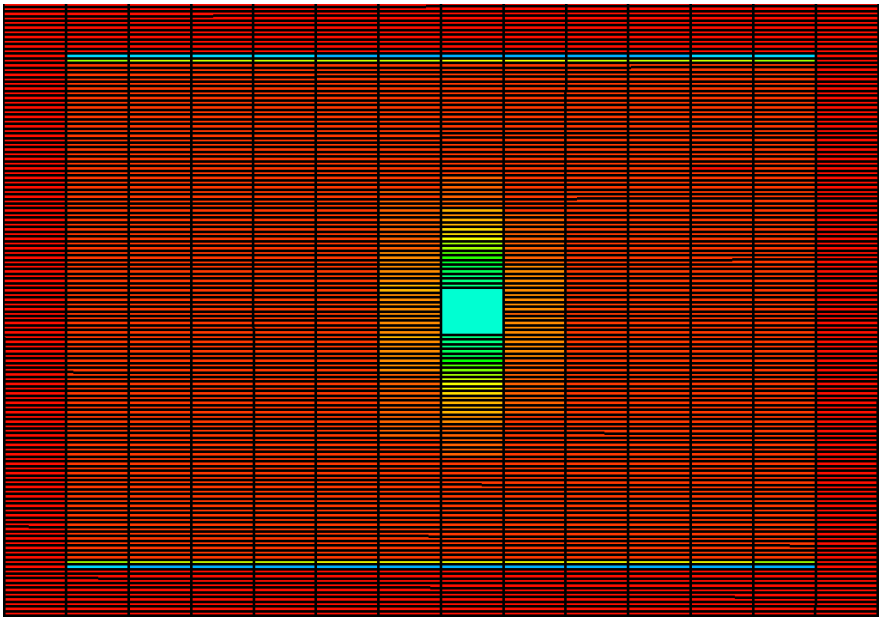

Oil saturation inside fracture after 500th end (end of production)

Figure 5.71: Oil saturation maps (Lean condensate- High drawdown) - Continued

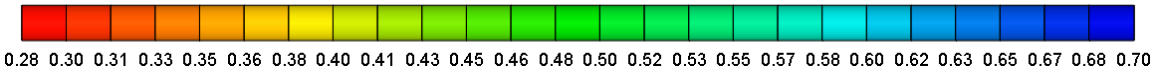

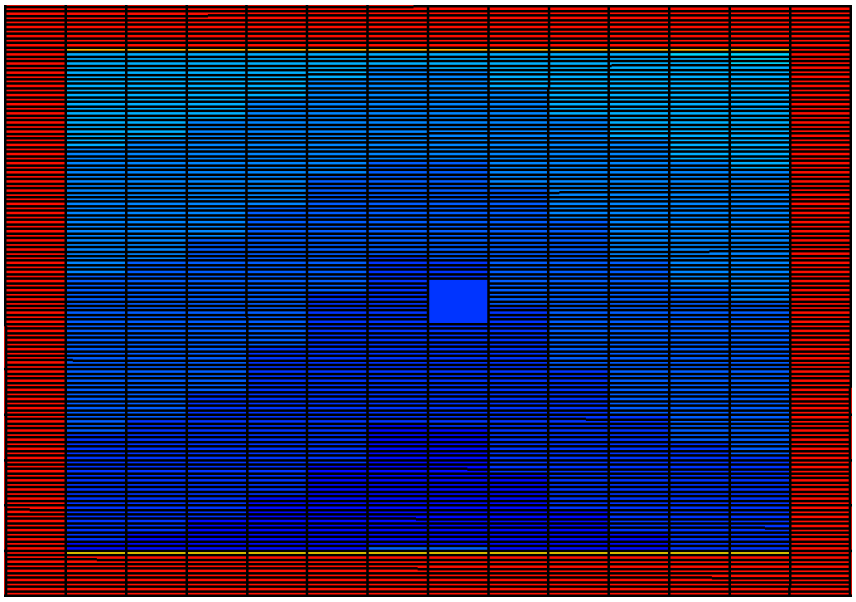

Water saturation after 30th day (end of shut-in, start of production)

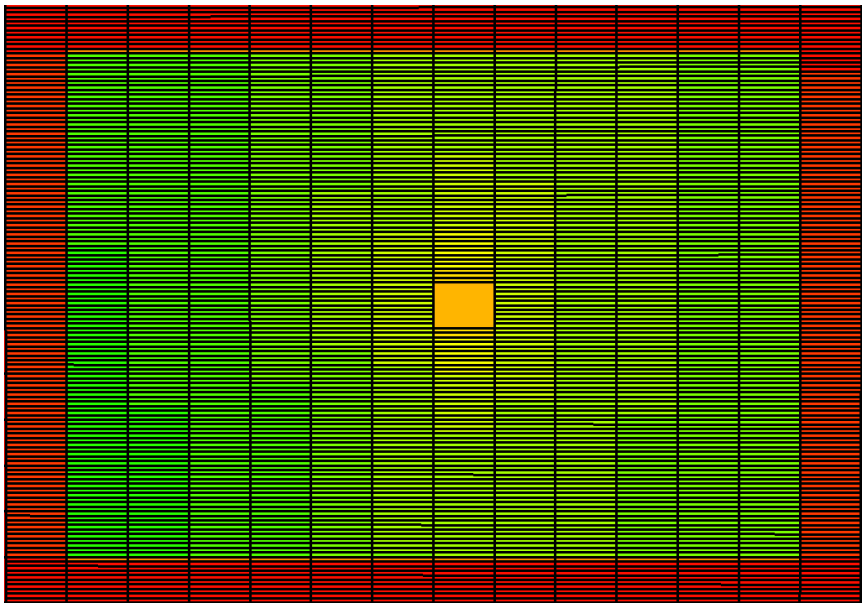

Water saturations after 80th day

Figure 5.72: Water saturation maps (Lean condensate- High drawdown)

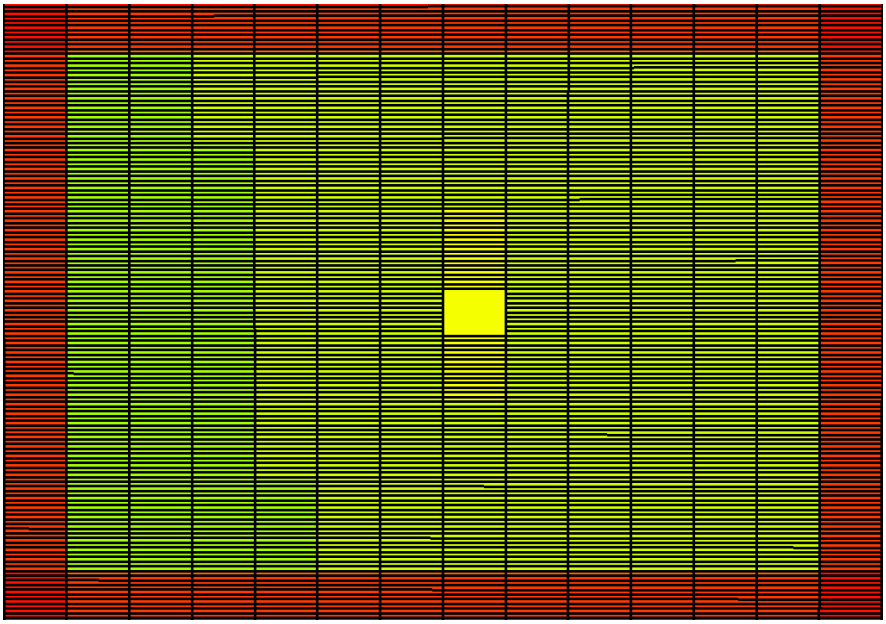

Water saturation inside fracture after 500th end (end of production)

Figure 5.72: Water saturation maps (Lean condensate- High drawdown) - continued

5.3.10. Rich Condensate – Base case (Relative permeability Set-2)

A bottomhole pressure of 3000 psi is applied to produce from the rich condensate reservoir. Water and oil cleanup profiles are shown below. It is observed that compared with Set-1 frac-water cleanup is poorer. However, condensate cleanup from fracture and matrix is better.

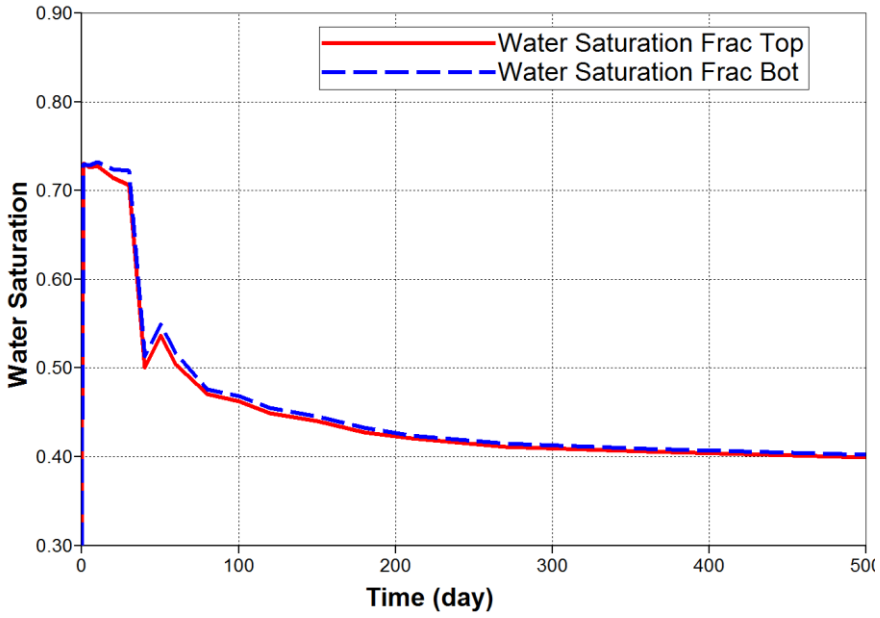

Figure 5.73: Variation of water saturation inside fracture over time (Rich condensate- Base)

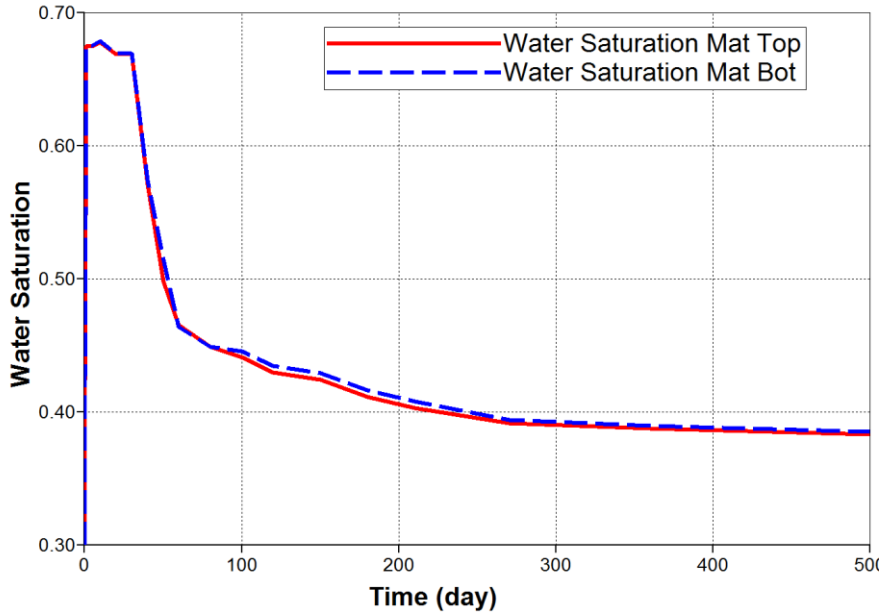

Figure 5.74: Variation of water saturation inside matrix 0.1 ft. from fracture face with time (Rich condensate- Base)

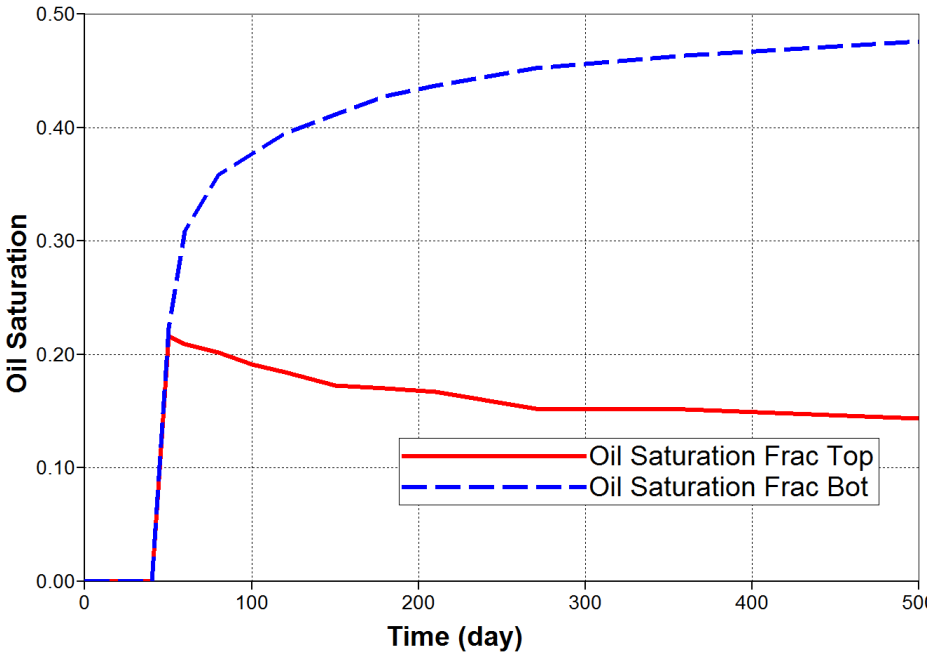

Figure 5.75: Variation of oil saturation inside fracture over time
(Rich condensate- Base)

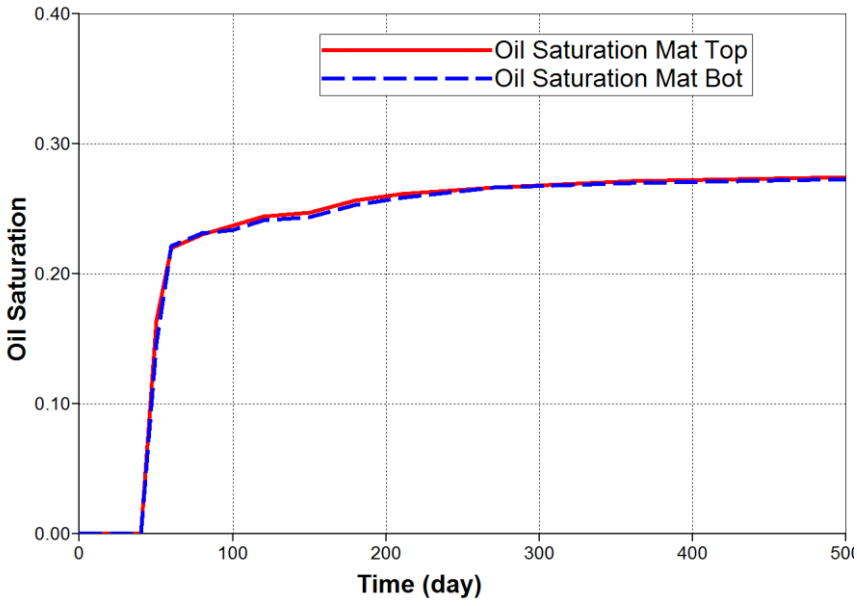

Figure 5.76: Variation of oil saturation inside matrix 0.1 ft. from fracture face with time
(Rich condensate- Base)

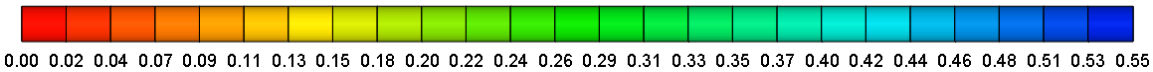

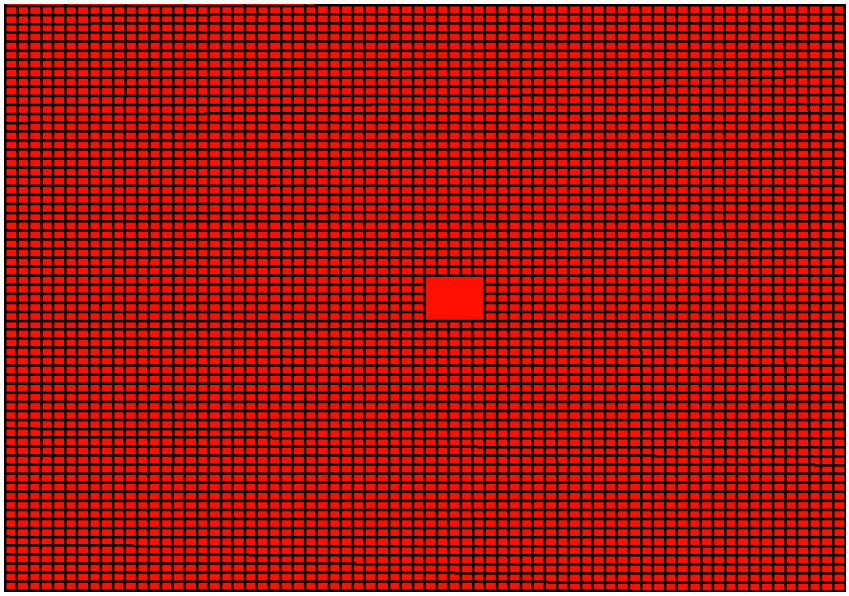

Oil saturation inside fracture after 30th day (end of shut-in)

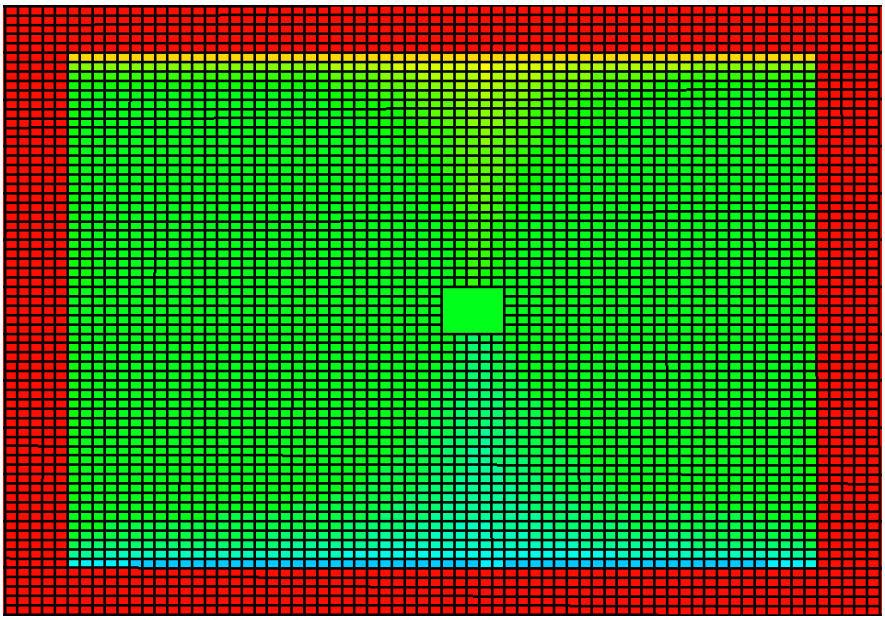

Oil saturation inside fracture after 120th day

Figure 5.77: Oil saturation maps (Rich condensate- Base)

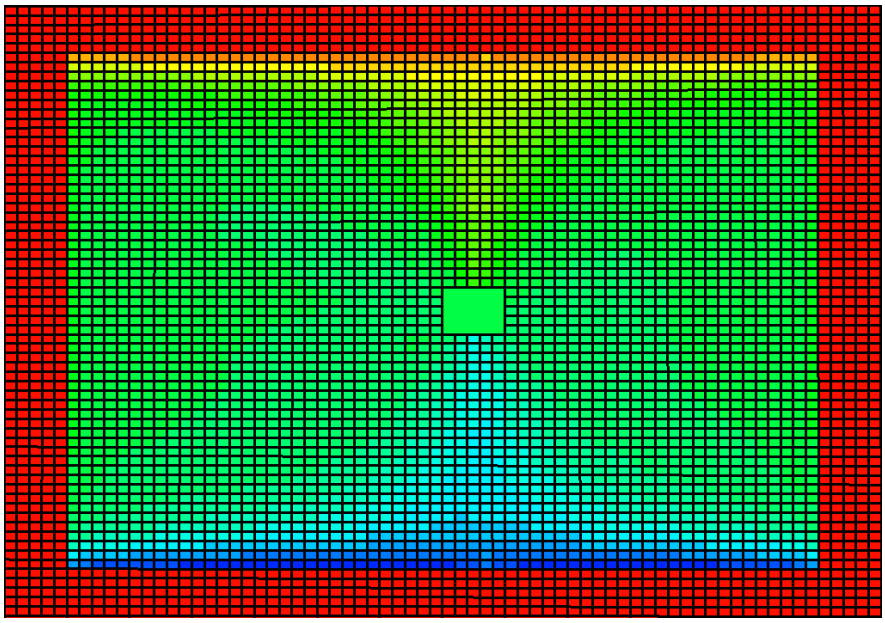

Oil saturation inside fracture after 500th end (end of production)

Figure 5.77: Oil saturation maps (Rich condensate- Base) - continued

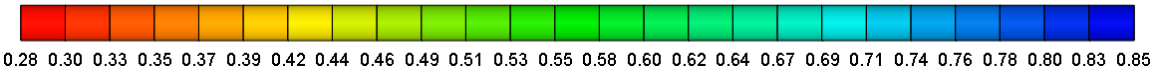

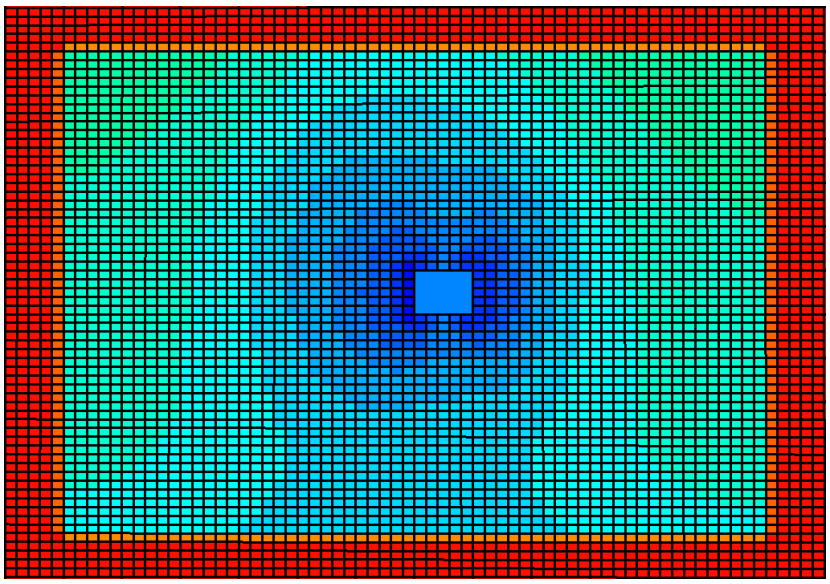

Water saturation after 30th day (end of shut-in)

Figure 5.78: Water saturation maps (Rich condensate- Base)

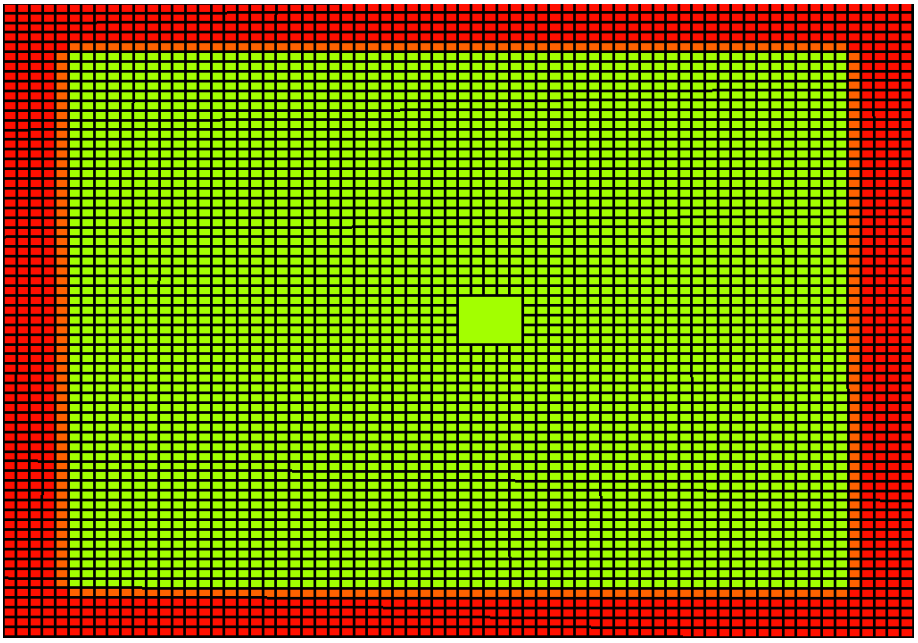

Water saturation after 80th day

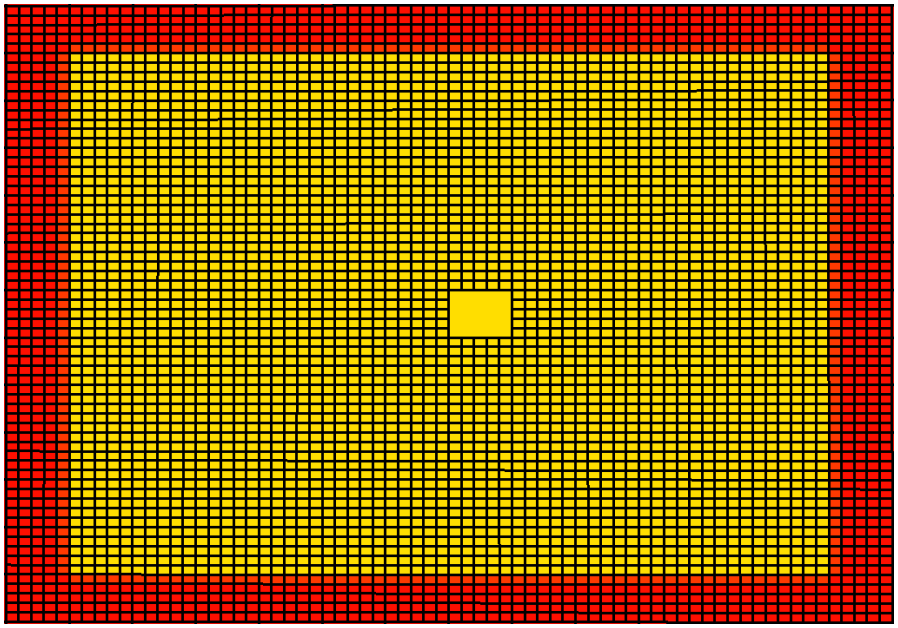

Water saturation inside fracture after 500th end (end of production)

Figure 5.78: Water saturation maps (Rich condensate- Base) - continued

5.3.13. Rich Condensate – Low drawdown (Relative perm. Set-2)

Wellbore pressure of 5500 psi is used to flow back the well in this low drawdown scenario. Since P_{wf} is greater than condensate dew point, no liquid drop out is expected. Lower drawdown leads to worse cleanup compared with the base case. Compared with Set-1, initial cleanup just after flowback is faster but long term cleanup is practically unaffected.

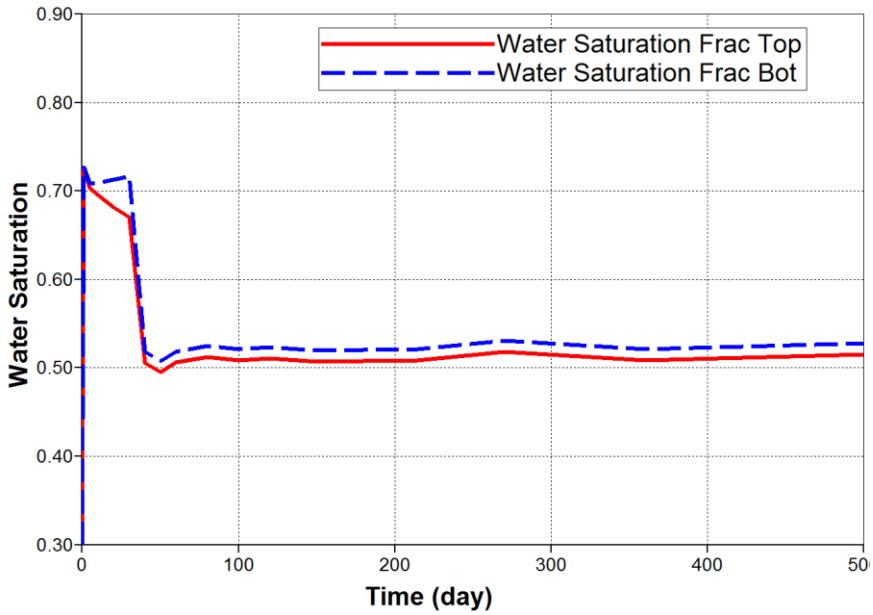

Figure 5.79: Variation of water saturation inside fracture over time (Rich condensate- Low drawdown)

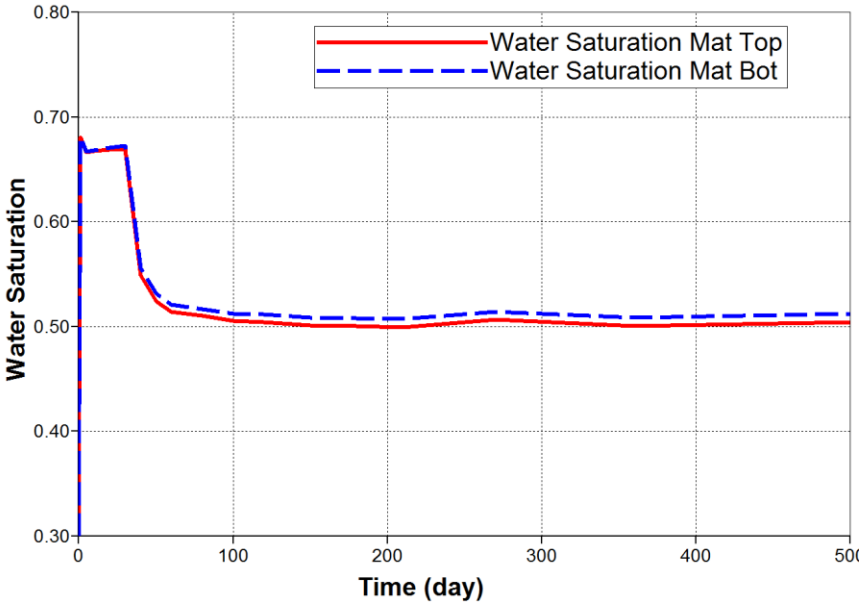

Figure 5.80: Variation of water saturation inside matrix 0.1 ft. from fracture face with time (Rich condensate- Low drawdown)

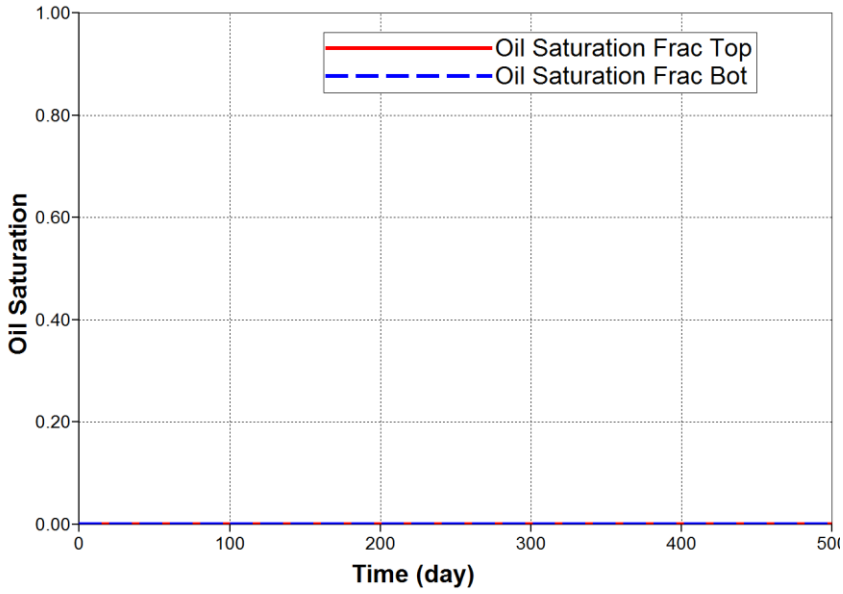

Figure 5.81: Variation of oil saturation inside fracture over time (Rich condensate- Low drawdown)

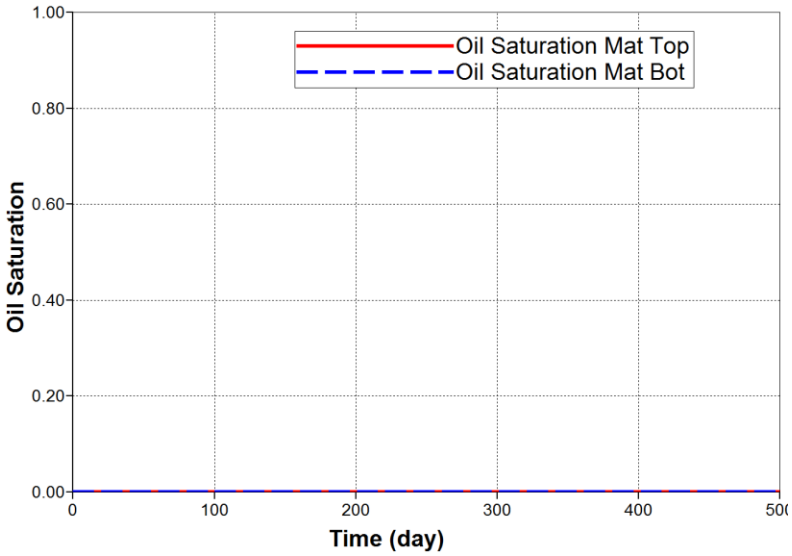

Figure 5.82: Variation of oil saturation inside matrix 0.1 ft. from fracture face with time (Rich condensate- Low drawdown)

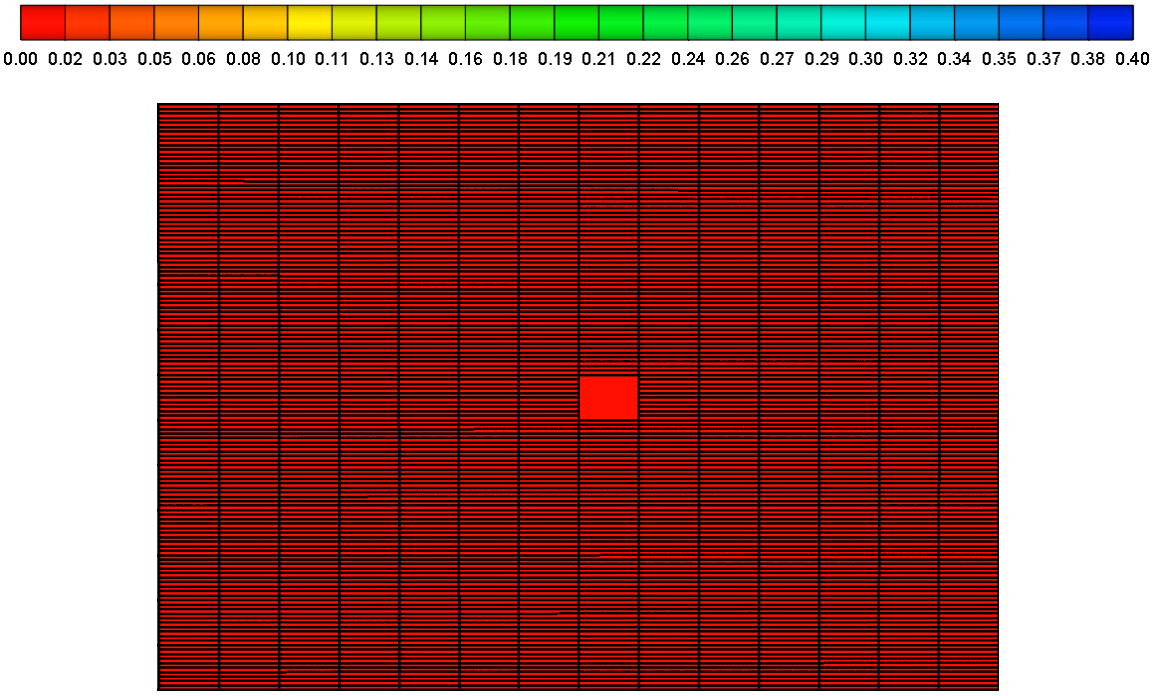

Oil saturation within fracture after 30th day (end of shut-in)

Figure 5.83: Oil saturation maps (Rich condensate- Low drawdown)

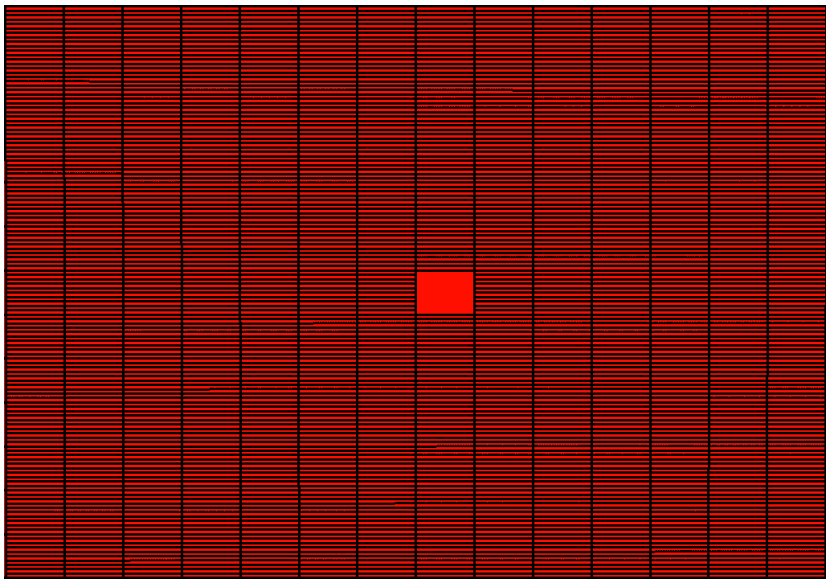

Oil saturation inside fracture after 500th end (end of production)

Figure 5.83: Oil saturation maps (Rich condensate- Low drawdown) - Continued

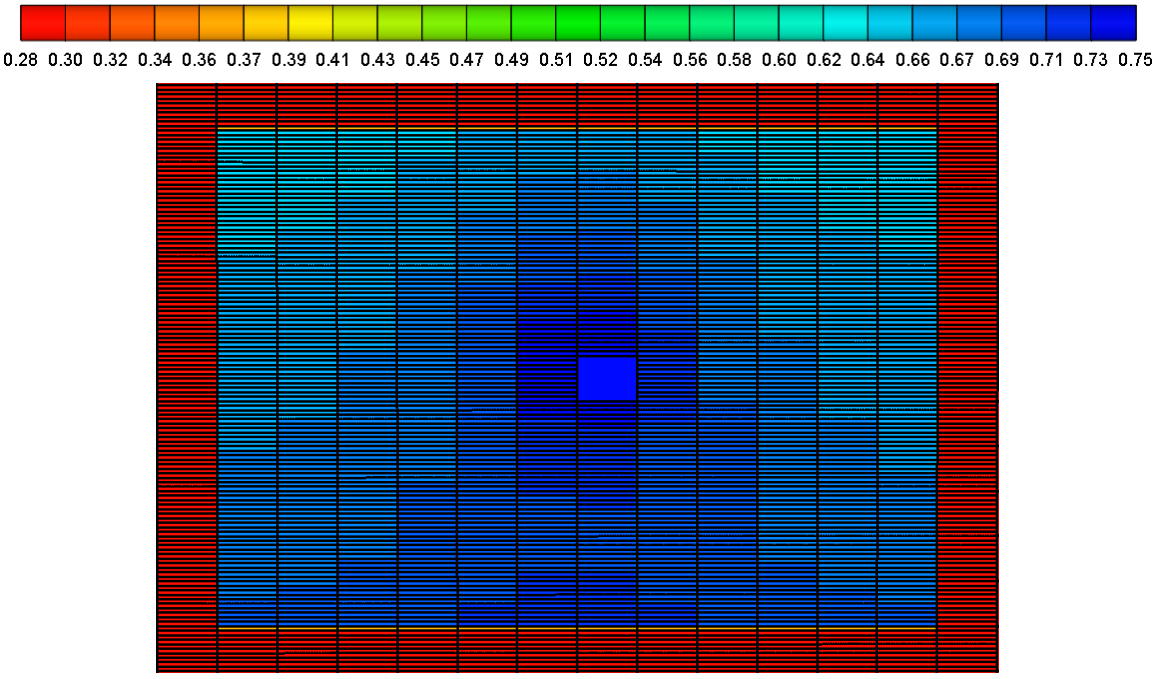

Water saturation inside fracture after 30th day (end of shut-in)

Figure 5.84: Water saturation maps (Rich condensate- Low drawdown)

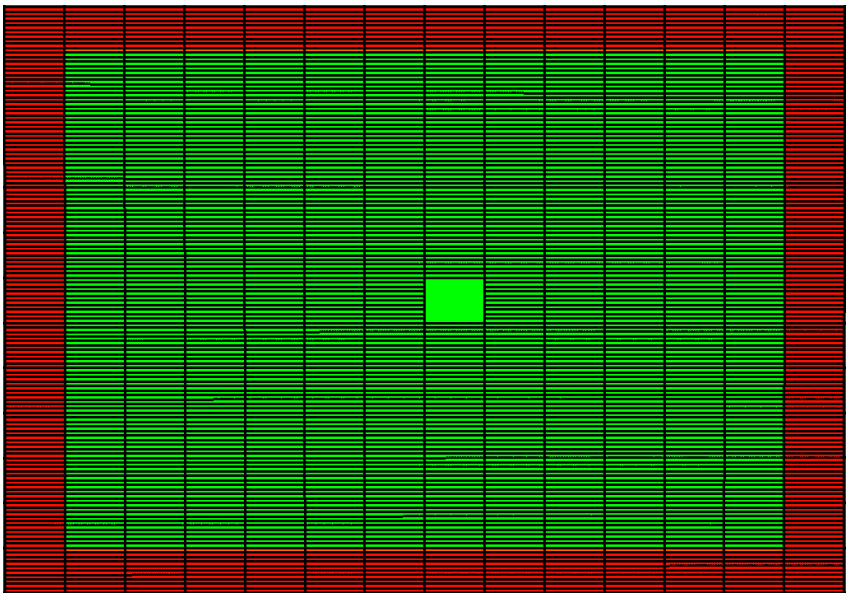

Water saturation inside fracture after 100th day

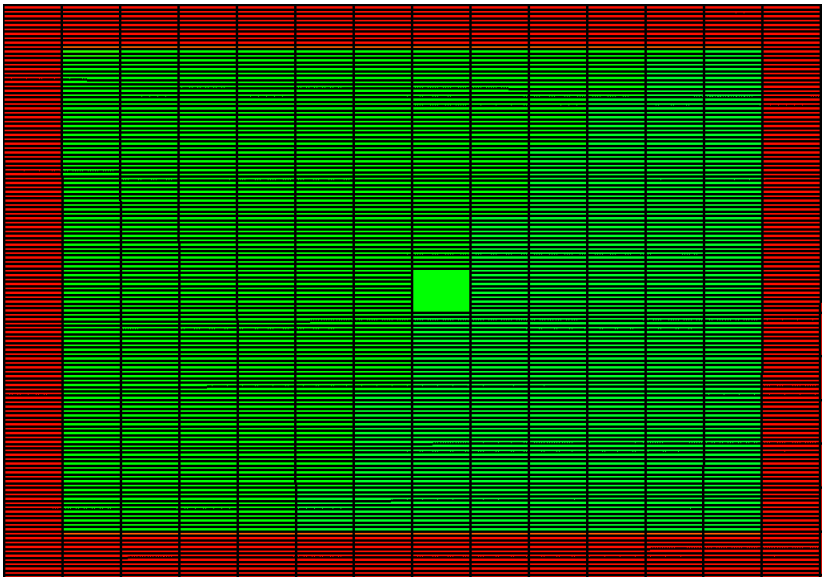

Water saturation inside fracture after 500th end (end of production)

Figure 5.84: Water saturation maps (Rich condensate- Low drawdown) - Continued

5.3.12. Rich Condensate – High drawdown (Relative perm. Set-2)

In this scenario, a bottom-hole pressure equal to 2500 psi is applied corresponding to the maximum liquid drop out pressure for the rich gas condensate. Higher drawdown leads to more efficient frac-water cleanup but also higher condensate loading inside the fracture. Compared to Set-1 under similar conditions, frac water cleanup is better though condensate cleanup is worse.

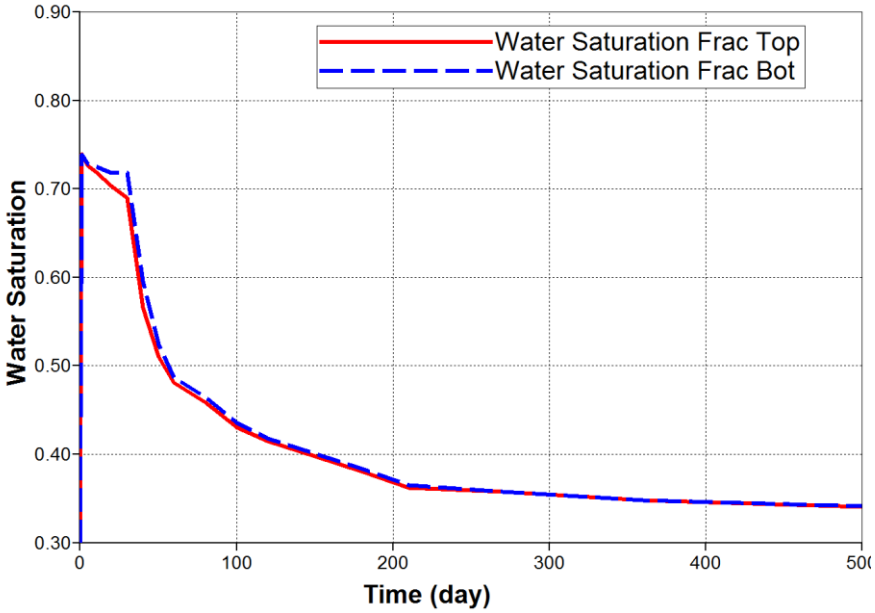

Figure 5.85: Variation of water saturation inside fracture over time (Rich condensate- High drawdown)

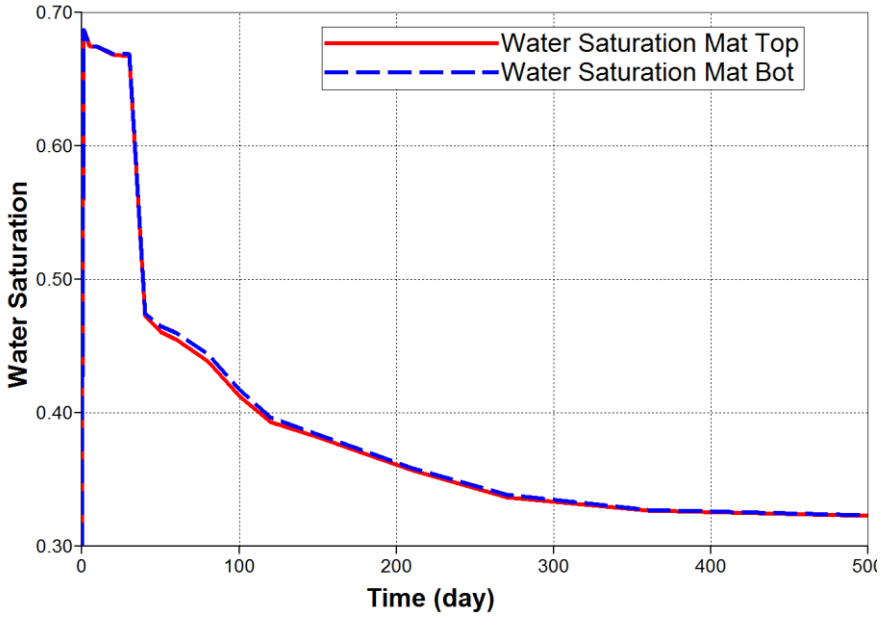

Figure 5.86: Variation of water saturation inside matrix 0.1 ft. from fracture face with time (Rich condensate- High drawdown)

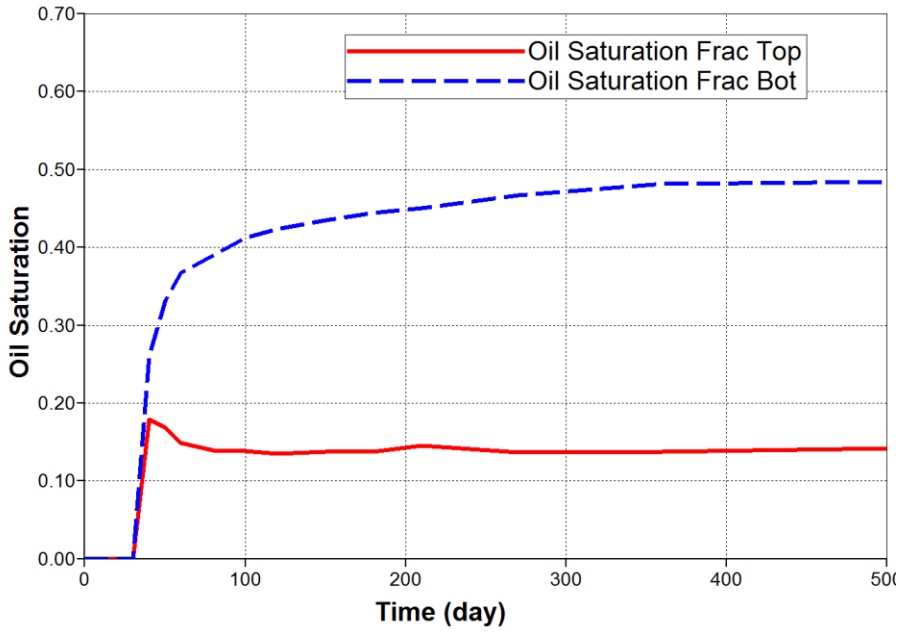

Figure 5.87: Variation of oil saturation inside fracture over time (Rich condensate- High drawdown)

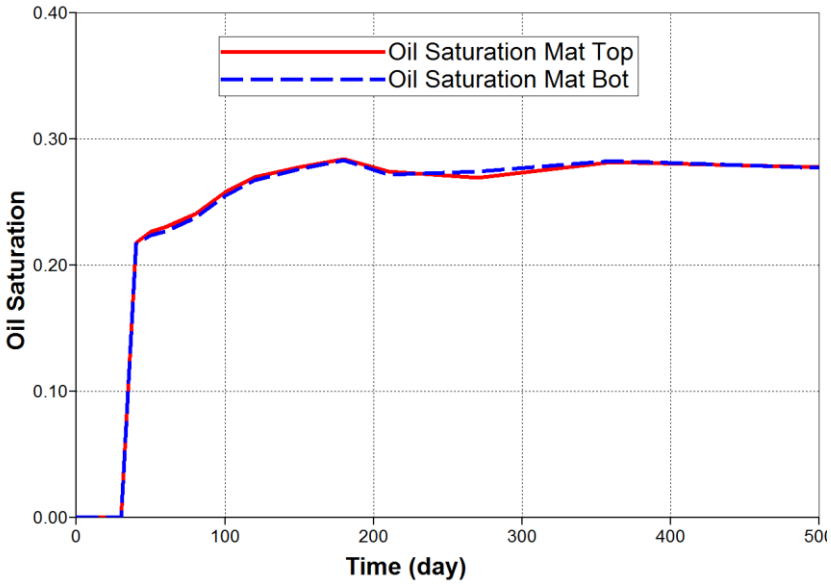

Figure 5.88: Variation of oil saturation inside matrix 0.1 ft. from fracture face with time (Rich condensate- High drawdown)

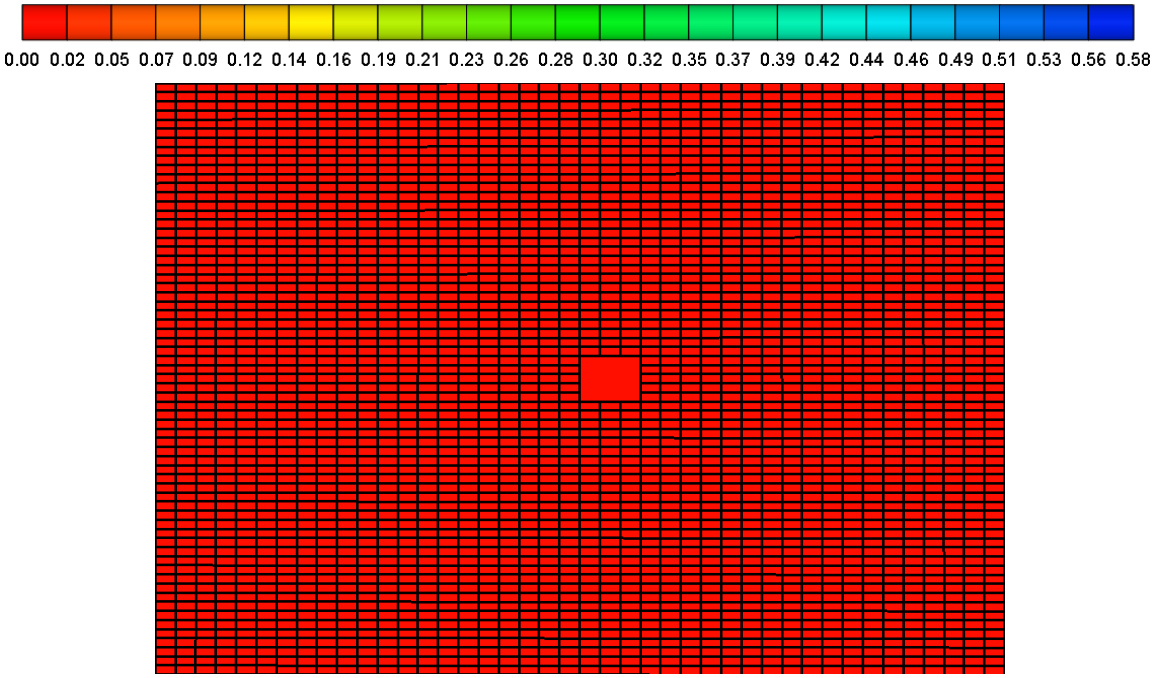

Oil saturation inside fracture after 30th day (end of shut-in, start of production)

Figure 5.89: Oil saturation maps (Rich condensate- High drawdown)

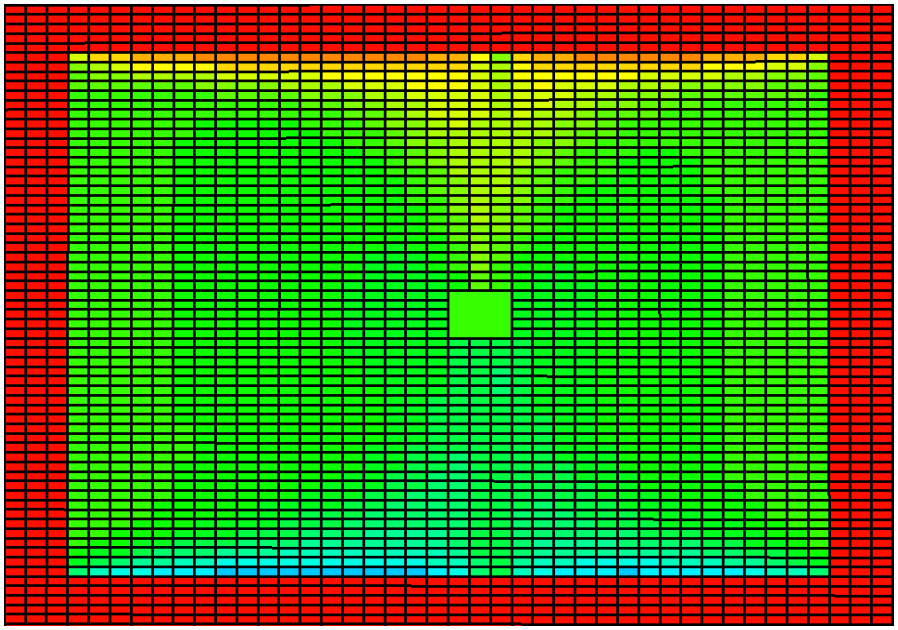

Oil saturation inside fracture after 100th day

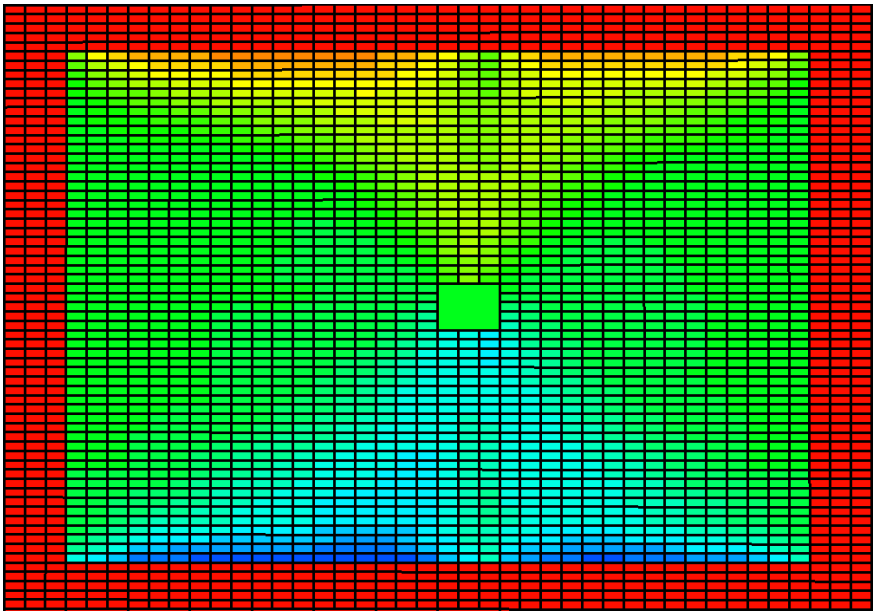

Oil saturation inside fracture after 500th end (end of production)

Figure 5.89: Oil saturation maps (Rich condensate- High drawdown) - Continued

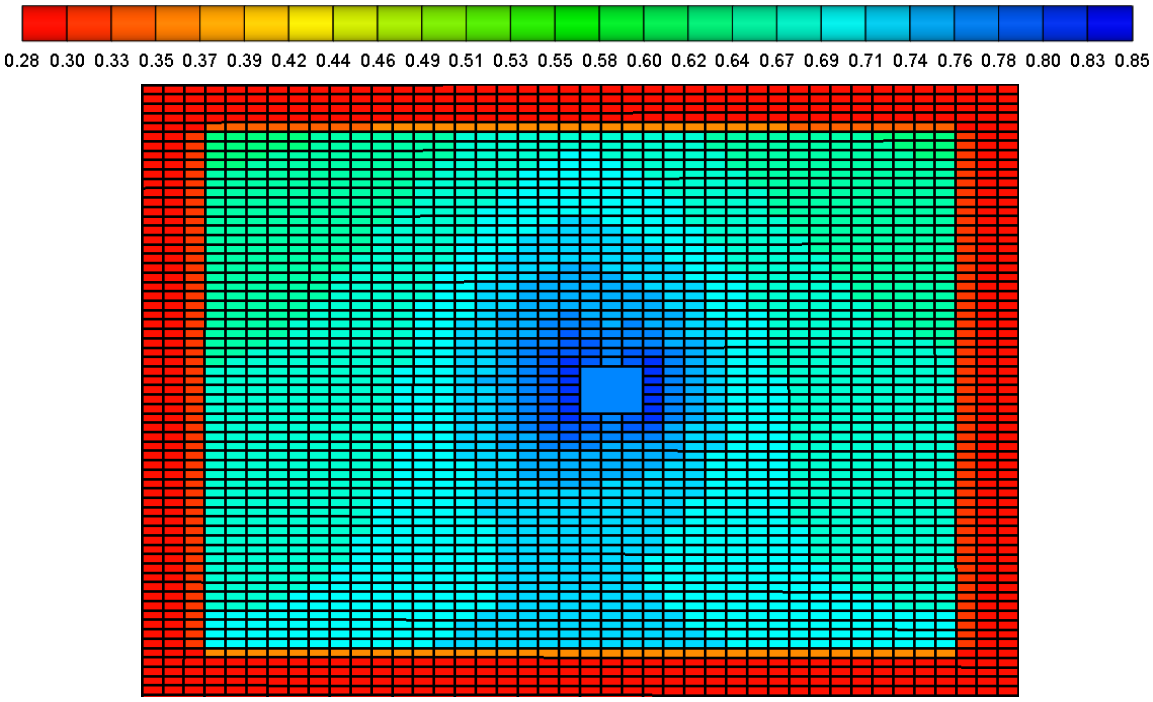

Water saturation inside fracture after 30th day (end of shut-in, start of production)

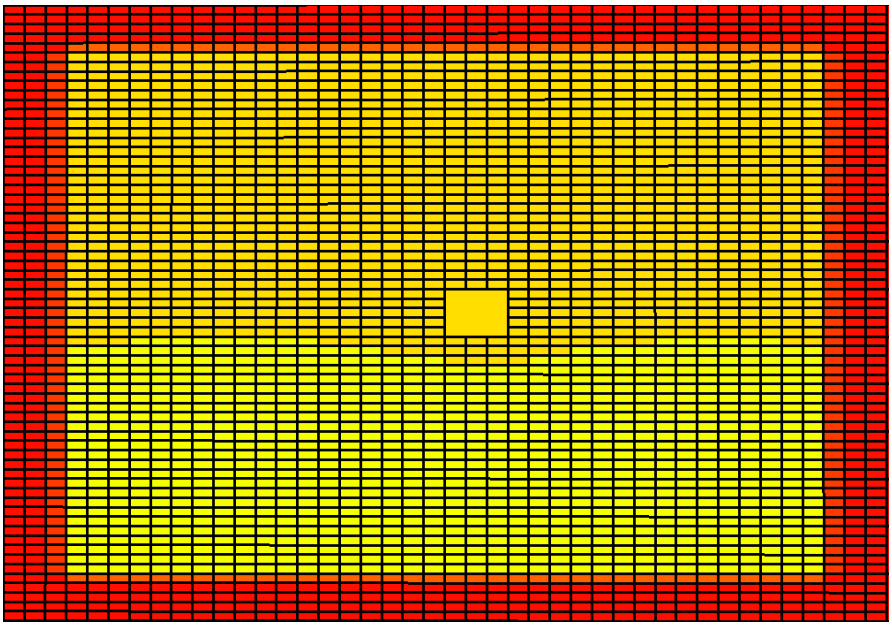

Water saturation inside fracture after 120th day

Figure 5.90: Water saturation maps (Rich condensate- High drawdown)

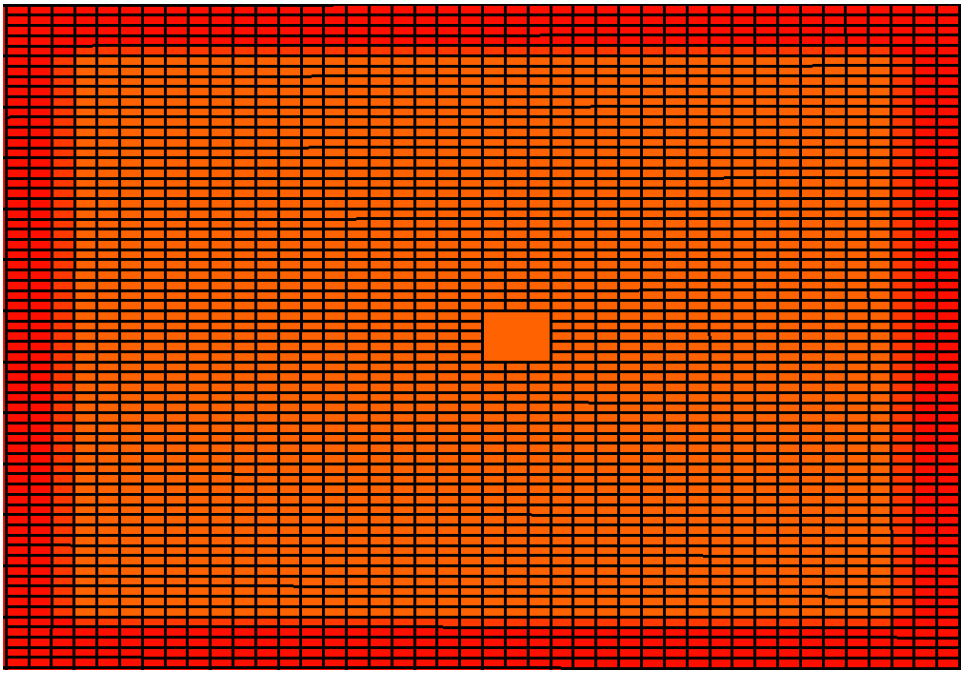

Water saturation inside fracture after 500th end (end of production)

Figure 5.90: Water saturation maps (Rich condensate- High drawdown) - Continued

5.3.13. Lean Condensate – Base case (Relative permeability Set-3)

Set-3 corresponds to the high water end point relative permeability set. In this case, a bottom-hole pressure of 4000 psi is applied for flowback. The fracture and matrix cleanup profiles in addition to the saturation maps are shown below. Compared to previous two sets, Set-3 provides much better frac-water cleanup. This cleanup could be attributed to higher water mobility at high water saturation immediately after flowback.

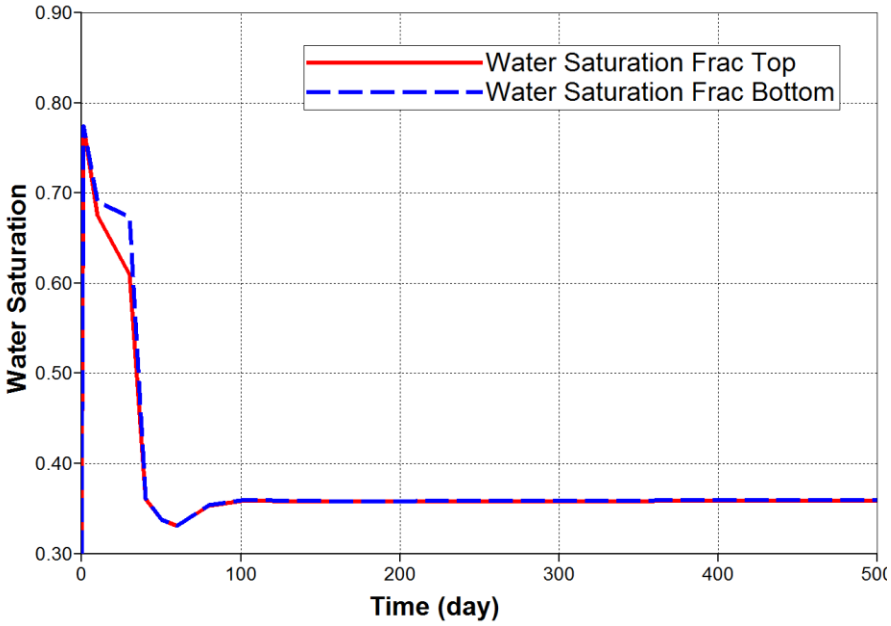

Figure 5.91: Variation of water saturation inside fracture over time (Lean condensate- Base)

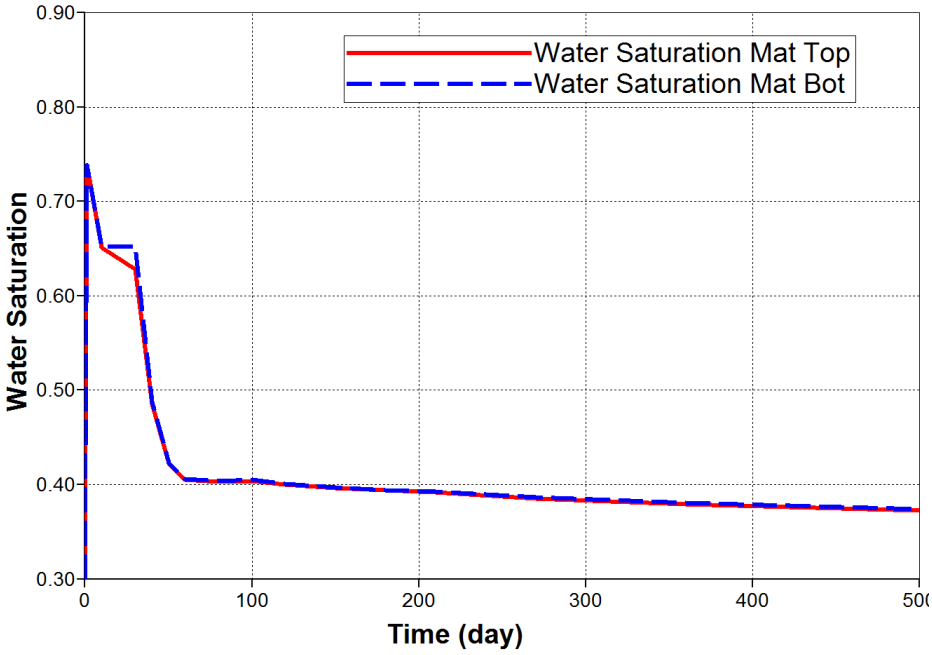

Figure 5.92: Variation of water saturation inside matrix 0.1 ft. from fracture face with time (Lean condensate- Base)

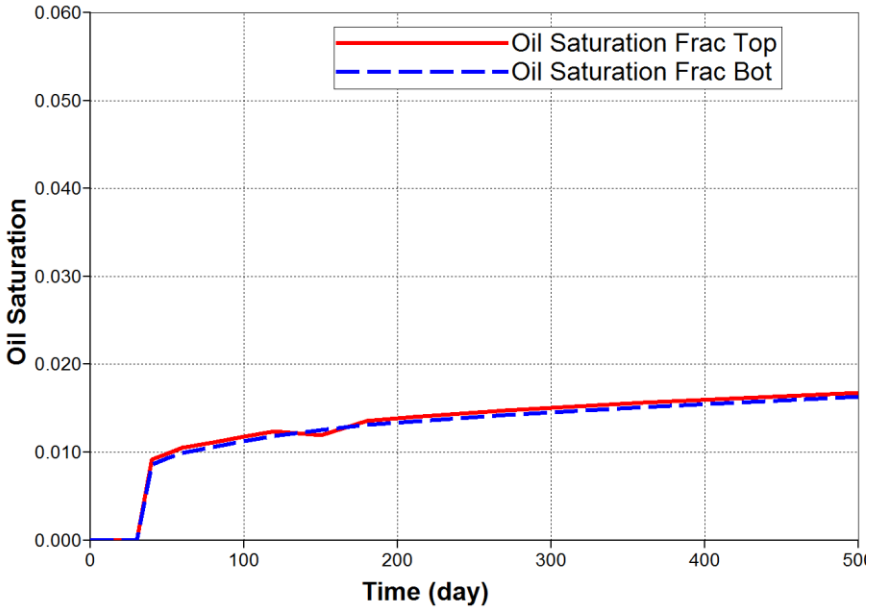

Figure 5.93: Variation of oil saturation inside fracture over time
(Lean condensate- Base)

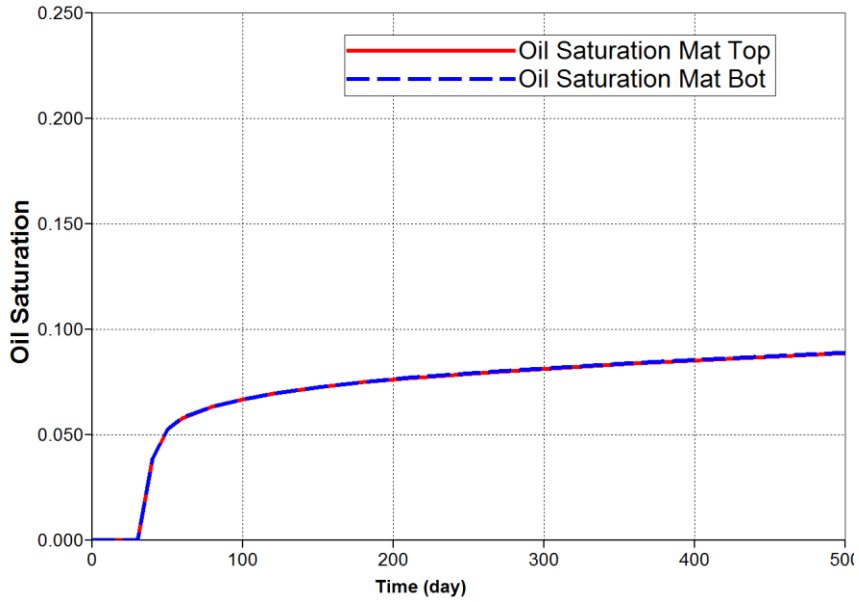

Figure 5.94: Variation of oil saturation inside matrix 0.1 ft. from fracture face with time
(Lean condensate- Base)

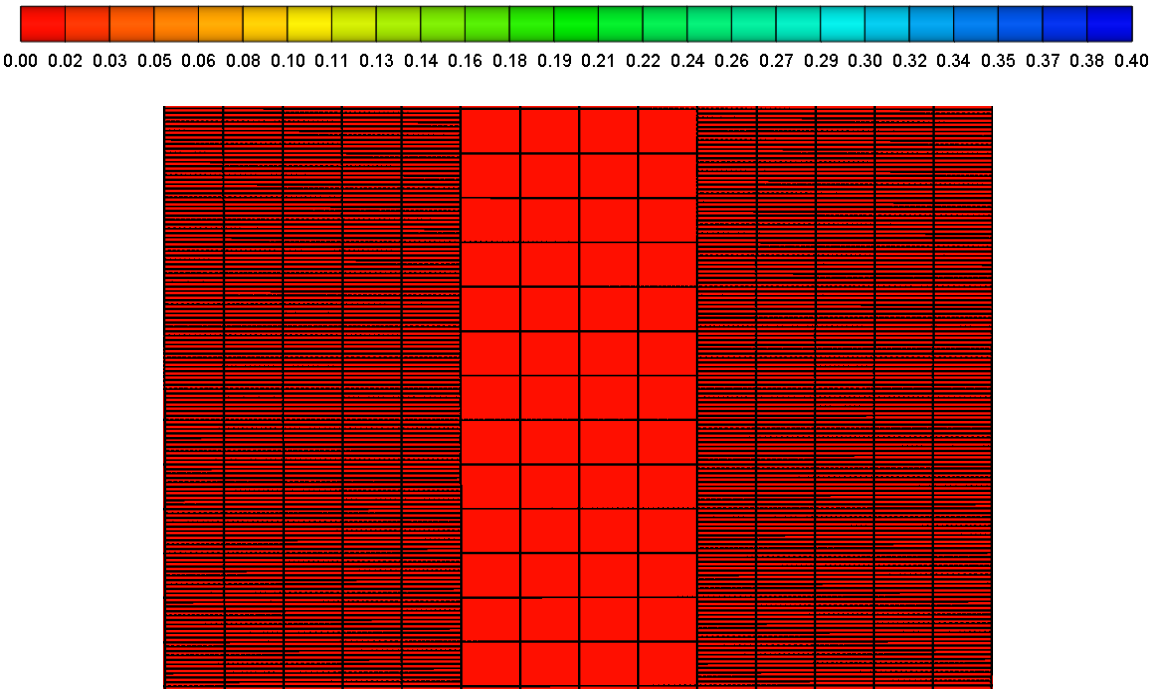

Oil saturation inside fracture after 30th day (end of shut-in, start of production)

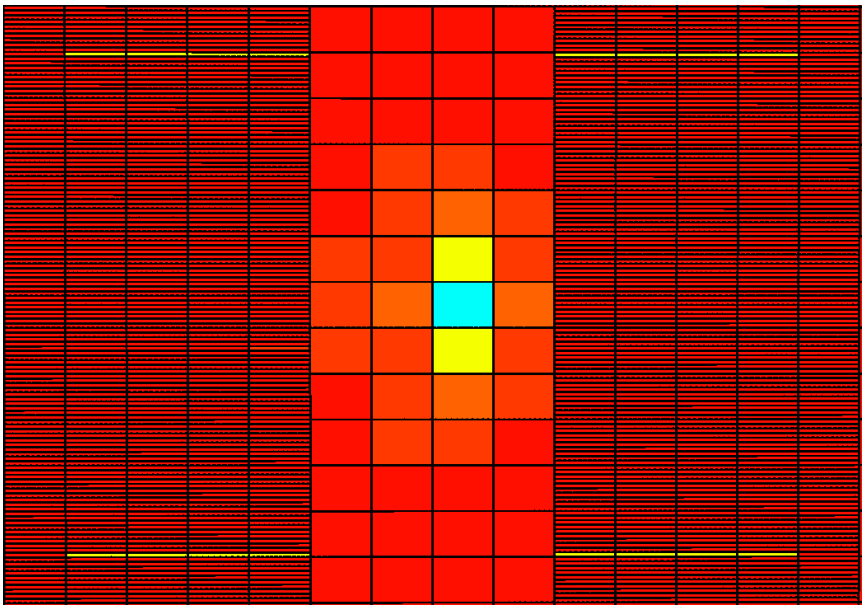

Oil saturation inside fracture after 30th day

Figure 5.95: Oil saturation maps (Lean condensate- Base)

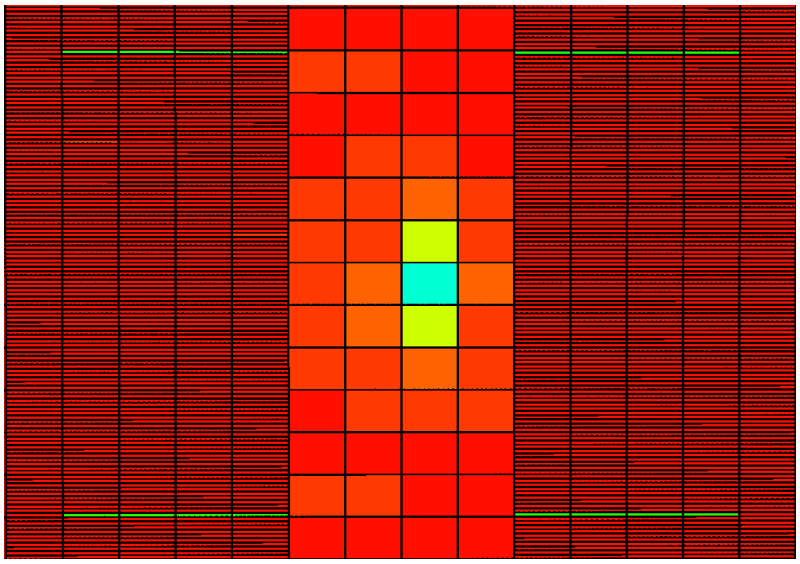

Oil saturation inside fracture after 500th day (end of production)

Figure 5.95: Oil saturation maps (Lean condensate- Base) - Continued

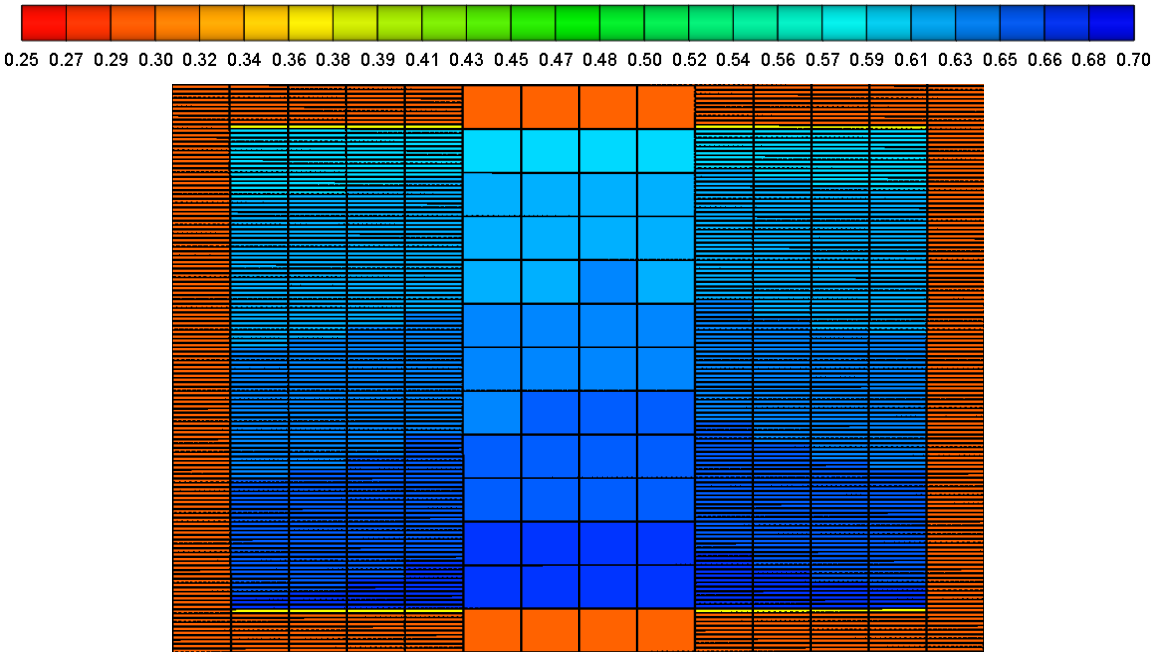

Water saturation inside fracture after 30th day (end of shut-in, start of production)

Figure 5.96: Water saturation maps (Lean condensate- Base)

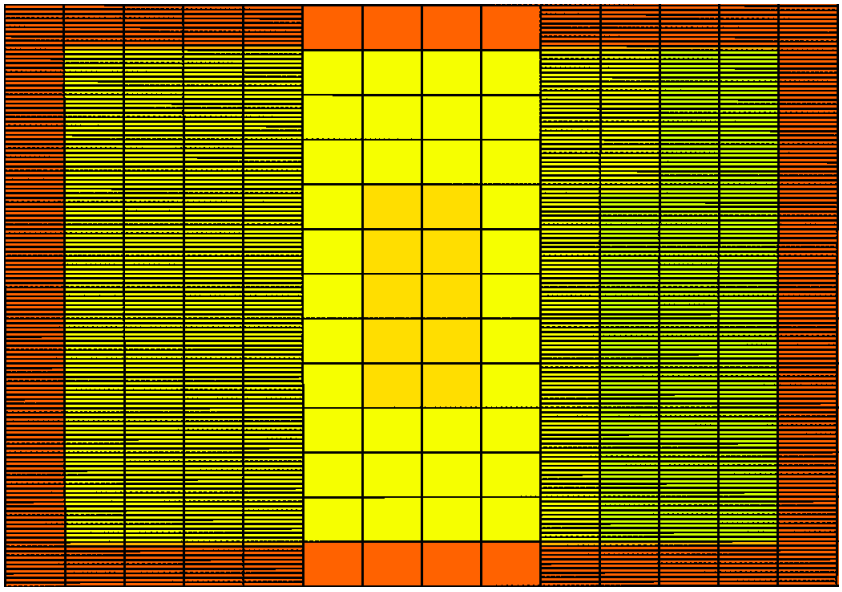

Water saturation inside fracture after 100th day

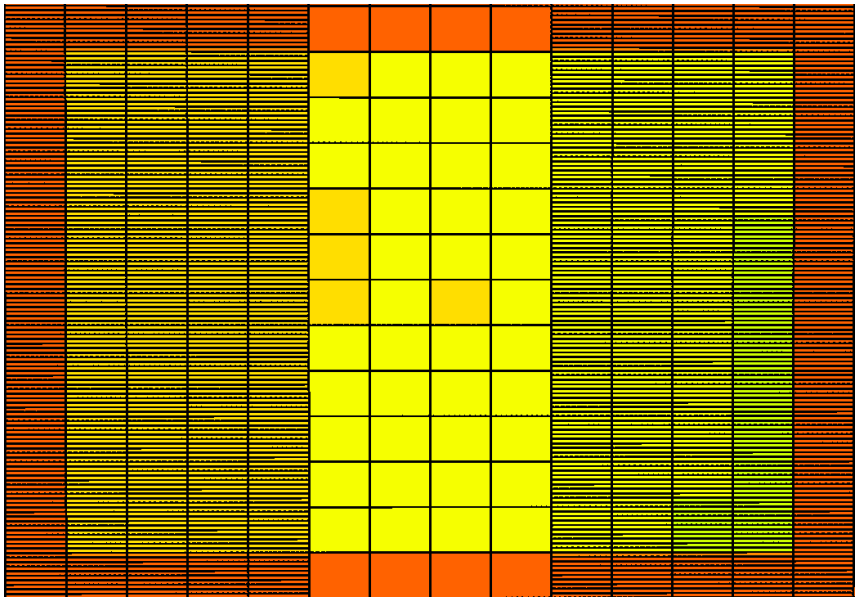

Water saturation inside fracture after 500th day (end of production)

Figure 5.96: Water saturation maps (Lean condensate- Base) - Continued

5.3.14. Lean Condensate – Low drawdown (Relative perm. Set-3)

A drawdown of 1000 psi is applied to initiate flowback in this case. Since the bottomhole pressure of 5500 psi is higher than the dew point of the lean condensate, no condensate drop-out is observed. Also, frac-water cleanup is slower than in the base case (for the same relative permeability set). However, compared with low drawdown case of Sets-1 & 2, water cleanup will be better due to higher mobility. Corresponding cleanup profiles and saturation maps are presented below.

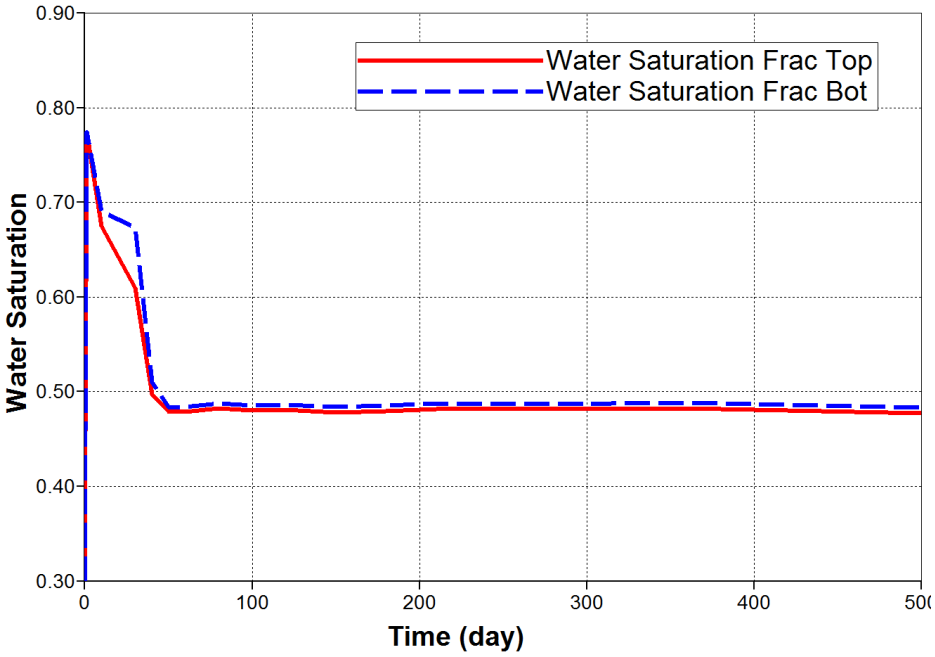

Figure 5.97: Variation of water saturation inside fracture over time (Lean condensate- Low drawdown)

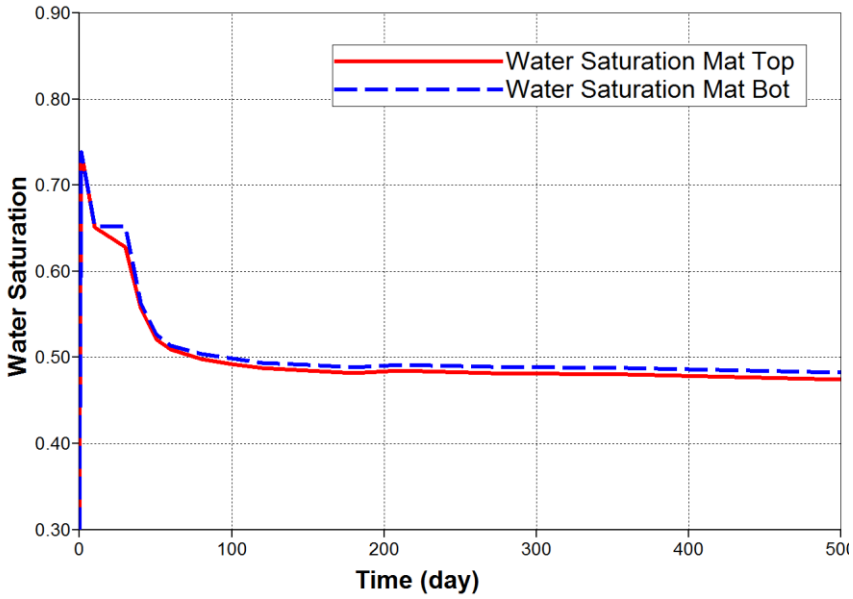

Figure 5.98: Variation of water saturation inside matrix 0.1 ft. from fracture face with time (Lean condensate- Low drawdown)

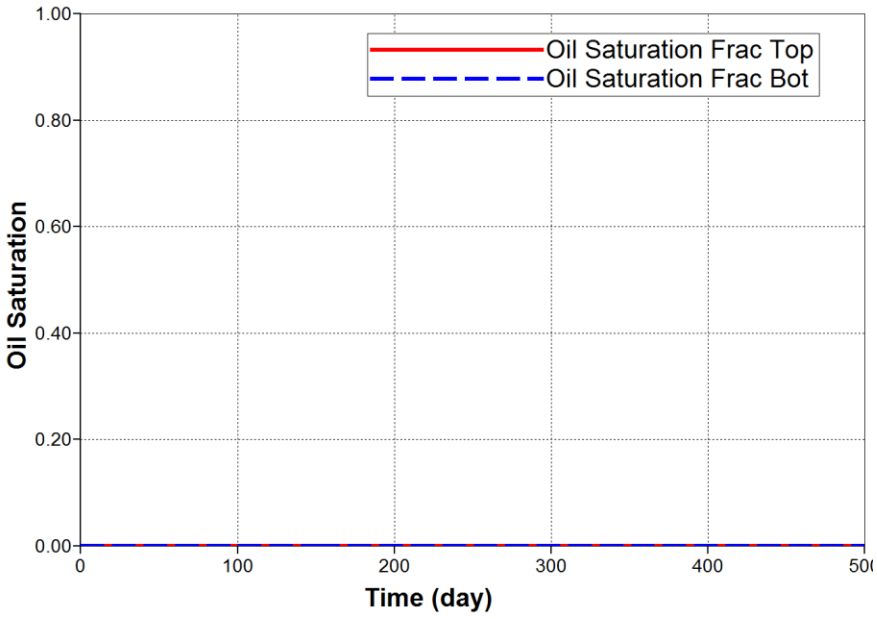

Figure 5.99: Variation of oil saturation inside fracture over time (Lean condensate- Low drawdown)

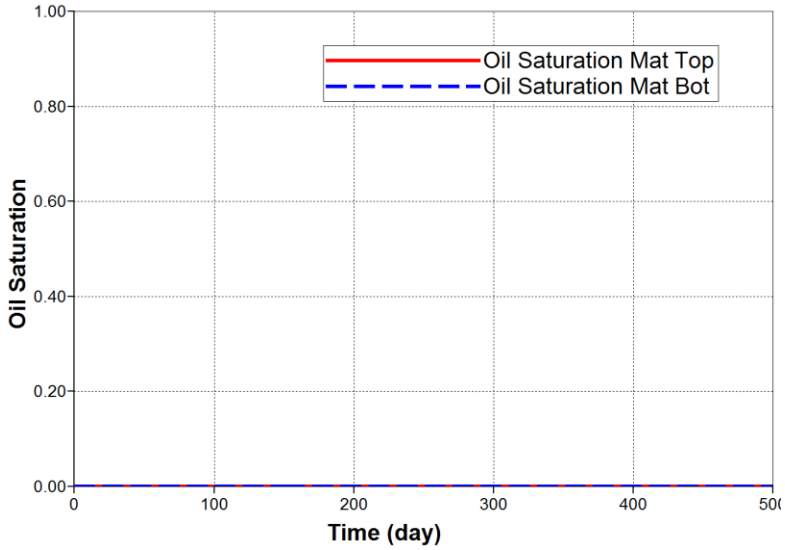

Figure 5.100: Variation of oil saturation inside matrix 0.1 ft. from fracture face with time (Lean condensate- Low drawdown)

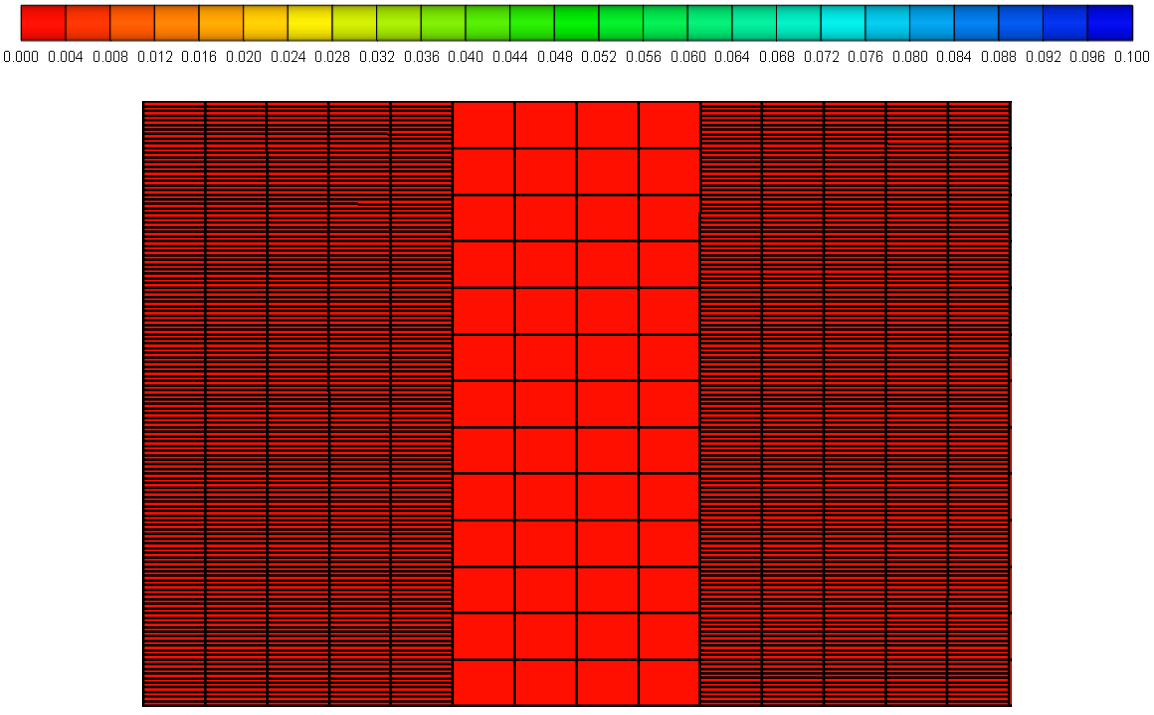

Oil saturation inside fracture after 30th day (end of shut-in)

Figure 5.101: Oil saturation maps (Lean condensate- Low drawdown)

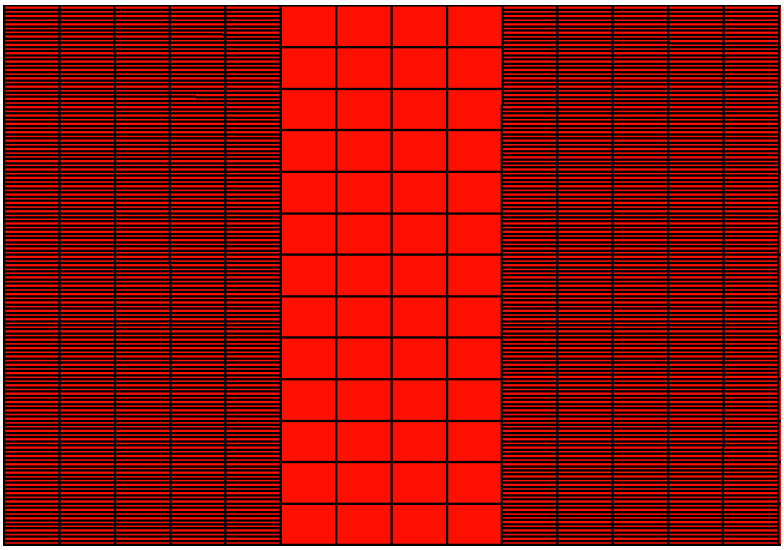

Oil saturation inside fracture after 500th day (end of production)

Figure 5.101: Oil saturation maps (Lean condensate- Low drawdown) - Continued

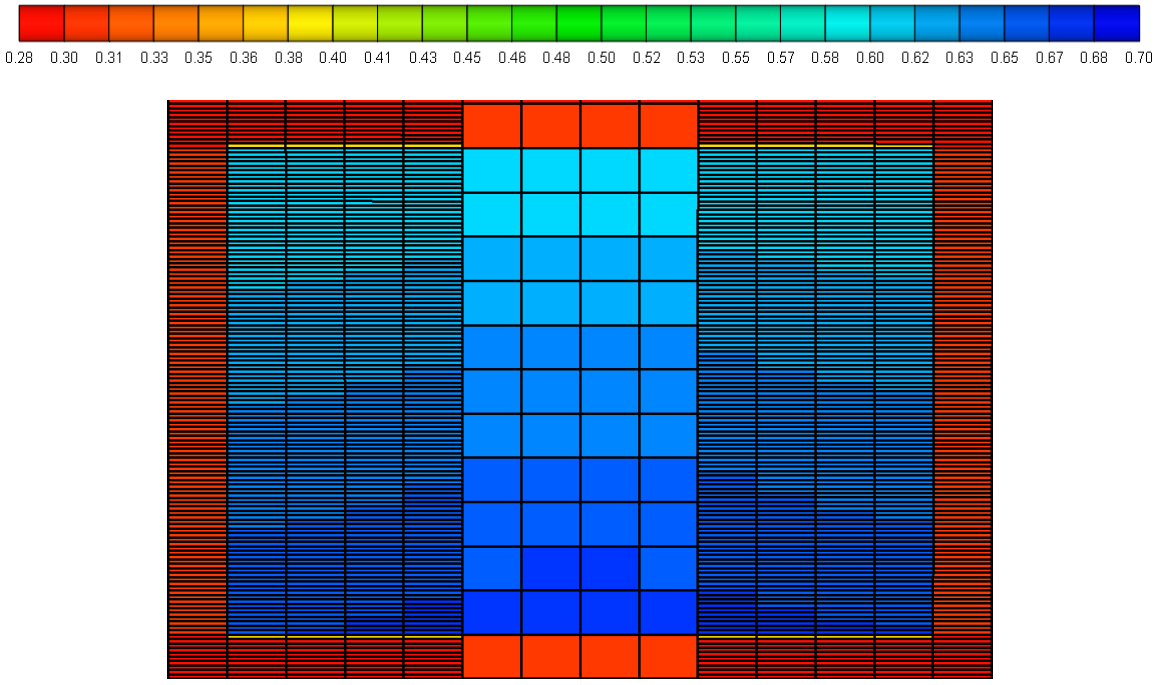

Water saturation inside fracture after 30th day (end of shut-in)

Figure 5.102: Water saturation maps (Lean condensate- Low drawdown)

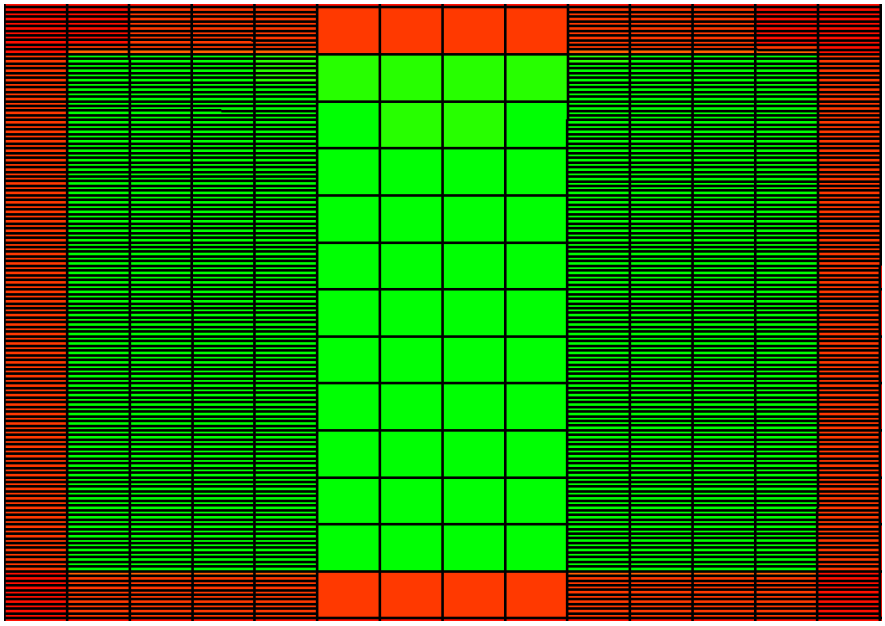

Water saturation inside fracture after 120th day

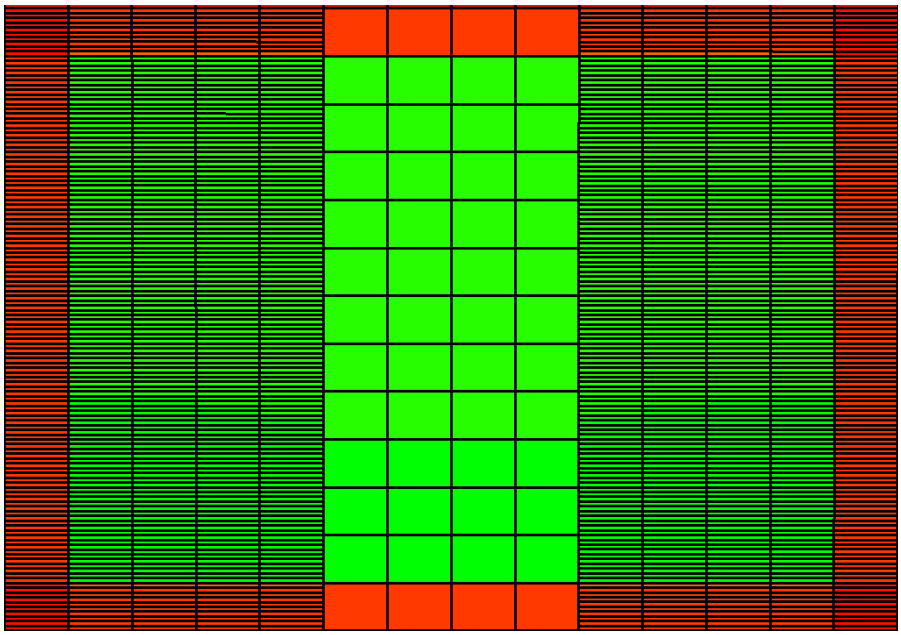

Water saturation inside fracture after 500th day (end of production)

Figure 5.102: Water saturation maps (Lean condensate- Low drawdown) - Continued

5.3.15. Lean Condensate – High drawdown (Relative perm. Set-3)

In this case, drawdown is increased to 3500 psi by applying a bottom-hole pressure of 3000 psi. Higher drawdown improves frac-water cleanup in fracture and matrix as expected. Cleanup profiles show frac-water is almost completely removed from fracture as saturation approaches residual value.

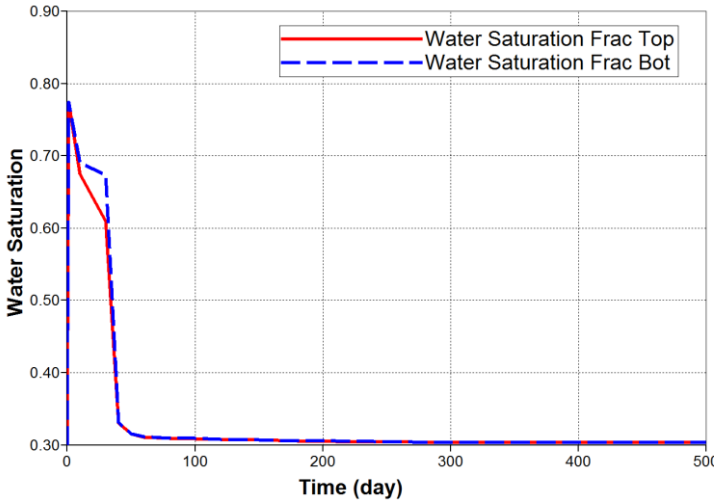

Figure 5.103: Variation of water saturation inside fracture over time (Lean condensate- High drawdown)

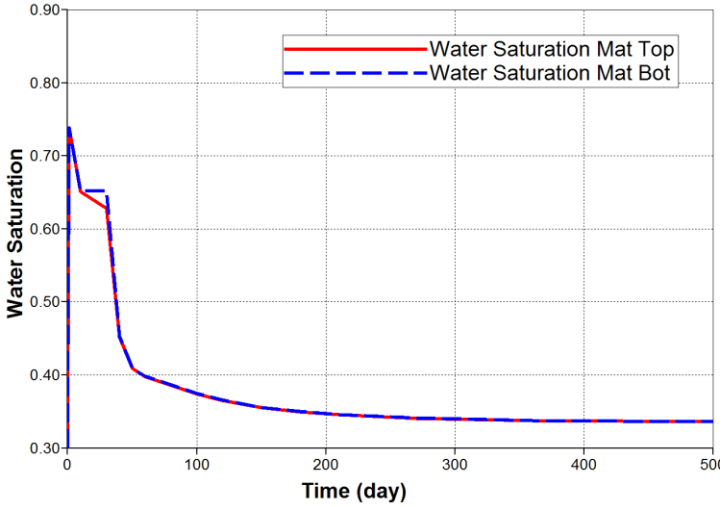

Figure 5.104: Variation of water saturation inside matrix 0.1 ft. from fracture face with time (Lean condensate- Low drawdown)

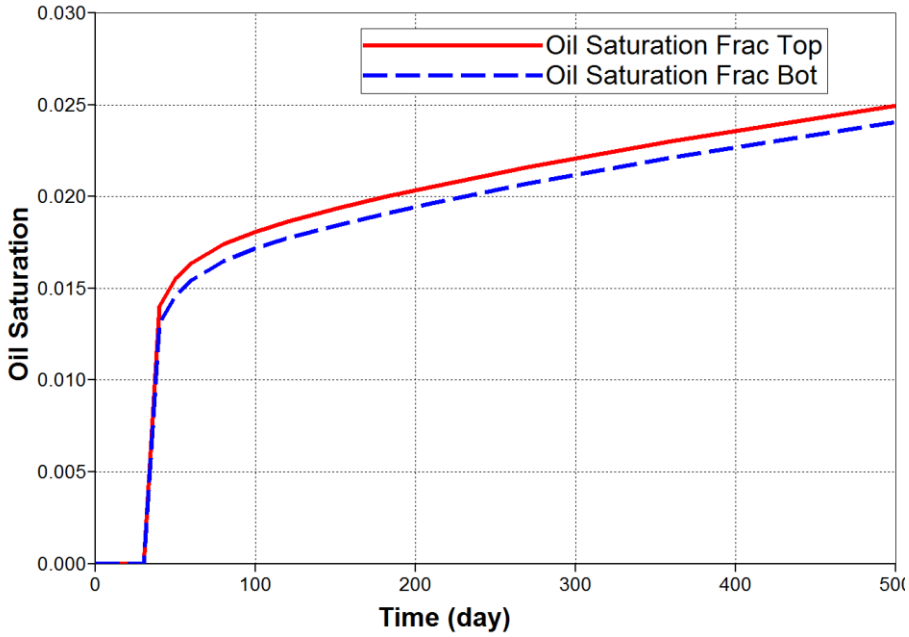

Figure 5.105: Variation of oil saturation inside fracture over time
(Lean condensate- High drawdown)

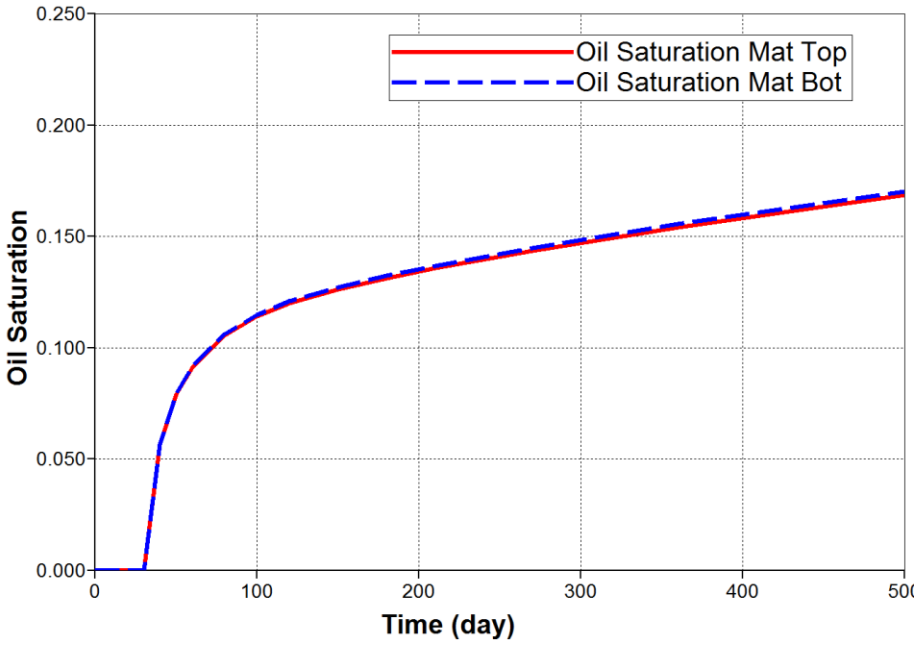

Figure 5.106: Variation of oil saturation inside matrix 0.1 ft. from fracture face with time
(Lean condensate- High drawdown)

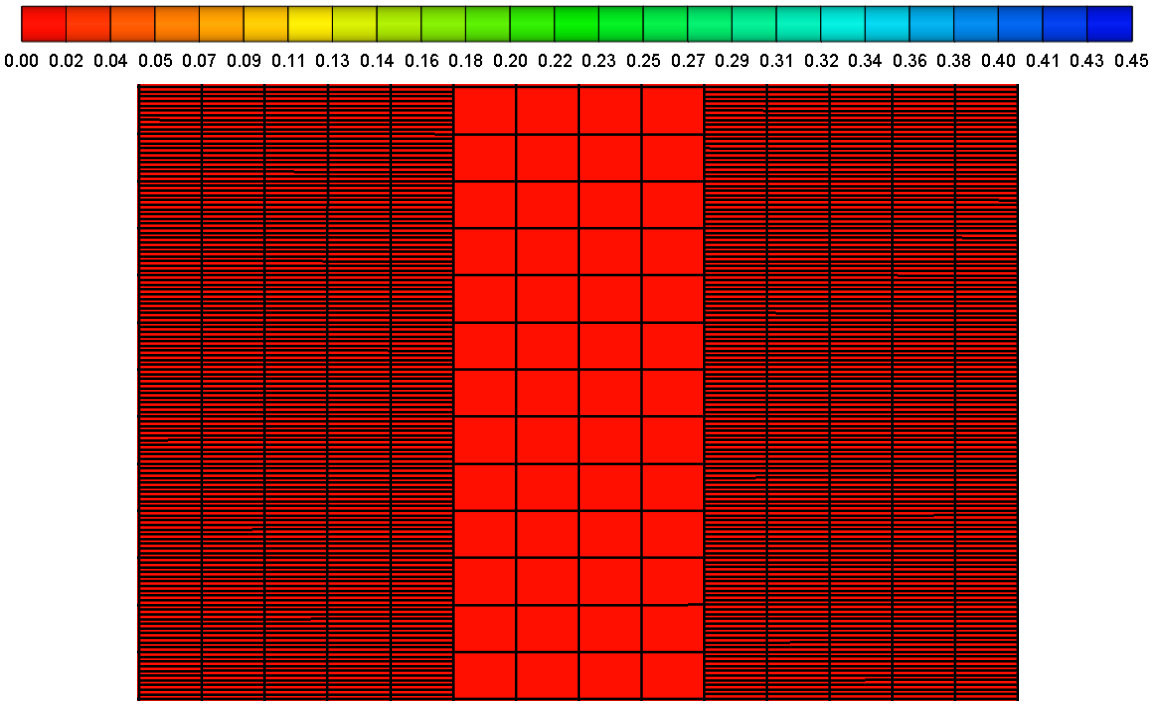

Oil saturation inside fracture after 30th day (end of shut-in)

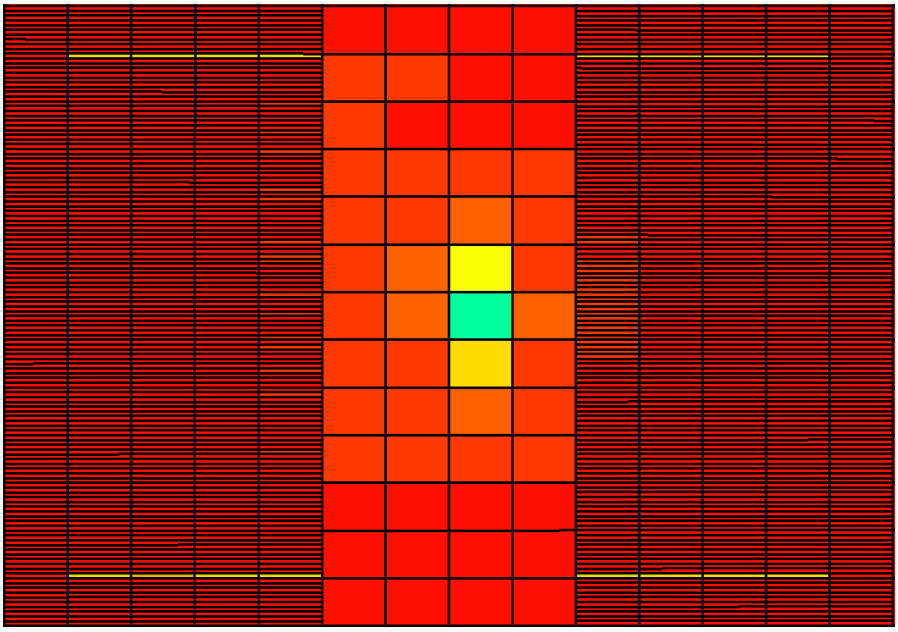

Oil saturation inside fracture after 100th day

Figure 5.107: Oil saturation maps (Lean condensate- High drawdown)

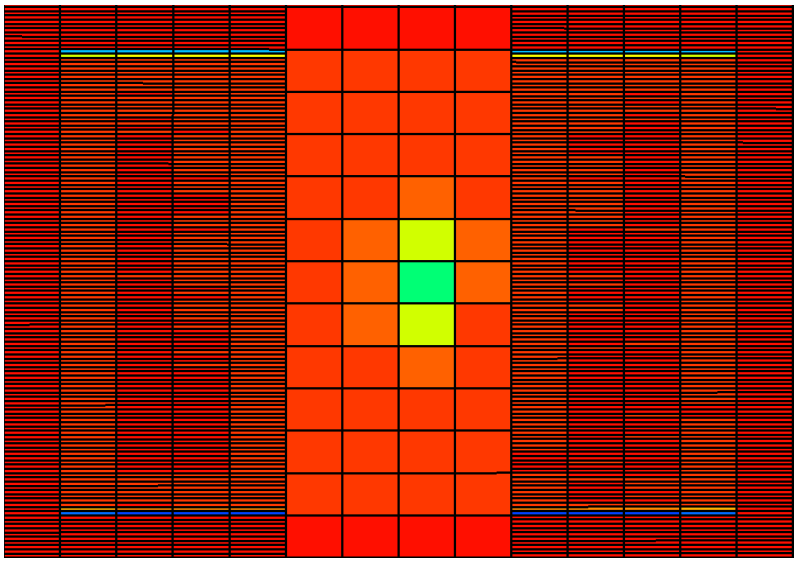

Oil saturation inside fracture after 500th day (end of production)

Figure 5.107: Oil saturation maps (Lean condensate- High drawdown) - Continued

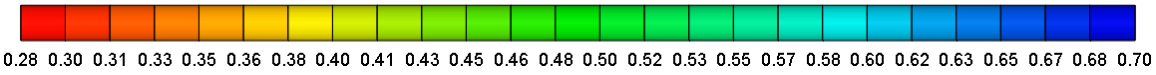

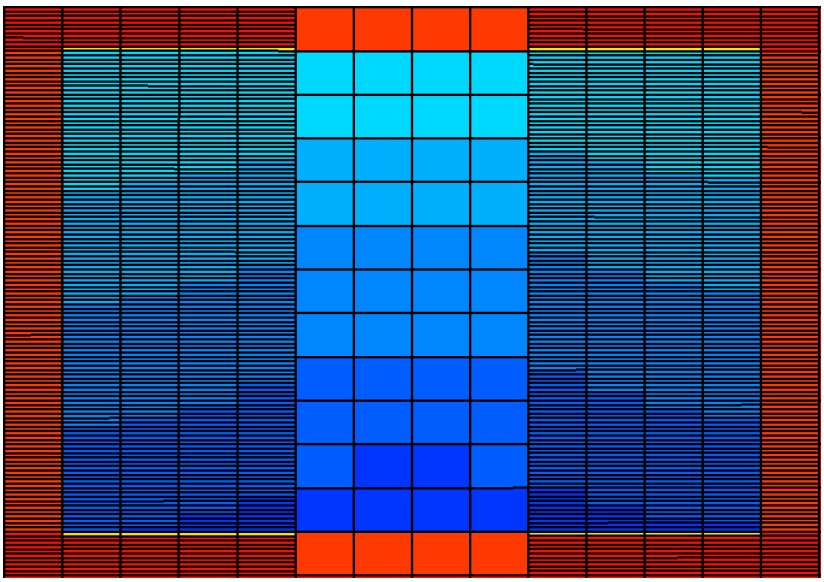

Water saturation inside fracture after 30th day (end of shut-in)

Figure 5.108: Water saturation maps (Lean condensate- High drawdown)

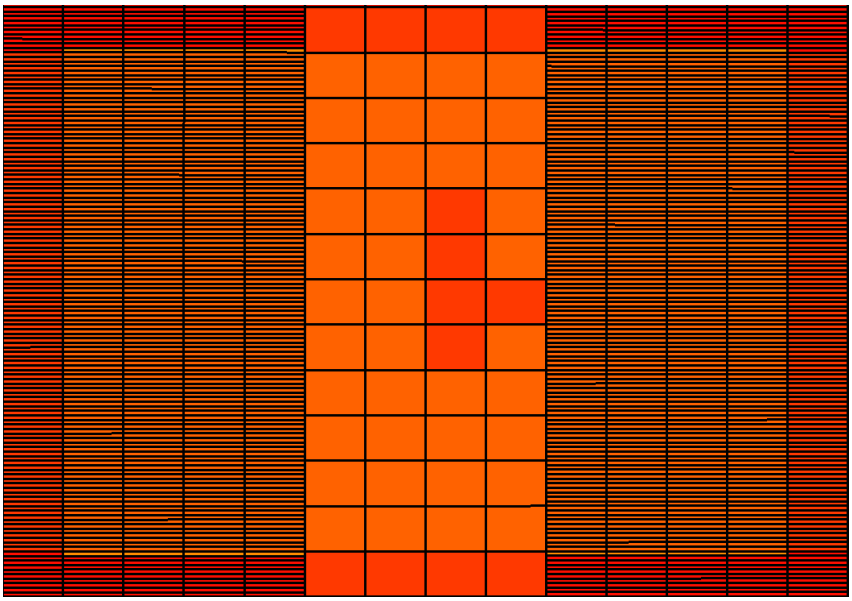

Water saturation inside fracture after 50th day

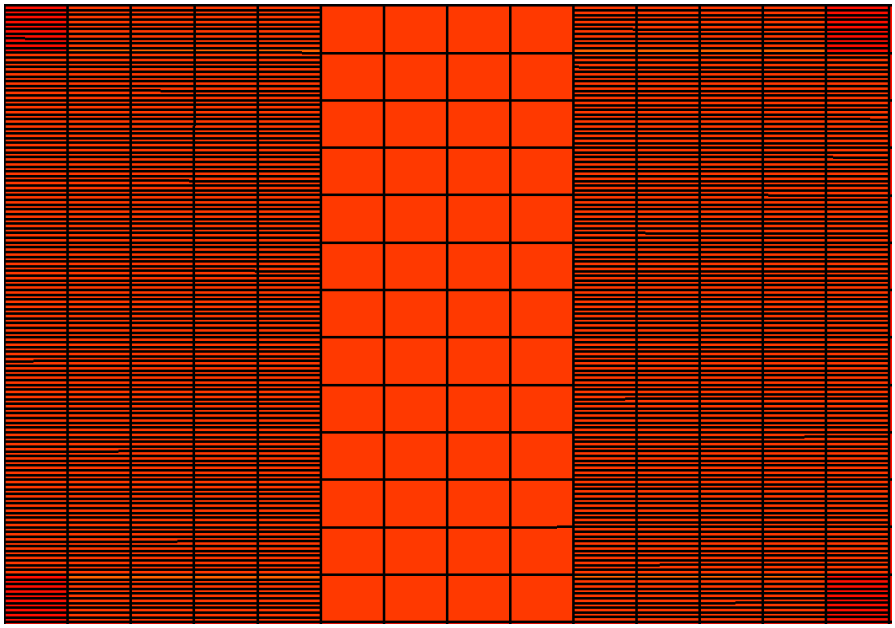

Water saturation inside fracture after 500th day (end of production)

Figure 5.108: Water saturation maps (Lean condensate- High drawdown) - Continued

5.3.16. Rich Condensate – Base Case (Relative perm. Set-3)

The following figures illustrate the cleanup profiles after flowback (P_{wf} = 3000 psi) for a rich condensate reservoir with Set-3 relative permeability curves. Compared with Set-1 and 2, frac-water cleanup is better. Condensate loading is observed at fracture bottom.

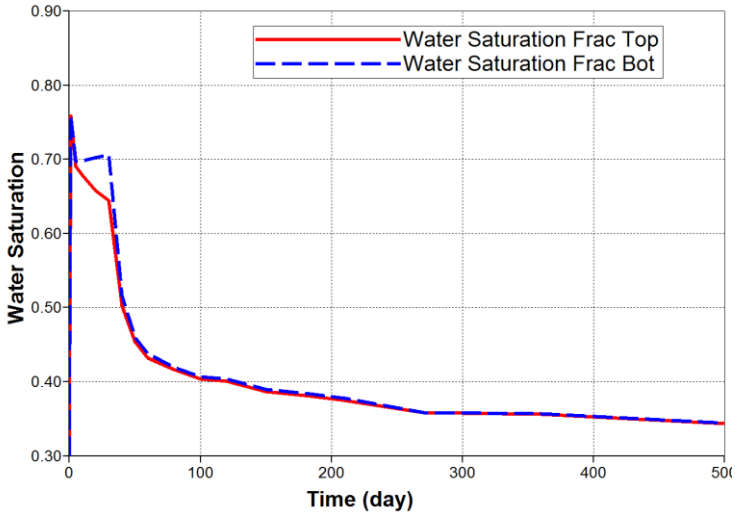

Figure 5.109: Variation of water saturation inside fracture over time (Rich condensate- Base)

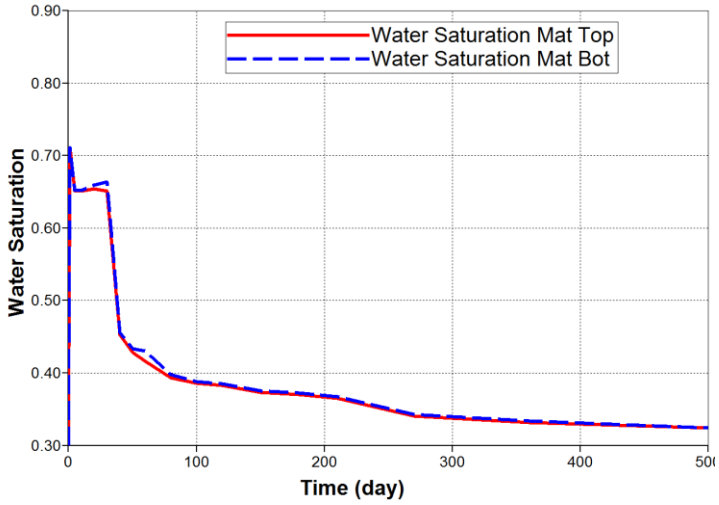

Figure 5.110: Variation of water saturation inside matrix 0.1 ft. from fracture face with time (Rich condensate- Base)

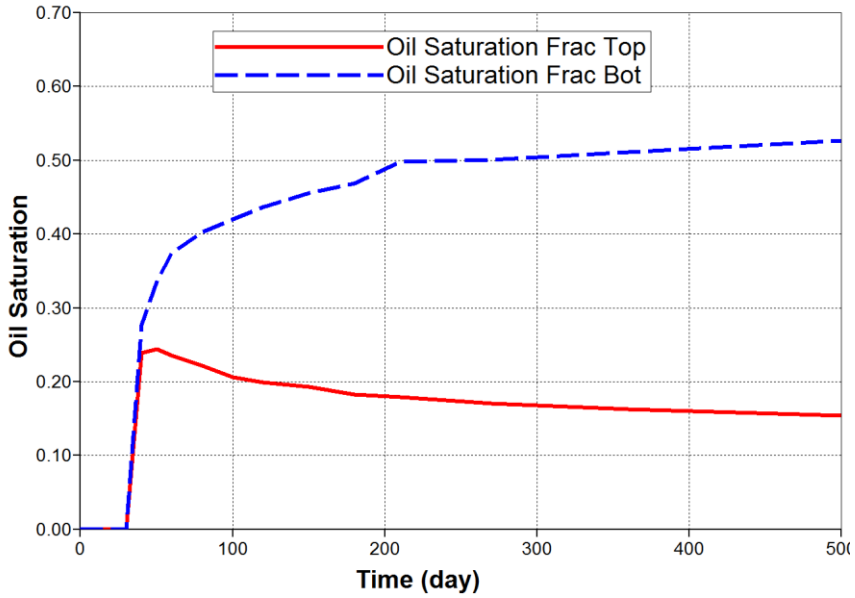

Figure 5.111: Variation of oil saturation inside fracture over time
(Rich condensate- Base)

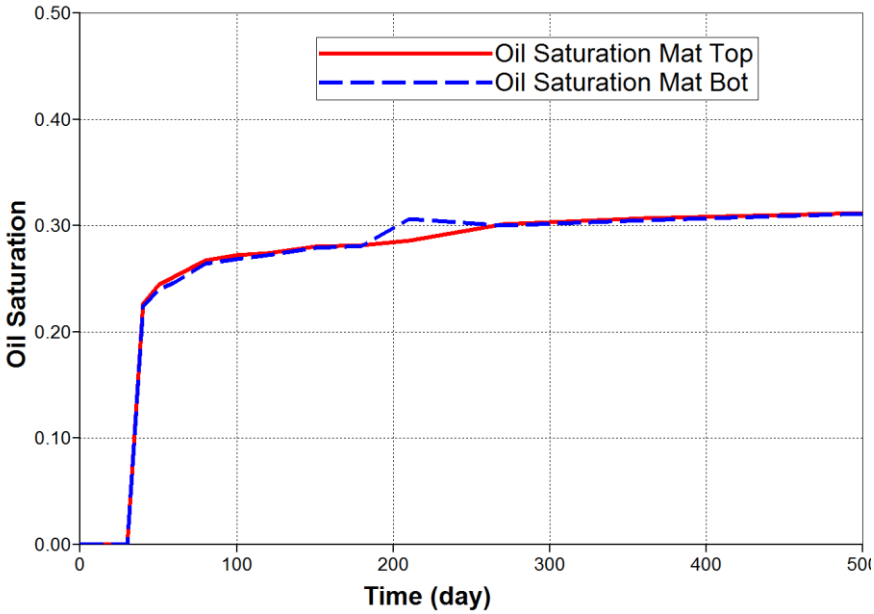

Figure 5.112: Variation of oil saturation inside matrix 0.1 ft. from fracture face with time
(Rich condensate- Base)

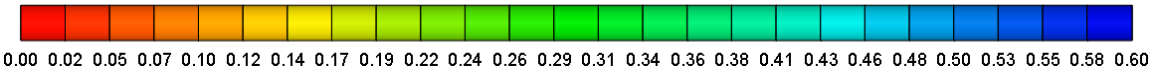

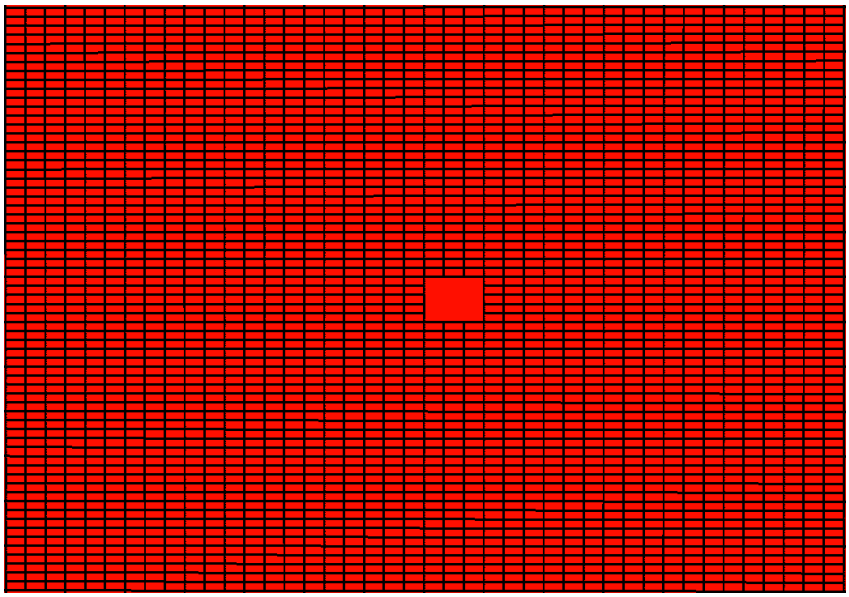

Oil saturation inside fracture after 30th day (end of shut-in)

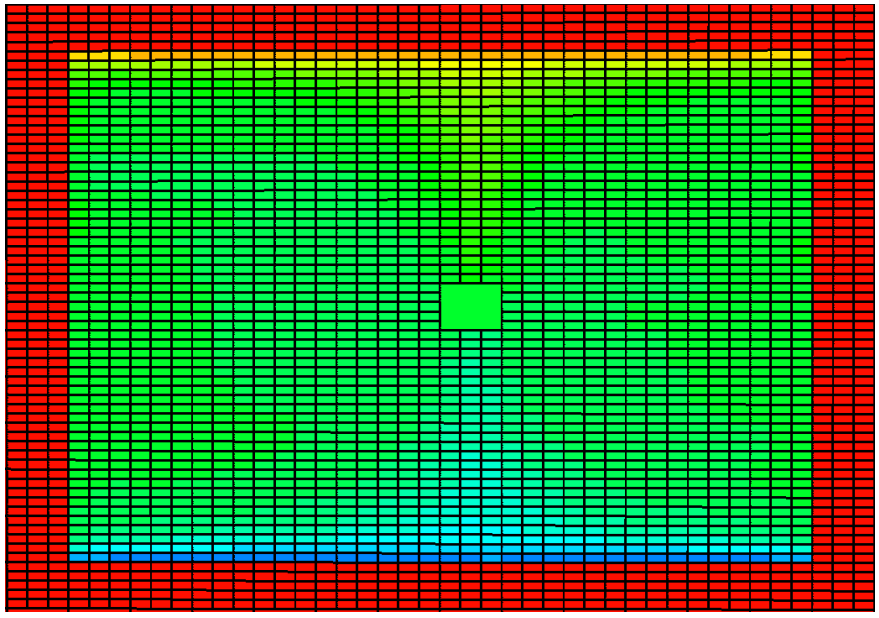

Oil saturation inside fracture after 150th day

Figure 5.113: Oil saturation maps (Rich condensate- Base)

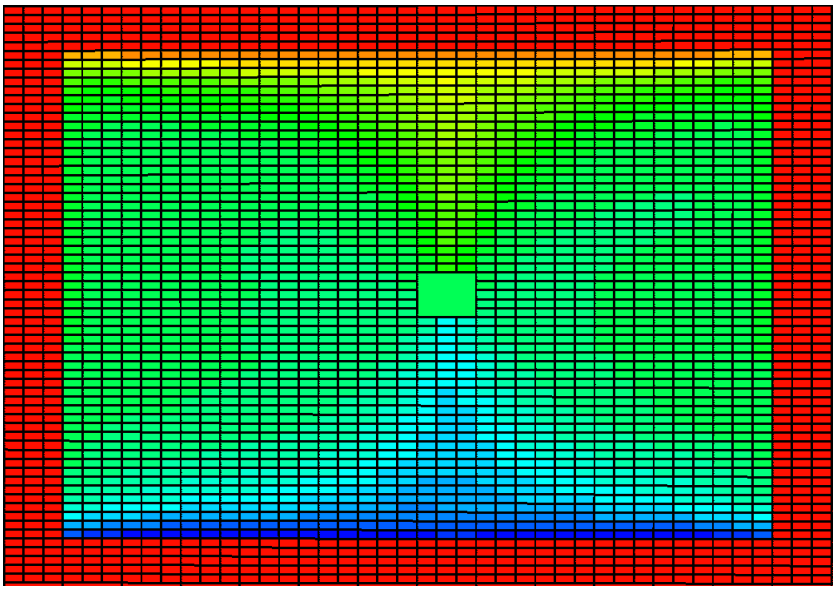

Oil saturation inside fracture after 500th day (end of production)

Figure 5.113: Oil saturation maps (Rich condensate- Base) - Continued

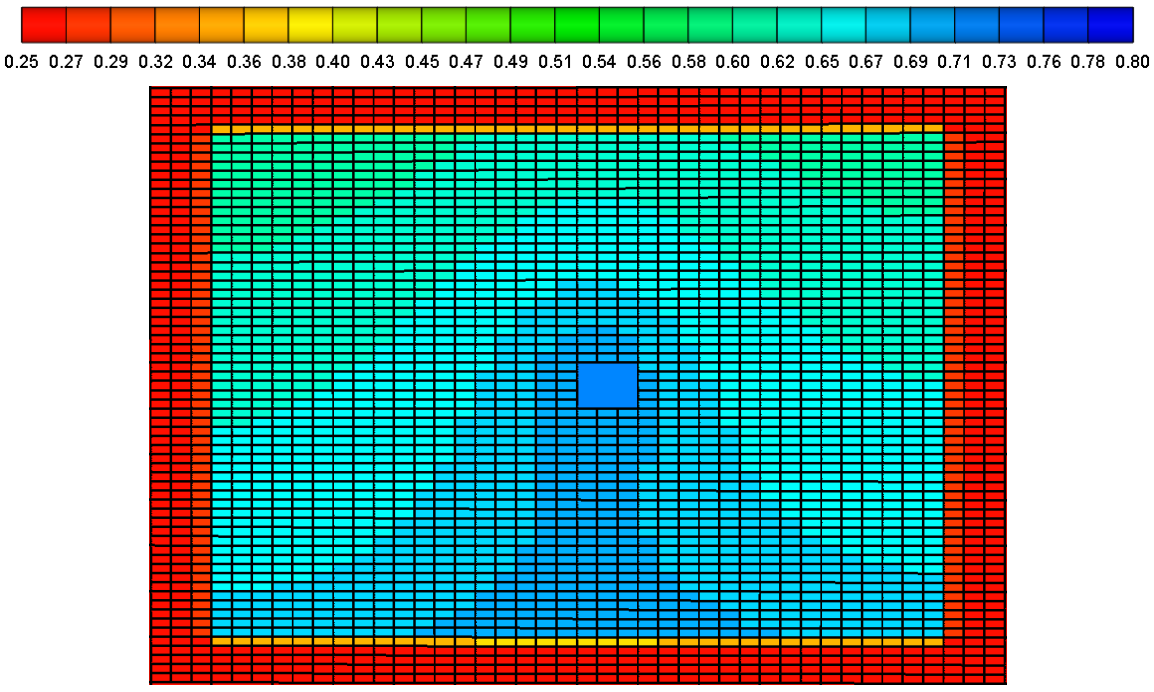

Water saturation after 30th day (end of shut-in)

Figure 5.114: Water saturation maps (Rich condensate- Base)

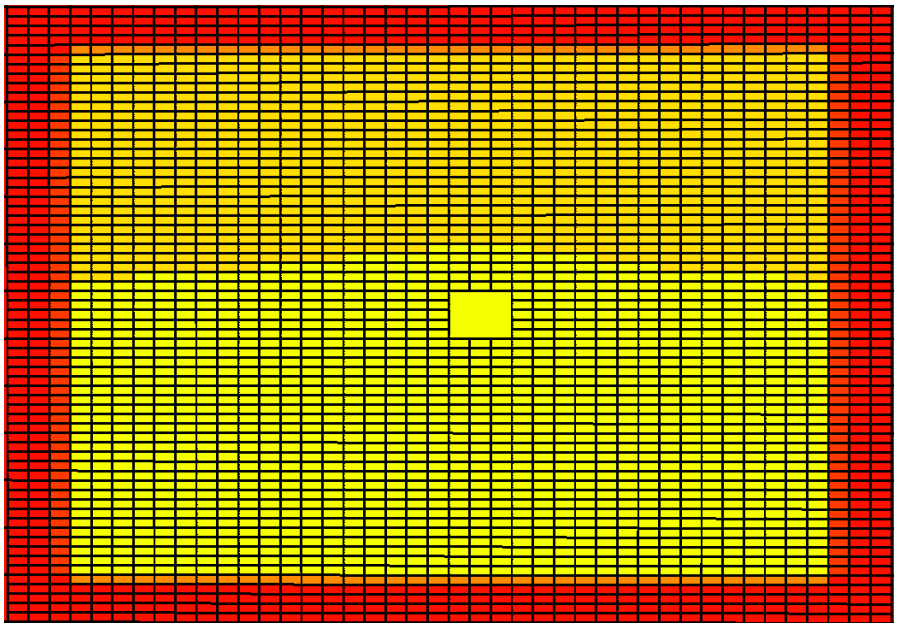

Water saturation after 100th day

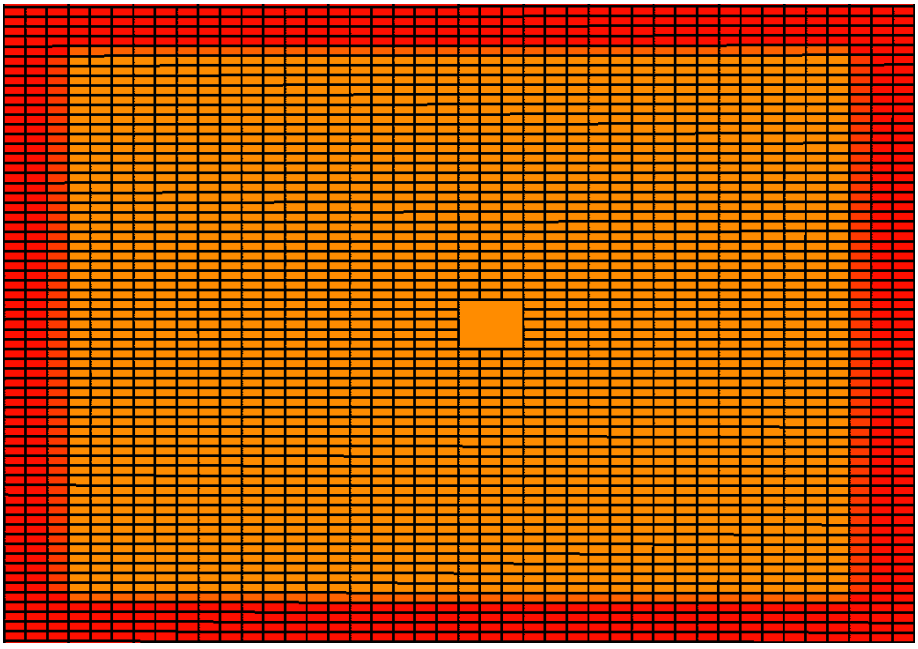

Water saturation inside fracture after 500th day (end of production)

Figure 5.114: Water saturation maps (Rich condensate- Base) - Continued

5.3.17. Rich Condensate – Low Drawdown (Relative perm. Set-3)

The rich condensate reservoir is produced by applying a bottom-hole pressure above the dew point, P_{wf} =5500 psi. Since wellbore pressure is above dew point, no condensate drop out is observed. The cleanup profiles are shown in following figures.

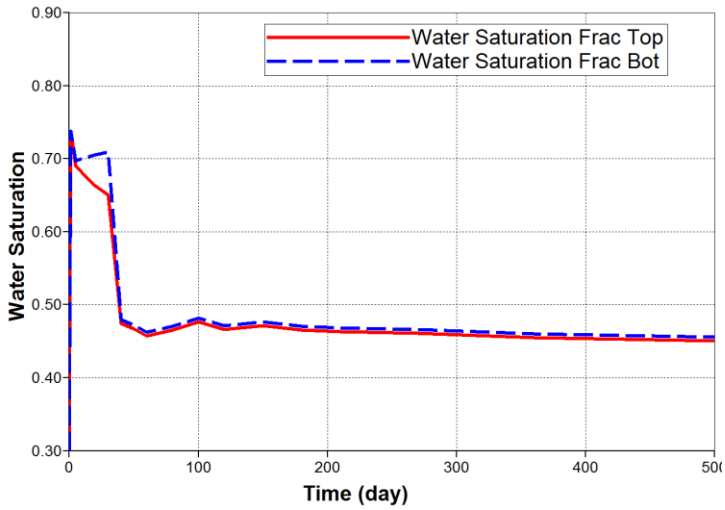

Figure 5.115: Variation of water saturation inside fracture over time (Rich condensate- Low drawdown)

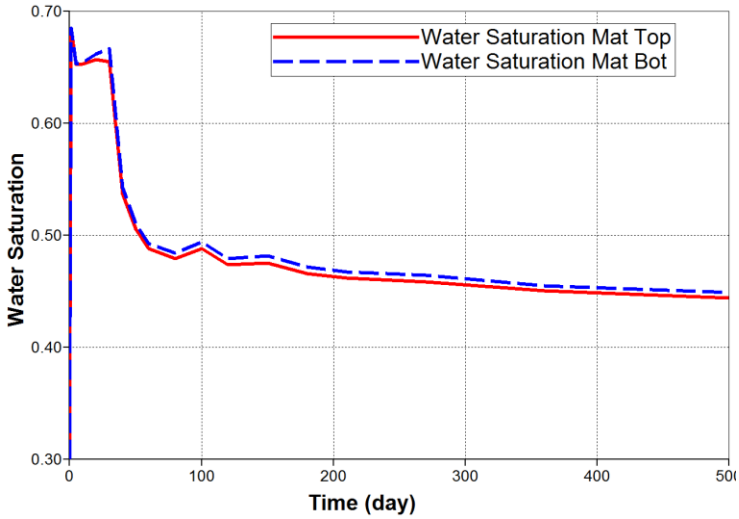

Figure 5.116: Variation of water saturation inside matrix 0.1 ft. from fracture face with time (Rich condensate- Low drawdown)

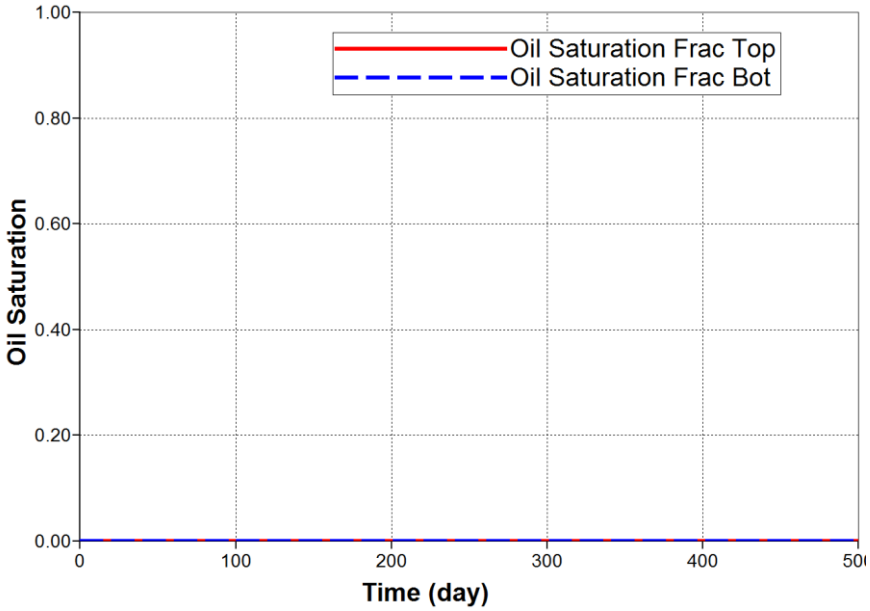

Figure 5.117: Variation of oil saturation inside fracture over time
(Rich condensate- Low drawdown)

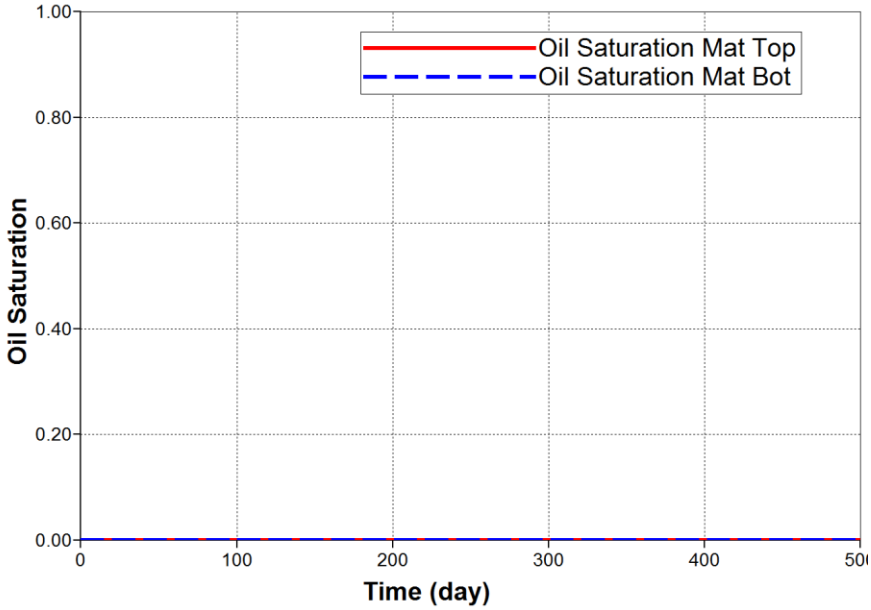

Figure 5.118: Variation of oil saturation inside matrix 0.1 ft. from fracture face with time
(Rich condensate- Low drawdown)

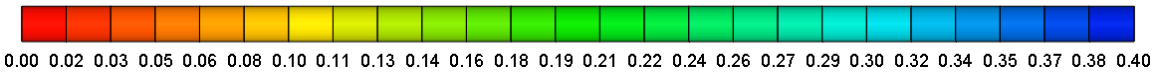

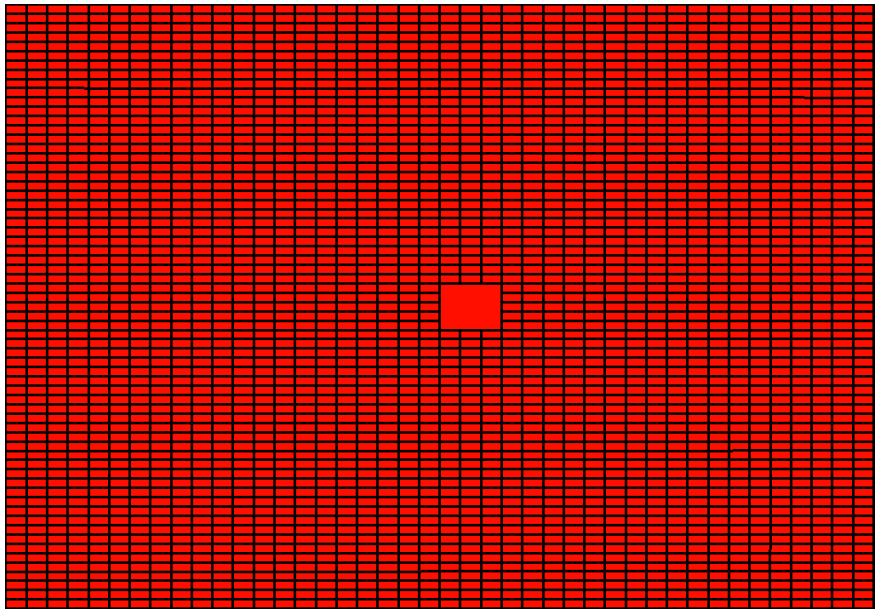

Oil saturation inside fracture after 30th day (end of shut-in)

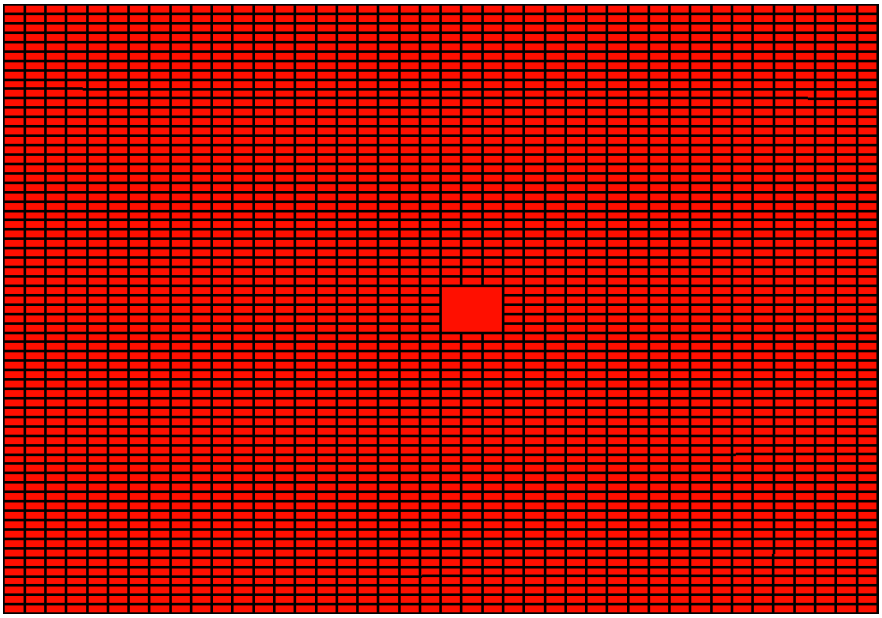

Oil saturation inside fracture after 500th day (end of production)

Figure 5.119: Oil saturation maps (Rich condensate- Low drawdown)

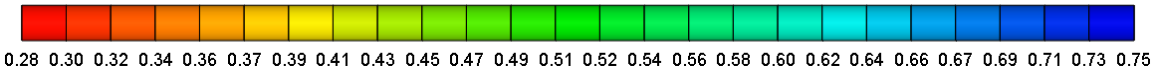

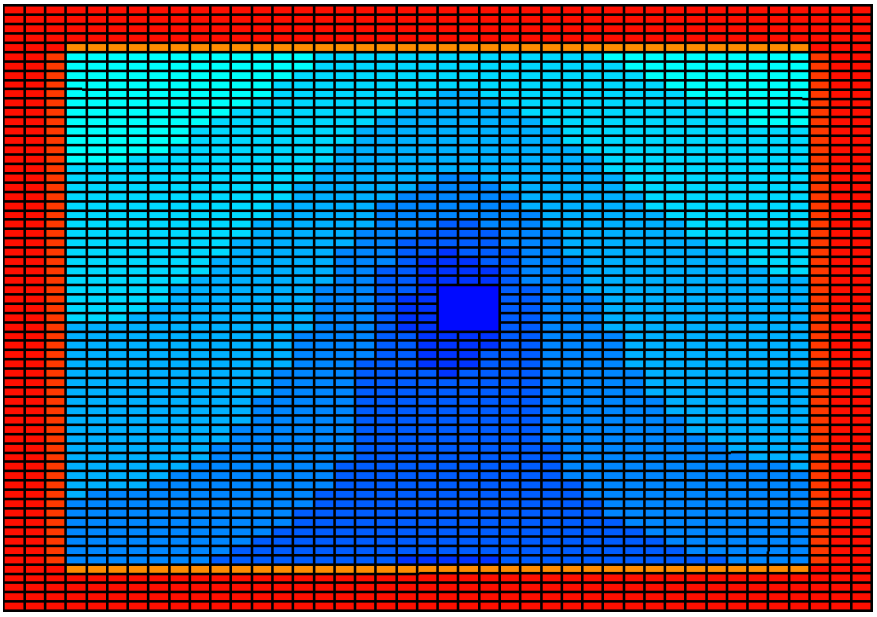

Water saturation inside fracture after 30th day (end of shut-in)

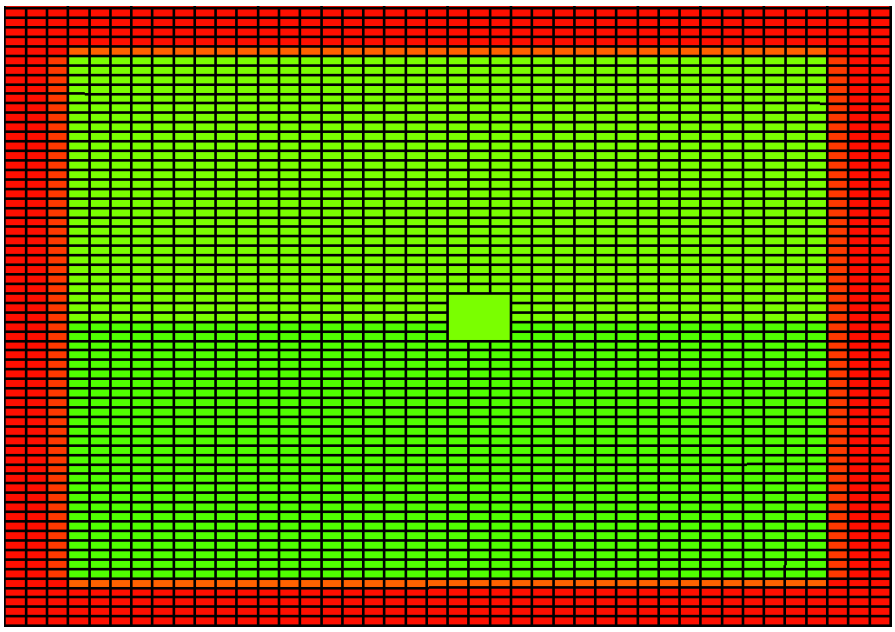

Water saturation inside fracture after 180th day

Figure 5.120: Water saturation maps (Rich condensate- Low drawdown)

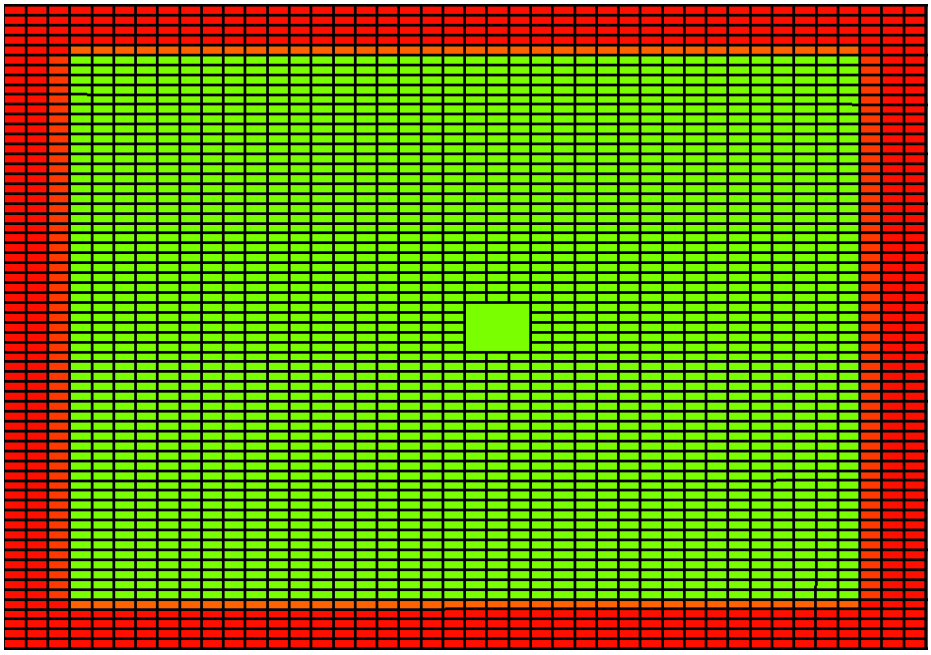

Water saturation inside fracture after 500th day (end of production)

Figure 5.120: Water saturation maps (Rich condensate- Low drawdown) - Continued

5.3.18. Rich Condensate – High Drawdown (Relative perm. Set-3)

A drawdown of 4000 psi is applied to the reservoir by applying a wellbore pressure of 2500 psi. This is the peak liquid drop out pressure for the rich condensate as mentioned earlier. The cleanup corresponding to Set-3 relative permeability curves is shown below. The frac-water cleanup is much faster and better than previous cases. This is due to higher drawdown as well as higher end point water relative permeability is Set-3. On the contrary, higher drawdown leads to higher condensate drop out and loading within the fracture.

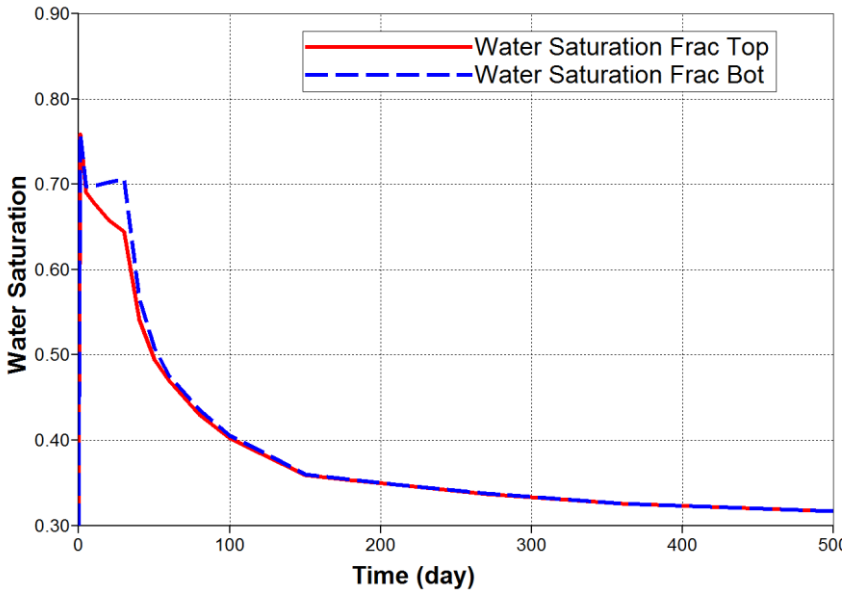

Figure 5.121: Variation of water saturation inside fracture over time (Rich condensate- High drawdown)

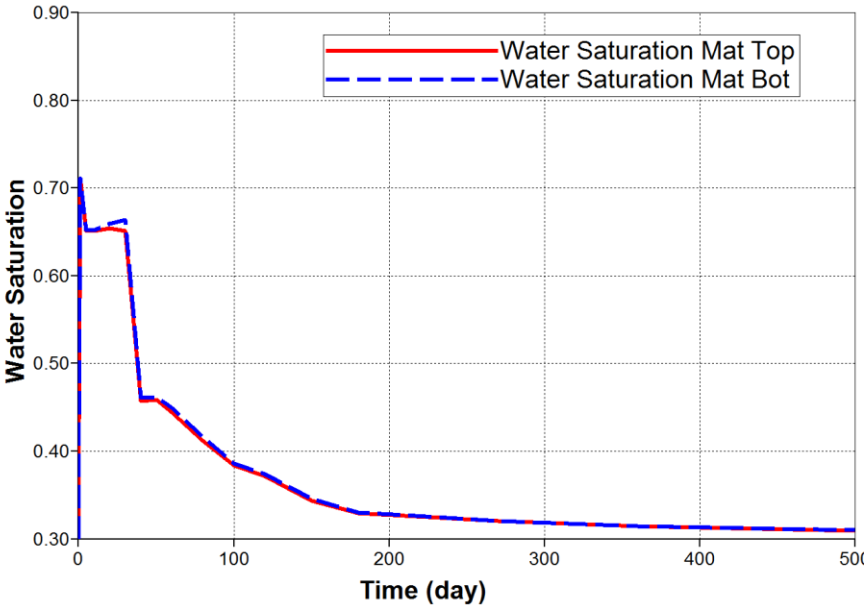

Figure 5.122: Variation of water saturation inside matrix 0.1 ft. from fracture face with time (Rich condensate- High drawdown)

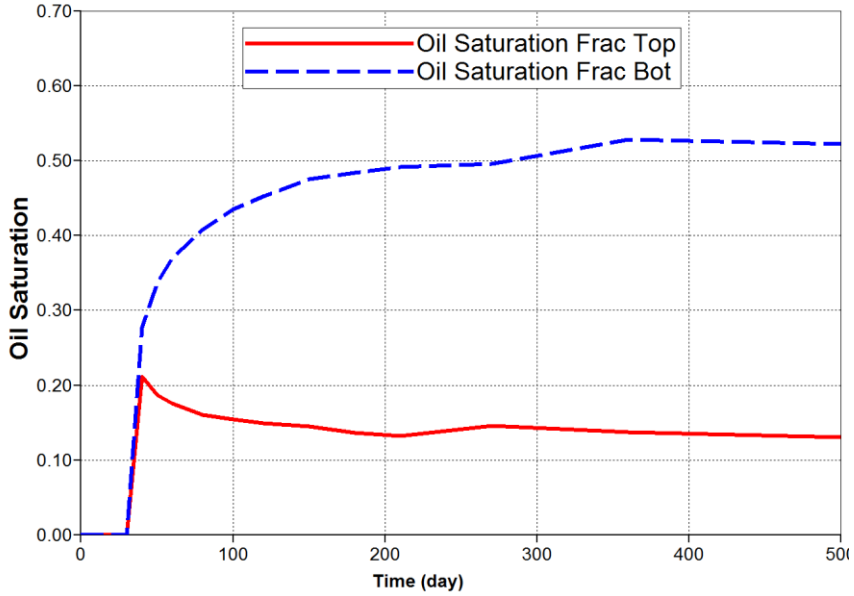

Figure 5.123: Variation of oil saturation inside fracture over time
(Rich condensate- High drawdown)

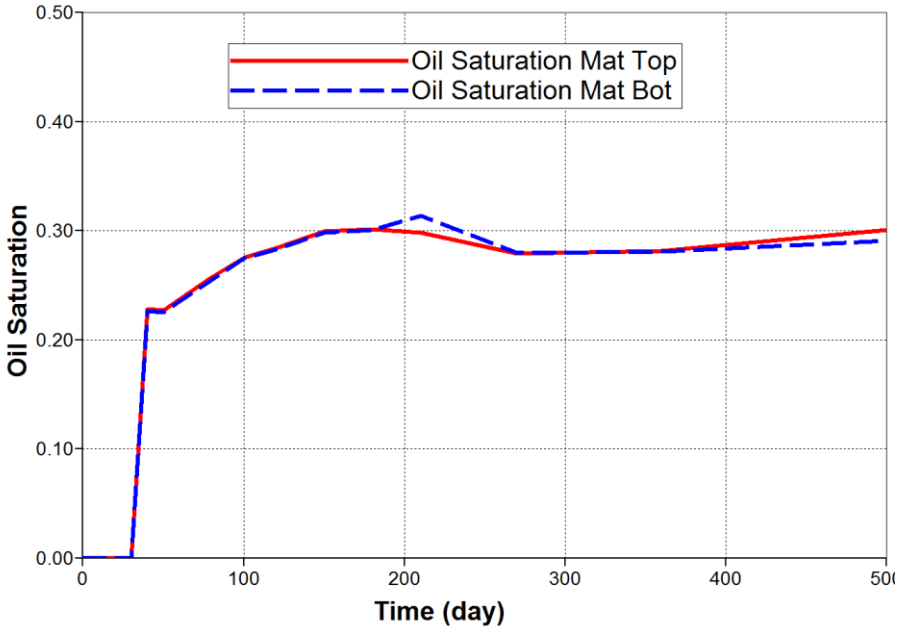

Figure 5.124: Variation of oil saturation inside matrix 0.1 ft. from fracture face with time
(Rich condensate- High drawdown)

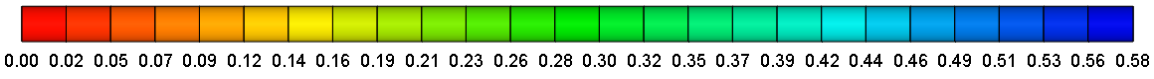

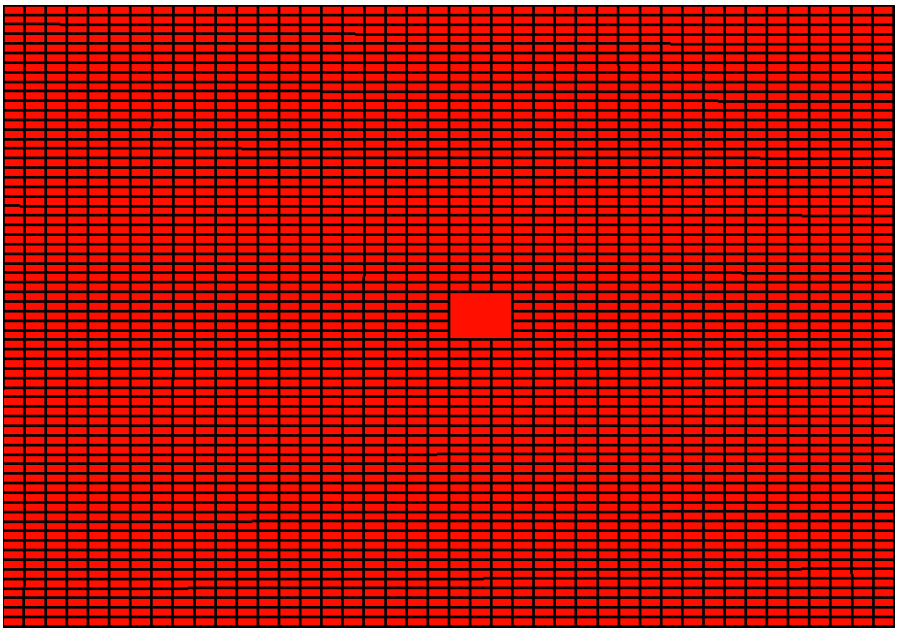

Oil saturation inside fracture after 30th day (end of shut-in)

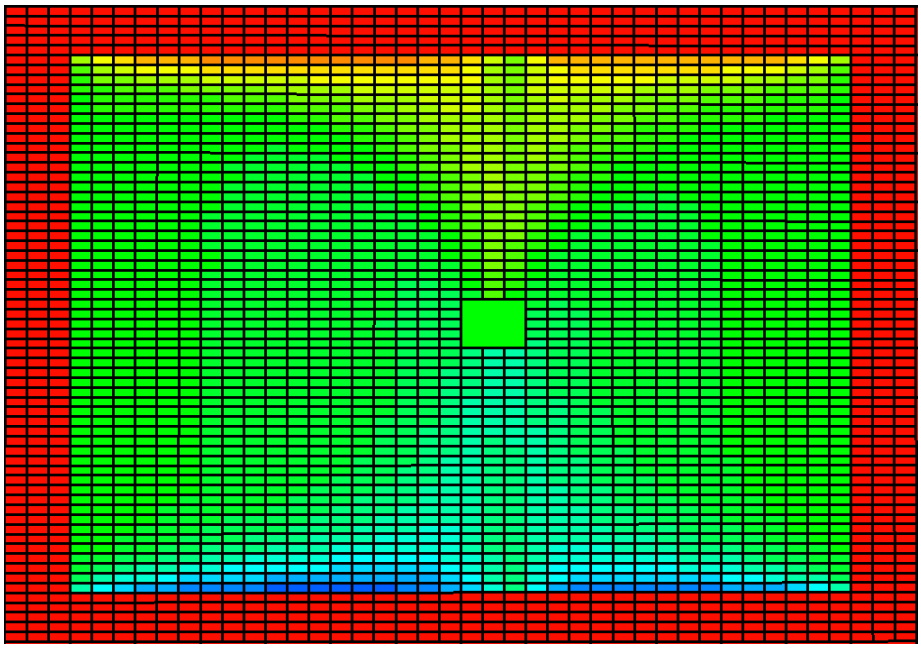

Oil saturation inside fracture after 120th day

Figure 5.125: Oil saturation maps (Rich condensate- High drawdown)

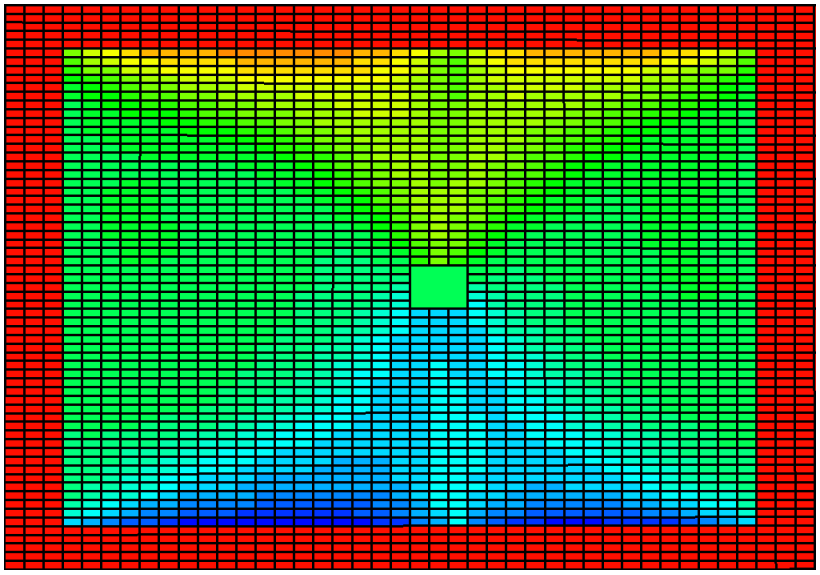

Oil saturation inside fracture after 500th day (end of production)

Figure 5.125: Oil saturation maps (Rich condensate- High drawdown) - Continued

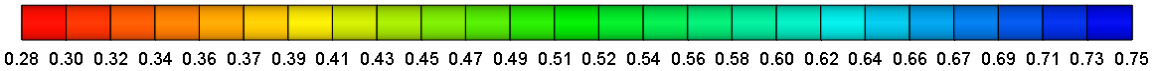

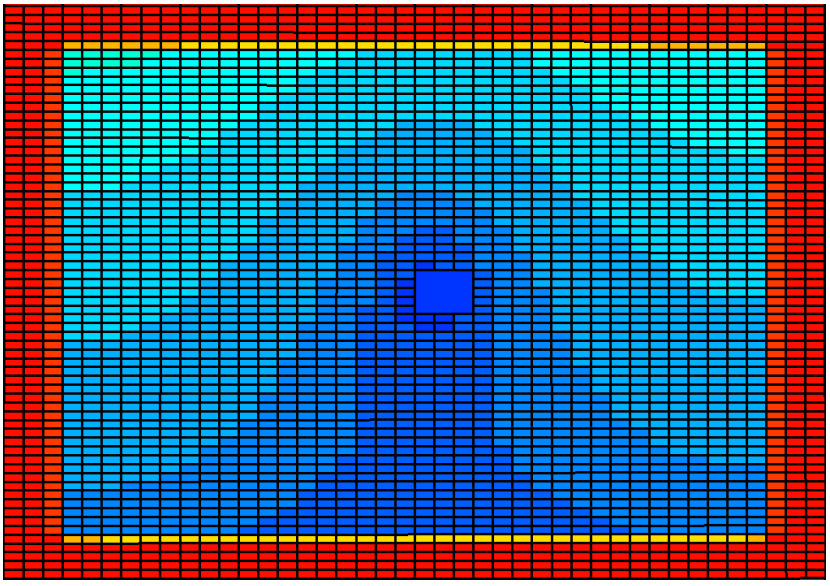

Water saturation inside fracture after 30th day (end of shut-in)

Figure 5.126: Water saturation maps (Rich condensate- High drawdown)

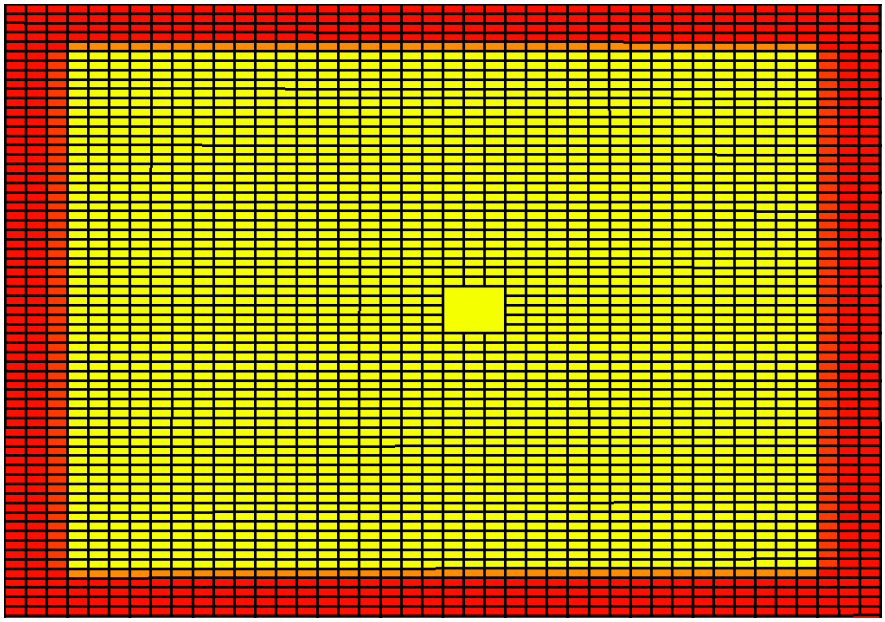

Water saturation inside fracture after 100th day

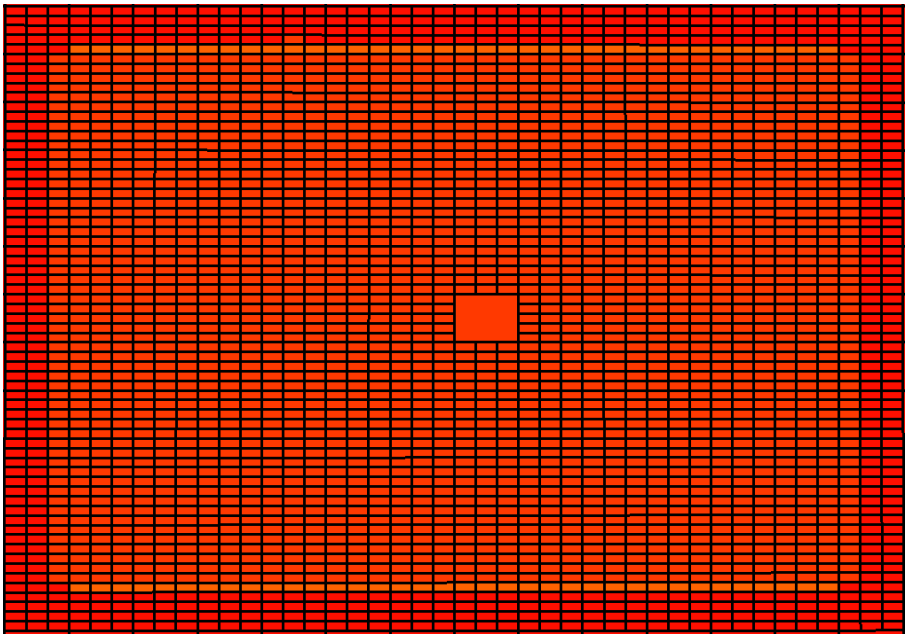

Water saturation inside fracture after 500th day (end of production)

Figure 5.126: Water saturation maps (Rich condensate- High drawdown) - Continued

5.4 DISCUSSIONS

5.4.1. Gas production from lean condensate reservoir

The cumulative gas production for lean condensate reservoirs, under different scenarios considered above is summarized in Table 5.9. It shows that going from Set-1 to Set-3 under similar drawdown conditions improves the cumulative gas production. This is because water cleanup improves leading to increase in gas productivity.

Rel perm set Simulation case	Relative permeability Set-1	Relative permeability Set-2	Relative permeability Set-3
Low drawdown (P_{wf} = 5500 psi)	9.3	9.12	9.65
Base case (P_{wf} = 4000 psi)	21.84	22.24	23.04
High drawdown (P_{wf} = 3000 psi)	32.75	31.52	32.84

Table 5.9: Cumulative gas production (MMscf) for lean condensate reservoir under different drawdown and relative permeability scenarios

Rel perm set Simulation case	Relative permeability Set-1	Relative permeability Set-2	Relative permeability Set-3
Low drawdown (P_{wf} = 5500 psi)	0	0	0
Base case (P_{wf} = 4000 psi)	3.9	3.8	1.7
High drawdown (P_{wf} = 3000 psi)	3	7.4	1.8

Table 5.10: Cumulative oil (condensate) production (Reservoir Barrels) for lean condensate reservoir under different drawdown and relative permeability scenarios

Cumulative oil (condensate recovery) at reservoir conditions is summarized in Table 5.10. As expected, when the wellbore pressure is greater than dew point no condensate is produced since there is no drop out. However, for relative permeability Set-1 reservoir, even with maximum drawdown the cumulative oil production is lower than Set-2 reservoir. Early time gas productivity variation for different relative permeability sets is plotted below in Figures 5.127-5.129. It shows that application of higher drawdown doesn't necessarily lead to higher initial gas productivity. But it impacts the fluid cleanup as seen in results from previous sections. As expected, lower drawdown leads to delayed and lower peak gas productivity. This trend is observed for all the three relative permeability sets. As liquid drop out is very low for lean condensate reservoirs, frac-water cleanup and productivity are not impacted by the condensate drop-out. Both of them are primarily dependent on the drawdown applied and therefore, the results obtained here are very similar to the ones observed for dry gas simulations.

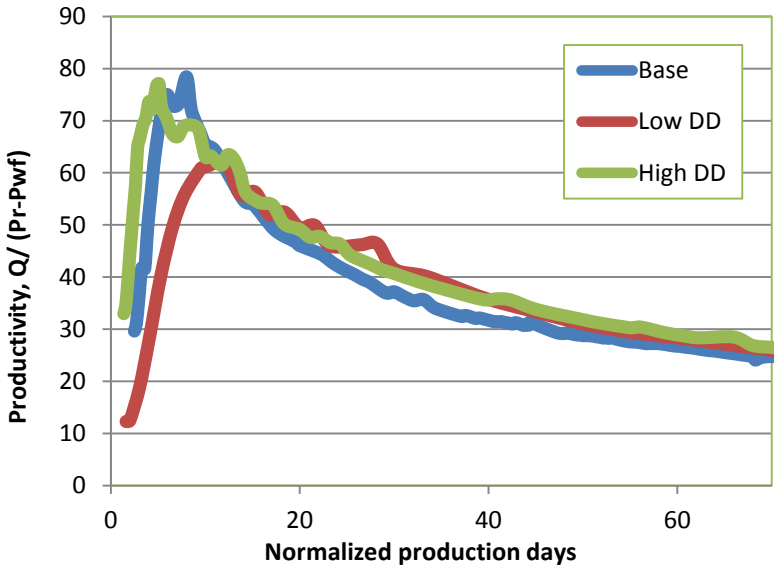

Figure 5.127: Gas productivity variation under different drawdown (Lean condensate – Set 1)

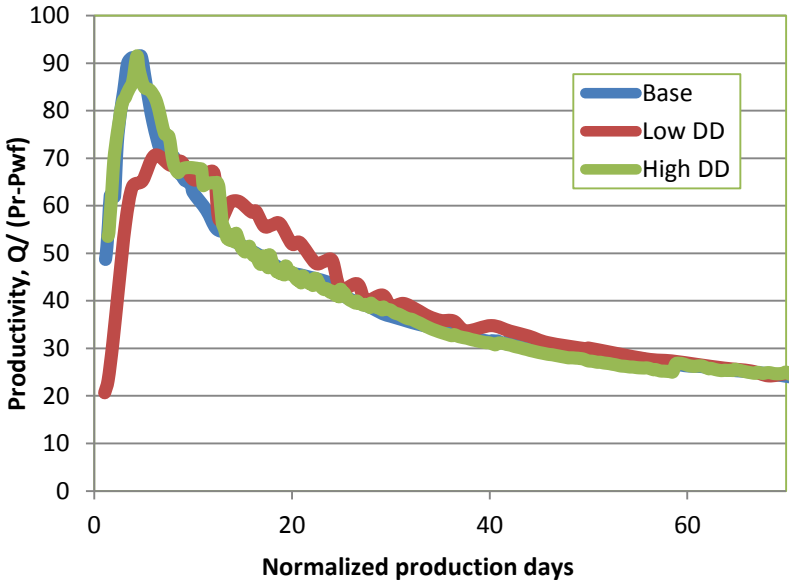

Figure 5.128: Gas productivity variation under different drawdown (Lean condensate – Set 2)

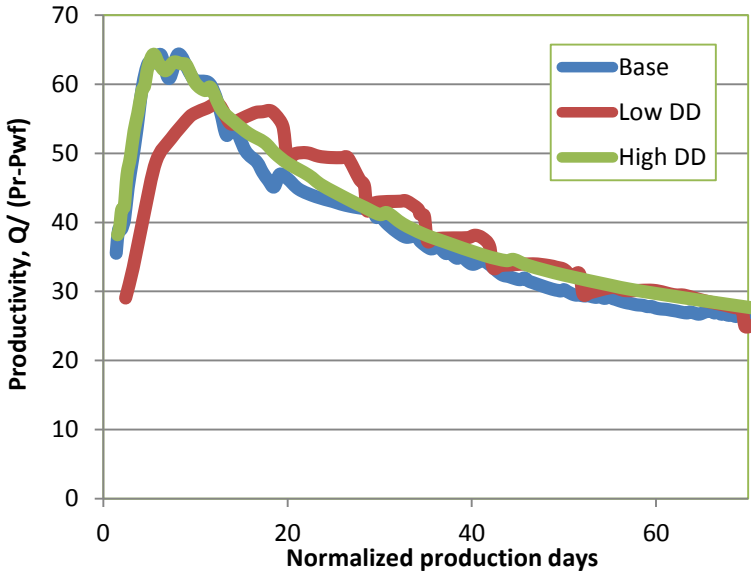

Figure 5.129: Gas productivity variation under different drawdown (Lean condensate – Set 3)

5.4.2. Gas production from rich condensate reservoir

The cumulative gas production for rich condensate reservoirs under different scenarios considered above is summarized in Table 5.11.

Rel perm set Simulation case	Relative permeability Set-1	Relative permeability Set-2	Relative permeability Set-3
Low drawdown (P_{wf} = 5500 psi)	3.06	3.21	3.28
Base case (P_{wf} = 3000 psi)	9.95	10.13	9.78
High drawdown (P_{wf} = 2500 psi)	11.9	11.51	11.33

Table 5.11: Cumulative gas production (MMscf) for rich condensate reservoir under different drawdown and relative permeability scenarios

It is interesting to note that for the rich condensate reservoir cumulative gas recoveries are significantly lower than for the lean condensate reservoir. (Table 5.9) This is attributed to higher gas relative permeability impairment due to higher condensate saturation. The cumulative condensate recovery at reservoir conditions for different scenarios is shown in Table 5.12. As expected higher drawdown leads to higher condensate drop-out and production. Gas productivity variation in early time is shown in Figures 5.130-5.132. For Sets 1 & 3 lower drawdown led to lower and delayed peak productivity. However, for Set 2 the peak productivity was approximately the same for all three drawdown conditions indicating that liquid blocking had more impact on gas productivity in this set.

Rel perm set Simulation case	Relative permeability Set-1	Relative permeability Set-2	Relative permeability Set-3
Low drawdown (P_{wf} = 5500 psi)	0	0	0
Base case (P_{wf} = 3000 psi)	7901.54	7417.85	8165.74
High drawdown (P_{wf} = 2500 psi)	9822.56	9575.05	9484.6

Table 5.12: Cumulative oil (condensate) production (Reservoir Barrels) for rich condensate reservoir under different drawdown and relative permeability scenarios

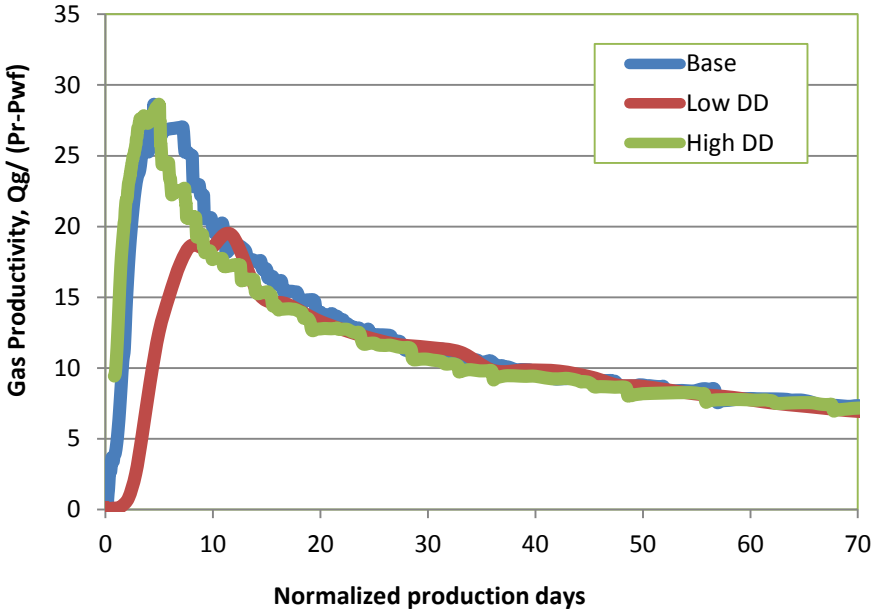

Figure 5.130: Gas productivity variation under different drawdown (Rich condensate – Set 1)

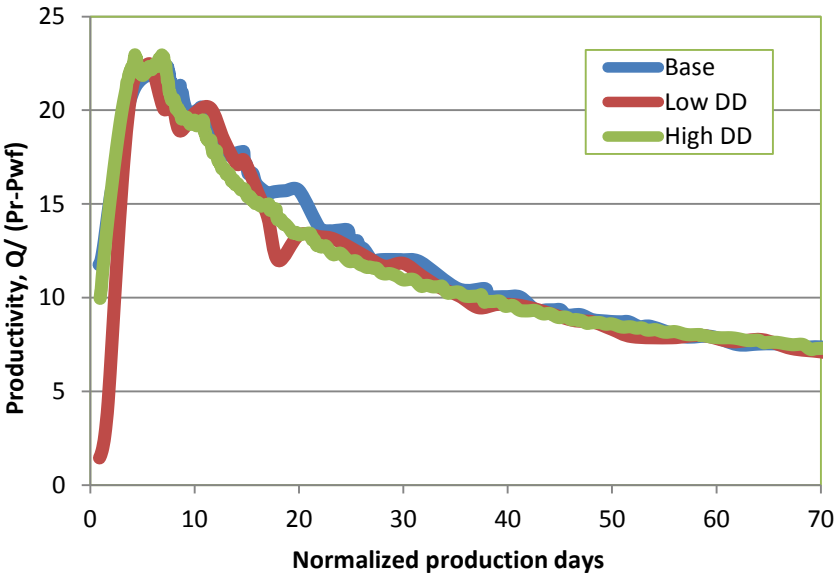

Figure 5.131: Gas productivity variation under different drawdown (Rich condensate – Set 2)

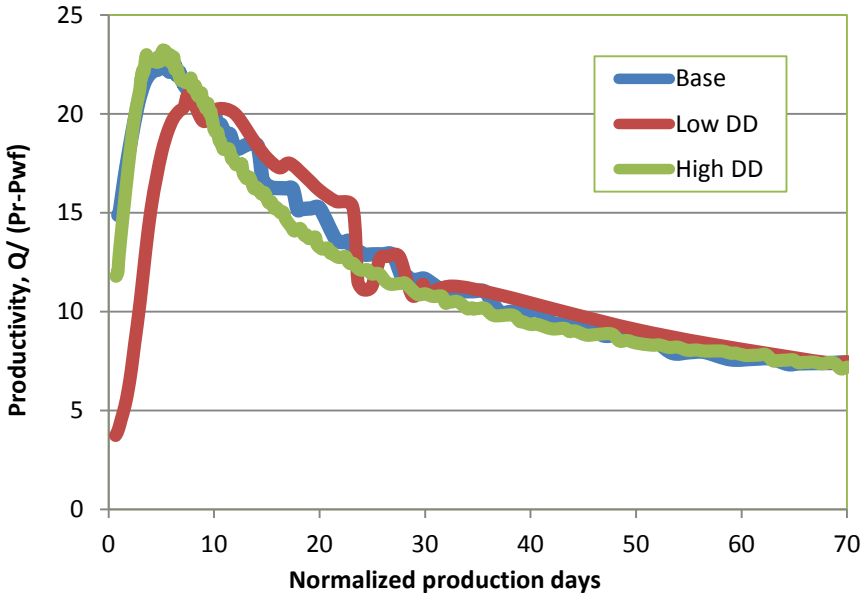

Figure 5.132: Gas productivity variation under different drawdown (Rich condensate – Set 3)

The oil saturation maps for the rich condensate reservoirs show that even after 500th day of production there is considerable condensate saturation within the fracture and more so towards the bottom of the fracture. This oil can't be imbibed by the matrix and has to be cleaned only through displacement.

This simulation study shows that for rich gas reservoirs the condensate has a tendency to load within the fracture and thereby, reduce gas relative permeability. This explains why cumulative gas recovery for rich condensate reservoirs was lower than for lean condensate reservoirs under similar drawdown conditions.

5.4.3. Frac-water cleanup in presence of condensate

CMG GEM 2011 doesn't provide the option to calculate the amount of water recovered in vapor phase after an Oil-Gas-Water flash. So an indirect approach is adopted to study the extent of cleanup in each scenario. Tables 5.13 and 5.14 below shows the post-500 day water and oil saturation values for each of the scenarios investigated above. The amount of residual water saturation both within the fracture and on fracture face in the matrix is indicative of the cleanup achieved. As can be seen, higher drawdown leads to lower water saturation within the fracture and in matrix near fracture. Also, Set-3 relative permeability curves enhance frac-water cleanup since water mobility is higher. For lean condensates, as long as oil saturation is below residual, the phase is immobile but saturation keeps rising. For the rich condensate reservoir, three phase flow is observed within the fracture and in the matrix. Flowing gas is displacing both water and oil in this scenario. Depending on the relative permeabilities of the aqueous and oil phase,

one or both of the phases might load inside the fracture. It was observed that presence of condensate phase somewhat improves frac water cleanup. Similar results were reported by Jamiolahmady et al. (2007) in their study. This could be attributed to the fact that condensate being a denser phase than gas, will provide a better displacement of frac water. On the other hand, presence of additional liquid saturation (oil and water instead of just water) further reduces gas relative permeability. This may lead to not only lower cumulative gas recovery but also increased condensate trapping within and around the fracture owing to the lower gas velocity.

		Frac Top Water Saturation	Frac Bot Water Saturation	Mat Top Water Saturation	Mat Bot Water Saturation	Frac Top Oil Saturation	Frac Bot Oil Saturation	Mat Top Oil Saturation	Mat Bot Oil Saturation
Set-1	Low DD	0.52	0.54	0.51	0.53	0	0	0	0
	Base	0.42	0.42	0.43	0.43	0.034	0.034	0.11	0.11
	High DD	0.37	0.37	0.39	0.39	0.128	0.13	0.23	0.23
Set-2	Low DD	0.53	0.55	0.52	0.54	0	0	0	0
	Base	0.4	0.4	0.4	0.4	0.033	0.033	0.078	0.078
	High DD	0.4	0.4	0.4	0.4	0.066	0.066	0.14	0.14
Set-3	Low DD	0.48	0.48	0.48	0.48	0	0	0	0
	Base	0.36	0.36	0.38	0.38	0.017	0.017	0.07	0.07
	High DD	0.3	0.3	0.33	0.33	0.025	0.024	0.17	0.17

Table 5.13: Water and oil saturations at top and bottom, within fracture and matrix, for Lean condensate

		Frac Top Water Saturation	Frac Bot Water Saturation	Mat Top Water Saturation	Mat Bot Water Saturation	Frac Top Oil Saturation	Frac Bot Oil Saturation	Mat Top Oil Saturation	Mat Bot Oil Saturation
Set-1	Low DD	0.49	0.51	0.49	0.50	0	0	0	0
	Base	0.37	0.37	0.36	0.36	0.15	0.50	0.29	0.29
	High DD	0.42	0.43	0.4	0.42	0.14	0.38	0.24	0.25
Set-2	Low DD	0.49	0.51	0.49	0.5	0	0	0	0
	Base	0.40	0.40	0.39	0.39	0.14	0.48	0.27	0.27
	High DD	0.34	0.34	0.32	0.32	0.14	0.48	0.28	0.28
Set-3	Low DD	0.45	0.46	0.44	0.45	0	0	0	0
	Base	0.34	0.34	0.32	0.32	0.15	0.53	0.31	0.31
	High DD	0.32	0.32	0.31	0.31	0.13	0.52	0.29	0.3

Table 5.14: Water and oil saturations at top and bottom, within fracture and matrix, for Rich condensate

5.5 SUMMARY

This chapter has looked at the impact of frac-fluid flowback from condensate rich gas reservoirs, both lean and rich. Three different water relative permeability sets, along with three different drawdown scenarios were simulated to study the cleanup effectiveness. Impact on gas production was also quantified. Following were the primary observations:

- Lean gas production is not significantly impacted due to condensate drop out.
- For rich condensate system, oil saturation in the fracture and the matrix reduces gas relative permeability.
- Frac-water cleanup is improved in presence of condensate.
- Clean-up of frac-water is uniform at top and bottom of the fracture. However, even after 500^{th} day of production there is mobile water saturation inside the fracture.
- Clean-up of condensate below dew point pressure is non-uniform and leads to condensate loading at fracture bottom.
- Higher water mobility relative permeability set (Set-3) shows faster frac-water cleanup.
- Cumulative gas recovery for rich condensate system is much lower than lean condensate under similar drawdown scenarios. This can be attributed to relative permeability damage due to condensate drop out.
- For rich condensate reservoirs, higher drawdown may not significantly improve cumulative gas production. This is because higher oil saturation reduces gas relative permeability.

Chapter 6: Summary, Conclusion and Recommendations

6.1 SUMMARY

This study investigated the possibility of liquid loading within hydraulic fractures in tight unconventional gas reservoirs. 3D, black oil and compositional simulation scenarios were tested to understand the impact of various mechanisms in operation. The hypothesis of frac-fluid/condensate retention at the fracture bottom was analyzed by replicating the fluid injection and flowback process through a single, lateral, bi-wing fracture in a horizontal wellbore. The impact of liquid loading on gas production was also quantified.

Black oil simulations using CMG's IMEX 2011 simulator were used for sensitivity analysis. The effect of matrix permeability, fracture permeability, fracture height, drawdown applied and shut-in period before flowback, on liquid loading within fracture was studied. This was followed by compositional simulations using CMG GEM for simulating liquid flowback from dry gas reservoirs. The effect of evaporative cleanup of water and velocity dependent relative permeability was investigated.

Lastly, frac-water cleanup from a gas condensate reservoir was studied for both lean and rich gas systems. Impact of water end point relative permeability and bottom hole wellbore pressure (above or below dew point) on liquid loading was demonstrated. In the case of gas condensates, the realistic possibility of condensate loading within fracture was highlighted. It was also shown that condensate drop out impacts gas production severely.

6.2 CONCLUSIONS

The following conclusions can be drawn from this study:

- Bottom hole wellbore pressure during flowback is an important control on the amount of frac-water loading within the fracture and therefore on the gas productivity.
- Extremely low matrix permeabilities (< 1 μD) can face significant liquid retention within fracture.
- High fracture conductivities can improve cleanup in the upper section of the fracture but gravity can overpower viscous forces, leading to liquid loading at fracture bottom.
- Shutting the well for a long duration after fracturing operation and before flowback, didn't show significant long term performance gains, as reported in certain shale gas field studies. Other mechanisms not captured in these simulations maybe responsible for this observation.
- Evaporative cleanup of water from the fracture face can enhance the amount of frac-water recovery. However, it is dependent on the amount of gas flow. Therefore, for a nano-Darcy reservoir under limited drawdown, the effect of evaporative cleanup might not be significant until after a couple of years.
- Velocity dependent relative permeability impacts the fracture and matrix water saturation during frac-water injection as well as immediately after flowback. The long term impact of using this model is minimal, considering the low steady state flow velocities (low capillary number) in tight reservoirs.
- Relative permeability set with higher water mobility allowed better frac-water cleanup as compared to low water mobility set.
- Higher drawdown led to better frac-water cleanup for lean condensate reservoir.

- For rich condensates, higher drawdown (P_{wf} below P_{dew}) may not necessarily lead to proportionately higher gas recovery. This is due to increased oil saturation in fracture and in matrix, which impacts the gas relative permeability adversely.
- Under similar drawdown conditions and reservoir properties, cumulative gas recovery was higher for lean condensate system in comparison with rich condensate system.

6.3 RECOMMENDATIONS

- Efficient vertical placement of the lateral in the pay zone may help reduce the impact of liquid loading.
- For dry gas reservoirs an optimal drawdown should be used to maximize liquid recovery yet minimize proppant flowback and embedment.
- Efficient proppant placement techniques must be adopted to minimize the impact of liquid loading in bottom portion of the fracture.
- Use of surfactants or other wettability modifiers in the pad fluid can help in the cleanup of frac-fluid.
- Use of non-aqueous fracturing fluids maybe considered under specific conditions such as low pressure reservoirs.
- More realistic, experimental values for rock wettability and capillary pressures can be investigated in the future.
- Effect of relative permeabilities hysteresis can be modeled for more accurate modeling of drainage and imbibition processes.
- Presence of natural fracture network can further exacerbate low frac-water recovery problem. Impact of dense or sparse fracture networks on liquid recovery should be modeled in the future.

APPENDICES

A1. SAMPLE INPUT FILE: BLACK OIL MODEL

```
RESULTS SIMULATOR IMEX 201110

INUNIT FIELD
WSRF WELL 1
WSRF GRID TIME
WSRF SECTOR TIME
OUTSRF WELL LAYER NONE
OUTSRF RES ALL
OUTSRF GRID SO SG SW PRES OILPOT BPP SSPRES WINFLUX
** WPRN GRID 0
OUTPRN GRID NONE
OUTPRN RES NONE

**$  Distance units: ft
RESULTS XOFFSET         0.0000
RESULTS YOFFSET         0.0000
RESULTS ROTATION         0.0000  **$  (DEGREES)
RESULTS AXES-DIRECTIONS 1.0 -1.0 1.0



**$ ************************************************************************
**$ Definition of fundamental cartesian grid
**$ ************************************************************************

GRID VARI 46 16 20
KDIR DOWN

DI IVAR
 52.22 38.6 28.53 21.09 15.59 11.52 8.52 6.3 4.65 3.44 2.54 1.88 1.39 1.03 0.76 0.56 0.41 0.31 0.23 0.17
0.12 0.09 0.05
 0.05 0.09 .12 .17 .23 .31 .41 .56 .76 1.03 1.39 1.88 2.54 3.44 4.65 6.3 8.52 11.52 15.59 21.09 28.53 38.6
52.22

DJ CON 25

DK CON 5

DTOP
 736*9960

**$ Property: Net Pay (ft)   Max: 10  Min: 10
```

```
NETPAY CON          10
**$ Property: NULL Blocks  Max: 1  Min: 1
**$  0 = null block, 1 = active block
NULL CON          1

**$ Property: Porosity  Max: 0.2  Min: 0.2
*POR  *IJK 1:46 1:16 1:20 0.1
          23:24 2:15 5:15 0.6    ** fracture porosity

**$ Property: Permeability I (md)
PERMI CON       1000E-006
*MOD 23:24 2:15 5:15 = 2000        ** fracture permeability

**$ Property: Permeability J (md)
PERMJ EQUALSI

**$ Property: Permeability K (md)
PERMK EQUALSI * 0.1


PINCHOUTARRAY CON          1
CPOR 4e-6
MODEL GASWATER
TRES 150

PVTG EG 1

**$        p        Eg       visg
      14.696   4.43757  0.0180751
     280.383   84.5546  0.0180772
      546.07   164.367  0.0180803
     811.757   243.736  0.0180839
     1077.44   322.532   0.018088
     1343.13   400.633  0.0180923
     1608.82   477.929   0.018097
      1874.5   554.322  0.0181018
     2140.19   629.726  0.0181068
     2405.88   704.066  0.0181119
     2671.57   777.283  0.0181172
     2937.25   849.327  0.0181225
     3202.94   920.158  0.0181279
     3468.63    989.75  0.0181334
     3734.31   1058.08  0.0181389
        4000   1125.15  0.0181444

GRAVITY GAS 0.2
REFPW 14.696
DENSITY WATER 60.5501
BWI 1.03776
CW 3.3202e-006
VWI 0.319053
CVW 0.0
```

```
ROCKFLUID

*JFUNC
*SRFTNW *CON  40

RPT 1

**$        Sw           krw      Pcgw
SWT
         0.2             0        4
        0.25  1.52588e-005       1.5
         0.3   0.000124141       0.8
        0.35    0.00063596       0.5
         0.4    0.00190625       0.4
        0.45    0.00483674      0.33
         0.5     0.0097754      0.28
        0.55     0.0186364      0.24
         0.6        0.0425      0.21
        0.65      0.090113      0.19
         0.7      0.152588      0.18
           1             1      0.16

**$        Sl           krg

SLT
         0.2         0.8
       0.2375    0.652476
        0.275    0.526182
       0.3125    0.415806
         0.35    0.316406
       0.3875    0.223404
        0.425    0.152588
       0.4625    0.100113
         0.5      0.0625
       0.5375   0.0366364
        0.575   0.0197754
       0.6125  0.00953674
         0.65  0.00390625
       0.6875  0.00123596
         0.70           0

RPT 2

**$        Sw       krw      Pcgw
SWT
         0.2        0        4
        0.25       0.03      1.5
         0.3       0.06      0.8
        0.35       0.09      0.5
         0.4       0.12      0.4
        0.45       0.15      0.33
```

```
        0.5       0.18      0.28
       0.55       0.21      0.24
        0.6       0.24      0.21
       0.65       0.27      0.19
        0.7        0.3      0.18
          1          1      0.16

**$       Sl      krg
SLT
       0.2       0.8
      0.70         0


*RTYPE  *IJK
  1:46  1:16 1:20  1
  23:24 2:15 5:15  2

SWCRIT CON          0.2

INITIAL

*VERTICAL *BLOCK_CENTER *WATER_GAS

REFDEPTH 10000
REFPRES 6500
DWGC 30000            ** Depth of water gas contact

NUMERICAL

*MAXSTEPS 100000
*NCUTS 100
*DTMIN 0.0000001

RUN
DATE 2012 1 1

**$
WELL  'Well-1'
INJECTOR 'Well-1'
INCOMP  WATER
OPERATE  STW  1000  CONT
**$ UBA    ff  Status  Connection
**$              rad  geofac  wfrac  skin
GEOMETRY  I  0.25  0.37  1.  0.
PERF  GEOA  'Well-1'
**$ UBA      ff  Status  Connection
   23 8 10  1.  OPEN    FLOW-FROM  'SURFACE'  REFLAYER
   24 8 10  1.  OPEN    FLOW-FROM  1
OPEN 'Well-1'
WELL  'Well-2'
PRODUCER 'Well-2'
```

```
OPERATE  MIN  BHP  4500.  CONT
**$ UBA    ff  Status  Connection
**$              rad  geofac  wfrac  skin
GEOMETRY  I  0.25  0.37  1.  0.
PERF  GEOA  'Well-2'
**$ UBA      ff  Status  Connection
   23 8 10  1.  OPEN    FLOW-TO  'SURFACE'  REFLAYER
   24 8 10  1.  OPEN    FLOW-TO  1
SHUTIN 'Well-2'

TIME 1                        ** 1 day injection

SHUTIN 'Well-1'               ** Shut-in well after injection

TIME 30
OPEN 'Well-2'                 ** Open producer after 30th day
TIME 40
TIME 50
TIME 60
TIME 80
TIME 100
TIME 120
TIME 150
TIME 180
TIME 210
TIME 270
TIME 360
TIME 500

STOP
```

A2. SAMPLE INPUT FILE: COMPOSITIONAL MODEL OF DRY GAS-WATER SYSTEM (INCLUDING VELOCITY DEPENDENT RELATIVE PERMEABILITY AND WATER EVAPORATION MODELS)

```
RESULTS SIMULATOR GEM 201110

INUNIT FIELD
WSRF WELL 1
WSRF GRID TIME
OUTSRF WELL YWEL 'H2O' 'Well-2'
OUTSRF GRID SO SG SW PRES W 'H2O' Y 'H2O'
OUTSRF RES
WPRN GRID 0
OUTPRN GRID NONE
OUTPRN RES NONE
**$  Distance units: ft
RESULTS XOFFSET          0.0000
RESULTS YOFFSET          0.0000
RESULTS ROTATION         0.0000  **$  (DEGREES)
RESULTS AXES-DIRECTIONS 1.0 -1.0 1.0
**$ *************************************************************************
**$ Definition of fundamental cartesian grid
**$ *************************************************************************

GRID VARI 50 20 20
KDIR DOWN

DI IVAR
 250 150 52.22 38.6 28.53 21.09 15.59 11.52 8.52 6.3 4.65 3.44 2.54 1.88 1.39 1.03 0.76 0.56 0.41 0.31 0.23 0.17 0.12
0.09 0.05
 0.05 0.09 .12 .17 .23 .31 .41 .56 .76 1.03 1.39 1.88 2.54 3.44 4.65 6.3 8.52 11.52 15.59 21.09 28.53 38.6 52.22 150 250

DJ JVAR 300 100 100 14*40 100 100 300

DK CON 5

** FINE GRIDDING THE FRACTURE VOLUME

*REFINE 25:26 4:7 4:9 *INTO 1 1 10
*REFINE 25:26 4:7 11:16 *INTO 1 1 10
*REFINE 25:26 14:17 4:9 *INTO 1 1 10
*REFINE 25:26 14:17 11:16 *INTO 1 1 10
*REFINE 25:26 4:7 10 *INTO 1 1 10
*REFINE 25:26 14:17 10 *INTO 1 1 10

DTOP
 1000*7960

**$ Property: Net Pay (ft)   Max: 10  Min: 10
NETPAY CON           10
**$ Property: NULL Blocks  Max: 1  Min: 1
**$  0 = null block, 1 = active block
NULL CON           1
**$ Property: Porosity  Max: 0.2  Min: 0.2

*POR  *IJK 1:50 1:20 1:20 0.1
```

```
        25:26 5:16 5:15 0.6    ** fracture porosity

**$ Property: Permeability I (md)
PERMI CON       0.0001
*MOD 25:26 5:16 5:15 = 2000        ** fracture permeability

**$ Property: Permeability J (md)
PERMJ EQUALSI

**$ Property: Permeability K (md)
PERMK EQUALSI * 0.1

PINCHOUTARRAY CON           1
CPOR 4e-6

**$ Model and number of components
*MODEL PR
*NC 2 2

 *COMPNAME
 'CH4'  'H2O'

 *HCFLAG
 1  2

 *PCRIT
 45.4  217.6

 *TCRIT
 190.6  647.3

 *AC
 0.008  0.344

 *MW
 16.043  18.015

 *VSHIFT
 -0.153860496  -0.14966408

 *VCRIT
 0.099  0.056

 *VISVC
 0.099  0.056

 *OMEGA
 0.4572355289  0.4572355289

 *OMEGB
 0.0777960739  0.0777960739

 *SG
 0.3  1.0

 *TB
 -258.61  212.0
```

```
*PCHOR
77.0  52.0
*HEATING_VALUES
844.2900105  0.0

*VISCOR   *HZYT
*MIXVC   1.0

*VISCOEFF
0.1023  0.023364  0.058533  -0.040758  0.0093324

*PVC3    1.2

*BIN
0.4907

** Using Water Evaporation model

H2O_INCLUDED
PHASEID GAS
TRES 300
DENW 60
VISW 0.3049
OGW_FLASH ON

**$ Property: EOS Set Number  Max: 1  Min: 1
EOSTYPE CON           1

ROCKFLUID

*JFUNC
*SRFTNW *CON  40


RPT 1
**$       Sw          krw         krow      Pcow
SWT
            0.3                  0                  0.7                4

            0.33125              1.22E-05           0.540733           1.5

            0.39375              0.001              0.305064           0.8

            0.45625              0.008              0.156383           0.5

            0.51875              0.0293091          0.070079           0.3

            0.58125              0.08               0.0256454          0.22

            0.64375              0.14               0.00667572         0.2

            0.70625              0.24               0.000865173        0.185

            0.76875              0.37               1.07E-05           0.16

            0.8                  0.45               0                  0.15
```

```
**$       Sl                    krg                        krog
SLT
           0.3                   1                          0
          0.33125               0.586182          0.000170898
          0.39375               0.316406          0.00273437
          0.45625               0.152588          0.0138428
          0.51875               0.0625            0.04375
          0.58125               0.0197754         0.106812
          0.64375               0.00390625        0.221484
          0.70625               0.001             0.410327
          0.76875               0.000244141       0.6
          0.8                   0                 0.7

RPT 2
**$       Sw      krw     krow     Pcow
SWT
           0.3      0        0.8       4
          0.3625   0.0875   0.7       1.2
          0.425    0.175    0.6       0.7
          0.4875   0.2625   0.5       0.4
          0.55     0.35     0.4       0.27
          0.6125   0.4375   0.3       0.21
          0.675    0.525    0.2       0.19
          0.7375   0.6125   0.1       0.175
          0.8      0.7      0         0.15

**$       Sl      krg     krog
SLT
       0.3      0.9       0
       0.8       0      0.8

*RTYPE  *IJK
 1:50  1:16 1:20  1
 25:26 5:16 5:15  2


**Using Velocity Dependent Rel Perm model
*VELDEPRP *MODEL1
*GAS 24556. 0.  1.0 0. 1. 4.00
```

```
*CONDENSATE 3000. 0.  1.0 0. 1. 2.9
*WATER 250. 0. 1.0 0. 1. 1.0
INITIAL

VERTICAL BLOCK_CENTER WATER_GAS

REFPRES
 6500

REFDEPTH
  8000

DWGC
   15000

*SWINIT *CON 0.3

*ZGAS 0.7 0.3

NUMERICAL
*MAXSTEPS 100000000
*DTMIN 0.0000000000000001
*MODILU *ON


RUN
DATE 2011  1 1

WELL  'Well-1'
INJECTOR 'Well-1'
INCOMP  WATER
OPERATE  STW  1000  CONT
**$ UBA    ff  Status  Connection
**$         rad  geofac  wfrac  skin
GEOMETRY  I  0.25  0.37  1.  0.
PERF  GEOA  'Well-1'
**$ UBA      ff  Status  Connection
   25 10 10  1.  OPEN    FLOW-FROM  'SURFACE'  REFLAYER
   26 10 10  1.  OPEN    FLOW-FROM  1
OPEN 'Well-1'


WELL  'Well-2'
PRODUCER 'Well-2'
OPERATE  BHP  4500.  CONT
**$ UBA    ff  Status  Connection
**$         rad  geofac  wfrac  skin
GEOMETRY  I  0.25  0.37  1.  0.
PERF  GEOA  'Well-2'
**$ UBA      ff  Status  Connection
   25 10 10  1.  OPEN    FLOW-TO  'SURFACE'  REFLAYER
   26 10 10  1.  OPEN    FLOW-TO  1
SHUTIN 'Well-2'

TIME 1                          ** 1 day injection
SHUTIN 'Well-1'
```

TIME 5
TIME 10
TIME 20
TIME 30

OPEN 'Well-2' **Producer starts after 30th day

TIME 40
TIME 50
TIME 60
TIME 80
TIME 100
TIME 120
TIME 150
TIME 180
TIME 210
TIME 270
TIME 360
TIME 500
STOP

A3. SAMPLE INPUT FILE: COMPOSITIONAL MODEL OF WET GAS-WATER SYSTEM (INCLUDING VELOCITY DEPENDENT RELATIVE PERMEABILITY AND WATER EVAPORATION MODELS)

```
RESULTS SIMULATOR GEM 201110

INUNIT FIELD
WSRF WELL 1
WSRF GRID TIME
OUTSRF GRID SO SG SW PRES W 'H2O' Y 'H2O'
OUTSRF RES
WPRN GRID 0
OUTPRN GRID NONE
OUTPRN RES NONE
**$  Distance units: ft
RESULTS XOFFSET          0.0000
RESULTS YOFFSET          0.0000
RESULTS ROTATION           0.0000  **$  (DEGREES)
RESULTS AXES-DIRECTIONS 1.0 -1.0 1.0
**$ *************************************************************************
**$ Definition of fundamental cartesian grid
**$ *************************************************************************

GRID VARI 50 20 20
KDIR DOWN

DI IVAR
 250 150 52.22 38.6 28.53 21.09 15.59 11.52 8.52 6.3 4.65 3.44 2.54 1.88 1.39 1.03 0.76 0.56 0.41 0.31 0.23 0.17 0.12
0.09 0.05
 0.05 0.09 .12 .17 .23 .31 .41 .56 .76 1.03 1.39 1.88 2.54 3.44 4.65 6.3 8.52 11.52 15.59 21.09 28.53 38.6 52.22 150 250

DJ JVAR 300 100 100 14*40 100 100 300

DK CON 5

** LOCAL GRID REFINEMENT WITHIN FRACTURE AND AT FRACTURE-MATRIX INTERFACE

*REFINE 24:27 4:17 4:9 *INTO 1 3 5
*REFINE 24:27 4:17 11:16 *INTO 1 3 5
*REFINE 24:27 4:9 10 *INTO 1 3 5
*REFINE 24:27 11:17 10 *INTO 1 3 5

DTOP
 1000*7960

**$ Property: Net Pay (ft)   Max: 10  Min: 10
NETPAY CON           10
**$ Property: NULL Blocks  Max: 1  Min: 1
**$  0 = null block, 1 = active block
NULL CON           1
**$ Property: Porosity  Max: 0.2  Min: 0.2

*POR  *IJK 1:50 1:20 1:20 0.1
         25:26 5:16 5:15 0.6    ** fracture porosity

**$ Property: Permeability I (md)
```

```
PERMI CON       0.0001
*MOD 25:26 5:16 5:15 = 2000        ** fracture permeability
**$ Property: Permeability J (md)
PERMJ EQUALSI

**$ Property: Permeability K (md)
PERMK EQUALSI * 0.1

PINCHOUTARRAY CON           1

CPOR 4e-6

**$ Model and number of components
*MODEL PR
*NC 9 9

 *COMPNAME
'N2'  'CO2'  'CH4'  'C2-3'  'C4-6'
'C7P1'  'C7P2'  'C7P3'  'H2O'

 *HCFLAG
0  3  1  1  1
1  1  1  2

 *PCRIT
33.5  72.8  45.4  45.03  34.6
19.9  14.42  8.48  217.6

 *TCRIT
126.2  304.2  190.6  337.91  461.72
508.82  814.39  1096.89  647.3

 *AC
0.04  0.225  0.008  0.1253  0.2348
0.3319  0.5931  1.0344  0.344

 *MW
28.013  44.01  16.043  35.82  69.2
109.33  210.23  424.84  18.015

 *VSHIFT
0.0  0.0  0.0  -1.0  -1.0
-1.0  -1.0  -1.0  0.0

  *VCRIT
0.0895  0.094  0.099  0.17232709  0.29625603
0.5503263  1.112666  2.1502311  0.056

 *VISVC
0.0895  0.094  0.099  0.1723270913  0.2962560372
0.5503263043  1.112666051  2.150231111  0.056

 *OMEGA
0.4572355289  0.4572355289  0.4572355289  0.4572355289  0.4572355289
0.4572355289  0.4572355289  0.4572355289  0.4572355289

 *OMEGB
0.0777960739  0.0777960739  0.0777960739  0.0777960739  0.0777960739
```

```
0.0777960739  0.0777960739  0.0777960739  0.0777960739

*SG
0.809  0.818  0.3  0.4838870093  0.6263314259
0.5982206404  0.9003389617  1.068512273  1.0

*TB
-320.35  -109.21  -258.61  -88.39549091  79.3502792
194.1782707  672.9837237  1232.409426  212.0

*PCHOR
41.0  78.0  77.0  102.3429  197.7143
312.3714  600.6571  1213.8286  52.0

 *HEATING_VALUES
0.0  0.0  844.2900105  0.0  0.0
0.0  0.0  0.0  0.0

 *VISCOR   *HZYT
*MIXVC   1.0

 *VISCOEFF
0.1023  0.023364  0.058533  -0.040758  0.0093324

 *PVC3    1.2

*BIN

0.00E+00
-0.05       0.05
-0.05       0.05        0
-0.05       0.05        0           0
-0.05       0.05        0           0           0
-0.05       0.05        0           0           0           0
-0.05       0.05        0           0           0           0           0
0.275       0.2         0.4907      0.00E+000.00E+000.00E+000.00E+000.00E+00

*CRITDELD -1

** USING WATER EVAPORATION MODEL

H2O_INCLUDED
PHASEID GAS
TRES 300
DENW 60
VISW 0.3049
OGW_FLASH ON

**$ Property: EOS Set Number  Max: 1  Min: 1
EOSTYPE CON           1

ROCKFLUID

*JFUNC
*SRFTNW *CON  40
```

RPT 1

**$	Sw	krw	krow	Pcow
SWT				
	0.3	0	0.7	4
	0.33125	1.22E-05	0.540733	1.5
	0.39375	0.001	0.305064	0.8
	0.45625	0.008	0.156383	0.5
	0.51875	0.0293091	0.070079	0.3
	0.58125	0.08	0.0256454	0.22
	0.64375	0.14	0.00667572	0.2
	0.70625	0.24	0.000865173	0.185
	0.76875	0.37	1.07E-05	0.16
	0.8	0.45	0	0.15

**$	Sl	krg	krog
SLT			
	0.5	1	0
	0.525	0.586182	0.000170898
	0.55	0.316406	0.00273437
	0.575	0.152588	0.0138428
	0.6	0.0625	0.04375
	0.625	0.0197754	0.106812
	0.65	0.00390625	0.221484
	0.675	0.000244141	0.410327
	0.7	0	0.7

RPT 2

**$	Sw	krw	krow	Pcow
SWT				
	0.3	0	0.8	4
	0.3625	0.0875	0.7	1.2
	0.425	0.175	0.6	0.7
	0.4875	0.2625	0.5	0.4
	0.55	0.35	0.4	0.27

```
            0.6125    0.4375    0.3         0.21

            0.675     0.525     0.2         0.19

            0.7375    0.6125  0.1           0.175

            0.8       0.7       0           0.15

**$       Sl      krg     krog
SLT
        0.5      0.9       0
        0.8       0      0.8

*RTYPE  *IJK
 1:50  1:16 1:20  1
 25:26 5:16 5:15  2

**Using Velocity Dependent Rel Perm model
*VELDEPRP *MODEL1
*GAS 24556. 0.  1.0 0. 1. 4.00
*CONDENSATE 3000. 0.  1.0 0. 1. 2.9
*WATER 250. 0. 1.0 0. 1. 1.0


INITIAL

VERTICAL BLOCK_CENTER WATER_GAS

*SWINIT *CON 0.3

*ZGAS 0.0283  0.0613  0.462498  0.162399  0.143899
 0.100689  0.039438  0.001477  0.0

REFPRES
  6500

REFDEPTH
  8000

DWGC
  15000

NUMERICAL
*MAXSTEPS 100000000

**DTMIN 0.0000000000000001
**MODILU *ON

DTMIN 1.E-06
DTMAX 75

NORM *PRESS  150 **field unit
NORM *SATUR  0.05 **0.3
NORM *GMOLAR 0.05 **0.02
NORM AQUEOUS 0.3

MAXCHANGE *SATUR  0.8
```

```
MAXCHANGE *GMOLAR 0.8
MAXCHANGE *PRESS  2000

CONVERGE PRESS 1.E-03
CONVERGE HC 1.E-03
CONVERGE WATER 1.E-03
CONVERGE *MAXRES  5.E-03


AIM THRESH 0.001

RUN

DATE 1901 1 1
AIMWELL

WELL  'Well-1'
INJECTOR 'Well-1'
INCOMP  WATER
OPERATE  STW  1000  CONT
**$ UBA    ff  Status  Connection
**$ UBA      ff  Status  Connection
**$         rad  geofac  wfrac  skin
GEOMETRY  I  0.25  0.37  1.  0.
PERF  GEOA  'Well-1'
**$ UBA       ff  Status  Connection
   25 10 10  1.  OPEN    FLOW-FROM  'SURFACE'  REFLAYER
   26 10 10  1.  OPEN    FLOW-FROM  1
OPEN 'Well-1'

WELL  'Well-2'
PRODUCER 'Well-2'

OPERATE  BHP  2500.  CONT
**$ UBA    ff  Status  Connection
**$ UBA      ff  Status  Connection
**$         rad  geofac  wfrac  skin
GEOMETRY  I  0.25  0.37  1.  0.
PERF  GEOA  'Well-2'
**$ UBA       ff  Status  Connection
   25 10 10  1.  OPEN    FLOW-TO  'SURFACE'  REFLAYER
   26 10 10  1.  OPEN    FLOW-TO  1
SHUTIN 'Well-2'

TIME 1                          ** 1 day injection
SHUTIN 'Well-1'


TIME 5
TIME 10
TIME 20
TIME 30

OPEN 'Well-2'        **Producer opened after  30th  day

TIME 40
TIME 50
TIME 60
```

```
TIME 80
TIME 100
TIME 120
TIME 150
TIME 180
TIME 210
TIME 270
TIME 360
TIME 500
STOP
```

A4. CAPILLARY PRESSURE

Modeling of capillary pressures is very important in this study. Capillary trapping within the matrix, near the fracture face is a dominant mechanism for frac fluid retention. It is also important in gas flow through the proppant pack. However due to lack of published literature about the nature of capillary pressure curves in unconventional (tight) gas reservoir matrix and in proppant packs, a Leverett J-function approach is adopted in this study to scale the capillary pressures based on permeability and porosity. The Leverett J-function used in this study is based on conventional reservoir rocks and is depicted in the Illustration below.

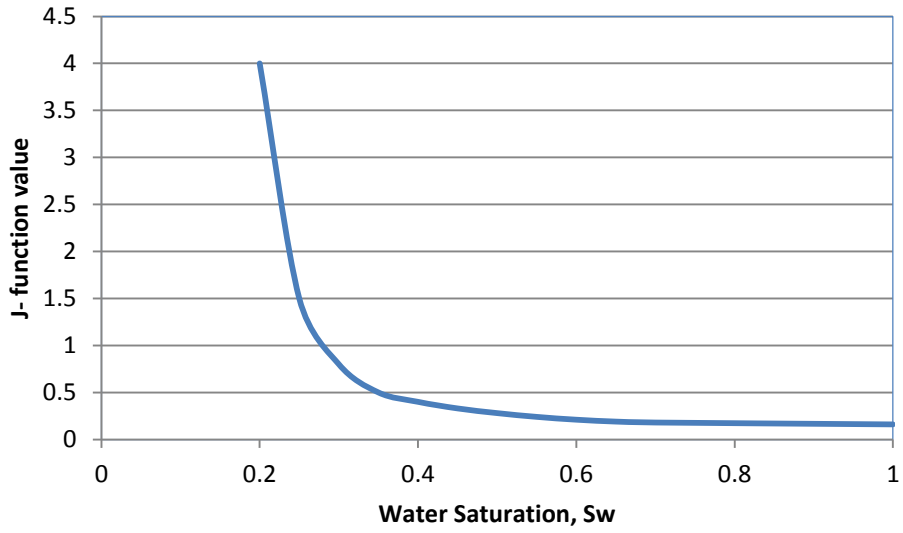

Illustration 4: Leverett J-function

CMG provides an option to invoke capillary scaling based on Leverett J-function using the *JFUNC keyword and requires relevant surface tension values. The J-function values are entered as Pc values in the respective relative permeability tables.

REFERENCES

Abacioglu, Y., Sebastian, H.M. and Oluwa, J.B.: Advancing reservoir simulation capabilities for tight gas reservoirs. SPE 122793 presented at the SPE Rocky Mountain Petroleum Technology Conference, Denver, Colorado, 14-16 April, 2009.

Afidick, D., Kaczorowski, N.J. and Bette, S.: Production performance of a retrograde gas reservoir: A case study of the Arun field. SPE 28749 presented at the SPE Asia Pacific Oil and Gas Conference, Melbourne, Australia, 7-10 November, 1994.

Ahmed, T., Evans, J., Kwan, R. and Vivian, T. : Wellbore liquid blockage in gas condensate reservoirs. SPE 51050 presented at the SPE Eastern Regional Meeting, Pittsburg, Pennsylvania, 9-11 November, 1998.

Al-Anazi, H.A., Pope, G.A. and Sharma, M.M.: Laboratory measurement of condensate blocking and treatment for both low and high permeability rocks. SPE 77546 presented at the SPE Annual Technical Conference and Exhibition, San Antonio, Texas, 29 September- 2 October 2002.

Bang, V.,: Phase behavior study of hydrocarbon-water-alcohol mixtures. MS Thesis, The University of Texas at Austin, May 2005.

Bang, V., Yuan, C., Pope, G.A., Sharma, M.M., Baran, J.R., Skildum, J.D. and Linnemeyer, H.C. SPE 19599 presented at the Offshore Technology Conference, Houston, Texas, 5-8 May, 2008.

Barnum, R.S., Brinkman, F.P., Richardson, T.W. and Spillette, A.G.: Gas condensate reservoir behavior: Productivity and recovery reduction due to condensation.

Bazin, B., Bekri, S., Vizika, O., Herzhaft, B. and Aubry, E. : Fracturing in tight gas reservoirs: Application of SCAL methods to investigate formation damage mechanisms. SPE 112460 presented at the SPE International Symposium and Exhibition on Formation Damage Control, Lafayette, Louisiana, 13-15 February, 2008.

Bennion, D.B., Bietz, R.F., Thomas, F.B. and Cimolai, M.P.: Reductions in the productivity of oil and low permeability gas reservoirs due to aqueous phase trapping. Journal of Canadian Petroleum Technology (November 1994), 45-54.

Boom, W., Wit, K., Zeelenberg, J.P.W. and Maas, H.C.: On the use of model experiments for assessing improved gas condensate mobility under near well bore flow conditions. SPE 36714 presented at the SPE Annual Technical Conference and Exhibition, Denver, Colorado, 6-9 October 1996.

Chopra, A.K., Carter, R.D.: Proof of two phase steady state theory for flow through porous media. SPE Formation Evaluation (December 1986), 603-608.

Chowdhury, N.S., Sharma, R., Pope, G.A. and Sepehrnoori, K. : A semi-analytical method to predict well deliverability in gas condensate reservoirs. SPE 90320 presented at SPE Annual Technical Conference and Exhibition, Houston, Texas, 26-29 September, 2004.

Cipolla, C.L., Lolon, E.P. and Dzubin, B.: Evaluating stimulation effectiveness in unconventional gas reservoirs. SPE 124843 presented at the SPE Annual Technical Conference and Exhibition, New Orleans, Louisiana, 4-7 October, 2009.

Clark, T.J.: The application of a 2D compositional, radial model to predict single well performance in a rich gas condensate reservoir. SPE 14413 presented at the

Annual Technical Conference and Exhibition, Las Vegas, Nevada, 22-25 September, 1985.

Cullick, A.S., Lu, H.S., Jones, L.G., Cohen, M.F. and Watson, J.P.: WAG may improve gas condensate recovery. SPE 19114 published in SPE Reservoir Engineering (August 1993), 207-213.

Darishchev, A., Lemouzy, P. and Rouvroy, P.: On simulation of flow in tight and shale gas reservoirs. SPE 163990 presented at the SPE Middle East Unconventional Gas Conference and Exhibition, Muscat, Oman, 28-30 January, 2013.

Du, L., Walker, J.G., Pope, G.A., Sharma, M.M. and Wang, P.: Use of solvents to improve the productivity of gas condensate wells. SPE 62935 presented at the Annual Technical Conference and Exhibition, Dallas, Texas, 1-4 October, 2000.

Ehrl, E. and Schueler, S.K.: Simulation of a tight gas reservoir with horizontal multifractured wells. SPE 65108 presented at the SPE European Petroleum Conference, Paris, France, 24-25 October, 2000.

El-Ahmady, M.H. and Wattenbarger, R.A.: Coarse scale simulation in tight gas reservoirs. PETSOC 2004-181 presented at Canadian International Petroleum Conference, Calgary, Alberta, Canada, 8-10 June, 2004.

El-Banbi, A.H., Forrest, J.K., Fan, L. and McCain, W.D.: Producing rich gas condensate reservoirs- Case history and comparison between compositional and modified black-oil approaches. SPE 58988 presented at the SPE International Petroleum Conference and Exhibition, Villahermosa, Mexico, 1-3 February, 2000.

Fishlock, T.P. and Smith, R.A.K.: Three phase studies of gas condensate flow behavior. SPE Advanced Technology Series (Vol.1, No.1, 1993), 127-132

Friehauf, K.E., Suri, A. and Sharma, M.M.: A simple and accurate model for well productivity for hydraulic fractured wells. SPE 119264 presented at the SPE

Hydraulic Fracturing Technology Conference, The Woodlands, Texas, 19-21 January, 2009.

Fussell, D.D.: Single well performance predictions for gas condensate reservoirs. JPT (July 1973), 860-870

Gdanski, R., Weaver, J., Slabaugh, B., Walters, H. and Parker, M.: Fracture face damage: It matters. SPE 94649 presented at SPE European Formation Damage Conference, Sheveningen, The Netherlands, 25-27 May, 2005.

Gdanski, R. and Walters, H.: Impact of fracture conductivity and matrix relative permeability on load recovery. SPE 133057 presented at the SPE Annual Technical Conference and Exhibition, Florence, Italy, 19-22 September, 2010.

Gdanski, R., Funkhouser, G.P.: Surfactant modeling for insight into load recovery enhancement for fracturing treatments. SPE 141296 presented at the SPE International Symposium on Oilfield Chemistry, The Woodlands, Texas, 11-13 April, 2011.

Hill, A.C. and Thomas, G.W.: A new approach for simulating complex fractured reservoirs. SPE 13527 presented at the SPE Middle East Oil Technical Conference and Exhibition, Bahrain, 11-14 March, 1985.

Holditch, S.A.: Factors affecting water blocking and gas flow from hydraulically fractured gas wells. JPT (December 1979), 1515-1524.

Hwang, J. : Gas injection for condensate recovery and remediation of liquid banking in gas-condensate reservoirs. MS Thesis, The University of Texas at Austin, May 2011.

Jamaluddin, A.K.M., Ye, S., Thomas, J., D'Cruz, D. and Nighswander, J.: Experimental and theoretical assessment of using propane to remediate liquid buildup in

condensate reservoirs. SPE 71526 presented at the Annual Technical Conference and Exhibition, New Orleans, Louisiana, 30 September- 3 October, 2001.

Jamiolahmady, M., Ganesh, D., Sohrabi, M. and Danesh, A. : The effects of fracture cleanup on the productivity of gas condensate systems. SPE 107432 presented at the SPE European Formation Damage Conference, Scheveningen, The Netherlands, May 30- 1 June,2007.

Kamath J. and Laroche, C.: Laboratory based evaluation of gas well deliverability loss caused by water blocking. SPE Journal. (March 2003), 71-80.

Karimi-Fard, M. and Firoozabadi, A.: Numerical simulation of water injection in fractured media using the discrete- fracture model and the Galerkin method. SPE 83633 published in SPE Reservoir Evaluation and Engineering (April 2003), 117-126.

King, G.R. and Ertekin, T.: State-of-the-art modeling for unconventional gas recovery. SPE 18947 published in SPE Formation Evaluation (March 1991), 63-71.

Kossack, C.A., Opdal, S.T.: Recovery of condensate from a heterogeneous reservoir by the injection of a slug of methane followed by nitrogen. SPE 18265 presented at the SPE Annual Technical Conference and Exhibition, Houston, Texas, 2-5 October, 1988.

Kumar, R.: Productivity improvement of gas condensate wells by fracturing. MS Thesis, The University of Texas at Austin, August 2000.

Mahadevan, J. and Sharma, M.M.: Cleanup of water blocks in low permeability formations. SPE 84216 presented at Annual Technical Conference and Exhibition, Denver, Colorado, 5-8 October, 2003.

May, E.A., Britt, L.K. and Nolte, K.G.: The effect of yield stress on fracture fluid cleanup. SPE 38619 presented at SPE Annual Technical Conference and Exhibition, San Antonio, Texas, 5-8 October, 1997.

Mirzaei, M. and Cipolla, C.L.: A workflow for modeling and simulation of hydraulic fractures in unconventional gas reservoirs. SPE 153022 presented at the SPE Middle East Unconventional Gas Conference and Exhibition, Abu Dhabi, UAE, 23-25 January, 2012.

Moinfar, A., Varavei, A., Sepehrnoori, K. and Johns, R.T.: Development of a coupled dual continuum and discrete fracture model for the simulation of unconventional reservoirs. SPE 163647 presented at the SPE Reservoir Simulation Symposium, The Woodlands, Texas, 18-20 February, 2013.

Montgomery, K.T., Holditch, S.A. and Berthelot, J.M. : Effects of fracture fluid invasion on cleanup behavior and pressure buildup analysis. SPE 20643 presented at SPE Annual Technical Conference and Exhibition, New Orleans, Louisiana, 23-26 September, 1990.

Osorio, J.G., Chen, H.Y. and Teufel, L.W.: Numerical simulation of coupled fluid-flow/geomechanical behavior of tight gas reservoirs with stress sensitive permeability. SPE 39055 presented at the SPE Fifth Latin American and Caribbean Petroleum Engineering Conference and Exhibition, Rio de Janeiro, Brazil, 30 August- 3 September, 1997.

Pope, G.A., Wu, W., Narayanaswamy, G., Delshad, M., Sharma, M.M. and Wang, P.: Modeling relative permeability effects in gas condensate reservoirs. SPE 49266 presented at the SPE Annual Technical Conference and Exhibition, New Orleans, Louisiana, 27-30 September, 1998.

Rai, R.R.: Gas condensates relative permeability parametric study and core flood simulation. Thesis, The University of Texas at Austin, December 2003.

Sanger, P.J. and Hagoort, J.: Recovery of gas condensate by nitrogen injection compared with methane injection. SPE 30795 published in the SPE Journal (March 1998), 26-33.

Settari, A., Sullivan, R.B. and Bachman, R.C.: The modeling of the effect of water blockage and geomechanics in waterfracs. SPE 77600 presented at SPE Annual Technical Conference and Exhibition, San Antonio, Texas, 29 September – 2 October, 2002.

Shaoul, J., Zelm, L. and de Pater, C.J.: Damage mechanisms in unconventional gas well stimulation- A new look at an old problem. SPE 142479 published in SPE Production & Operations (November 2011), 388-400.

Solimon, M.Y. and Hunt, J.L.: Effect of fracturing fluid and its cleanup on well performance. SPE 14514 presented at SPE Easter Regional Meeting, Morgantown, West Virginia, 6-8 November, 1985.

Tannich, J.D.: Liquid removal from hydraulically fractured gas wells. JPT (November 1975), 1309-1317

Wang, J.Y., Holditch, S.A. and McVay, D.A.: Modeling fracture fluid cleanup in tight gas wells. SPE 119624 presented at SPE Hydraulic Fracturing Technology Conference, The Woodlands, Texas, 19-21 January, 2009.

Wang, P., Pope, G.A. and Sepehrnoori,K.: Development of equations of state for gas condensates for compositional petroleum reservoir simulation. In Situ, 24(2&3), 2000.

Wang, Q., Guo, B. and Gao, D.: Is formation damage an issue in shale gas development?. SPE 149623 presented at the SPE International Symposium and Exhibition on Formation Damage Control, Lafayette, Louisiana, 15-17 February 2012.

Whitson, C.H., Fevang, O. and Sevareid, A.: Gas condensate relative permeability for well calculations. SPE 56476 presented at the SPE Annual Technical Conference and Exhibition, Houston, Texas, 3-6 October, 1999.

Wu, Y.S., Li, J., Ding, D., Wang, C. and Di, Y.: A generalized framework model for simulation of gas production in unconventional gas reservoirs. SPE 163609 presented at the SPE Reservoir Simulation Symposium, The Woodlands, Texas, 18-20 February, 2013.

Xie, J., Yang, C., Gupta, N., King, M.J. and Datta-Gupta, A.: Integration of shale gas production data and microseismic for fracture and reservoir properties using Fast Marching Method. SPE 161357 presented at the SPE Eastern Regional Meeting, Lexington, Kentucky, 3-5 October, 2012.

Yu, X. and Guo, B.: How significant is the formation damage in multi-fractured horizontal wells?. SPE 125905 presented at the SPE International Symposium and Exhibition on Formation Damage and Control, Lafayette, Louisiana, 10-12 February, 2010.

Zhang, Y., Yang, C., King, M.J. and Datta-Gupta, A.: Fast-Marching methods for complex grids and anisotropic permeabilities: Application to unconventional reservoirs. SPE 163637 presented at the SPE Reservoir Simulation Symposium, The Woodlands, Texas, 18-20 February, 2013.